Development of miRNA-mimic nanoparticles for the treatment of brain tumours

Shubaash Anthiya Ramamoorthi

Thèse de Doctorat

Shubaash
ANTHIYA RAMAMOORTHI GOPALRAM

Mémoire présenté en vue de l'obtention du
grade de Docteur de l'Université d'Angers
sous le label de L'Université Nantes Angers Le Mans
et
Mémoire présenté en vue de l'obtention du
grade de Docteur de l'Université de Nottingham

École doctorale : Biologie – Santé Nantes-Angers (ED-502)

Discipline : Biomolécules, pharmacologie, thérapeutique
Spécialité : *(7)*
Unité de recherche : *INSERM UMR_S 1066*

Soutenue le 04 November *2016*
Thèse N° : *s78173*

Development of miRNA-mimic nanoparticles for the treatment of brain tumours

JURY

Rapporteurs :	**Patrick MIDOUX,** Directeur de recherche (DR1 INSERM), CBM - CNRS UPR4301, Université d'Orléans, FR. **Stephen HART,** Professeur d'Université, University College London, United Kingdom.
Examinateurs :	**Jean-Paul ISSARTEL,** Directeur de recherche (DR2 CNRS), INSERM U1216, Université Grenoble-Alpes, FR. **Snow STOLNIK,** Professeur d'Université, University of Nottingham, United Kingdom.
Directeur de Thèse :	**Martin GARNETT,** Professeur d'Université, University of Nottingham, United Kingdom. **Emmanuel GARCION,** Directeur de recherche (DR2 INSERM), INSERM U1066, Université d'Angers, FR.
Co-directeur de Thèse:	**Beth COYLE,** Professeur d'Université, University of Nottingham, United Kingdom.

2012-2016

Diplôme : Docteur
Spécialité : PHARMACOLOGIE EXPERIMENTALE ET CLINIQUE

Development of miRNA-mimic nanoparticles for the treatment of brain tumours

ANTHIYA RAMAMOORTHI GOPALRAM Shubaash

Sous la direction de
Docteur GARNETT Martin
Docteur GARCION Emmanuel

Membres du jury
MIDOUX Patrick | Rapporteur
HART Stephen | Rapporteur
STOLNIK Snow | Examinateur
ISSARTEL Jean-Paul | Examinateur
COYLE Beth | Co-directeur de Thèse

Soutenu le :
04 Novembre 2016

université angers

Development of miRNA-mimic nanoparticles for the treatment of brain tumours

Shubaash ANTHIYA RAMAMOORTHI GOPALRAM

Thesis submitted to

The University of Nottingham and the University of Angers

for the degree of Doctor of Philosophy

November 2016

Development of miRNA-mimic nanoparticles for the treatment of brain tumours

Shubaash ANTHIYA RAMAMOORTHI GOPALRAM

Thesis submitted to

The University of Nottingham and the University of Angers

for the degree of Doctor of Philosophy

04 November 2016

NanoFar – Erasmus Mundus Joint Doctoral Programme

(2012 – 2016)

Thesis Committee Members/ Internal Examiners:

Snow STOLNIK, Professor, University of Nottingham, United Kingdom.
Jean-Paul ISSARTEL, Research Director (DR2 CNRS), University of Grenoble-Alpes, France.

External Examiners:

Patrick MIDOUX, Research Director (DR1 INSERM), University of Orléans, France.
Stephen HART, Professor, University College London, United Kingdom.

Directors of the Thesis :

Martin GARNETT, Associate Professor, University of Nottingham, United Kingdom.
Emmanuel GARCION, Research Director (DR2 INSERM), University of Angers, France.

Co-Supervisor of the Thesis:

Beth COYLE, Associate Professor, University of Nottingham, United Kingdom.

Acknowledgments

I thank Prof. Jean-Pierre Benoit, director of the MINT [Micro et Nanomédecines Biomimétiques, INSERM UMR-S1066], for allowing me to perform this thesis work in his laboratory.

I thank NanoFar, an Erasmus Mundus Joint Doctorate (EMJD) Programme, for funding this project. I thank Prof. Frank Boury, for his hard-work, vision and efforts in creating this wonderful programme that allows many students like me to follow our research dreams.

I express my deepest gratitude to Dr. Martin Garnett and Dr. Emmanuel Garcion, my thesis directors, for their immense support and guidance throughout this project. I remember my telephone interview with Martin as it happened yesterday. It was a great pleasure to be able to work on this project and share your great knowledge in the field of nucleic acid delivery. I always admire your patience and scientific rigor. I thank Emmanuel for believing in me and my abilities even when nothing was working and extending your support in every possible way. Without this scientific, financial and moral support, the project would not have progressed to the current level. I admire your scientific curiosity and our walk-in discussions.

I thank Dr. Beth Coyle, my co-supervisor, for her great support, guidance, advice, motivation to participate in conferences, joyful and assertive approach on science and life. You are a great supervisor and I learnt to be organized and to conduct research in a more structured way.

I thank Dr. Snow Stolnik and Dr. Jean-Paul Issartel, my thesis committee members, for the stimulating discussions, deep insights and different perspectives they had provided for the project.

I thank Dr. Patrick Midoux and Prof. Stephen Hart, for accepting to be the jury and evaluating this thesis.

I thank the imaging platform SCIAM [Service Commun d'Imageries et d'Analyses Microscopiques – Dr. Guillaume Mabilleau, Rodolphe Perrot, Florence Manero and Romain Mallet] for their great help with confocal and electron microscopy imaging performed during this work. I also thank Dr. Catherine Guillet and Jerome Cayon from platform PACeM [Plateforme d'Analyse Cellulaire et Moléculaire] for their help with flowcytometry and PCR. I thank Dr. Jean-Christophe Gimel for the training on Nanoparticle Tracking Analysis, Dr. Laurent Lemaire for his help with MRI imaging, Dr. Franck Lacoeuille for the training on *in vivo* imaging system, and Sylvie Avril for helping with cell culture. I thank Laurence Sindji, Nolwenn Lautram and Jerome Bejaud for their technical support and training at Angers. Thank you Edith Greleau, Patricia Le Grand and Céline Lépine for helping with the administrative procedures and ordering.

I thank Becky [Dr. Rebecca Chapman] and Dr. Lisa Storer for their help with cell culture and training at CBTRC [Children's Brain Tumour Research Centre]. I thank Dr. Philip Clarke for his invaluable help with live cell luciferase imaging with IVIS system. I thank Dr. Anna Grabowska for providing the sequence of luciferase siRNA. I also thank Christy [Christine Grainger-Boultby], Paul Cooling, Amy Nairn and all other staffs at the Boots Science Building for their invaluable technical support at Nottingham.

I thank Delyan and Nelly, it was wonderful times we had during my stay at Nottingham. I cannot forget the traditional Bulgarian dinners and home-made beers. Delyan, you inspire me with your scientific discussions and it has always helped me when I was feeling lost. Thank you Aishah for all your help, late-night discussions and teaching me Spongebob steps to stay awake at night. I thank Ammar, Zainab, Fahad, Ibteisam, Aseel, Aleksandra for all your help and wish you all the best for your PhDs. Thank you Aseel and Vincenzo for helping me with the NMR analysis, Aleksandra for helping with 3D-spheroid imaging, Victoria for all your help during the initial days, Maria for providing the siRNA sequence and Lee Moir for his kind help with TEM imaging. I thank everyone (Masar, Hiteshri, Emanuela, Naim, Daniel Wan, Alam, Laura, Tamara, Yasmin, Durga and Anbarasu) for the pleasant and memorable moments that we shared in the lab and in the office (A03, B14 and D16).

I thank Audrey for helping me with different experiments during the initial days of my PhD and thanks for answering all my silly questions during your busy final year experiments. Thank you Delphine for your kind help with the lentiviral transfection and generation of luciferase reporter cell lines; Thank you Claire for encouraging me during the difficult periods of thesis writing; and Thank you Mathie for help with luciferase assay and other “champagne” moments. Thank you Natasha and Clement for helping with cell culture and animal experiments. Thank you Hélène Malhaire, Emilie - Kévin, Aurélien - Angelique, Nada, Claire - Julian, Angélique - William, Hélène Lajous for all the scientific and non-scientific discussions, encouragement, lab lunches, home lunches and your support. I thank everyone (Anne-Laure, Nathalie, Maud, Alejandro, Leila, Lousineh, Rosemonde, Anne-Claire, Thomas Cordonnier, Anita, Alison, Milad, Janske, Flonja, Chantal, Bathabile, Carl, Marion, Thomas Perrier, Giovanna, Florence, Sai Krishna, Tian, Sravan, Gulfam) for all the beautiful moments we shared during these years of PhD.

I thank everyone from the University of Angers [INSERM U1066] and the University of Nottingham [School of Pharmacy and School of Medicine] for helping me with this thesis work.

I thank Catea, Zofia, Marta, Yannig, Jey (Jayasheelan), Aishu, Deepak, Shree and Gopal Jadhav for all the wonderful moments, movies, travels, delicious dinners, cooking experiments, shopping and all your help during my stay at Lakanal and Nottingham.

I thank my friends and mentors who encouraged me and acted as a motivation to pursue for a PhD, Prof. Siddhartha Sankar Ghosh, Pallab, Gokey, Amit, Anbarasu, Murugavel, Thamarai Selvan, Anoop, Muthukumaran, Debatosh, Aditya, Saravanan, Chockalingam and Santhosh.

A special thanks to Marion Toucheteau and Elise. Marion, you are a great person. I am very happy to know you; your help to me and all other NanoFar students is invaluable. I cannot imagine going through all the complex administrative and visa processes without your help. I wish you all the very best in all your endeavours. Elise, thank you very much for everything you have done. I can never forget my first Christmas celebration, with you, your parents and relatives, and our trip to Mt. Saint Michel. I wish you “Bon Courage!” for finishing your thesis and wish happiness and good health to you and your family.

Finally, thanks Dad, Mom, Kartik, Aunts (Veda, Rathai, Bhuvana, Sumathi, Lakshmi, Sabitha, Ganga), Uncles (Jothiram, Sakthi, Logu, Kannan, Ramesh, Murali, Jegatheesan, Ananthakrishnan), my cousins (Swathy, Prasanna, Aravind, Abi, Nishi, Pranay, Santhosh, Theju, Sindhu, Anesh and Suprabhaa) and grandparents (Annger amba, Aiyyo) for your encouragement, motivation to pursue research and providing emotional support during all these years. Thank you for letting me follow my dreams and your sacrifices for supporting it.

Table of Contents

List of Figures

List of Tables

List of Abbreviations

ABC transporters - ATP-binding cassette transporters
AFU - Arbitrary Fluorescence Unit
AGO – Argonaute
AKT - viral-Akt Murine Thymoma Viral Oncogene Homolog 1; [viral-AKT was discovered from AKT-8 viral strain. "t" stands for transforming capability; AKT-8 virus was isolated from AKR mice. "Ak" – Sequential in-bred mouse strain number [Aa, Ab, Ac, …, Ak, ..]. "R" Rockefeller Institute. [Source: http://www.scienceforums.net/topic/4627-what-does-akt-stand-for/]
ALU - Arbitrary Luminescence Unit
ATCC - American Type Culture Collection
ATP - Adenosine triphosphate
BBB - Blood Brain Barrier
bFGF - Basic Fibroblast Growth Factor
BGS - Bovine Growth Serum
BMI1- B-Lymphoma Mo-MLV Insertion Region 1 Homolog
BuNHAc – Acetyl - NH - Butyl - NH2
BuNic – Nicotinamide - Butyl - NH2
CBA – N, N′-cystamine bisacrylamide
CCD - Charge-Coupled Device
CED - Convection Enhanced Delivery
CL – Crosslinking
CMV – Cytomegalovirus
CN – Cell number
CNS - Central Nervous System
CoA-SH - Coenzyme A (Reduced form)
CP – Copolymer [PEG-PAA-PEG]
CP2k – $PEG_{1.7kDa}$–(DMEDA-Cysteamine)$_{2.4kDa}$-(DMEDA-MBA)$_{11kDa}$—(DMEDA-Cysteamine)$_{2.4kDa}$–$PEG_{1.7kDa}$
CP2k(R) – Reduced copolymer [CP2k] with free-thiols
CP5k - PEG_{5kDa} –$PAA_{3.1kDa}$–PEG_{5kDa}
CpG – 5′-Cytosine-phosphate-Guanine-3′
CRC - cysteine–arginine–cysteine motifs.
CSC - Cancer stem-like Cells
CSF - Cerebrospinal Fluid
DAH-Arg - 1,6-diaminohexane – Arginine conjugate
DAH-Arg-His - 1,6-diaminohexane – (Arginine-Histidine) conjugate
di (Boc) - N, N′ -bis-(tert-butoxycarbonyl)
DLR - Dual Luciferase Reporter assay
DLS - Dynamic Light Scattering
DMEDA - dimethyl-ethylene-diamine
DMEM - Dulbecco's Modified Eagle's Medium

DMSO - Dimethyl sulfoxide
DNA - Deoxyribonucleic acid
DTNB - [3, 3'-dithio-bis (6-nitrobenzoic acid)]
DTT - 1,4-Dithiothreitol
EDTA - Ethylenediaminetetraacetic acid
EGF - Epidermal Growth Factor
EGFR - Epidermal Growth Factor Receptor
EMEM - Eagle's Minimal Essential Media
EPR - Enhanced Permeation and Retention effect
Et-Br - Ethidium bromide
FB83 - Foetal Brain Cells 83
FBS - Foetal Bovine Serum
FGF - Fibroblast Growth Factor
FGFR - Fibroblast Growth Factor Receptor
GalNAc - N-acetylgalactosamine
GBM - Glioblastoma
GSH – Glutathione
H or His – Histidine
HDL - High density lipoproteins
HP – Homopolymer
IDH - Isocitrate Dehydrogenase
K or Lys – Lysine
Kcps – kilo counts per second
LDL - Low density lipoproteins
LNA - Locked Nucleic Acids
Luc - Firefly luciferase
MAb – Monoclonal Antibody
MBA - methylene bisacrylamide
MBP – Mono-block Polymer
MES - 2-(N-morpholino) ethanesulphonic acid
miR – miRNA – microRNA – micro-Ribonucleic acids
miRISC – microRNA Induced Silencing Complex
MOI - Multiplicity of Infection
Mono (Boc) - N-(tert-butoxycarbonyl)
MTS - [3-(4,5-dimethylthiazol-2-yl)-5-(3-carboxymethoxyphenyl)-2-(4-sulfophenyl)-2H-tetrazolium assay
MTT - (3-(4,5-Dimethylthiazol-2-yl)-2,5-Diphenyltetrazolium Bromide)- 2H-tetrazolium, inner salt
MWCO - Molecular Weight Cut-off
NEAA - Non-Essential Amino Acids
NHEJ - Non-homologous end-joining
NIH - National Institutes of Health, United States of America
NMR - Nuclear Magnetic Resonance spectroscopy
NSC83 - Neural Stem Cells 83

NSF – Neurosphere Formation Media
NTB - 2-nitro-5-thiobenzoic acid
PAA – Linear chain Poly(amidoamine) polymers with $(DMEDA\text{-}MBA)_m$-$(DMEDA\text{-}Cysteamine)_n$ backbone
PBS - Phosphate Buffered Saline
PDGFR - Platelet-derived growth factor receptor
PEG – Poly(ethylene glycol)
PEI – Polyethylenimine
PIPES - Piperazine-N, N′-bis (2-ethanesulfonic acid)
PMS - Phenazine methosulfate
RCN - Relative Cell Number
RES - Reticuloendothelial System
RFU - Relative Fluorescence Unit
RIPA - Radio immunoprecipitation assay
RLU - Relative Luminescence Unit
RNA - Ribonucleic acid
RNAi – RNA interference
ROS - Reactive Oxygen Species
RSD – Relative Standard Deviation
RTK - Receptor Tyrosine Kinase
RT-q-PCR - Real Time – Quantitative Polymerase Chain Reaction
RU – Repeating units (of the polymer)
RU/Nt - Polymer repeating unit to RNA nucleotide mol/mol ratios
SH – thiol
SHH – Sonic Hedgehog
siRNA - Small interfering RNA
SPy – Thio-pyridine
TAE – Tris – Acetic Acid – EDTA buffer
TBE – Tris – Borate – EDTA
TBP – Tri-block Polymer
TEM - Transmission Electron Microscopy
TP53 – Tumour Protein 53kDa
UA – University of Angers
UoN – University of Nottingham
UTR – Un-translated Region
UV-Vis – Ultra-violet / Visible (light)
VEGFR - Vascular Endothelial Growth Factor
W or Trp – Tryptophan
WHO - World Health Organisation
Wnt - Wingless-type, Mouse Mammary Tumour Virus related integration site

Chapter – I

General Introduction

1 General Introduction

1.1 Brain Tumours

Primary brain tumours occur both in children and adults. More than 50 % of brain tumours are gliomas that arise from the glial cells from different parts of the brain[1,2]. The new 2016 classification of tumours of the Central Nervous System (CNS) by the World Health Organisation (WHO) is based on both phenotype (histopathological appearance) and genotype (signature genetic changes)[3]. The tumours are also graded on a scale of I to IV by the WHO grading system. Grade I are well-differentiated, low-risk benign tumours that resemble normal cells; Grade II are moderately differentiated, slightly abnormal looking, slow growing tumours; Grade III are poorly differentiated, actively growing, abnormal looking malignant cancers; and Grade IV are undifferentiated, abnormal looking, highly malignant, fast growing, infiltrating tumours with poor prognosis[4,5]. Glioblastoma and medulloblastoma are classified as grade IV tumours[3]. Glioblastoma are currently categorised as diffuse astrocytic and oligodendroglial tumours; while the medulloblastoma are categorised under embryonal tumours (phenotype)[3]. Based on genotype, medulloblastoma are classified as WNT-activated group 1 [Wnt - Wingless-type, Mouse Mammary Tumour Virus related integration site], SHH-activated group 2 with or without TP53 mutation [SHH – Sonic Hedgehog; TP53 – Tumour Protein 53], non-WNT/non-SHH group 3 and 4; while the glioblastomas are classified based on the mutation status of IDH gene [Isocitrate Dehydrogenase]. Primary glioblastoma is the most frequent adult brain tumour with un-mutated, wild-type IDH gene with a median survival of a mere 15 months even with the best possible treatments available (surgery + radiotherapy + chemotherapy)[3,6] while the secondary glioblastoma patients with mutated IDH gene have a longer median survival of 31 months[3]. IDH mutations are known to contribute to tumorigenesis of multiple cancers including gliomas[7], while the mutation also sensitizes the cancer cells to radiotherapy under hypoxic condition, but not under normoxic condition[8].

1.2 Glioblastoma and Current Treatments

The general multi-modal treatment for gliomas includes surgery, radiation and adjuvant chemotherapy with temozolomide. Surgery removes most of the tumour mass preserving the normal functioning of the brain. The presence of residual tumour after the surgery, dispersion of cancer cells during surgery and metastasis to inaccessible organs are then treated with radio and chemotherapies, Figure 1-1.

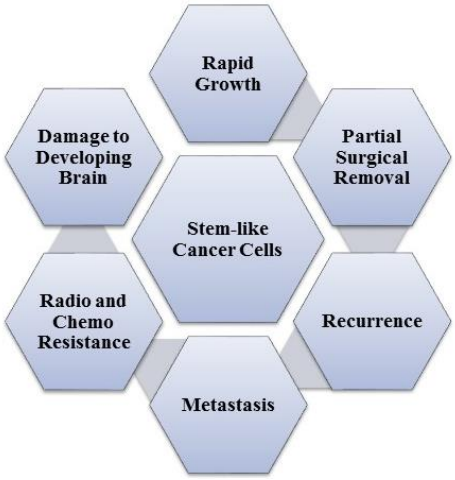

Figure 1-1: Challenges in treating brain tumour.

Due to the presence of the blood brain barrier (BBB), only a limited number of the available drugs given orally or through intra-venous injections can reach the tumour in sufficient concentration to be effective. Other strategies are being optimized to circumvent the problem of the blood brain barrier e.g. intrathecal injections, ommaya reservoirs (external reservoir connected to the ventricles by a capillary tube) for direct cerebrospinal fluid (CSF) drug delivery, post-operative implants like gliadel (polymer matrix wafers slowly releasing Lomustine into the surrounding) and loco-regional convection enhanced delivery (CED)[9-12]. These techniques give the option of using other chemotherapeutic drugs that do not readily cross the BBB. So far, however, all the treatment options available are only palliative without a cure. In order to devise better solutions to manage brain tumours, it is important to have an overview of current available strategies and treatment resistance mechanisms.

1.3 Radiotherapy

The paradigm of cancer treatment relies on chemo and radiotherapy. Radiation therapy is the preferred mode of treatment for brain tumours due to the non-invasive nature of the procedure and increase in life expectancy of the patients[13]. Ionizing radiation can damage the DNA either by direct-energy transfer or indirectly through the generation of reactive oxygen free radicals (ROS) that react with DNA to create double-strand breaks which could become lethal if left unrepaired[14]. Double strand breaks are much more difficult to repair than single strand breaks.

The problems associated with the partial effectiveness of radiotherapy are hypoxia and radio-resistance. The presence of hypoxia in the tumour environment leads to the generation of fewer free radicals and hence reduced DNA damage. Multiple radio-resistant pathways are also present that facilitate the repair of double strand breaks[15]. Side-effects of radiation include, oncogenic mutations caused in the cancer cells and surrounding normal tissues resulting in progression to an aggressive tumour phenotype and induction of secondary malignancies respectively[16,17].

Also, in recent years there is increasing evidence suggesting that the outcomes are affected by the presence of stem-cell like tumour initiating cell populations that display radio- and chemo-resistance characteristics. These unique characteristics of cancer-stem-like cells arise due to the activation of certain biological pathways controlling DNA repair and apoptosis[18,19].

1.4 Chemotherapy (Genotoxic Drug Treatment)

Most of the conventional genotoxic drugs act on actively dividing cells by inhibiting DNA replication or causing damage to DNA[20]. This assault to DNA is expected to trigger cell death in rapidly dividing cancer cells. Cell-cycle specific drugs act only at certain stages of replication. For example, antimetabolites (e.g. methotrexate, 5-fluorouracil, gemcitabine) inhibit DNA synthesis (S phase); Cytarabine inhibits DNA polymerase (S phase); Topoisomerase inhibitors (e.g. doxorubicin, epirubicin, irinotecan, etoposide) intercalate with DNA and inhibit DNA unwinding which results in strand-breaks and inhibition of replication (S, G2 phase); Vinca alkaloids (e.g. vincristine) and toxoids (e.g. paclitaxol) affect normal functions of microtubules and chromosomal segregation (M phase)[21]. In tumours, not every cell is dividing at the same time, hence increase in efficiency of cell cycle specific drugs can be achieved by extending the duration of drug exposure instead of increasing the dosage[21].

Other drugs are not specific to certain stages of cell cycle, such as alkylating agents (e.g. temozolomide, cyclophosphamide, lomustine, mitomycin C) and platinum derivatives (e.g. cisplatin) which show dose-dependent toxicity and can kill both proliferating and non-proliferating cells[21]. These are highly reactive chemicals that form chemical bridges between the strands of nucleic acids or proteins, affecting DNA replication and other normal functions[21]. Other drugs such as Bleomycin cause DNA fragmentation.

The major disadvantage of these cytotoxic drugs are the lack of specificity to cancer cells which results in adverse side effects leading to poor quality of life in people with cancer. Moreover, the presence of inter- and intra-tumour heterogeneity, altered blood supply, micro-environment changes, cellular phenotype, genetic composition, gene expression patterns[22,23], alternative metabolic pathways[24,25], drug efflux pumps[26], detoxifying enzymes[26], DNA repair mechanisms[27], mutations[27], activation and amplification of oncogenes[25,27] and resistance to cell death, these factors together dilute the cytotoxic effect of genotoxic agents on cancer cells. Also, these drugs do not affect the cancer cell populations that are dormant, metastatic (e.g. epithelial-mesenchymal transition)

and/or undifferentiated stem-like cells that are highly treatment-resistant[26,28]. As there are no other options available for cancer treatment, conventional genotoxic drugs and radiation are used as the first-line treatment for most of the cancers. Improvement in current treatment outcomes can be achieved by targeting the stem-like population of cancer cells[26,29,30] and the chemo and radio-resistance mechanisms[18,26,31].

1.5 Chemo-Radio Resistance and Stem cells

The main mode of action of both chemotherapeutics and radiation is by causing damage to DNA. Hence, many of the resistance pathways are shared, like DNA repair mechanisms (see section: 1.6.3, page: 7). But there are also several other survival pathways that are inter-related with one another and have overlapping functions (see section: 1.6.4, page: 9)[28]. Interestingly, some of these pathways are also implicated in stemness[26,28].

Stem cells (SC) are specialized undifferentiated or partially differentiated cells that can give rise to an entire organism [totipotent zygote], closely related tissue types [pluripotent embryonic stem cells, ESC and adult stem cells, ASCs] or a heterogeneous tumour resembling their tumour of origin [tumorigenic cancer stem-like cells, CSCs][32]. All these stem-cells have an ability to differentiate into different cell types upon exposure to specific extracellular cues while maintaining a stem-cell niche [i.e. asymmetric cell division, self-renewal and differentiation][33]. Cancer stem-like cells (CSCs) are characterized by the expression of certain markers [e.g. CD133, CD44, CXCR4, ALDH], some of the stem-cell related transcription factors [e.g. POU5F1, SOX2, KLF4, BMI1, NANOG], high levels of detoxifying efflux pumps [e.g. ABC transporter family] and sometimes markers of epithelial-mesenchymal transition-inducing factors[34] [EMT-IF, e.g. SNAI, TWIST][26]. Adult stem-cells are known to be dormant and can become active upon certain triggers such as an injury. Similarly, it has been shown in multiple instances that the CSC population in a tumour increases following chemo-[35] or radiotherapy[28,36]. As a result, these therapies enrich resistant CSC population and eliminate non-resistant cancer cells. CSCs are also implicated in tumour relapse after a surgery as just a small number of CSCs are capable of recapitulating an entire tumour. Hence, targeting CSC-specific

pathways that are involved in treatment resistance, self-renewal and survival would not only increase the efficiency of conventional therapies, but also might reduce the chance of relapse[26].

1.6 Resistance Genes and Signalling Pathways

1.6.1 Efflux Pumps

The concentration of cytotoxic drug reached at the site of action is critical to have a therapeutic response. The first hurdle to achieve effective drug concentration can be addressed by using novel drug delivery systems. However, cancer cells also express detoxifying efflux pumps which can actively expel the drug molecules from the cytoplasm hence reducing the effective concentration inside the cell[26]. The ATP-binding cassette transporters (ABC transporters) comprise a large family consisting of 48 members, many of which can contribute to drug efflux. Most notably ABCB1 [MDR1 "multidrug resistance protein 1" or P-gp "permeability glycoprotein"], ABCC1 [MRP1 "multidrug resistance protein 1"] and ABCG2 [BCRP "breast cancer resistance protein"] have been extensively studied in cancer drug resistance[26]. Cancer cells can express several of these efflux pumps at the same time or can over-express upon chemo-challenge.

1.6.2 Detoxifying Enzymes

Cancer cells can also inactivate the drug after cellular entry either by high expression of detoxifying enzymes or epigenetic silencing (promotor methylation by DNA methyltransferases) of prodrug activating enzymes[26]. Glutathione (GSH) reduction is known to inactivate platinum derivatives[26]; aldehyde dehydrogenase (ALDH) is known to inactivate cyclophosphamide, temozolomide, irinotecan, paclitaxel, epirubicin and doxorubicin[26]; O6-methylguanine-DNA methyltransferase (MGMT) is known to inactivate temozolomide[26]; UDP glucuronosyltransferase 1 (UGT1A1) is known to inactivate irinotecan and cytarabine[26,37].

Radiation results in generation of reactive oxygen species (ROS) that react with DNA to create double-strand breaks. ROS scavenging molecules [e.g. GSH, α-Lipoic acid (ALA), Melatonin, vitamin E and C] and ROS metabolizing

enzymes [e.g. Glutathione peroxidases (GPXs), Peroxiredoxins (PRDXs), Catalase (CAT), Superoxide dismutases (SODs), Isocitrate dehydrogenase 1 (IDH1)], neutralize ROS and hence reduce radiation-induced damage[38-40]. CSCs have been shown to over-express ROS scavenging enzymes allowing them to reduce oxidative stress[38]. Aldehyde dehydrogenase (ALDH1A1)[41] and cyclo-oxygenase-2 (COX-2)[42] have also been strongly implicated in radio-resistance although the mechanisms are not yet clearly understood.

1.6.3 DNA Repair Pathways

DNA damage would be caused by drugs that has escaped efflux pumps and detoxifying enzymes. The damaged cells activate cell cycle inhibitors and several DNA repair mechanisms to fix the DNA damage[26].

Dormancy / Cell Cycle Arrest: The DNA damage can only affect the dividing cells. There exists a dormant cancer cell population which inherently express dormancy associated proteins (e.g. histone deacetylase, histone demethylase) which slows down the cell cycle. This dormant population is not affected by DNA damage. Upon DNA damage, the dividing cells can also enter a dormant state by activating these dormancy-associated proteins and other checkpoint proteins to have more time to fix the damaged DNA[26]. The MRN (MRE11-RAD50-NBS1) complex recognizes DNA lesions and activates ataxia telangiectasia mutated (ATM), ataxia telangiectasia and Rad3-related (ATR) kinases, which in turn activate checkpoint kinases (CHEK1, CHEK2). Other checkpoint proteins include WEE1, TP53, BRCA, XRCC5, RBP-1. All these checkpoint proteins cause cell cycle arrest and delay in cell division in response to DNA damage.

DNA Repair: DNA repair involves single strand and double strand repair enzymes depending on the nature of the DNA damage. Single strand repair includes base excision repair (BER), nucleotide excision repair (NER), and mismatch repair (MMR). Double strand breaks (DSBs) are fixed by homologous recombination (HR) or non-homologous end joining (NHEJ). About 130 distinct proteins are involved in human DNA repair mechanisms, many of which have one or more replaceable partners[43].

MGMT (O6-methylguanine-DNA methyltransferase) is able to directly remove an alkylated base[26,43,44].

BER enzymes include DNA glycosylases [e.g. UNG "uracil DNA glycosylase", SMUG1 "single-strand-selective monofunctional uracil-DNA glycosylase 1", MBD4 "methyl-CpG binding domain 4, DNA glycosylase", MPG "N-methylpurine DNA glycosylase"] which remove the damaged base from the nucleotide. Apurinic/Apyrimidinic (AP) endonucleases cleave the abasic nucleotide, Poly(ADP-ribose) polymerase (PARP) or a DNA polymerase [POLB "Polymerase Beta" or POLG "Polymerase Gamma"] add the missing nucleotides, and a ligase (LIG3-XRCC1) joins the nick[26,43].

NER involves several DNA binding proteins for recognition and stabilization of the lesioned DNA strand [e.g. Damage-Specific DNA Binding Proteins (DDBs), Xeroderma Pigmentosum - Complementation Group A and C (XPA, XPC) and Replication Protein (RPA)], DNA helicase for unwinding (XPB, XPD), 3′-specific endonuclease (XPG) and 5′- specific endonuclease [Excision Repair Cross Complementing 1 - (ERCC1-XPF)] excise on either side of the lesion, a DNA polymerase [POLD1 or POLE1 (Polymerase δ1 or ε1)] adds the missing complementary DNA segment and a ligase (LIG1) joins the nick[26,43].

MMR proteins [MutS homolog (MSH2 to MSH6), MutL homolog (MLH1, MLH2)] recruit endonucleases and polymerases to rectify the mismatch errors occurring during the replication process[43]. The major importance of these MMR proteins is distinguishing and rectifying the errors produced in the newly synthesized strand while preserving the original template stand[26,43].

DSBs are lethal when left unrepaired. DSBs and other lesions are marked by phosphorylated histone (γH2AX) which recruits available repair proteins. Binding of 53BP1 [p53-Binding Protein 1] recruits NHEJ repair machinery while binding of BRCA1 [breast cancer 1] inhibits 53BP1 and recruits homologous recombination (HR) repair machinery [e.g. PALB2, BRCA2, RAD51][45]. In HR, the DSBs are bound by exonucleases and helicases which create ssDNA (end resection)[43]. BRCA2 recruits RAD51 recombinase to the ssDNA resulting in strand invasion to homologous DNA sequence which is used

as a template for the synthesis of the missing sequence, followed by recombination[45]. Alternatively, error prone NHEJ repair involves the recruitment of DNA end-binding heterodimeric protein complex [XRCC6-XRCC5, XRCC: X-ray repair cross complementing] to the DSB ends which results in end protection. NHEJ ligases [LIG4 and XRCC4] directly ligate any two adjacent DSB ends[45].

Targeting DNA repair to sensitize cancer cells to chemo and radio-therapy has been explored widely[27]. Due to the presence of multiple proteins and pathways for DNA repair, loss of function by targeting one repair mechanism can be replaced by a complementary pathway. Along with a genotoxic agent, targeting of a DNA repair mechanism in patients who inherit a defective complementary repair pathway would cause an excessive accumulation of DNA lesions and genome instability resulting in effective tumour killing [e.g. PARP inhibitors in BRCA defective patients][26,46]. Such an approach is called synthetic lethality[47]. However, non-cancerous cells might acquire carcinogenic mutations[27], due to treatment-induced defects in DNA repair, causing secondary malignancies.

1.6.4 Survival Pathways in Brain Tumours

Even if the DNA damage is not completely fixed, the cancer cells can still survive by suppressing apoptotic signals and activating other survival pathways that allow the propagation of cancer cells with an abnormal but stable genome.

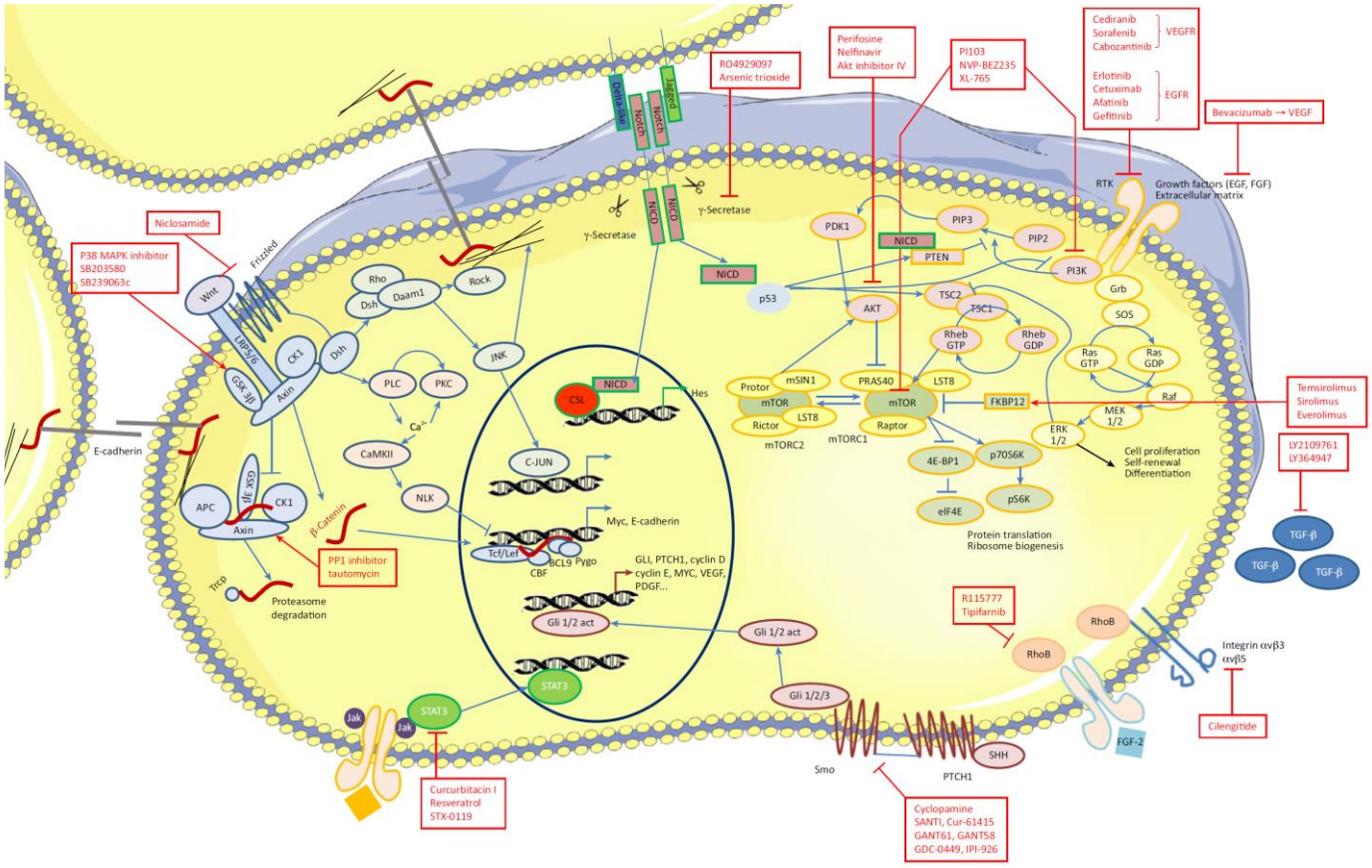

Figure 1-2: Key survival and resistance pathways in brain tumours.

[Image Source: Sehedic D, Cikankowitz A, Hindre F, Davodeau F, Garcion E. Nanomedicine to overcome radioresistance in glioblastoma stem-like cells and surviving clones. *Trends Pharmacol Sci.* 2015;36(4):236-252]

Notch Signalling: Notch signalling is activated by a transmembrane ligand [Delta-like ligands - DLL1, 2, 4 and Jagged 1, 2] interacting with a transmembrane receptor (NOTCH1 – NOTCH4) which results in a two-step proteolytic cleavage of the receptor releasing the active form in the cytoplasm. The cleavage is carried-out sequentially by ADAM Metallopeptidase [A Disintegrin and Metalloproteinase, ADAM 10 or ADAM 17] and γ-secretase. The active intracellular fragment enters the nucleus where it forms a complex with other nuclear factors [e.g. Mastermind-Like Transcriptional Coactivator (MAML1)] and activates expression of several target genes [e.g. Cyclin D3 (CCND3), CDK inhibitor (CDKN1A), EGFR2, MYC, Hairy and Enhancer of Split (HES) family of transcription factors][48]. Notch signalling has a complex, multifaceted functional activity ranging from proliferation, self-renewal, angiogenesis, migration and immune-modulation[48].

Wnt/β-catenin: Canonical Wnt pathway controls proliferation, self-renewal, differentiation and other functions. Binding of wnt ligands [WNT 1 to 11] to its receptors [Frizzled (FZDs) and Low density lipoprotein receptor-related proteins (LPRs)] causes the disassembly of AXIN, Adenomatous Polyposis Coli (APC) and Glycogen Synthase Kinase (GSK3β)[49]. This stabilizes β-catenin from degradation as GSK3β is no longer able to phosphorylate it[49]. Forkhead Box M1 (FOXM1) aids the nuclear entry of β-catenin where it forms a complex with T-cell factor/lymphoid enhancer factor (TCF/LEF) and activates several target genes [e.g. Matrix Metallopeptidase (MMP2), Zinc Finger E-Box Binding Homeobox (ZEB1), Snail Family Zinc Finger transcription factor (SNAI1, SNAI2), Twist family Basic Helix-Loop-Helix Transcription Factor (TWIST), N-cadherin][49]. FOXM1 directly upregulates SOX2 and RAD51[49].

Wnt signalling is inhibited by several families of antagonistic ligands like Dickkopf (DKK), Naked (NKD) and soluble Frizzled-related proteins (sFRPs)[49] and hence these have the ability to sensitize glioblastoma to chemotherapeutics and suppress clonogenic properties[50,51]. Hedgehog signalling is also implicated in negative regulation of wnt-signalling and these appear to be mutually exclusive to one another[49]. These wnt-antagonists are frequently downregulated in glioblastoma[49-51]. Alternatively, glioblastomas over-express

some of the wnt-signalling-enhancers such as Pleomorphic Adenoma Gene-Like 2 (PLAGL2) transcription factor[49,52], human achaete-scute homolog (ASCL1) transcription factor[53], Forkhead Box M1 - Maternal Embryonic Leucine Zipper Kinase (FOXM1-MELK)[54] and wnt-ligand secreting transmembrane protein (WLS)[49,55]. Altogether, enhanced wnt-signalling causes highly clonogenic CSC population maintenance, tumorigenesis, invasion, increased chemo[56]- and radio[36]-resistance[49].

Hedgehog/GLI Signalling: Hedgehog (HH) signalling is activated by secreted ligands [Sonic (SHH), Indian (IHH) or Desert (DHH)] binding to patched transmembrane receptors (PTCH) which relieves its inhibitory effect from smoothened transmembrane receptor (SMO)[48]. SMO subsequently releases the transcription factor Glioma-Associated Oncogene Homolog [GLI1 or GLI2], through a signalling cascade[48]. GLI enters the nucleus and activates several HH target genes [Cyclin D1 (CCND1), Cyclin E1 (CCNE1), B-Lymphoma Mo-MLV Insertion Region 1 Homolog (BMI1), GLI1, PTCH1, MYC, HES family][48]. Also irrespective to HH ligands, GLI can be regulated by several other pathways including AKT, RAS, MYC. GLI signalling is key for glioblastoma pathogenesis, tumour progression and chemo-radio resistance[28,57,58].

Receptor Tyrosine Kinase (RTK) Signalling: Transmembrane tyrosine kinases play an important role in glioblastoma and other cancers. RTKs include several growth factor receptors like Epidermal growth factor receptor (EGFR), Fibroblast Growth Factor Receptor (FGFR), Vascular Endothelial Growth Factor (VEGFR), Platelet-derived growth factor receptor (PDGFR), Receptor for hepatocyte growth factor (MET) and insulin-like growth factor receptor (IGFR)[59]. Binding of growth factor to their corresponding receptors results in direct activation of PI3K/AKT/mTOR and RAS/RAF/MAPK (ERK) signalling[59]. AKT inhibits activation of caspases [CASP9 and CASP3] and prevents apoptosis at a post-mitochondrial level[60]. Hyperactive AKT and mTOR are associated with aggressive tumours, increased resistance, cell survival, invasion and angiogenesis[28]. AKT can also be activated by several other

pathways that are independent of RTKs and PI3K, [e.g. cAMP, calmodulin and heat shock protein (HSPB1)][28,61].

Signal Transducer and Activator of Transcription (STAT) is activated by ciliary neurotrophic factor (CNTF) family of cytokine receptors or janus kinase (JAK) activated by RTKs (e.g. EGFR, PDGFR), non-receptor tyrosine kinases [SRC "sarcoma (Schmidt-Ruppin A-2) viral oncogene homolog", ABL "Abelson murine leukaemia viral oncogene homologs"], AKT/mTOR and RAS/ERK[28,62,63]. Phosphorylated STAT proteins dimerizes and enters the nucleus where it activates MYC "avian myelocytomatosis viral oncogene homolog", BCL2L1 "B-cell CLL/lymphoma (BCL2)-like 1", MCL1 "Myeloid Cell Leukaemia 1", survivin. STAT overexpression is also implicated in CSC maintenance, radio-chemo resistance, DNA repair, angiogenesis and invasion[62,63].

Nuclear Factor (NF)-κB: NF-κB can be activated upon irradiation by Ataxia Telangiectasia Mutated (ATM), AKT, DNA-Activated Protein Kinase (DNA-PK), Mitogen-Activated Protein Kinase (MAPK) and Tumour Necrosis Factor (TNF)[22]. It is also activated by Mitogen-Activated Protein Kinase Kinase Kinase (MEKK1, MEKK3), Transforming Growth Factor – Activating Kinase 1, NFκB – activating kinase, Protein Kinase C, interleukin-1 (IL1), T- and B-cell mitogens [e.g. bacteria, lipopolysaccharide (LPS), viruses, viral proteins, double-stranded RNA-dependent protein kinase (PKR)] and physical and chemical stress[22]. Most of these signals are also associated with the activation of TGFB1. Although TGFB1 has tumour-suppressor activity, in glioblastoma TGFB1 is associated with proliferation, aggressiveness and therapy resistance[64].

NFκB induces resistance by the activation of anti-apoptotic proteins [XIAP "X-chromosome-linked inhibitor of apoptosis", GADD45B "growth arrest and DNA damage-inducing protein βeta", Cytokine Induced Apoptosis Inhibitor (CIAPIN1 and CIAPIN2), TNF receptor-associated factor (TRAF1, TRAF2), cellular FLICE-inhibitory protein (cFLIP), B-Cell CLL/Lymphoma 2 (BCL2), BCL2-Like1 (BCL2L1), and Survivin], cell cycle regulators [cyclin B1, cyclin D1][15], ROS neutralizers [COX2 "Cytochrome C Oxidase II", MnSOD "Manganese-Containing Superoxide Dismutase" and γ-glutamylcysteine

synthetase (the rate limiting enzyme of GSH synthesis)] and other survival proteins [intercellular adhesion molecule-1 (ICAM1), galectin, P-selectin, AKT][15].

Hypoxia-Associated Signalling: Radiation causes vascular damage resulting in increased hypoxia which in turn induces Hypoxia Inducible Factor 1 Alpha (HIF1A)[65]. HIF1A promotes angiogenesis, migration, proliferation, survival, therapy resistance and revival[65]. HIF1A enhances the expression of VEGF for neovascularization. The inflammation and injury induced by radiation causes the tumour and surrounding stromal cells [cancer associated fibroblast (CAF)] to secrete growth factors (e.g. TGFB1) and chemokines [e.g. stromal cell-derived factor (SDF1 or CXCL12)] aiding angiogenesis and invasion of glioblastoma[66].

Hypoxia also induces expression of fibroblast growth factors (FGFs)[67] and integrins (αvβ3 and αvβ5)[68]. Both activate RHOB by farnesylation. Activated RHOB inhibits radiation induced mitotic cell death[28,69].

Targeting these resistance pathways to improve the effect of conventional therapies had been the main focus of recent decades.

1.7 Current Target-Specific Drugs and Antibodies (MAb)

Unlike conventional genotoxic drugs, target-specific drugs were designed to inhibit specific proteins and cellular process that are critical for the survival, proliferation, resistance, angiogenesis or invasion of cancer. These drugs have a much better safety profile compared to genotoxic drugs.

Imatinib, a tyrosine kinase inhibitor for a cancer-specific fusion protein BCR-ABL [(breakpoint cluster region)-(Abelson murine leukaemia viral oncogene homolog)], most effectively treats Philadelphia chromosome-positive leukaemia and other cancers as a single therapeutic agent and without affecting the quality of life[70]. Bortezomib is a proteasome inhibitor used in multiple myeloma patients[71].

Other cellular targets and drugs are presented in **Table 1-1 [page: 15]**. Most of these drugs are in clinical trials or in late stage pre-clinical evaluation. Those

drugs tested in clinical trials have only shown modest antitumor activity, either as a single agent or in combination with conventional genotoxic drugs, in unselected populations[48]. This class of drugs are a form of personalized medicine. As multiple pathways are active or can be activated in cancer cells, different combination of these drugs are expected to be more beneficial[72]. In order to obtain better clinical outcomes, an initial screening of patients' tumour for the identification of key tumour-survival genes and pathways must be performed to predict the right combination of drugs for which the tumours would respond [e.g. treatment with imatinib for BCR-ABL fusion protein in patients' tumour cells].

Table 1-1: Cellular targets and target-specific drugs.

Cellular Targets	**Drugs and Antibodies[26,28,48,49]**
Epidermal Growth Factor Receptor (EGFR)	Gefitinib[73,74], Erlotinib[74], Trastuzumab, Cetuximab
Vascular Endothelial Growth Factor Receptor (VEGFR)	Cediranib[75], Sorafenib[76], Apatinib[77]
Vascular Endothelial Growth Factor (VEGF)	Bevacizumab (Avastin®)
Fibroblast Growth Factor (FGF2)	Tipifarnib
Transforming Growth Factor (TGFB1)	LY364947
MET	Cabozantinib
AKT	Nelfinavir, Harmine
mTOR/PI3K	XL765
MAPK	Imatinib
Survivin	LLP-3
BCL-2	ABT-737
MCL-1	Omacetaxine
Integrins (αvβ3 and αvβ5)	Cilengitide
HIF1A	17-AAG
NOTCH*	Retinoic acid, Resveratrol, γ-secretase inhibitors
WNT*	Celecoxib, Aspirin, Diclofenac, Sulforaphane[49]
HH*	Sonidegib[48]

* - The drugs affecting NOTCH, WNT and SHH pathways are less specific and hence show off-target related side-effects.

1.8 MicroRNA - A Single Agent Multimodal Therapeutic

One of the new potential modalities which could control several resistance mechanism is by delivery of treatment-sensitizing microRNAs (miRNA replacement therapy). microRNAs (miRNAs) are natural small interfering RNAs (siRNAs) that have the ability to target multiple genes by binding to the 3′-UTR of the targeting mRNA, **Figure 1-3**.

1.8.1 MicroRNA – Biogenesis and Function

MiRNA genes are transcribed by RNA polymerases in the nucleus forming large primary-miRNA (Pri-miRNA, > 500 bases) which may harbour one or more stem-loop structures[78], Figure 1-3. The RNA-binding protein (Di George syndrome Critical Region gene 8, DGCR8/Pasha) and a RNAse III endonuclease (Drosha) recognizes the stemloop structures and releases the stem-loop Precursor miRNA (Pre-miRNA, ~70 nucleotides)[79]. Pre-miRNA is transported out of the nucleus by Exportin-5 (XPO5)[80]. The pre-miRNA has two arms (5′ and 3′) encoding the active miRNA sequence named as miR-X-5p (Red strand) or miR-X-3p (Blue strand) respectively, Figure 1-3 (see, Precursor miRNA). Once in the cytoplasm, the pre-miRNA loads into a pre-RISC (RNA induced silencing complex) consisting of Dicer, TAR RNA binding protein (TRBP), one of the argonautes (AGO1 - AGO4) and chaperones (Heat Shock Proteins, HSP70/HSP90)[81]. Dicer cleaves the stem-loop structure creating a ~23bp miRNA duplex which loads into an argonaute (AGO)[81]. Either miR-5p or miR-3p strand can load into the AGO, the choice is partially determined by the first nucleotide[82] and partially determined by the ease of unwinding of the first few base-pairs at the 5′ ends, i.e. weak-base pairing or presence of mismatch bulge[83,84]. AGO has higher affinity for loading U > (2-fold) A > (13-fold) G ≈ C[82]. The complementary strand is then eliminated from the AGO resulting in the formation of an active RISC complex with a mature miRNA sequence. The 2 – 7 nucleotides (seed sequence, highlighted in green in Figure 1-3, see miRNA Duplex) at the 5′-end of the miRNA scans for the complementary sequence on different mRNAs[85]. Binding to the target mRNA 3′-UTR (Untranslated Region) results in the inhibition of protein synthesis either by degradation of the mRNA

or blocking the transcription process without affecting the messenger RNA (mRNA) level[86].

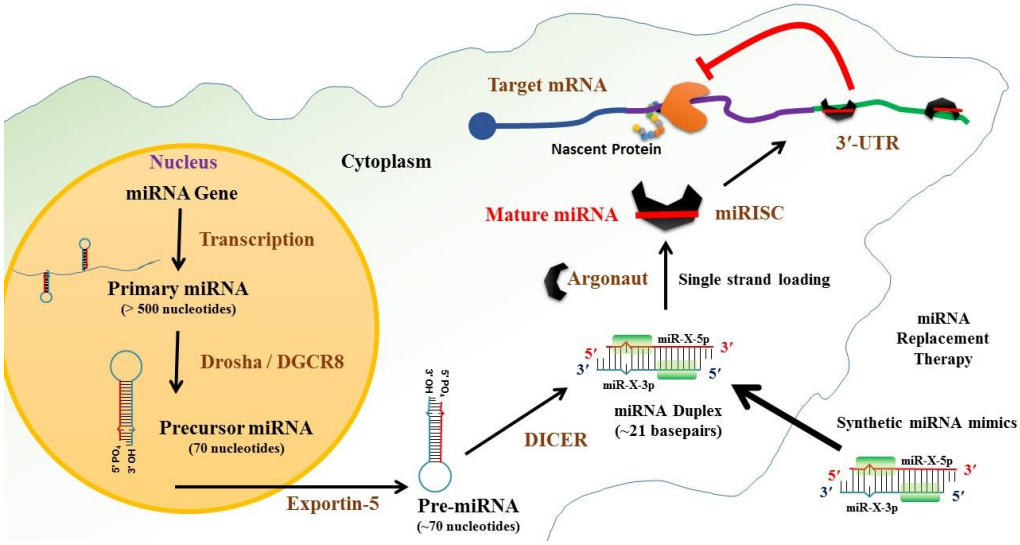

Figure 1-3: MicroRNA Biogenesis and Gene Silencing.

When miRNA mimics (synthetic miRNA duplexes) are delivered into the cell, they directly load into argonautes forming the RISC complex and exhibiting the same functional role as natural miRNAs.

1.8.2 Tumour Suppressor MicroRNAs

MicroRNAs can be classified as tumour suppressors (ts-miRs) or oncogenic miRNAs (onco-miRs). Suppression of a single onco-miR using Locked Nucleic Acids (LNAs, antegomiRs) can reactivate multiple tumour suppressor genes leading to tumour regression and other related benefits[87,88]. Conversely, introduction of a single tumour suppressor miRNA can suppress multiple oncogenes and tumour-survival factors, hence could also act as a single agent therapeutic or a sensitizing agent for conventional therapies[89]. This property of targeting multiple functionally related target genes makes miRNAs very attractive candidates for cancer treatment. Several tumour suppressor miRNAs have been identified which could be potentially used for miRNA-replacement therapy including, miR-34a[89], let-7[90], miR-16[91,92], miR-29[93], miR-101[94], miR-122[95], miR-124[96], miR-128[97], miR-145[98], miR-154[99], miR-181[100], miR-218[101], miR-302/367 cluster[102] and many more. Among them, miR-128 (hsa-miR-128-3p), miR-145 (hsa-miR-145-5p) and members of miR-302/367 cluster (hsa-

miR-302a-3p and hsa-miR-367-3p) were selected for this project. These microRNAs were selected for their ability to suppress self-renewal, metastasis and chemo or radio-resistance. miR-128 was implicated in normal brain development or function, but it is suppressed during the development of brain tumours. miR-128[103,104], miR-145[105,106] and miR-302[102,107,108] were implicated in the radio- or chemo-sensitization and reversal of stem-ness or tumour-forming ability by targeting stem-cell specific transcription factors and pathways.

1.8.3 MicroRNA-128

MiR-128 is a brain enriched miRNA expressed in high levels in normal brain tissue[109]. There exists an inverse correlation between miR-128 expression and grade of the glioma[110]. It is down-regulated in most tumour types including, acute lymphocytic leukaemia[111], lung[112], pituitary[113], colon[114] and ovarian[115] cancers.

Table 1-2: Direct target genes of miR-128.

Target genes	Major Function	Cancer Type
Stem-cell factors		
E2F3a[116], BMI1[113,117]	Stem cell transcription factors	Pituitary tumour[113], Glioma[116]
Chemo and Radio Resistance factors		
VEGF-C[118], EGFR[119], PDGFR[119]	Growth factors and receptors	Bladder[118], Glioma[119]
WEE1[120], SIRT1[114], RND3[121], SMAD2[122], BAX[123], truncated NTRK3[124]	Survival, Cell cycle, Apoptosis	pituitary adenomas[120], colon carcinoma[114], Glioma[121]
ABCC5[103], ABCA1[104], ABCG1	Efflux Pump	Breast
p70S6K1[110]	Angiogenesis	Glioma[110], ovarian[115]
DCX[125], RELN[125]	Invasion and metastasis	Neuroblastoma[125]
PFKL[112]	Metabolic regulator	Lung[112]

Cancer cells switch their metabolism from oxidative phosphorylation to glycolysis which increases glucose uptake, lactate production, rapid proliferation and tumorigenesis[112]. miR-128 directly targets phosphofructokinase liver type (PFKL), a rate limiting enzyme in glycolysis, suppressing cell proliferation and colony forming ability of lung cancer cells[112].

MiR-128 directly targets receptor tyrosine kinases (RTKs) like Epidermal Growth Factor Receptor (EGFR)[119], Platelet Derived Growth Factor Receptor

(PDGFR)[119], one of the RTK ligands – Vascular Endothelial Growth Factor C (VEGFC)[118], cell cycle checkpoint nuclear protein WEE1, G2 Checkpoint Kinase (WEE1)[120], Rho family GTPase 3 (RND3 or RHOE) involved in anti-apoptotic proliferative behaviour[121], Mothers Against Decapentaplegic Homolog 2 (SMAD2) downstream effector of TGFβ signalling[122], BCL2 Associated X Protein (BAX) a pro-apoptotic molecule[123] and truncated Neurotrophic Receptor Tyrosine Kinase 3 (NTRK3)[124], a neuronal plasticity regulator.

MicroRNA-128 has been shown to directly downregulate BMI1, an oncogene and a stem cell renewal factor, widely over-expressed in brain tumours. BMI1 down-regulation increases intracellular-ROS which triggers the senescence signalling pathway mediating cell growth arrest in medulloblastomas[117,126]. As BMI1 is a known transcriptional suppressor of Phosphatase and tensin homolog (PTEN), BMI-1 suppression increases PTEN expression. The tumour suppressor gene, PTEN, suppresses the activation (phosphorylation) of AKT[113]. Inhibition of AKT in turn increases the expression of miR-128[112] probably via p70S6 kinase1 (p70S6K1). p70S6K1 is an important down-stream effector of PI3k/ AKT/ mTOR pathway, highly expressed in glioma[110] and other types of cancer[115]. This kinase is known to modulate carcinogenesis, cell cycle, apoptosis, chemo-resistance, angiogenesis and miRNA processing[110,115]. p70S6K phosphorylates tristetraprolin (TTP) inhibiting its ability to bind Dicer and hence blocking the maturation of several miRNAs including miR-145[115], a tumour suppressor (see 1.8.4). p70S6K activates hypoxia-inducible factor 1 (HIF-α) which in turn activates vascular endothelial growth factor (VEGF) promoting angiogenesis[110]. miR-128 and miR-145 directly target p70S6K inhibiting angiogenesis and invasion. miR-128 is known to reduce the inflammatory response and cause immune tolerance by inhibiting the phosphorylation of MAPK14 (p38) and reducing the production of TNF in macrophages[127]. miR-128 is capable of inducing apoptosis in a TP53-dependant and TP53-independent manner. It also inhibits sirtuin-1 (SIRT1), a (NAD)-dependent histone deacetylase, hence preventing the inactivation of tumour suppressor TP53[114], Table 1-2.

MiRNA-128 is a bona fide tumour suppressor which can reduce tumour growth, invasion, induce apoptosis and senescence, hence can be used a single agent therapeutic against cancer, if it can be delivered at high dose at regular intervals. It can also be used as sensitizing agent for conventional treatments.

1.8.4 MicroRNA-145

MicroRNA-145 directly targets the stem cell maintenance factors OCT4 (Octamer-Binding Transcription Factor 3), SOX2 [SRY (Sex-Determining Region Y)-Box 2] and KLF4 (Kruppel-Like Factor 4)[128] and the glioma invasiveness factor, NEDD9 [Neural Precursor Cell Expressed, Developmentally Down-Regulated 9][129], Table 1-3. It blocks Insulin-like growth factor receptor I (IGF-IR) and its ligand Insulin Receptor Substrate-1 (IRS1)[130] thereby making cancer cells susceptible to apoptosis, blocks proliferation and migration[131]. It also downregulates angiogenesis factors, plasminogen activator inhibitor-1 (PAI1)[132] and p70S6K1[133]. It inhibits tumour growth by downregulating anti-apoptotic and cell cycle proteins like Cyclin-Dependent Kinase 6 (CDK6)[134,135], MYC[136], Specificity Protein 1 transcription factor (SP1)[134] and Phospholipase C epsilon 1 (PLCE1)[137]. It downregulates STAT1, one of the downstream effectors of JAK and MAPK kinase pathway[138]. It reduces growth of breast cancer cells by downregulating Rhotekin (RTKN) which is involved in the Rho-mediated activation of NF-κB pathway[139]. MiR-145 is able to induce chemo-sensitization by directly inhibiting transmembrane permeability of glycoprotein-1 (P-gp)[134,140]. miR-145 also indirectly downregulates up to 20 different DNA repair proteins[141], and directly blocks EMT factors such as NEDD9[129], SOX9[142], Mucin 1 (MUC1)[143], Yamaguchi Sarcoma Oncogene Tyrosine Kinase (YES)[138], adducin 3 (ADD3)[142], Zinc Finger E-Box Binding Homeobox 2 (ZEB2)[144], metadherin (MTDH)[145,146], Fascin Actin-Bundling Protein 1 (FSCN1)[147], Mothers Against Decapentaplegic Homolog 3 (SMAD3)[148] and Cluster of differentiation 40 (CD40)[149]. Together miR-145 expression induces radio- and chemo-sensitivity in gliomas, bladder[144,147], prostate[141] and cervical[150] cancer. It also blocks invasion, metastasis and clonogenic properties of several cancers including brain[129,142], lung[145,148] and ovarian[146] cancers. It has been reported that the overexpression of long-non-coding RNAs (LncRNAs) like Taurine Upregulated Gene 1 (TUG1)[144]

and Metastasis Associated Lung Adenocarcinoma Transcript 1 (MALAT1)[150] act like miRNA sponge sequestering miR-145 from its functional activity, thereby inducing radio-resistance in bladder and cervical cancers respectively.

Table 1-3: Direct target genes of miR-145.

Target genes	Major Function	Cancer Type
Stem-cell factors		
OCT4[128], SOX2[128], KLF4[128]	Stem cell associated transcription factors	(Tested in human embryonic stem cells)
Chemo and Radio Resistance factors		
IRS1[130], IGF-1R[131]	Growth factors and receptors	Colon[130], Bladder[131] cancer
MYC[136], CDK6[134,135], SP1[134], PLCE1[137], STAT1[138], RTKN[139]	Cell cycle, Survival, Apoptosis	Ovarian[134], Cervical[135], Colon[138], Breast[139] cancer; oral[136] and oesophagus[137] squamous cell carcinoma
ABCB1 (P-gp)[140]	Efflux Pump	Gastrointestinal (GI) cancer
PAI-1[132], p70S6K1[133]	Angiogenesis	Bladder[132], Colon[133] cancer
FSCN1[147], MTDH[145,146], MUC1[143], YES[138], NEDD9[129], SMAD3[148], SOX9[142], ADD3[142], CD40[149]	EMT, invasion and metastasis	Bladder[147], Ovarian[146], Breast[143], Colon[138], Lung[145,148], Glioma[129,142]

Like miR-128, miR-145 is also a bona fide tumour suppressor targeting multiple oncogenes and resistance genes and hence can either be use as single agent miRNA replacement therapeutic or in combination therapy.

1.8.5 MicroRNA-302/367 family

The miR-302/367 cluster is represented by several miRNAs, miR-302-a-3p, -a-5p*, b-3p, b-5p*, c-3p, c-5p*, d-3p, d-5p* and miR-367-3p, -5p*; (* - represents less dominant form). miR-302a-3p share the same seed sequence with miR-302 -b, -c and -d (see, Figure 1-4), while miRbase enlisted miR-367-3p as the dominant form expressed in cells. The miR-302/367 family is conserved across vertebrates[151]. In humans, this cluster resides in chromosome 4 (4q25 region) within the intron of LARP7 gene [La Ribonucleoprotein Domain Family Member 7][151]. This family of miRNAs is transcribed along with LARP7 gene or independently with its own promotor[151]. Several transcription factors like OCT3/4, NANOG, REXO1 and SOX2 are able to activate the expression of

these miRNAs[151]. These miRNA are strongly implicated in the induction of pluripotency (iPSCs)[152], tumour-suppressor[153] and tumour promotor activity[151].

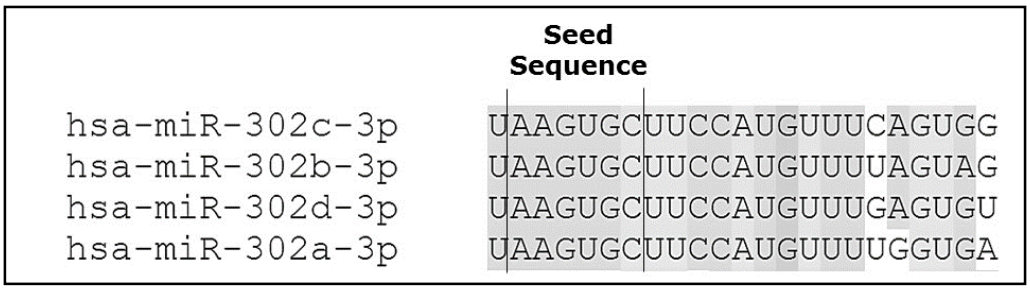

Figure 1-4: Sequence alignment of miR-302-(a, b, c, d) -3p

Tumour-Suppressor: MiR-302b was shown to directly target Epidermal Growth Factor Receptor (EGFR or HER1) in hepatocellular carcinoma cells (HCC)[154] and EGFR4 or HER4 in oesophageal squamous cell carcinoma (ESCC)[155]. The expression of miR-302b with a plasmid DNA resulted in the inhibition of proliferation of both cancer types. In ESCC, miR-302b was also able to induce apoptosis and reduce *in vitro* cell invasion, Table 1-4. miR-302 directly targets resistance genes like AKT1 and RAD52, resulting in radio-sensitization of breast cancer cells[107]. miR-302 also targets stem cell transcription factor BMI1 and inhibits the tumorigenecity[153], **Table 1-4**.

Table 1-4: Direct target genes of miR-302.

Target genes	Major Function	Cancer Type
Stem-cell factors		
BMI1[153], NR2F2[156]	Stem cell associated transcription factors	
Chemo and Radio Resistance factors		
EGFR1 (HER1)[154], EGFR4 (HER4)[155], CXCR4[102], TGFβR2[152],	Growth factors and receptors	Oesophagus[155], Liver[154], Glioma[102]
CDK2, CDK4[153], Cyclin D1[157], AKT1[107], RAD52[107], CCL5[158], RBP-1[158], RHOC[152], TOB2[159], DAZAP2[159] and SLAIN1[159]	Cell cycle, Survival, Apoptosis	Breast[107]
MECP1 and MECP2 AOF1 and AOF2[160], MBD2[161]	Epigenetic Reprogramming	Normal cells
ABCA1[162]	Efflux Pump	Normal cells

MiR-302 directly targets key cell cycle proteins like cyclin D1[157] and cyclin dependant kinase (CDK2/4)[153] modulating cell cycle arrest or G1 – S phase transition. The miR-302/367 cluster has been reported to suppress self-renewal and invasiveness of glioblastoma initiating cells (GICs) by directly targeting CXCR4 receptor and its ligand SDF1, thereby blocking the CXCR4/SDF1 mediated SHH/GLI/NANOG activation[102]. miR-302 regulates cellular plasticity [e.g. Epithelial-Mesenchymal Transition (EMT)] by directly downregulating Transforming Growth Factor Beta Receptor 2 (TGFBR2), its upstream regulators Lefty1, 2 and one of the downstream effectors, Ras Homolog Family Member C (RHOC)[152], **Table 1-4**.

Somatic Cell Reprogramming: MiR-302 can induce somatic cells to enter a pluripotent stem-cell (iPSC) like state, under certain culture conditions, by promoting genome-wide demethylation. This is achieved by direct downregulation of epigenetic regulators like methyl-CpG binding proteins (MECP1 and MECP2) and lysine-specific histone demethylase 1 and 2 (AOF1 and AOF2). Absence of these proteins destabilizes DNA methyltransferase (DNMT1) which in turn induces genome-wide demethylation[160]. Human umbilical cord blood (CB) cells transduced with OCT4, SOX2, MYC, KLF4 form iPSCs. Introduction of miR-302-a, b, c, d improves the efficiency of iPSC formation, by rescuing Nanog expression by down-regulating its transcriptional inhibitor [methyl-DNA binding domain protein 2 (MBD2)][161]. miR-302 can modulate the self-renewal capabilities by promoting Bone morphogenetic proteins (BMP) signalling. BMP signalling is promoted by downregulating three of different BMP inhibitors: Transducer Of ERBB2, 2 (TOB2)[159], Deleted In Azoospermia-Associated Protein 2 (DAZAP2)[159] and SLAIN Motif Family Member 1 (SLAIN1)[159], **Table 1-4**.

In general, miRNA does not completely block the expression of its target genes, and hence the cell fate is context specific, i.e. the outcome is decided by the synergistic effect of several different microRNAs and the abundance of different target genes expressed in the cell of interest[152].

1.9 MicroRNA Delivery

Because of the multiple gene targets, miRNA is a multi-modal therapeutic molecule that can be used for treating many pathologies, especially cancer. The potential of RNAi therapeutics and gene therapy are huge and the major limitation with nucleic acid therapeutics is the delivery. An ideal microRNA delivery system that could be used in a clinical setting should have the following properties: The size of the delivery system should be uniform and in nano-dimension (20 – 200 nm). Nanoparticles less than 5 nm are able to reach the tissue by crossing the vascular endothelial barrier but also have fast renal clearance rate; whereas larger particles (>20 nm) have less renal clearance, longer circulation half-life but are not able to cross the vascular endothelial barrier unless it is leaky (EPR, enhanced permeation and retention effect) and they are effectively captured by immune and reticuloendothelial system (RES) present in liver, lungs and kidney[163]; PEGylation can also slow down this process of rapid elimination[163]; The delivery system should be able to package large quantities of miRNA; Should be stable under storage and physiological conditions; Should have good cellular uptake; It should be able to escape the endosomal compartment and release the miRNA in to the cytoplasm, the site of action; addition of recognition ligands may enhance localisation or cellular uptake. Finally, it should be non-toxic, non-immunogenic, biocompatible, simple cost-effective formulation with the ease of scalability.

1.9.1 Cellular uptake of naked- and complexed miRNA

Naked unmodified negatively charged miRNA or siRNA are large, highly hydrophilic macromolecules that have minimal interaction with the cell membrane, hence show marginal uptake and functional activity compared to ligand conjugated or nanoparticle mediated delivery systems[164].

The main mode of uptake of oligonucleotides (naked and in combination with a delivery system) is by endocytosis (clathrin-mediated, caveolar, macropinocytosis or any other mode of uptake)[165]. The choice of endocytic pathway and intracellular fate depends on the size, nature of interaction and type of conjugated ligand[165]. Endocytosis results in the entrapment of oligonucleotides in an endosomal vesicle which then fuses with an early

endosome (sorting endosome)[165]. The oligonucleotides can be sorted in to recycling vesicles and expelled out, trafficked to intracellular organelles [e.g. golgi apparatus or endoplasmic reticulum] or to the late endosomes [(LE) or multi-vesicular body (MVB)][165]. The RISC machinery for siRNA and miRNAs were found to be associated with outer wall of rough endoplasmic reticulum (rER) and hence trafficking to ER might lead to some biological activity[165,166]. The oligonucleotides reaching the late endosomes (LE) can be expelled out by exosome-mediated exocytosis or degraded after acidification (pH 5 – 6) and fusion with lysosome (pH 4.5). Evidence suggests that even a few molecules, of free siRNA (>10) or miRNA (>100)[167], in the cytoplasm could produce potent functional effects[164]. Hence, for the nanoparticles with high cellular uptake, strategies that allow endosomal escape and intra-cellular release of oligonucleotides should be addressed more seriously to achieve highly functional delivery systems[168].

1.9.2 MicroRNA Delivery Systems and Strategies

Chemical Conjugates: MiRNA chemical conjugates are the simplest form of delivery systems where the 3′-end is conjugated to a hydrophobic moiety [e.g. cholesterol[168,169], squalene[170], fatty acids[171], α-tocopherol[172]] Hydrophobic ligand conjugated miRNAs/siRNAs form complexes with serum proteins or lipoproteins [e.g. low and high density lipoproteins (LDL or HDL)] which enhances oligonucleotide circulation and cellular uptake[169,171]. Alternatively a receptor-specific ligand [e.g. the RGD peptide targeting αvβ3 integrins[173], N-acetylgalactosamine (GalNAc) targeting asialoglycoprotein receptor[174], CpG DNA sequence targeting Toll like receptor 9 (TLR9)[175], peptides (e.g. H5WYG[176]), antibodies[177], aptamers[178]] can effectively improve the uptake of naked oligonucleotides both *in vitro* and *in vivo*[179].

Peptide Nanoparticles: Cell penetrating peptides and other cationic peptides can be complexed with nucleic acids to form high efficiency delivery systems like MPG-8[180], CADY[181], RVG-R9 [Rabies Virus Glycoprotein – Oligo-Arginine][182]. MPG-8 [probably this is N-TER™] is an improved 21 aminoacid peptide [βAFLGWLGAWGTMGWSPKKKRK-Cysteamide] derived from a parent sequence developed by M. C. Morris, P. Vidal, G. Divita

et al (MPG)[183]. MPG is a cell penetrating peptide derived from the fusion sequence of hydrophobic HIV gp41 (Human immunodeficiency virus, glycoprotein 41) and hydrophilic nuclear localization sequence from SV40 (Simian virus 40) T-antigen. CADY is a combined aromatic tryptophan (W) and cationic arginine (R) containing 20 aminoacid peptide with the following sequence, Acetylated-GLWRALWRLLRSLWRLLWRA-Cysteamide developed by "L. Crombez, G. Aldrian-Herrada, G. Divita *et al*[181]. The cysteamide group at the C-terminus is required for the cellular uptake of these peptide-siRNA nanoparticles[180], acetylation at the N-terminus of CADY improved cellular uptake but it was dispensable, the β-Alanine at the N-terminus of MPG-8 allows functionalization if needed, while lysine (Lys, K) and arginine (Arg, R) are positively charged aminoacids to allow complexation with negatively charged siRNA or miRNAs.

Metallic Nanoparticles: Spherical nucleic acids (SNA) consist of a core gold nanoparticle (AuNP) with its surface densely packed with oligonucleotides attached via thiolate-Au interaction. The passenger strand bearing a thiol (SH) group could react with gold nanoparticles to deliver miRNA or siRNA. The guide strand would be separated from the passenger strand inside the cells by the RNAi machinery[184]. These nanoparticles show high transfection efficiency, low toxicity and ability to cross blood brain barrier (BBB) without a targeting ligand[184]. AuNP can also be loaded with miRNA via cysteamine coating at its surface[185]. PEI coated iron oxide nanoparticles were used for the delivery of miRNA *in vitro* with promising transfection efficiency and low toxicity[186]. Gadolinium-DTPA (Diethylenetriaminepentaacetic acid) loaded nano graphene-oxide (GO) were used for imaging and co-delivery of miRNA and epirubicin[187].

Lipid Based Nanoparticles: Lipid based delivery systems can be broadly classified as liposomes (made of lipid bilayers) and lipid nanoparticles (LNPs)[188]. LNPs are sometimes referred as stable nucleic acid lipid particle (SNALP) or solid lipid nanoparticles (SLN). LNPs are made with the same cationic lipids used for the preparation of liposomes. The complexes formed between cationic lipids and anionic nucleic acid are called lipoplexes. The major

difference between liposomes and LNPs is that liposomes have an aqueous core while the LNPs have a lipophilic matrix at its core which dramatically increases the *in vivo* stability and transfection efficiency of LNPs compared to liposomes[189-192].

Components of Lipid-based nanoparticles: The most commonly used components are cationic lipids [e.g. N-1-[(2,3-dioleyloxy)propyl]-N,N,N-trimethylammonium chloride (DOTMA), dioleyloxy-N,N-dimethyl-3-aminopropane (DODMA), 1,2-dioleoyl-3-dimethylammonium-propane (DODAP), 2,3-di-oleyloxy-N-[2(spermine-carboxamido)ethyl]-N,N-dimethyl-l-propan-aminium (DOSPA), 5-carboxyspermylglycine dioctadecylamide (DOGS)], a neutral lipid [e.g. 1,2-distearoyl-sn-glycero-3-phosphocholine (DSPC)], an unsaturated, amphiphilic, pH-sensitive fusogenic lipid [e.g. Dioleoylphosphatidylethanolamine (DOPE), Dilinoleyl-methyl-4-dimethylaminobutyrate (DLin-MC3-DMA)], a PEGylated-lipid [e.g. PEG ceramides, PEG-succinoyl-diacylglycerols (PEG-s-DAG)] and cholesterol[188,189].

Liposomes: Cationic liposome preparation, in general, starts with solvent evaporation to obtain lipid bilayers coated onto a flask which are then resuspended in aqueous phase to obtain crude liposomes. Extrusion through porous membranes (e.g. 100 nm) then results in cationic liposomes with a uniform size distribution. Finally, lipoplexes are obtained by mixing the cationic liposomes with nucleic acids. Several commercial transfection agents are cationic liposomal formulations including Lipofectamine™ [DOSPA: DOPE, 3:1 w/w], Lipofectin™ [DOTMA: DOPE (1:1)], TRANSFECTAM™ [DOGS][193]. Liposomal formulations work better in the absence of serum, however using certain cationic cholesterol derivatives along with DOPA has shown to partly overcome the serum stability issues[194].

The fate of ~70 % of siRNA delivered by lipid nanoparticles reach late endosomes (LE), packed into exosomes for exocytosis[195] and the remaining would be degraded after fusion with lysosome[165,188]. Only a small fraction (1 – 2%) of the oligonucleotides reach the cytoplasm that account for the functional activity. This cytoplasmic release was predicted to happen either by direct fusion

of liposomal delivery systems with cell membrane or destabilization of the endosomal bilayer causing the oligonucleotides to leak out into the cytoplasm[165,196].

Lipid nanocapsules (LNCs) are a class of LNPs with an oily hydrophobic core [e.g. Labrafac WL1349 (Caprylic/Capric triglycerides)] stabilized by surfactants [e.g. Solutol HS15 (PEG_{600} -15-hydroxy stearate) and Lipoid S75 (70% Soybean phosphatidylcholine)]. Oligonucleotides like siRNA or LNAs can be delivered with LNCs following one of the two strategies: nucleic acid lipoplexes embedded in the LNCs[197] or nucleic acids complexed on to a cationic peptide grafted on LNC's surface[198].

Dioleyl-Glu-Orn-Orn are a new class of hybrid nanoparticles made of a combination of a lipid and peptide. These hybrid molecules are also able to form stable nanoparticles with siRNA and showed efficient gene silencing both *in vitro* and *in vivo*[192]. Lipopolyplexes (LPN) are hybrid nanoparticles made of lipid, polymer and nucleic acid[199,200]. These delivery systems are capable of encapsulating all kinds of nucleic acids and exhibit high transfection efficiency with low toxicity[199].

Polymeric Nanoparticles: The polymeric nanoparticles can be prepared by two different strategies, (1) Polyelectrolyte complexes (PEC or polyplexes); (2) Encapsulation. Most of the polymeric nanoparticles are formed as by mixing a cationic polymer with an anionic nucleic acid (polymer-nucleic acid complexes - polyplexes). The poly(amidoamine)-miRNA nanoparticles used in this work belongs to polyplex type.

A typical example for encapsulation type of nanoparticles is a Polylactide-co-glycolic acid (PLGA)-coated spermidine-nucleic acid complex[201]. Here, cationic spermidine acts as a nucleic acid condensing agent, while the PLGA acts an encapsulating and stabilizing agent. (PLGA) is a biocompatible FDA approved polymer, hence PLGA-coating of polyplexes is an attractive strategy for nucleic acid delivery[201,202]. All the other polymeric nanoparticles discussed below belong to polyplex type.

Chitosan is a biodegradable polymer widely used for nucleic acid delivery. Chitosan alone[203] and in combination with hyaluronic acid[204] were able to delivery miRNA *in vivo* without any signs of toxicity (weight loss) in animals.

Dendrimers, like polyamidoamine (PAMAM), are hyper-branched, mono-disperse, multi-functional nanoparticles with high cellular uptake and able to deliver a wide range of cargo, including miRNA and miRNA inhibitors[205]. Polyethylenimine (PEI) is a gold standard cationic polymer used in the nucleic acid delivery. Its use in clinic is limited by its toxicity[206]. The toxicity issue was overcome by either chemically modifying the more toxic primary and secondary amines into less toxic secondary and tertiary amines. High molecular weight (HMW) and branched cationic polymers show high toxicity while the low molecular weight (LMW) and linear polymers show poor nucleic acid binding and transfection efficiency[206]. One way to overcome this issue is by using hybrid polymers, e.g. linear PEI-chitosan hybrid nanoparticles showed better transfection efficiency and improved safety profiles[206]. Another way is by cross-linking LMW polymers with bioreducible disulphide linkages. For example, thiol cross-linked LMW-PEI polyplexes conjugated with brain targeting rabies virus glycoprotein (RVG) were useful for the delivery of miR-124a[207]. These nanoparticles displayed low toxicity and brain targeting capabilities. A comprehensive list of such bio-reducible nanoparticle delivery systems and strategies are enlisted in the section:1.9.5, page: 33.

The polymeric delivery systems can destabilize the late endosomal (LE) compartment by proton-sponge effect during its acidification (pH 5 – 6)[188]. Therefore, endosomal escape of polyplex has to accompany the escape of oligonucleotides from the polymers for a functional activity. Evidence suggests that just a few molecules, of free siRNA or miRNA, in the cytoplasm could produce potent functional effects[164]. Hence, strategies that allow the intra-cellular release of oligonucleotides after internalization should be addressed more seriously to achieve highly functional delivery systems[168].

Natural and Bio-mimetic Nanoparticles: Exosomes and microvesicles are naturally secreted miRNA loaded vesicles, which are known to act as natural delivery and signalling systems for cell to cell communication[208]. These vesicles

can be charged with miRNA either by transfecting huge amount of exogenous miRNA in to the packaging cells or by directly transfecting the exosomes by electroporation or chemical methods[208,209].

Targeted Brain Delivery: Active brain targeting of delivery systems can be achieved by ligand conjugation which can improve blood brain barrier (BBB) transport and cellular uptake. Nanoparticles conjugated with transferrin[210], lactoferrin[211], peptides derived from Kunitz domain (Angiopeps[212,213]), leptin (leptin30)[214], snake neurotoxin candoxin (CDX)[215], HIV-1 TAT protein (TAT peptide)[216], cationic cell penetrating peptide $(RXRRBR)_2XB$[217] and the rabies viral glycoproteins [RVG29 – a 29 amino-acid peptide with the following sequence YTIWMPENPRPGTPCDIFTNSRGKRASNG][218] and [RDP39, a 39 amino-acid Rabies-virus derived protein with the following sequence - KSVRTWNEIIPSKGCLRVGGRCHPHVNGGGRRRRRRRRR][219] has successfully demonstrated BBB-crossing and brain-specific accumulation after intra-venous or intra-nasal administration. Polysorbate-80 coated nanoparticles have shown higher doxorubicin delivery to brain than the uncoated nanoparticles [6 µg/g vs 0.1 µg/g]. This was due to the preferential adsorption of apolipoprotein E (apoE) on the surface of these nanoparticles and the polysorbate-80's ability to inhibit P-gp drug efflux pump[220,221].

1.9.3 MicroRNA/ siRNA Delivery Systems in Clinical Trials

Most of the clinical trials with nucleic acids [siRNAs, antisense oligonucleotides and locked nucleic acids (Miravirsen)[222]] are performed without nano-carriers[223,224]. The unmodified phosphodiester form of nucleic acids can be easily degraded in the blood and body fluids if they are not associated with some kind of carrier system due to the nuclease activity. However, synthetic modified oligonucleotides [e.g. backbone modifications: phosphorothioate, morpholino; Ribose sugar modifications at 2′-OH: 2′-O-methyl, 2′-O-Fluoro; locked nucleic acids, a methylene bridge between 2′-O and 4′-C] are resistant to nuclease degradation and in some cases may have better cellular entry [e.g. phosphorothioate (PS)].

Miravirsen is the first anti-miRNA oligonucleotide in human clinical trials. It is a single stranded antagomiR targeting miR-122 which is abundantly expressed in liver and acts as an important host factor for hepatitis C viral genome stabilization and replication. Miravirsen is a locked nucleic acid modified phosphorothioate oligonucleotide delivered without any carrier system. The results from phase II clinical trials indicated that although Miravirsen was able to significantly reduce the serum miR-122 levels, there was no correlation observed with the viral load, probably due to poor uptake by liver cells (3, 5 and 7 mg/kg). Moreover, they found out that the virus developed resistance through a mutation that allows its replication independently of miR-122. Miravirsen development has been now discontinued by Santaris Pharma, Roche[222]. RG-101, the next generation GalNAc conjugated antagomiR against miR-122 is under phase II clinical trial conducted by Regulus Therapeutics (EudraCT Number: 2015-001535-21). The targeted RG-101 has shown significant reduction in the viral load with a single subcutaneous injection at 2 and 4 mg/kg of dosing[225].

The different delivery systems used for siRNA or miRNA include cyclodextrin containing polymer (ClinicalTrials.gov Identifier: NCT00689065), LODER (Local Drug EluteR) polymeric system (NCT01676259), Polyethylenimine (PEI) (NCT01435720), Lipid nanoparticles (LNPs), liposomes (NCT01808638) and GalNAc conjugates (NCT02292186)[223,224,226].

CALAA-01 is a cationic copolymer of β-cyclodextrin and a co-monomer [probably dimethyl suberimidate (βCD-DMS)][227,228]. The polyplexes are made by self-assembling with siRNA with the polymer, followed by grafting of PEG (AD-PEG) and targeting ligand (AD-PEG-Transferrin) using Adamantane-Cyclodextrin (AD-βCD) interaction[229]. The nanoparticles were administered by intravenous route and targeted towards solid tumour. This study conducted by Calando Pharma showed siRNA specific mRNA knockdown[226], however the trial was terminated in 2013 and no reasons were indicated for termination (NCT00689065)[229].

siR-LODER is a PLGA based biodegradable polymeric implant loaded with siRNA polyplexes (probably, siRNA-PEI complex with mannitol[230]) that releases the siRNA complexes in the local area for extended period of time [2 – 5 months][231]. Currently, Silenseed Ltd. is starting a Phase II clinical trial with siG12D-LODER (siRNA against mutated KRAS oncogene) in combination with gemcitabine for pancreatic cancer patients (NCT01676259).

Most of the clinical trials conducted by Alnylam (NCT01960348), Arbutus Biopharma/Tekmira (NCT02631096) and Mirna Therapeutics are based on lipid nanoparticles (LNP) formulated either with proprietary amphoteric Di-alkylated Amino Acid (DiLA^2) or SMARTICLES® technologies[232]. The patents suggest that it may contain a mixture of Palmitoyl-oleoylphosphatidylcholine (POPC), Dioleoyl-phosphatidylethanolamine (DOPE) or (DOTAP), Cholesterol or Cholesterol hemisuccinate (CHEMS) or 4-(2-Aminoethyl)-Morpholino-Cholesterol hemisuccinate (MoChol) or dimyristoylglycerol-hemisuccinate (DMG-Succ) and possibly few more components with fusogenic properties[233-236]. Dicerna Pharmaceuticals uses EnCore™ Lipid Nanoparticles (NCT02314052) or GalNAc conjugates (preclinical evaluation) for the delivery of DsiRNA (Dicer substrate short-interfering RNA). Classical siRNAs are 21 – 23 nucleotides long and are loaded directly into the RISC complex, whereas DsiRNAs are ~27 nucleotides long which requires DICER processing before RISC loading. DICER mediated RISC loading is more efficient that direct RISC loading. A detailed list of clinical trials with siRNA therapeutics is enlisted in the following review by Yin *et la*[223] and Ozcan *et al*[224].

MRX34 by Mirna Therapeutics is the only miRNA therapeutic in clinical trials and uses SMARTICLE® lipid based formulation. Phase I clinical trial (NCT01829971) evaluating maximum tolerated dose has been completed and detail reports about the outcomes are yet to be published. Two Phase II clinical trials have been planned to start by the end of 2016.

1.9.4 Crosslinked Delivery Systems

Crosslinked polymeric systems, broadly referred as nanogels[237], are versatile multi-functional drug delivery systems extensively studied in the field of nanomedicine[238]. The rationale for cross-linking is to increase drug loading and *in vivo* stability of nano-assemblies, reduce toxicity by increasing biodegradability[239] and to tailor the release of cargo in response to specific stimuli[240,241]. Various types of stimuli-responsive chemical crosslinking include pH sensitive acetal, ketal, imine, hydrazone, carboxylate esters and carbonates; photo-cleavable linkers like biscoumarin and ortho-nitrobenzyl ester; enzyme cleavable phosphoesters; concentration responsive boronate esters; bio-reducible disulphides and many more[241].

1.9.5 Bio-reducible Nucleic Acid Delivery Systems

Bio-reducible delivery systems have an advantage of preferential disassembly in the intracellular compartment compared to extra-cellular body-fluids due to the differential abundance of glutathione. For this reason, they have been widely used for the delivery of nucleic acids where intra-cellular delivery is necessary. In most cases, crosslinked nanoparticles have shown to be more effective than their non-crosslinked counterparts[242,243]. The crosslinking (CL) refers to the intermolecular bond formation. Based on this definition, bio-reducible nanoparticles can be broadly classified into pre-crosslinked [Pre], post-crosslinked [Post] and non-crosslinked [Non], **Figure 1-5**, page: 34.

Pre-crosslinking refers to the inter-molecular bond formation occurring before the mixing with the nucleic acid, while the post-crosslinking refers to the inter-molecular bond formation occurring after the mixing with nucleic acid (caged nanoparticles)[242,244]. Pre- and Post- crosslinked nanoparticles are prepared either using thiol bearing polymers [Pre-SS or Post-SS][243,245] or employing a bioreducible chemical crosslinker [Pre-XY or Post-XY][246], **Figure 1-5**. Bioreducible chemical crosslinkers have a reactive group (Y) at either end of the molecule which readily reacts with a chemical group from the polymer chain (X). For example, dimethyl-3,3′-dithiobispropionimidate (DTBP) readily reacts with primary amines from poly-L-lysine (PLL) and hence stabilizing the PLL-DNA polyplexes when it is added after the formation of the complex[247].

High molecular weight (HMW) polymers that are obtained by polymerisation of disulphide monomers [e.g. cystamine derivative][239] are typical examples of non-crosslinked bioreducible systems. These bioreducible HMW polymers effectively binding and release nucleic acid while circumventing the toxicity posed by non-biodegradable HMW polymers[248]. Other types of non-crosslinked bio-reducible nanoparticles includes those that use thiol-chemistry for the attachment of detachable ligands, siRNA, PEG or other functional groups. All these nano-complexes [pre, post or non-CL] are bioreducible, the post-crosslinking yields better stability with smaller size and uniform size distribution[244]. A comprehensive list of bio-reducible nucleic acid delivery systems are listed in Table 1-5 (Peptides and lipids, page: 35), Table 1-6 (Polymers, page: 36) and Table 1-7 (Poly-amidoamines, page: 37). The nature of crosslinking [Pre-SS, Post-SS, Pre-XY, Post-XY or Non-CL] is presented in the last column of all the table.

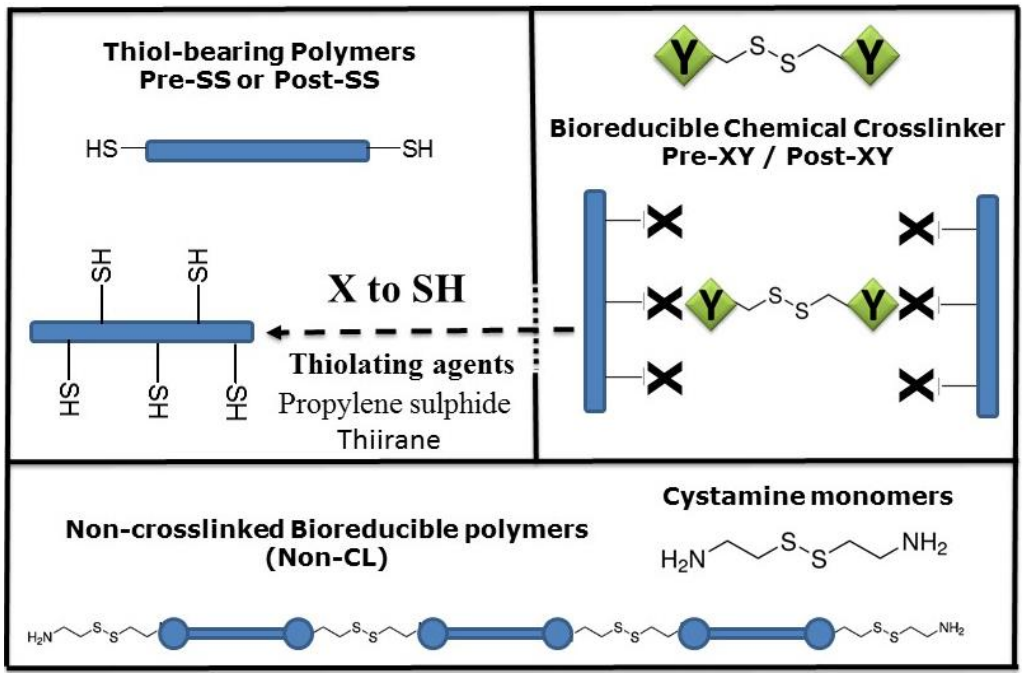

Figure 1-5: Bioreducible polymer strategies.

Thiol bearing polymers can be allowed to crosslink before [Pre-SS] or after [Post-SS] mixing with nucleic acids. For non-thiolated polymers, a chemical crosslinker can be added before [Pre-XY] or after [Post-XY] the formation of polyplex. Alternatively, those polymers can be thiolated using specific reagents. The cystamine bearing polymers do not involve in crosslinking before or after the polyplex formation [Non-CL].

Table 1-5: Bioreducible peptide and lipid-based delivery systems.

Nuc.A.	Peptide / Protein	Notes / Highlights	Type
pDNA	Poly(L-lysine)	Cross-linker: DTBP	Post-XY [247]
siRNA	PEG-*b*-(PLL - iminothiol) [244]	Monodisperse stable micelles (50 nm)	Post-SS
pDNA	Cys - Trp - Lys_{17} - Cys [242]	Chloroquine used for endosomal escape	Post-SS
pDNA	Cys - Lys_{16} - Cys [249]	Fusogenic peptide from influenza virus for escape	Pre-SS
pDNA mRNA siRNA	Cys -$H_{3/6}$ -Lys_{3}-$H_{3/6}$ -Cys	Histidine (H) residues facilitated endosomal escape	Pre-SS [243,250] / Post-SS [251]
pDNA	Multi-component Glycopeptide (+/-) PEG-peptide	Crosslinked peptides were rapidly metabolized in the liver at the same rate as the non-crosslinked peptides.	Post-SS [252]
pDNA	Polyacridine peptide -(Cys-P/S/M)-PEG_x	Penicillamine (P)/thiol (S)/ maleimide (M); PSM or SM or PS linkages increase *pharmacokinetics (PK)* of circulating NP.	Non-CL [253]
siRNA	Thiolated cationic helical polypeptides	Cross-linking resulted in size reduction.	Post-SS [254]
pDNA, siRNA	Oligoaminoethane polyplexes	PEG shielding and addition of ligand with CRC motif increased efficiency.	Post-SS [255]
Nuc.A.	Lipid Based	Notes	CL, ref.
pDNA	C_{14}-Cys-Ornithine	2 – 10 fold less efficient than Transfectam & PEI	Post-SS [256]
pDNA	Diolein liposomes encapsulating cross-linked PEI/ DNA complexes	Cross-linker: DSP or DTBP. Crosslinking of PEI reduced gene transfection.	Post-XY [257]
pDNA	DOPC/DOPE/SS14	GSH responsive transfection	Pre-SS [258]
siRNA	Multiple pH sensitive cross-linkable surfactants	Thiol oxidation faster with siRNA. Best performance = highest haemolysis (pH 5.4)	Post-SS [259]

Abbreviations: Cys (C) – Cysteine; CRC - Cys–Arginine–Cys motifs; His (H) – Histidine; Lys (K) – Lysine; Trp (W) – Tryptophan; PLL - Poly (L-lysine); DOPC - 1,2-dioleoyl-sn-glycero-3-phosphatidylcholine; DOPE - 1,2-dioleoyl-sn-glycero-3-phosphatidylethanolamine; PEG - Polyethylene glycol; DSP – Dithiobis(succinimidylpropionate); PEI – Polyethylenimine; NP – nanoparticle; DTBP – dimethyl,3,3′-dithiobispropionimidate,2HCl; SS14 - triazine-based gemini surfactant.

Table 1-6: Polymer-based bioreducible delivery systems.

Nuc.A.	Polymer	Notes	CL, ref.
pDNA	PEI[260] or PEI-$PEG_{20/30k}$[261]	Cross-linker: DSP	Post-XY [260,261]
pDNA, siRNA	LMW PEI (800 Da)	Cross-linker: DSP[246] or DTBP[246] or DTPA[262]	Pre-XY [246,262]
pDNA, siRNA	Linear PEI	Cross-linker: Lomant's reagent or di (boc)-cystine	Pre-XY [248,263]
miRNA	Branched PEI (1200 Da) – NHS – PEG – MAL – RVG	Thiolating agent: Propylene sulphide	Pre-SS [207]
pDNA	PEI (800, 1800 & 25,000 Da)	Thiolating agent: Thiirane	Pre-SS [264]
pDNA, siRNA	(SS-PEI) coated SPION (PEI-800 Da + DTBP)	Efficient nucleic acid delivery and near Infra-Red imaging	Pre-XY [265]
PNA	Shell crosslinked knedel-like (SCK) nanoparticles PAEA-*b*-PS poly(acrylamidoethylamine)-*b*-polystyrene	Polystyrene core with amine rich shell - amine partially cross-linked for stability and SS-PNA chemically conjugated onto the shell[266]	Non-CL [266]
pDNA	p(HPMA)-co-AEDP-K_{10}	Bio-reducible polymers were not able to form salt stable polyplexes.	Non-CL [267]
pDNA, siRNA	p(HPMA-DMAE-co-PDTEMA)-b-PEG-Folate	siRNA required more crosslinking for stable particle formation.	Non-CL [268,269]
pDNA	Polyaspartamide-based disulphide-containing brushed PDMAEMAs	Presence of bio-reducible brushes increased gene delivery.	Non-CL [270]
pDNA	PDMAEMA-SS-PEG-SS-PDMAEMA	Excellent colloidal stability compared to PDMAEMA.	Non-CL [271]
poly siRNA	Thiolated Glycol Chitosan	Thiol crosslinked Poly-siRNA (> 300 bp)	Post-SS [272,273]

Abbreviations: AEDP – 3-[(2-aminoethyl) dithio)] propionic acid; di(Boc) - N,N′-bis-(tert-butoxycarbonyl) ; DMAE - N,N′-dimethylaminoethanol; DSP – Dithio bis(succinimidylpropionate); DTBP – Dimethyl,3,3′-dithiobispropionimidate,2HCl; DTPA - 3′-dithiobispropanoic acid; HPMA - N-(2-Hydroxypropyl) methacrylate; Lys (K) – Lysine; NP – nanoparticle; NHS-PEG-MAL-RVG - N-hydroxysuccinimide-PEG-Maleimide-Ligand; Nuc.A. – Nucleic acid; PDMAEMA - poly(2-(dimethylamino) ethyl methacrylate); PDTEMA - N-[2-(2-pyridyldithio)] ethyl methacrylamide; PEG - Polyethylene glycol; PEI – Polyethylenimine; PNA – Peptide Nucleic Acid; SPION – Super-Paramagnetic Iron Oxide Nanoparticles. SS – dithiol crosslinking.

Table 1-7: Bioreducible linear poly(amidoamine) delivery systems.

Nuc.A.	Linear PAA	Notes	Type.
pDNA, ODNs, and siRNA	Multi-component Mono-block PAA + PEG – PAA – PEG + Nucleic acid PAA – p(MBA-Cystamine/ DMEDA)	Highly stable PEGylated nanoparticles obtained. Increase in PEG-length decreased transfection. Difference in complex formation observed between double-stranded RNA and DNA of similar lengths.	Post-SS [245,274,275]
pDNA	Hyper-branched PAA ABOL terminated p(CBA – DMEDA)	Hyper-branched PAA were more efficient than the linear PAA and active in the presence of serum.	Non-CL [276]
pDNA, ODN, siRNA [277]	p(CBA – AEP)[278] p(CBA/ HMBA-AEP)[239,279] p(CBA-Histamine/DMPA) p(CBA - ABOL)[277] p(CBA - APOL)[280] p(CBA - TEPA)[281] p(CBA - DMC)[282]	Cell membrane thiols are essential for the uptake of bio-reducible polyplexes. [279] Better transfection efficiency and lower toxicity compared to non-reducible PAA polymers	Non-CL [239,277-283]
pDNA, siRNA	p(CBA - (DAH-Arg))[284] + PEG[285]/ -SS-PEG-Paclitaxel[286] p(CBA-(DAH-Arg-His))[287] p(CBA - Guanidinylated-amino hexane)[288] p(CBA - DAH-Arg)) -SS-PAMAM[289] p(CBA - DAH-Arg)) -SS-PAMAM-PEG-cRGD[290]	Chloroquine ineffective. Histidinylated – more efficient than non-histidinylated polymer. Guanidinylated – higher cellular uptake and strong nuclear localization. PAMAM conjugation reduced the size, increased uptake and transfection.	Non-CL [284-291]
pDNA	p(CBA - BuNHAc/BuNic)	Efficient transfection and no toxicity	Non-CL [292]

Abbreviations: ABOL - 4-amino-1-butanol; AEP – 1-(2-aminoethyl) piperazine; APOL - 5-amino-1-pentanol; BuNHAc – Acetyl-NH-Butyl-NH2; BuNic – Nicotinamide - Butyl - NH2; CBA – N, N′-cystamine bisacrylamide; DAH-Arg - 1,6-diaminohexane – (Arginine) conjugate; DAH-Arg-His - 1,6-diaminohexane – (Arginine-Histidine) conjugate; DMC - N,N′-dimethyl cystamine; DMEDA - N, N′ - Dimethyl-ethylene-diamine; DMPA - 3-(dimethylamino)-1-propylamine; HMBA – N,N′-hexamethylenebisacrylamide; MBA - N, N′ - Methylene bisacrylamide; PAA – Poly (amido amines), linear; PAMAM – Poly(amido amine), hyper-branched dendrimers; TEPA – tetra-ethylene pentamine; Nuc.A. – Nucleic acid;

1.9.6 Crosslinkable Poly(amidoamines)

This thesis is about the development miRNA nanoparticle with thiol crosslinkable poly(amidoamines).

Poly(amidoamines) (PAA) are a family of linear polymers synthesized by stepwise Michael-type polyaddition of primary mono-amines ($R\text{-}NH_2$) or secondary diamines ($R_1\text{-}NH\text{-}R_2\text{-}NH\text{-}R_1$) with bisacrylamide (=CH-CO-NH-X-NH-CO-CH=)[293]. Linear PAA polymers should not be confused with polyamidoamine (PAMAM) dendrimers which have a similar linkage chemistry but a different structure and which are more commonly described in the literature. Bisacrylamides, the poly-addition agents, are regarded as an essential part of all the polymerization reactions of every PAA. A polymer made with an amine monomer and a bisacrylamide is considered as a homopolymer. Strictly by definition, if the polymer is made of two different amine monomers and a bisacrylamide then it is regarded as a copolymer[293].

The main backbone of the PAA polymers used in this work is made of methylene bisacrylamide (MBA) and two monomers, dimethyl-ethylene-diamine (DMEDA) and cysteamine (CySH), [see 1.9.7 (page: 38) for chemical structure and synthesis] and so strictly all the polymers used in this thesis are co-polymers. However, for simplicity, non-PEGylated homo-block polymer containing a single-block linear PAA segment will be referred to as HP or 'homopolymer'. PEGylated tri-block polymer (PEG-PAA-PEG) is a block co-polymer of PAA and PEG, and will be referred as CP [Copolymer].

1.9.7 Chemical Structure and Synthesis of Polymers

PAA block of HP was synthesized with three monomers, DMEDA, cystamine and MBA. Structure of monomers are presented in Figure 1-6. The reaction of these three monomers results in a cystamine cross-linked hydrogel[294], **Figure 1-7**, page: 40. Treatment with 2, 2′-dithio-dipyridine results in the formation of dithio-pyridine pendants through disulfide–disulfide exchange at the cystamine residues separating the crosslinked strands[294,295]. The final product is obtained as a filter-cake after ultra-filtration through a 10 kDa MWCO filter, **Figure 1-8**, page: 40[245,296-299].

PEGylated tri-block polymers (CP) is synthesized with DMEDA, mono-t-Boc cystamine and MBA (Figure 1-6). PEG chains are added on each end of the polymer[296]. CP2K and CP5K represents two different co-block polymers containing 1700 Da or 5000 Da PEG chains respectively. CP2K contains thiol repeating units at each edge of the central PAA block (11000 Da) (Figure 1-9) whereas CP5k contains the thiol repeating unit randomly distributed in the central PAA block (3100 Da) (**Figure 1-10**, page: 41).

Differences in thiol protecting groups: CP contains mono-Boc (t-butyloxycarbonylamino)ethyl-protected cysteamine groups (CyS-S-Boc)[293] whereas HP contains thiopyridine protected cysteamine (CyS-S-Py). These thiol-protecting groups prevent disulphide bridge formation during storage and hence increase their usability[294].

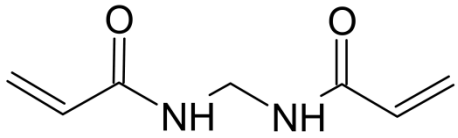

N, N′ - Methylene bisacrylamide (MBA)

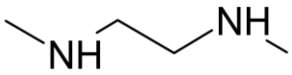

N, N′ - Dimethyl-ethylene-diamine (DMEDA)

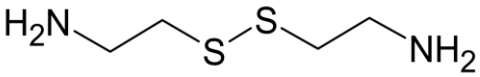

Cystamine

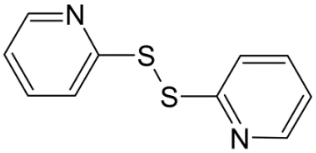

2, 2′- Dithio-dipyridine

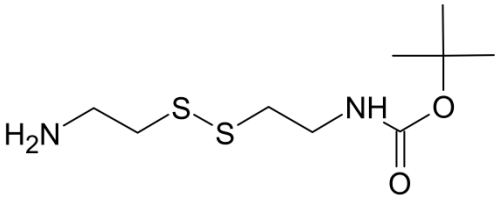

mono-(tertiary-butyloxycarbonyl) cystamine
[mono-t-Boc cystamine]

Figure 1-6: Building block of homo- and copolymers.

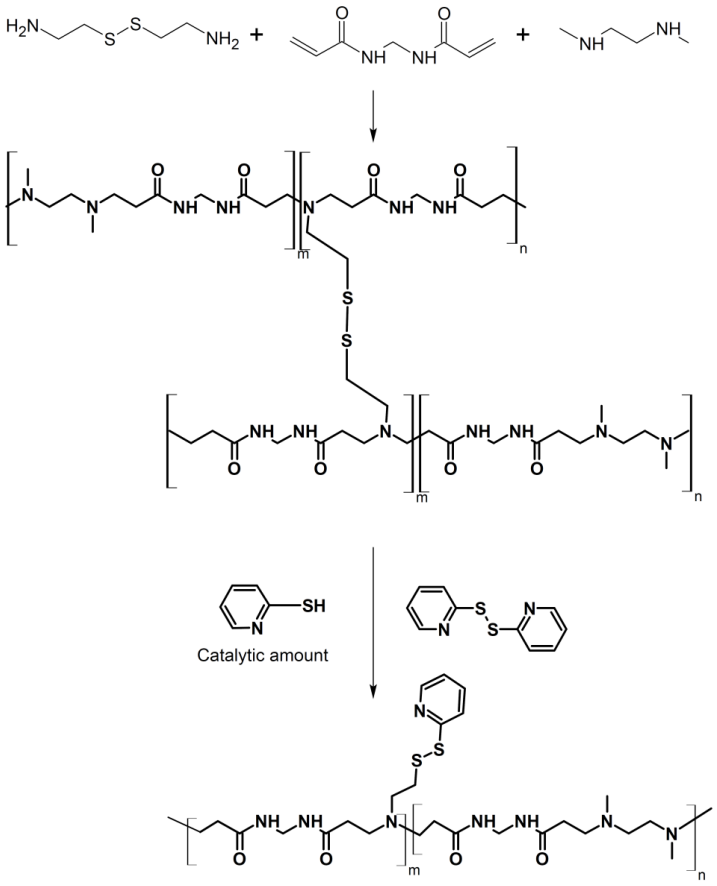

Figure 1-7: Synthesis of homopolymer (HP).

Formation of cystamine-linked PAA and thiopyridine (SPy) pendant incorporation. (Reaction scheme adapted and modified from Ranucci *et al,* DOI: 10.1002/marc.200700139[294]).

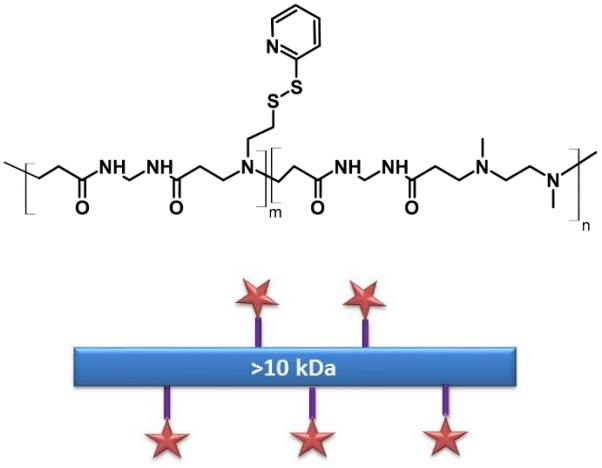

Figure 1-8: Structure and schematic representation of homopolymer (HP).

HP contains thiol (MBA-Cysteamine-SPy pendant, stick and star representation) and non-thiol (MBA-DMEDA) repeating units. Thiol repeating units are randomly distributed in the PAA structure.

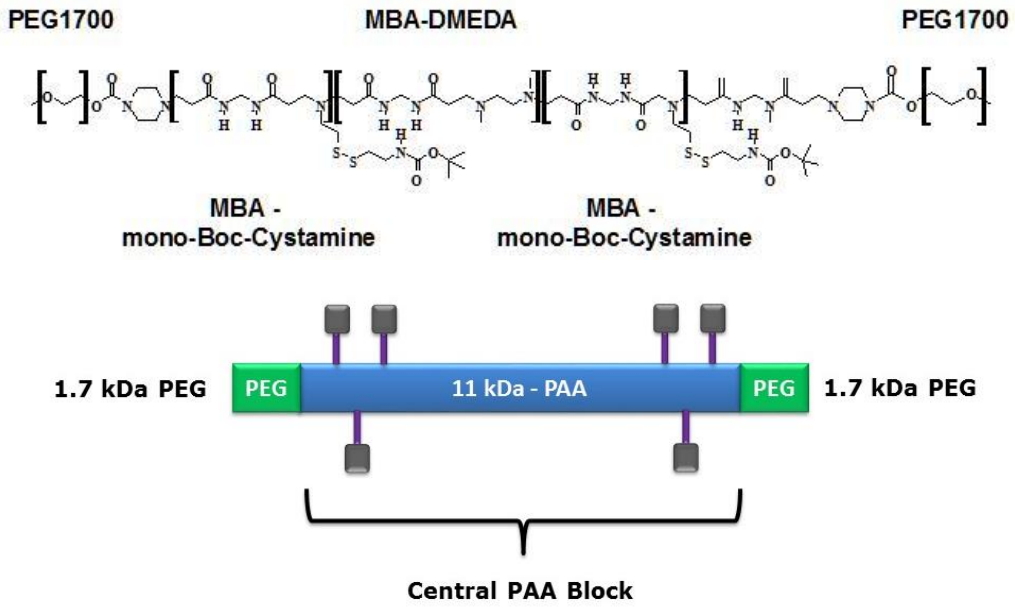

Figure 1-9: Structure and schematic representation of copolymer [CP2k].
PAA segment of CP2k contains thiol (MBA-Cystamine-Boc pendant, stick and box representation) and non-thiol (MBA-DMEDA) repeating units. The thiol repeating units are present at the edges of the PAA block. The image is scaled to represent relative length of PEG and PAA block with respect to their molecular weight. In the linear structure, the PEG chain might appear much shorter than PAA block if the length of repeating units is taken into consideration.

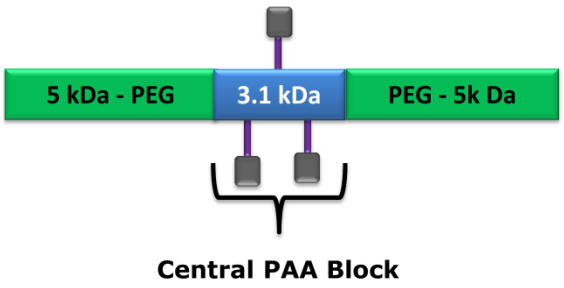

Figure 1-10: Schematic representation of copolymer [CP5k].
CP5k contains thiol (MBA-Cystamine-Boc pendant) and non-thiol (MBA-DMEDA) repeating units similar to HP and CP2k. The thiol repeating units randomly distributed through the length of the PAA block (represented in blue). The PAA block is attached to PEG_{5000} at either of its ends.

1.9.8 Polyplex formation and thiol crosslinking

Two component systems are complexes made by mixing one polymer, either PEGylated (CP) or non-PEGylated PAA (HP), with the microRNA, Figure 1-11 (Top image). Three component complexes are prepared by mixing a nucleic acid with a polymer blend solution, containing PEGylated (CP) and non-PEGylated (HP) polyamidoamine polymers in a required HP:CP (mol/mol) RU ratio, Figure 1-11 (Bottom image). The negatively charged miRNA self-assembles with the positively charged polymers (HP and CP), while the free thiols are expected to form disulphide bridges by crosslinking with adjacent thiols or by reacting with HP that contains dithiopyridine pendants. The reaction between a free thiol and a dithiopyridine results in the formation of a disulphide bond while releasing a thiopyridine (SPy) group. This disulphide crosslinking stabilizes the polymer-miRNA nano-complex. Homo-block polymer (HP) refers to the non-PEGylated polyamidoamine (PAA) and co-block polymer (CP) refers to the PEGylated polyamidoamine (PEG-PAA-PEG). The reduced form of the polymer is represented by "(R)".

Three-component polyplexes have an advantage over two-component systems. It allows the flexibility of using different ratios of polymers hence controlling the amount of PEG or thiol crosslinking in the nanoparticles. This also allows integrating different types and forms of nucleic acids hence expanding its usability in multiple applications ranging from eco-friendly molecular water-tracers to nucleic acid delivery systems for medical applications[245].

Advantages of thiol crosslinking: Danish *et al.,* showed the serum stability of the siRNA loaded in the crosslinked polyplexes were higher compared to non-crosslinked polyplexes (HP:CP PAA RU ratio 1:1, PAA:RNA RU ratio 2.5:1 mol/mol)[275]. It was demonstrated that in the presence of reducing agents like glutathione or dithiothreitol (5 mM), the crosslinked polyplexes were able to partially release the siRNA (~ 30 – 50%)[275]. When the crosslinked polyplexes were treated in combination with low concentration of heparin (Heparin to siRNA, 0.25: 1 w/w) and one of the reducing agents (5 mM), a complete release was observed[275]. In another experiments, it was shown that the amount of heparin required for complete release of siRNA from crosslinked polyplexes

was 2:1 w/w ratio[275]. At low heparin concentration (0.25:1), the amount of siRNA released was very low[275]. These results indicated that the thiol-crosslinked PAA-siRNA nanoparticles can release the cargo siRNA under intracellular reducing environments[275]. Thiol-crosslinking also improved the stability of the polyplexes under physiological salt concentrations (150 mM NaCl) and above (until 750 mM NaCl for the HP:CP RU ratio 1:1, PAA to RNA RU ratio 2.5:1)[275]. Similarly, Aljaeid *et al* demonstrated these properties for crosslinked PAA-DNA polyplexes[274]. He also showed that crosslinked polyplexes strongly bind to DNA compared to non-crosslinked polyplexes by ethidium-bromide exclusion assay[274].

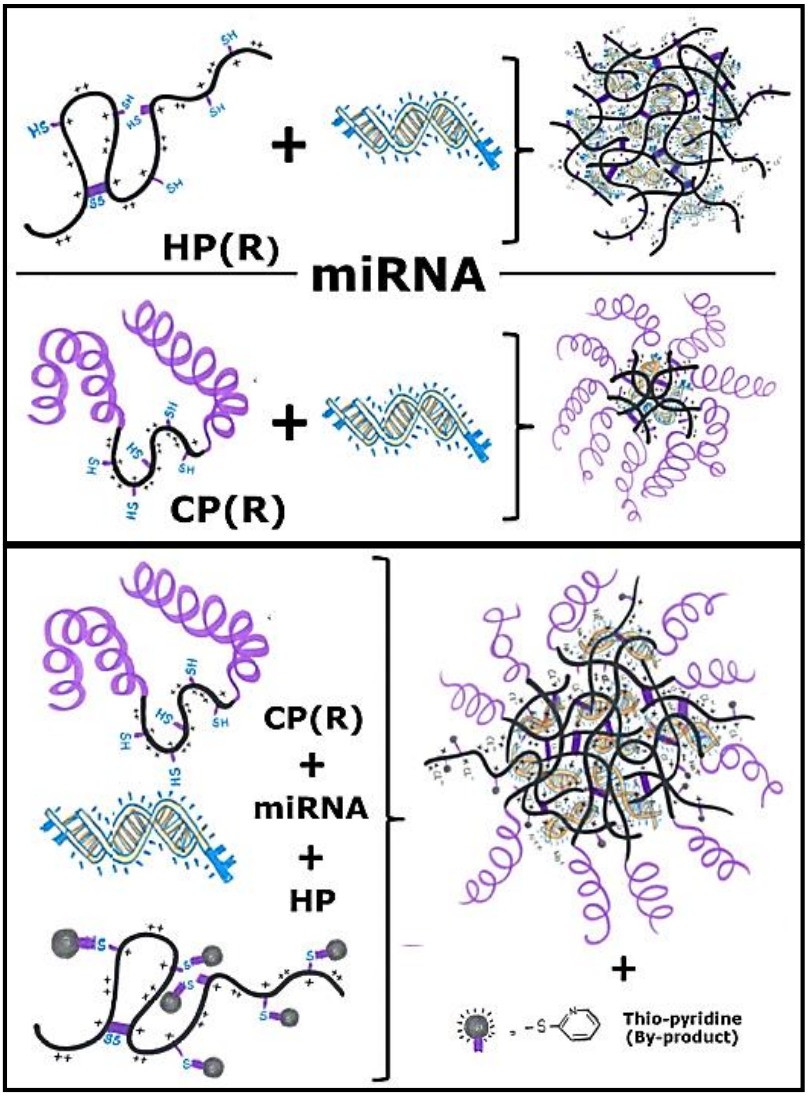

Figure 1-11: Schematics of two- and three- component polyplexes.

Top image: Two component miRNA polyplexes [HP(R)-miRNA or CP(R)-miRNA].

Bottom image: Three-component polyplexes [HP – CP(R) – miRNA]. The disulphide crosslinking can happen via thiol-thiol or thiol-dithiopyridine interactions.

1.10 Aims and objectives

Since the discovery of RNA interference (RNAi), siRNA and other RNAi molecules have attracted the central attention as a safe alternative for gene therapy. microRNAs are emerging as a novel therapeutic molecule for cancer therapy due to the ability to target multiple genes. Lack of an efficient and safe non-viral delivery systems has hindered the progress of RNAi into clinics. Glioblastoma are an aggressive form of brain tumours with a median survival of 15 months even with the currently available best treatment options[6]. Treatment of glioblastoma with tumour-suppressor microRNAs (miRNA replacement therapy) has shown promising results either as a single agent[89] or in combination with conventional chemo and radio therapy[103,105,107,300-302]. In a clinical setting, the treatment of glioblastoma begins with surgery to remove the bulk of the tumour without affecting the functions of the brain. The residual tumour is treated with chemo- and radio-therapy. The residual tumour and the spread of tumour cells (cancer-stem like cells) during surgery are two main reasons for the tumour recurrence and treatment failure[303]. The microRNA replacement therapy can be performed during and after primary tumour resection, i.e. the tumour-suppressor miRNA nanoparticles delivered by one of the many available options of local delivery [e.g. the nanoparticles can be stereotaxically injected for in-operable tumours[304] or injected around the tumour resection site[305] or sprayed in the surgical cavity during surgery]. The sprayed nanoparticles could temporarily impair the dislodged cancer cells to implant and grow, while the injection of nanoparticles in the surgical margin can inhibit the growth of the residual tumour, make it less aggressive and sensitize against the following chemo- and radiotherapy. Hence, this strategy may reduce the rate of tumour recurrence. As the injected miRNA would be active only for short amount of time (few days to weeks depending on the delivery system), other loco-regional delivery options might be needed to regularly deliver miRNA nanoparticles to keep the micro-tumour from relapsing. Due to the presence of blood-brain barrier, the loco-regional route of nanoparticle administration might be more effective than systemic delivery. Less invasive procedures like implantation of catheters in the surgical cavity or ventricles (nanoparticle delivery in the cerebrospinal fluid) might enable long-term delivery of nanoparticles[9-12].

For such a loco-regional application, the ideal properties of the miRNA-nanoparticles for efficient delivery would require the following properties, 1. Safe and with low toxicity to the brain (non-toxic polymers and nanoparticle components); 2. Stable, non-aggregating nanoparticles in the physiological media (cerebrospinal and extracellular fluid) (Thiol crosslinking and PEG); 3. Less interaction with the environment to enable deeper tissue penetration (PEG); 4. Small size (20 – 200 nm) for fast and extended tissue distribution (Polymer to miRNA stoichiometry, preparation method); 5. High and selective uptake of nanoparticles by tumour cells and intracellular release of miRNA (Targeting Ligand). Hence, the aim is of this project is to develop miRNA nanoparticles that are suitable for loco-regional miRNA delivery in glioblastoma. PEGylated (CP) and non-PEGylated (HP) linear chain cationic polyamidoamine (PAA) polymers that have thiol-crosslinkable groups were used for the formulation of the PAA-miRNA nanoparticles.

Chapter 3: Optimization of miRNA-polymer interaction; Physico-chemical and biological evaluation of poly(amidoamine)-microRNA polyplexes prepared by "Salt in Polymer" method

This chapter was aimed at the development and screening of efficient PAA-miRNA-nanoparticles. Primary screening would be based on physico-chemical characterization while the secondary screening would be based on the *in vitro* performance. The three major selection criteria for the primary physico-chemical selection of polyplexes were defined as, (a) high miRNA incorporation (≥ 90% of miRNA complexation efficiency); (b) No or minimal free polymer in the miRNA-polyplexes to avoid excess free-polymer mediated cytotoxicity; and (c) Size of the polyplexes. Percentage miRNA-polymer complexation and presence of free polymer would be tested by agarose gel electrophoresis, while the size of the polyplexes would be determined by dynamic light scattering (DLS). The PAA-miRNA complexes satisfying the primary selection criteria would be tested for *in vitro* uptake and transfection efficiency on a glioblastoma cell line without or with a luciferase gene, U87MG and U87MG-Luc respectively.

Chapter 4: Improvements in the polymer purification, stability and biological activity of poly(amidoamine)-microRNA nanoparticles - "Salt-free complexation" method

This chapter was aimed at the development of a fast copolymer purification procedure to improve and maximise the free-thiol yield; To study the crosslinking behaviour of polymers under different salt and pH conditions for the deeper understanding of the crosslinking process; To select the nanoparticles for *in vitro* testing based on stability of the nanoparticles under physiological salt concentration; and to study the *in vitro* uptake and gene silencing behaviour of stable PAA-miRNA nanoparticle formulation.

Chapter 5: Formulation of stable crosslinked nanoparticles by "Salt in RNA" method and Development of *in-situ* ligand grafting technique

The first part of the final chapter was aimed at the improvement in the formulation process to produce stable PAA-miRNA nanoparticles by introducing optimal amount of salt in the microRNA solution; The second part of the chapter was aimed at the development of ligand conjugated nanoparticle preparation to improve cellular uptake and functional activity.

Additional Chapter (Appendix): Development of Normalization Technique for Live Cell Luciferase Assay with High Throughput Compatibility

Luciferase assay serves as a valuable tool for the evaluation of transfection efficiency of siRNA/ miRNA loaded nanoparticles. The reduction in luciferase signal after nanoparticle treatment indicates either successful RNAi delivery and associated luciferase knockdown and/or cytotoxicity of the nanoparticles. Meaning ful results can be obtained by data normalization. The most widely used data normalization technique for single luciferase expression system is based on protein quantification (ALU "arbitrary luminescence unit"/ mg of protein). The major limitation of protein quantification is the difficulty of processing multiple samples. As this work would involve testing of several different formulations, this additional chapter was aimed at the development of a simple and sensitive live-cell luciferase assay with high-throughput capability for reporting luciferase expression and cytotoxicity in the same sample.

Chapter – II

General Materials and Methods

2 General Materials and Methods

2.1 Materials

All the materials used are of high purity grade and most of the chemicals and reagents were purchased from Sigma until and unless specified. The water used for the experiments was of very high-purity unless and otherwise specified. The water was produced on-site from a reverse osmosis/deionization process using ELGA PureLab [conductivity < 10 $Mohm^{-1}$, University of Nottingham] or Milli-Q [conductivity < 18 $Mohm^{-1}$, University of Angers] water systems.

Double second generation stranded mirVana^{TM} microRNA mimics were purchased from Life Technologies which had proprietary optimized chemical modifications to suppress the passenger strand activity better than their first generation mimics. The guide strand of the therapeutic human miRNAs used in this study includes miR-128 (-3p), miR-145 (-5p), miR-302a (-3p), miR-367 (-3p) and a negative control mimic, mirVana miRNA mimic Neg#1, see **Table 2-1** (page: 48) for the sequence information. The fluorescent miRNA-mimics were purchased from Dharmacon or Sigma. The details of the miRNA-mimics and siRNA used in this study are listed in the following table, **Table 2-1**.

The polyamidoamine polymers were designed and synthesised for this nucleic acid delivery work by our collaborators Prof Paolo Ferruti and Prof Elisabetta Ranucci of the Department of Organic and Industrial Chemistry, University of Milan, Italy. A non-PEGylated mono-block PAA with molecular weight greater than 10 kDa was used in this study and will be referred as homopolymer or HP, (**Figure 1-8**, page: 40). Two different PEGylated tri-block PAAs were referred as copolymers (CP) and indicated as CP2k or CP5k based on the length of the PEG chains on each polymer. CP2k has cystamine repeating units distributed at the either ends of PAA block as $PEG_{1.7kDa}$–$Cystamine_{2.4kDa}$-PAA_{11kDa}–$Cystamine_{2.4kDa}$–$PEG_{1.7kDa}$ (**Figure 1-9**, page: 41); while the CP5k has a randomly distributed cystamine in the short PAA block as PEG_{5kDa} –$PAA_{3.1kDa}$–PEG_{5kDa} (**Figure 1-10**, page: 41). The reduced form of HP, CP2k, CP5k were denoted as HP(R), CP2k(R), CP5k(R) respectively. The polymer data sheet and values essential for the calculations are provided in the, **Table 2-2**, page:49.

Table 2-1: miRNA mimics and siRNA sequence information.

Name of the miRNA/ siRNA miRBase ID (LifeTech Product ID) Sequence (5′ → 3′) (Guide Strand / *Passenger Strand*) Molar Mass (g/mol) - Nucleotides	**Pre-miR stem-loop structure** * (Actual miRNA mimics sequence) * Source : www.mirbase.org
hsa-miR-128-3p MIMAT0000424 (MC11746) UCACAGUGAACCGGUCUCUUU *CGGGGCCGUAGCACUGUCUGAGA* MW: 14469 g/mol – 44 Nt	
hsa-miR-145-5p MIMAT0000437 (MC11480) GUCCAGUUUUCCCAGGAAUCCCU *GGAUUCCUGGAAAUACUGUUCU* MW: 14643 g/mol – 45 Nt	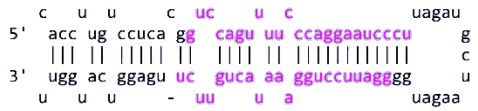
hsa-miR-302a-3p MIMAT0000684 (MC10936) UAAGUGCUUCCAUGUUUUGGUGA *ACUUAAACGUGGAUGUACUUGCU* MW: 15055 g/mol – 46 Nt	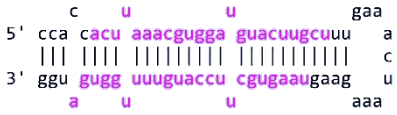
hsa-miR-367-3p MIMAT0000719 (MC10832) AAUUGCACUUUAGCAAUGGUGA *ACUGUUGCUAAUAUGCAACUCU* MW: 14393 g/mol – 44 Nt	
mirVana miRNA mimic Neg#1 Sequence information not available.	No known gene target on the whole human genome.
Fluorescent miRNA Control cel-miR-67-Dy547 (Dharmacon: CP-004500-01) (5′-DyLight547 conjugated miRNA) cel-miR-67-Cy3 (Sigma - Custom design) (3′-Cyanine3 conjugated miRNA, miR-Cy3) UCACAACCUCCUAGAAAGAGUAGA-Cy3 *CGCUCAUUCUGCCGGUUGUUAUG* MW: 15950 g/mol – 47 Nt	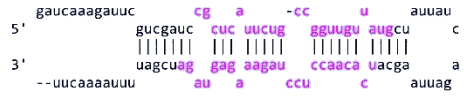
Firefly Luciferase siRNA [£] (Sigma – Custom design siRNA) CCGCAAGAUCCGCGAGAUU[dT][dT] *AAUCUCGCGGAUCUUGCGG[dT][dT]* MW: 12722 g/mol – 42 Nt	Completly complemetary dsRNA with two nucleotide overhangs
MISSION® siRNA Universal Negative Control #1 (Sigma: SIC001)	Sequence information not available.

[£] - siRNA sequence was kindly provided by *Prof. Anna Grabowska*, Faculty of Medicine & Health Sciences, University of Nottingham, UK.

Table 2-2: Polymer data sheet and derived values.

The table represents the essential numbers required for theoretical calculations. thiol inactive/ thiol protected polymers and active-thiol bearing reduced polymers. "(R)" represents the reduced form of the polymer that is normally obtained after reduction with DTT (Dithiothreitol).

Polymer	Percentage of PAA in the polymer [PAA/(PAA+2.PEG)]x100 mass %	MW of PAA non-thiol RU, (DMEDA-MBA) g/mol	Percentage of disulphide RU or thiol RU in PAA (SS or SH RU) [Cys block/(Cys+PAA)]x100 mol %	MW of PAA SS or SH RU, g/mol	Average molecular weight of PAA RU, g/mol
HP	100.00 %	315	20.80 %	377	326
HP (R)	100.00 %		15.72 %	268	304
CP2K	83.20 %		15.79 %	443	330
CP2K (R)	82.28 %		11.30 %	268	309
CP5k	23.66 %		35.50 %	443	351
CP5k (R)	21.04 %		31.76 %	268	295

2.2 Ellman's Assay and Assay Validation

Quantitative Ellman's Assay: Ellman's assay was used to quantify the amount of free thiol in the reduced polymer. Ellman's reagent, DTNB [3, 3'-dithio-bis(6-nitrobenzoic acid)], which reacts with free sulfhydryl groups (-SH) yielding a coloured compound (2-nitro-5-thiobenzoic acid) which can be measured at 412 nm. This reaction was reported to be sensitive to pH (optimal at pH 8.0), steric hindrance and electrostatic effect[306]. The following quantitative procedure was adapted from the Thermo Scientific Ellman's reagent manual[306]. Ellman's reagent was prepared by dissolving DTNB (40 mg) in reaction buffer [10 mL, 0.1 M phosphate buffer with 1 mM EDTA, pH 8.0]. Freshly prepared L-Cysteine or N-Acetyl cysteine stock solution (5 mM, in water) was diluted in water to obtain standard solutions of different concentrations [0 to 1000 µM]. Polymer solution (2 mg/mL) was prepared in acidified water [pH 4.0]. The polymer or the standard solution [100 µL] was added to the Ellman's reagent [20µL], followed by the addition of reaction buffer [1000 µL]. This assay mixture [200 µL] was transferred to a microplate reader and the absorbance was measured at 412 nm. The amount of the thiol in the polymer was determined from the cysteine standard curve.

Qualitative Ellman's Assay: Alternatively, a quick qualitative Ellman's assay could be performed by mixing polymer solution [100 µL] with Ellman's reagent [20 µL]. Instant colour change from pale to bright yellow indicates the presence of free thiol in the polymer solution. This technique was useful when it was necessary to know the presence or absence of free thiol, but the actual concentration of active thiols was not required [e.g. as a quality control measure after thiol reduction and purification, see page no.:54, 55, 56].

2.2.1 Validation of Ellman's Assay

The efficiency of the Ellman's assay to accurately identify the number of thiol groups in a test sample is dependent on the many factors, like the accessibility of free thiols, pH, temperature, incubation time, concentration of sample and Ellman's reagent. It has been reported that using sub-optimal concentrations (10 µM) DTNB, even when present in excess will result in under-estimation of thiol.

Hence, the concentration of Ellman's reagent we use is optimal. The polymer solution (CP2K-R) was incubated with different concentrations [1 mL, 0.2 – 10 mM] of the DTNB for 30 minutes at room temperature. The absorbance was recorded at 412 nm.

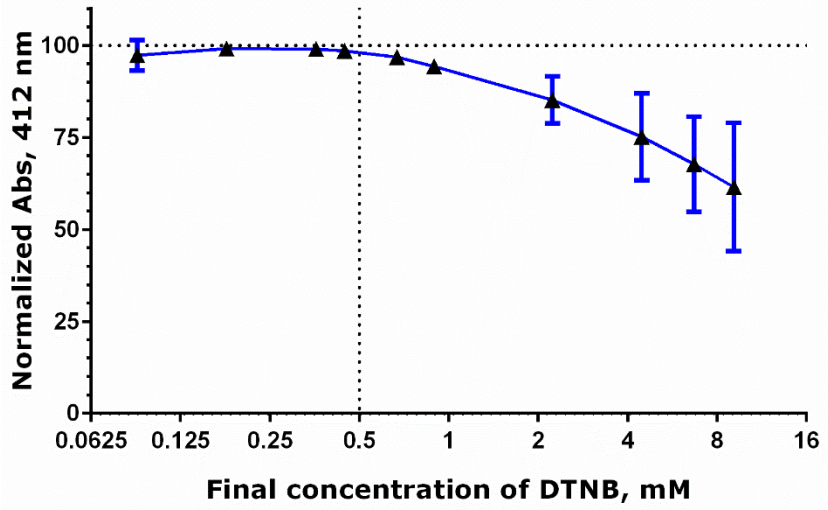

Figure 2-1: Validation of DTNB concentration.

Higher concentrations of the DTNB (< 2 mM) resulted in very high backgrounds and hence reduced the sensitivity of the assay procedure. The recommended concentration of DTNB by the Thermo-Scientific protocol is 0.179 mM and the optimal concentration observed was between 0.09 – 0.5 mM. Hence the concentration from Thermo-Scientific protocol was found to be suitable for thiol determination on PAA polymers.

2.3 Polymer Reduction and Purification

2.3.1 Polymer Dissolution

In general, the PAA polymers are hygroscopic. It is normally stored at -20˚ C. To minimise absorption of moisture, the cold polymer was equilibrated to room temperature before the lid was opened to use the polymer.

The pH of water was adjusted to pH 4.0 and deoxygenated by passing nitrogen gas for 30 minutes under magnetic stirring. This acidified water (pH 4.0 or 0.1 mM HCl) was used for all the following steps. The 200 mg of polymer was dissolved in 20 mL of water to obtain a 10 mg/mL polymer solution. The pH was adjusted to pH 7.4 which was indicated as a favourable condition for the DTT to remove the mono-BOC protecting group. The polymer solution was transferred to a round-bottom flask with a rubber stopper or a glass vial sealed

with parafilm. The polymer solution was deoxygenated by passing nitrogen gas for 10 minutes.

2.3.2 Polymer Reduction with DTT

The optimal conditions for cleaving the di-sulphide bond in the presence of a reducing agent like DTT are, pH 7 – 9, temperature: 25˚ C - 37˚ C, duration: 10 – 30 minutes[307]. DTT was dissolved in deoxygenated water, pH 7.4 [1.5 to 5 molar equivalents of polymer thiols]. The formula for calculating required amounts of DTT is given in the next section (2.3.3). Freshly prepared DTT solution was added to the polymer solution prepared in the previous step. The mixture was constantly stirred for 1 hour in dark, under nitrogen atmosphere. After an hour, the pH of the reaction mixture was set to pH 3.5 to 4.0 by adding appropriate amounts of HCl [2 M].

2.3.3 Calculation of Amount of DTT Required

The amount of DTT is usually 1.5 to 5 molar equivalents of disulphide repeating units present in the polymer. The disulphide repeating units include mono-BOC-cysteamine as in the case of copolymers [CP2k or CP5k] or dithio-pyridine in the case of homopolymer [HP]. The general formula to calculate the amount of DTT is given by,

Amount of DTT required (g) = Moles of disulphide RU in the polymer (mol) X Required molar equivalents X Molecular weight of DTT (g/mol)

where,

Molecular weight of DTT = 154.25 g/mol

The value for "molar equivalents" can be chosen as required (1.5 to 10).

Moles of disulphide repeating units in the polymer can be estimated by the following equation,

$$\textbf{Disulphide Repeating Units in the polymer}, [(\mathbf{S-S})\ \mathbf{RU}]\ (\mathbf{mol}) = \frac{\textbf{Amount of polymer (g)} \times \left(\frac{\textbf{Percentage of PAA}}{\mathbf{100}}\right) \times \left(\frac{\textbf{Percentage of disulphide RU}}{\mathbf{100}}\right)}{\boldsymbol{MW\ of\ PAA\ disulphide\ RU}\ \textbf{before reduction}\ \left(\frac{\mathbf{g}}{\mathbf{mol}}\right)}$$

The specific values for each polymer was either supplied with the polymer data sheet or derived from the available information, **Table 2-2** (page: 49).

Table 2-3: Calculated amount of DTT for polymer reduction.
The table represents mass of DTT required for reduction of 100 mg of polymer [DTT/ Polymer disulphide RU molar ratio 1:1]. DTT was used in excess [1.5 to 10 molar equivalent of polymer disulphide RU] for the polymer reduction.

Polymer	Mass of DTT, (One molar equivalent of the polymer thiol RU present in 100 mg of polymer) (mg)
HP	8.5
CP2k	4.6
CP5k	3.0

2.3.4 Polymer Purification by Ultrafiltration

2.3.4.1 Priming and Regeneration of Membrane Filter

The membrane filter (PLCC-07610, 5k low-bind 76mm Amicon filters) was initially removed from the protective envelope. To remove sodium azide and glycerine coating, the membrane was soaked in water with its glossy side facing downwards for an hour by changing the water every 20 minutes. Then the membrane was soaked in NaCl solution [5 wt.%, 30 minutes] to remove any UV-absorbing material, followed by rinsing in water [10 minutes]. Finally, the membrane was immersed in water until needed to avoid drying of the membrane surface.

Membrane Regeneration: After use, the membrane was regenerated by rinsing with water [1 minute], NaOH [100 mM, 30 minutes] and water [10 minutes]. For long term storage, the membrane was immersed in ethanol [10 vol.%] and stored at 4˚ C with the glossy side facing towards the solution.

2.3.4.2 Assembly of the Ultrafiltration Unit

The components were arranged in a sequence as shown in the **Figure 2-3** (A), page: 55. Briefly, the wetted-porous support was placed on the base piece followed by placing the primed filter membrane with its glossy side facing up followed by the rubber gasket, sample cylinder, another rubber gasket, magnetic stirrer fitted top-piece. Finally, the whole setup was locked, filled with deoxygenated water and pressurized to 4 bar using a compressed nitrogen source.

2.3.4.3 Filtration cycles

The nitrogen cylinder was turned-off and the filtration unit was slowly de-pressurized by gently turning the head of the pressure release value. Once the pressure was released completely, the sample valve was removed and the DTT + Polymer reaction mixture obtained in section 2.3.2 was introduced into the filtration unit filled with deoxygenated water. The water level was adjusted to ~ 250 mL and the system was pressurized to 4 bar to start the ultra-filtration process. When the sample level reached about 10 mL (2 – 3 hours), the filtration cycle was repeated 3 times by adding 250 mL of water for each cycle as illustrated in Figure 2-2(C), page: 54. The final product was collected in 10 mL aliquots in pre-weighed glass scintillation vials; checked for thiol activity by qualitative Ellman's assay (section: 2.2, page: 50); set to pH 4.0; snap frozen in liquid nitrogen and lyophilized for 48 hours[275].

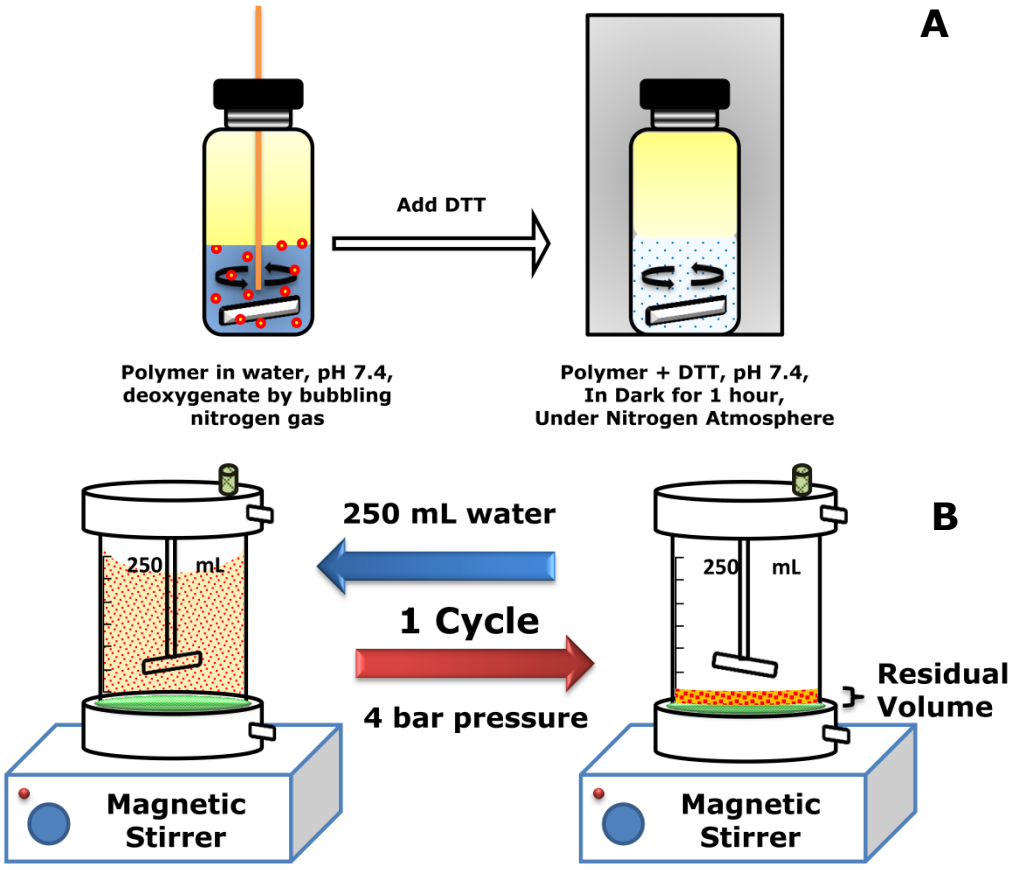

Figure 2-2: Schematic representation of polymer activation and purification.
(A) Deoxygenation and DTT treatment for polymer reduction. Figure (B) represents a cycle in ultrafiltration step for the purification of activated polymer from DTT and other by-products.

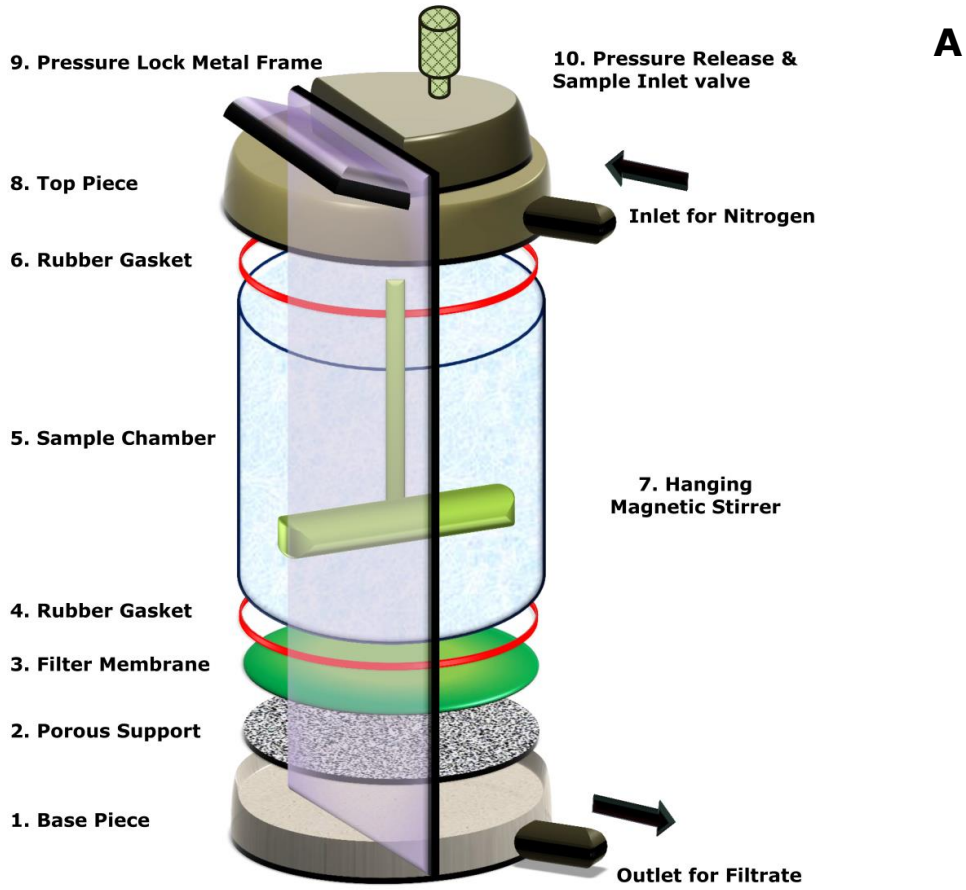

Figure 2-3: Assembly of ultra-filtration unit.

(A) Sequential assembly of Amicon ultra-filtration unit is shown. The numbers in front of each piece represents the assembling sequence.

2.3.5 Polymer Purification by Dialysis

The polymer + DTT reaction mixture solution was transferred into a sufficient length dialysis membrane, (Spectra/Por Dialysis membrane, MWCO: 6000-8000 Da). The edges were sealed and the dialysis was performed under dark against 5L acidified deoxygenated ultra-pure water, pH 4.0. The water was replaced every 3 - 5 hours, at least for 6 cycles. Finally, the dialysed polymer solution was collected in a glass scintillation vial. The polymer solution was set to pH 4.0 and filtered using 0.22 µm or 0.45 µm syringe filter. 5 mL aliquots were made in a 20 mL pre-weighed clean scintillation vials. Qualitative Ellman's assay was performed as described in section 2.2, page: 50. The vials were sealed with parafilm and pores were made with a sharp needle. The samples were then snap-frozen in liquid nitrogen and lyophilized until dried products are obtained.

2.3.6 Polymer Purification by PD-10 column

The PD-10 column was prepared by gravity method, as recommended. To prepare the column, the storage buffer was flushed out by passing ultrapure water [25 mL, column void volume ≈ 2.5 mL]. Then the column was equilibrated with elution buffer [25 mL, 0.1 mM HCl]. The reduced polymer solution with DTT [2.5 mL, pH 4.0 from section 2.3.2, page:52] was loaded on to the column. The flow-through was discarded. The reduced polymer was eluted from the desalting column by the addition of elution buffer [3.5 mL]. A pre-weighed glass scintillation vial (20 mL) was used to collect the final product (3.5 mL). A fraction of the eluted polymer solution [100 µL] was mixed with the Ellman's reagent [20 µL]. Immediate colour change to bright yellow indicated that the collected product has free thiols. The sample was snap frozen in liquid nitrogen and lyophilized for at least for 18 hours. The PD-10 column was regenerated by passing Milli-Q water [30 mL] or by re-suspending the column beads in water, NaOH (0.2 M), NaCl (500 mM) and Milli-Q water. For storage, the column was equilibrated with ethanol [20 vol.%, 15 mL] and stored at room temperature until next use. Each column was reused many times.

2.3.7 Lyophilisation

The freeze drying was carried out for 48 hours using VirTis® Sentry 2.0 SP Scientific Freeze dryer in Nottingham. Lyophilization was performed for 20 hours using STERIS LyoVac GT2 lyophilizer in Angers. The lyophilisation programme used in Angers includes several steps of sample drying by gradual regulation of sample-stage temperature,

-40º C to -40º C – 1 hour - Sample stabilization
-40º C to +15º C – 2 hours – Primary desiccation (Stage I)
+15º C to +15º C – 5 hours – Primary desiccation (Stage II)
+15º C to +25º C – 0.5 hour – Secondary desiccation (Stage I)
+25º C to +25º C – 10 hours – Secondary desiccation (Stage II)

2.3.8 Yield Calculation

Following polymer reduction with DTT and purification with one of the methods described above, the yield of the polymer can be calculated on the basis of mass recovery and thiol recovery.

$$\textbf{Percentage thiol recovery} = \left(\frac{\textbf{Actual moles of thiol obtained from Ellman's Assay (mol)}}{\textbf{Theoretical moles of thiol repeating units from the polymer (mol)}}\right) \textbf{X 100}$$

The moles of disulphide repeating units in the polymer can be obtained by,

$$\textbf{Disulphide Repeating Units in the polymer, [(SH) RU] (mol)} = \frac{\textbf{Amount of polymer (g) x } \left(\frac{\textbf{Percentage of PAA}}{\textbf{100}}\right) \textbf{ x} \left(\frac{\textbf{Percentage of thiol RU}}{\textbf{100}}\right)}{\textit{MW of PAA Thiol RU} \textbf{ after reduction } \left(\frac{\textbf{g}}{\textbf{mol}}\right)}$$

The values required for these calculations are supplied in the polymer data sheet, **Table 2-2** (page:49).

Percentage Mass Recovery

$$\textbf{Yield by mass, (\%)} = \frac{\textbf{Final amount of polymer recovered}}{\textbf{Theoretical yield of polymer}} \textbf{x 100}$$

where,

Theoretical Yield of the Polymer

= Initial mass of polymer (g) – Mass of leaving group (g)

where,

Mass of leaving group (g)

= Moles of disulphide repeating units in the polymer (mol)

x MW of leaving group (g/mol)

where,

MW of leaving group,

- mono-Boc (t-butoxycarbonylamino) ethyl mercaptan, ($C_7NO_2H_{14}S$-) = 176 g/mol
- 2-thio-pyridine (C_5NH_4S-) = 110 g/mol

2.4 Preparation of miRNA-polyplexes

miRNA complexes are prepared by mixing equal volumes of polymer and microRNA solutions. Two component systems are complexes made by mixing one polymer, either PEGylated or Non-PEGylated PAA, with the microRNA. microRNAs are an essential part of the polyplexes, hence counted as one component. Two component systems contain only one polymer in the polymer solution, whereas three component systems contain a mixture of two polymers. Here we explain the formulas involved in the calculation of required amount of polymer for mixing with microRNA solution.

2.4.1 Calculation of moles of RNA Repeating Units (Nt)

As the amount of RNA is usually known, we start our calculations by finding the moles of RNA repeating units (RNA RU or Nt, nucleotides). The repeating units of RNA are RNA nucleotides. microRNAs are 21 – 23 nucleotide double stranded RNAs. A 23-nucleotide long ds-miRNA would contain 46 nucleotides (Nt). For this condition, the moles of RNA RU can be obtained simply by multiplying the moles of RNA with 46. The moles of RNA are readily available when the molar concentration (M) of miRNA solution is known, where,

Moles of RNA (mol) = Molar concentration, (mol/L) X Volume (L)

$$\textbf{Moles of RNA nucleotides, Nt (mol)} = \textbf{Moles of RNA}_{(mol)} \textbf{X Total number of nucleotides per RNA molecule}$$

Example: Calculation of moles of RNA RU in a miRNA solution [10 µL, 20 µM].

$$\text{Moles of miRNA in 10 µL} = 20 \left(\frac{\mu mol}{L}\right) \text{ x } (10 \text{ x} 10^{-6} \text{ L}) = 200 \text{ pmol}$$

$$\text{Moles of miRNA nucleotides, Nt} = 200 \text{ pmol x } 46 \text{ Nt} = 9200 \text{ pmol}$$

Alternatively, moles of RNA RU can be obtained from its mass,

$$\textbf{Moles of RNA nucleotides, Nt} = \left(\frac{\textbf{Mass of RNA}_{(g)}}{\textbf{Avg. MW of RNA Nucleotide}_{(g/mol)}}\right)$$

where,

Average molecular weight of RNA nucleotide was used as 327 g/mol.

2.4.2 Two Component Complexes

The complexes were prepared according to the polymer RU to RNA nucleotide (RU/Nt) (mol/mol) ratio. For two component systems, the required amount of polymer for a given RU/Nt ratio and known amount of RNA can be calculated as follows,

Mass of HP required (g)

$$= \left(\textbf{Moles of RNA Nt}_{(mol)}\right) \textbf{X} \left(\frac{\textbf{RU}}{\textbf{Nt}} ratio\right) \textbf{X} \left(\textbf{Avg. MW of HP RU}_{(g/mol)}\right)$$

or

Mass of CP required (g)

$$= \left(\textbf{Moles of RNA Nt}_{(mol)}\right) \textbf{X} \left(\frac{\textbf{RU}}{\textbf{Nt}} ratio\right) \textbf{X} \left(\frac{\textbf{Avg. MW of CP RU}_{(g/mol)}}{PAA\ Ratio}\right)$$

2.4.3 Three Component Complexes

Three component complexes are prepared from a polymer blend solution, containing PEGylated (CP) and non-PEGylated (HP) polyamidoamine polymers mixed in a required HP: CP ratio (PAA RU mol/mol ratio) where the total polymer PAA repeating units are contributed by both the polymers in the mixture. HP: CP ratio was represented as Required Parts of HP PAA RU: Required Parts of CP PAA RU, [e.g: 3:1; 2:1; 1:1; 1:2; 1:3]

$$\textbf{HP ratio} = \left(\frac{\textbf{Required Parts of HP}}{Parts\ of\ HP + Parts\ of\ CP}\right)$$

$$\textbf{CP ratio} = \left(\frac{\textbf{Required Parts of CP}}{Parts\ of\ HP + Parts\ of\ CP}\right)$$

Therefore, amount of HP required for a given RU/Nt ratio can be calculated by,

Mass of HP (g)

$$= \left(\text{Moles of RNA Nt}_{(mol)}\right) \text{X} \left(\frac{\text{RU}}{\text{Nt}} ratio\right) \text{X (HP Ratio) X (Avg. MW of HP RU}_{(g/mol)}\text{)}$$

Mass of CP (g)

$$= \left(\text{Moles of RNA Nt}_{(mol)}\right) \text{X} \left(\frac{\text{RU}}{\text{Nt}} ratio\right) \text{X (CP Ratio) X} \left(\frac{\text{Avg. MW of CP RU}_{(g/mol)}}{PAA\ Ratio}\right)$$

Information on the average molecular weight of PAA RU and PAA ratio can be found in the **Table 2-2**, page: 49

2.5 Gel Retardation Assay

2.5.1.1 Background

Ethidium bromide [Et-Br] is a cationic dye that binds with nucleic acids via intercalation and electrostatic interactions[308]. Electrostatic interaction occurs most favourably under low salt concentrations (< 10 mM). Intercalation of Et-Br with double stranded nucleic acids increases the fluorescence of the dye due to the reduction in the accessibility of the dye with water molecules[308]. The fluorescence quenching of Et-Br by water was attributed to the effective proton transfer occurring between the excited state Et-Br to the water molecules[309]. When the dye binds to the phosphate of nucleic acid by electrostatic forces the dye is exposed to water molecules, hence the enhancement of fluorescence is only minor. Also, the amount of fluorescence depends on the amount of intercalated dye. In the presence of DNA condensing agents, like poly-cations, the number of binding sites of Et-Br is reduced. This property of reduced intercalation (Et-Br exclusion) is widely used to study the binding properties of poly-cations with nucleic acid. This ethidium bromide exclusion assay is usually performed with spectroflurometer, where the nucleic acid is initially allowed to bind to poly-cation and Et-Br is added just before measurement. This exclusion assay resembles the conditions of the gel electrophoresis, where the nucleic acid/poly-cation complexes are load on to the gel and ethidium bromide from the gel intercalated during the electrophoresis step. Hence, ethidium bromide exclusion can be observed with the gel electrophoresis setup as well.

2.5.1.2 Protocol

The agarose gel [1.2 wt.%] was prepared in 1x TAE (UoN) or 0.5x TBE (UA) running buffer. The agarose was dissolved by heating the mixture in a domestic microwave oven. The mixture was cooled down to 55˚ C and ethidium bromide was added to a final concentration of 0.5 µg/mL.

A constant amount of miRNA was loaded in each well (~500 ng/well) while varying the amount of polymer. The electrophoresis was conducted at 70 V for 40 minutes in 1X TAE or 0.5x TBE running buffer. The microRNA was imaged under the UV-trans-illuminator gel imaging system [Fluorescence Gel Documenter, Syngene - UoN/ Fluorescence-Chemi-luminescence Imaging System, Vilber Lourmat DP-001.SD – UA]. The densitometry analysis of microRNA on gel images were performed with ImageJ 1.47v, a free image analysis software from NIH, USA. Images acquired by auto mode were used for this semi-quantitative analysis.

For the visualization of free polymer, the gel was stained with coomassie blue staining solution [100 mg/mL - Coomassie Brilliant Blue R250, 50 % methanol, 10% acetic acid in water] followed by background elimination with de-staining solution [5 % methanol, 7.5 % acetic acid in water]. Coomassie stained gels were imaged against a white background using the trans-white mode. **Observational Note:** When the staining solution was re-used, it resulted in slow staining of polymer bands while the gel remained relatively clear, hence the de-staining step could be by-passed.

2.5.2 Gel Image Acquisition and ImageJ – Method Validation

Auto image acquisition mode uses the region emitting maximum fluorescence as reference point to calculate the optimal exposure time such that the maximum fluorescence does not exceed saturation point of the CCD detector. Hence, images obtained using this setting is ideal for quantitative analysis with ImageJ (Figure 2-4A). Although fainter signals are not visible on this image, they were picked up by the software while performing image analysis. [RU/Nt ratio 1.5 to 4 did not reach 100% complexation, Figure 2-5 – Blue line].

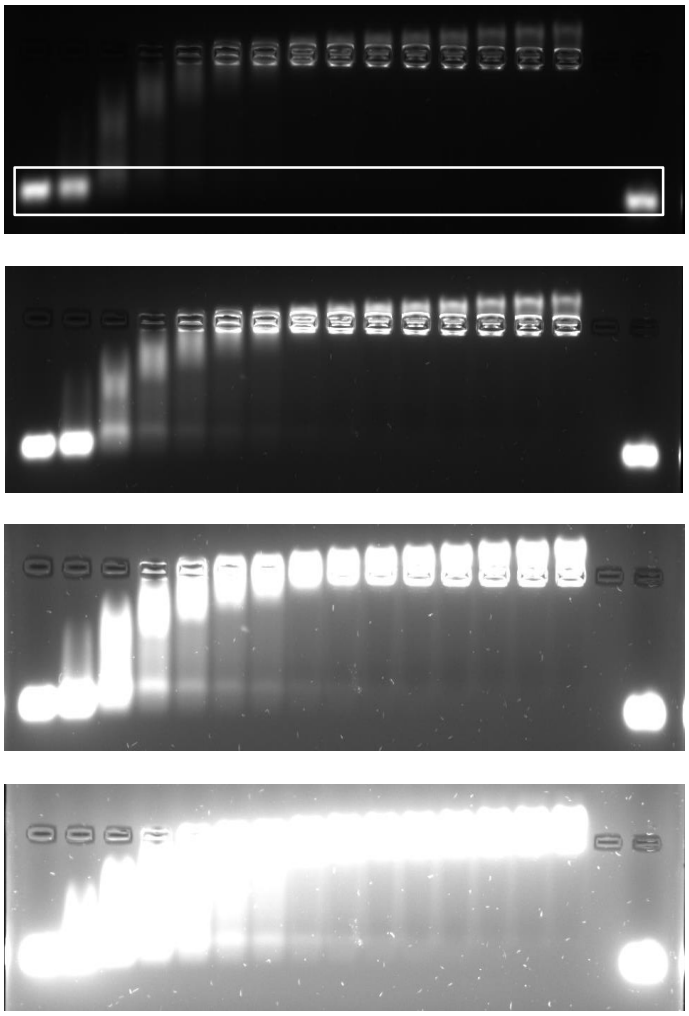

Figure 2-4: Effect of exposure time during a typical agarose gel imaging.
Representation of a typical gel loaded with 500 ng miRNA per well with increasing polymer to RNA (RU/Nt) ratio: 0, 0.5, 1, 1.5, 2, 2.5, 3, 4, 5, 6, 7.5, 10, 15, 20, 30, 0/0, 0). All these images represent the same gel but with increasing exposure time from optimal auto exposure (A) to gradual increase in saturation (B, C, D).

Other images were recorded with higher exposure times to enable the visualization of fainter signals and used for representation when it was considered appropriate. Saturated images with high background did not produce intensity plots on ImageJ hence did not contribute to quantification (e.g.: Figure 2-4: C, D).

Although it was possible to obtain intensity plots with the saturated image 6 (B), it was insensitive to small changes that was observed with the auto-exposed image 6 (A). This resulted in under-estimation of miRNA interactions for low polymer RU to RNA Nt ratios (RU/Nt < 2) as seen in the Figure 2-5.

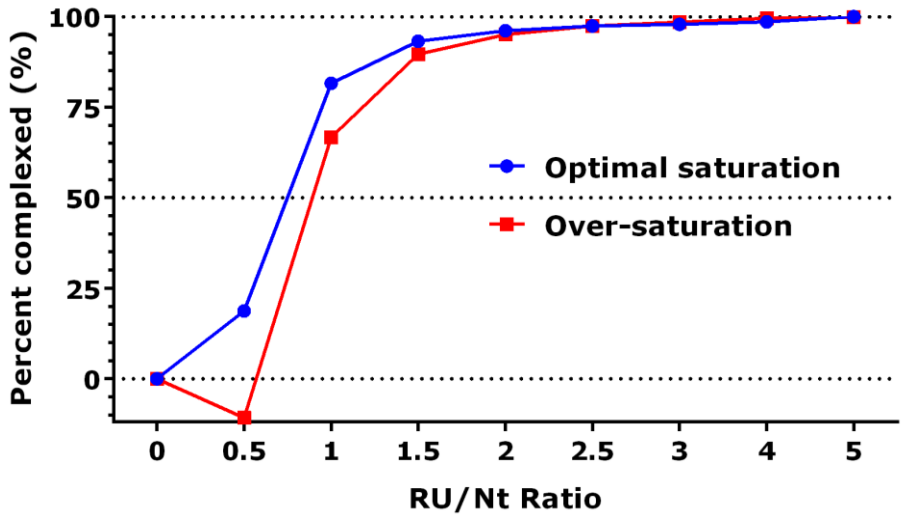

Figure 2-5: Influence of image saturation on data quality.

The graph represents the percentage of miRNA complexed with homopolymer (HP-R) at different RU/Nt ratios. Each curve represents data obtained from two different images of the same gel, Figure 2-4 (A, B), that were obtained from different exposure times.

Percentage complexed miRNA = 100 – Percentage of free miRNA in each sample,

The percentage of free microRNA was calculated from the intensity of miRNA fluorescence measured from the area of the gel that was parallel to the free microRNA florescence [White box in Figure 2-4(A) indicates the area of free microRNA measurement]. The fluorescence outside this region was considered as the fluorescence from different molecular weight species of PAA-miRNA complexes. The lane with no microRNA (RU/Nt: 0/0) was used as the blank to subtract the background signal.

2.6 Dynamic Light Scattering (DLS)

2.6.1 Principles of Dynamic Light Scattering

Particles in a liquid are constantly moving and colliding with neighbouring particles exhibiting random Brownian motion. Large particles move slowly while the smaller particles move faster defined by the Stokes-Einstein equation. Particles also have the property of scattering light. A group of particles in one spatial arrangement would produce a distinct pattern of scattering intensity. This pattern of intensity is constantly changing due to Brownian movement. Dynamic Light Scattering (DLS), also known as Photon Correlation Spectroscopy (PCS), measures the fluctuation in the intensity pattern of the scattered light to calculate the size of the particles. Briefly, the intensity pattern of the scattered light is collected between very small intervals of time (δt – micro or nanosecond). The first measurement (at time t) is compared between the successive measurements (t+ δt, t+ 2δt, t+ 3δt,..) to find a correlation. A correlator produces a value between 1 (perfect correlation) to 0 (no correlation). For nanoparticles, the time taken for the correlation value to reach 0 from 1 is typically in the order of milli-seconds. Comparatively, the time to reach zero correlation is slower for large particles, because of its slower motion, and faster for small particles. This produces a correlation plot with a decay time which is used by the software to calculate the particle size. Typically, the instrument produces the size distribution (on X-axis) against the intensity (on Y-axis) called distribution by intensity. This information is used to derive other meaningful plots like distribution by volume, mass or number which can be helpful to analyse the data when the sample contains more than one population of particles[310].

For example, when a sample contains equal proportion of 10 nm and 100 nm particles of same density and refractive index, the intensity plot would produce two size distribution peaks corresponding to 10 and 100 nm. By Rayleigh's approximation, the intensity of the light scattered by a particle is sixth power of its diameter. Hence, the smaller particles scatter less light the intensity of the 10 nm peak will be 1,000,000 times smaller than the 100 nm peak. When the intensity data is converted to volume or mass distribution, the peak of 10 nm particles will appear 1000 times smaller than the 100 nm particle, as the volume

of the sphere is third power of its radius ($4/3\ \pi r^3$). When the volume distribution is further converted to number distribution, ideally both the peaks should appear at the same height revealing actual relative quantities[310].

However, there exists limitations when using these derived plots, as they are calculated using many assumptions. The intensity data, information on refractive index and dispersing medium are used to derive distribution by volume using Mie theory. Also, Mie theory work well only for spherical particles[311]. Assuming that the densities of all measured particles are same, the volume is converted to distribution by mass. The volume distribution can also be converted to distribution by number, but it is indicated that this calculation has a high risk of huge errors[310]. Number distribution can be used if the quality of the measurement data is good, which can be found from the "Size Quality Report" and "Expert Advice" tabs on the Malvern Zetasizer software. In general, the size obtained from these plots have the following trend, d(intensity) > d(volume) > d(number)[312]. It is important to be aware of these assumptions and limitation for clear understanding and more meaningful interpretations of the data.

Table 2-4: Instruments used for DLS and Zeta-potential measurements.

Type	Instrument / Model / Software	Laser (output)	Optics	Size Range, hydrodynamic diameter
University of Nottingham (Pharmacy – Boots Science Building)				
Size	Viscotek 802 DLS without DAT S/W: OmniSIZE 3.0	830 nm Infra-red Diode (50 mW)	Classical - 90˚	1 nm – 2 µm
Zeta	Malvern Nano ZS with MPT-2 Autotitrator (Model: ZEN 3500) S/W: Zetasizer 7.0	532 nm Green Diode (50 mW)	173˚ Backscatter, 13˚ Forward scatter, Dual Angle	0.6 nm – 6 µm
University of Angers (U1066 – MINT)				
Size	Malvern Nano S (Model: ZEN 1600) S/W: Zetasizer 7.02	633 nm Red HeNe (4 mW)	173˚ Backscatter, 13˚ Forward scatter, Dual Angle	0.6 nm – 6 µm
Zeta	Malvern Nano ZS (Model: ZEN 3600) S/W: Zetasizer 7.02	633 nm Red HeNe (4 mW)	173˚ Backscatter, 13˚ Forward scatter, Dual Angle	0.6 nm – 6 µm

2.6.2 Viscotek 802 DLS - Measurements and Terminologies

To measure the particle size by Viscotek DLS instrument, about 14 - 30 µL of the sample was transferred to Hellma quartz cuvettes (105.251.15.40-QS). The count rate was set around 300 kcps by adjusting the LASER power between 1 – 95%. The acquisition time was set as 10s for each measurement and the size was obtained as an average of minimum 10 clean measurements. The calculation options were set as follows, resolution of peaks was set to 300 for better accuracy and first data point was ignored when a spike (mystery peak) was seen to appear between the first and second data points, which results in very small apparent size peak appearing mainly for the dilute samples[313]. The size distribution by intensity was used for all data interpretations until and otherwise specified. Polystyrene was used as the mass model. The standard deviation and equivalent percentage SD (% RSD) indicates the width of the peak relative to its height at the half-height point[313]. %RSD is the polydispersity indicator[313] and is calculated for each peak. %RSD < 20% represents mono-dispersity. 'Rh' represents hydrodynamic radius in nm. A small peak of very small Rh (around 1 nm), is often referred to as a 'solvent peak' but is more accurately described as a 'noise peak' and is the result of noise in the raw data, modelled by the fitting routine[313].

2.6.3 Malvern Instruments - Measurements and Terminologies

To measure the particle size by Malvern Nano S or ZS, about 12 - 50 µL of the sample was transferred to an ultra-low volume DLS quartz cuvette [UoN: Hellma -105.251.QS; UA: Hellma- 105.251.005-QS]. The nanoparticles were assumed to have the same refractive index as "polystyrene latex" and its values were used as a model system for obtaining volume and number distribution. Water was selected as the dispersant and sample viscosity was considered the same as the dispersant. Temperature was set to 25˚ C. ZEN 2112 was selected as the quartz cuvette model. The measurement angle was set to 173˚ non-invasive backscatter [NIBS default] mode. Measurement duration was set to "Automatic" which would calculate number of runs and run duration (usually 10 - 20s) depending upon the sample properties. Each sample was measured in triplicates. Attenuation and positioning method was also set to automatic for selecting the optimal measurement conditions.

The results are represented by Z-average (Z-avg), polydispersity index (Pdi) and peak means. Z-avg and Pdi are calculated by cumulants analysis of the size intensity data. Pdi, represents the width of the assumed Gaussian distribution[314]. Pdi < 0.2 (< 20 %) are considered as mono-disperse for protein samples. Z-avg is only meaningful for spherical, single population mono-disperse samples. For example, a sample containing 10 nm and 100 nm particles, the Z-average can be anywhere between 10 and 100 nm (e.g. 50 nm) and does not reflect any actual population in the sample. Even if the sample has only one peak, but broader distribution with Pdi > 0.5, Z-average is not useful for interpretations. In such cases, individual peak mean values give meaningful results[310,314].

2.7 Zeta-Potential

2.7.1 Principles of Zeta-potential measurements

Zeta-potential is defined as the electrostatic potential near the surface of the particles[310]. The surface of the nanoparticles exhibits a charge that is dependent on the pH of the solution[310]. When a charged particle is placed in an ionic solution, oppositely charged ions strongly binds to the particle surface forming the "Stern" layer which is the beginning of the electrical-double layer[310]. Surrounding the stern layer is the inner and outer "Diffuse" layer of ions[310]. The inner-diffuse layer contains counter-ions that move along with the particle, while the ions in the outer diffuse layer ions move independent of the particles[310]. The boundary between the inner- and outer- diffuse layers is called the slipping plane and the potential difference between the inner and outer diffuse layer is called the zeta-potential[310].

Malvern instruments measures the zeta-potential by Laser Doppler Velocimetry (LDV) using Mixed-Mode Measurement and Phase Analysis Light Scattering (M3-PALS) technique[310]. When a charged particle is placed in an ionic solution and exposed to oppositely charged electrodes, the solid particles and the ions in the liquid tend to move towards the oppositely charged electrodes defined as electrophoresis and electro-osmosis respectively[310]. The electrophoretic mobility of the particles in the centre of a capillary tube is affected by the electroosmotic motion of the surrounding liquid[310]. M3-PALS-LDV technique cancels out this electroosmotic effect, hence providing the true electrophoretic

velocity of the particles[310]. The zeta-potential is then calculated using the Henry equation,

$$U_E = [2\ \varepsilon\ z\ f(\mathrm{Ka})] / 3\ \eta,$$

where U_E is the electrophoretic velocity, ε is the dielectric constant; z is the zeta-potential; η is the viscosity; and *f(*Ka) is the Henry's function; *f(*Ka) = 1.5 (Smoluchowski approximation), when the particle size is > 200 nm and electrolytes > 1 mM salt; *f(*Ka) = 1 (Huckel approximation), when the particle size is < 200 nm dispersed in an non-aqueous solution [310].

2.7.2 Measurement

The initial nanoparticle solutions contained 2.5 µM (~ 38 µg/mL) miRNA in ~ 150 mM NaCl solution, pH 6.0. The nanoparticle solution was diluted 3.5 fold in water to obtain a nanoparticle solution containing ~ 10 µg/mL of miRNA which resulted in the dilution of the salt concentration to ~ 45 mM NaCl. The ideal ionic concentration required for zeta-potential measurement is 1-10 mM NaCl. However, the nanoparticle solution must contain at least 10 µg/mL of miRNA to obtain sufficient scattering signal. Due to this requirement, the minimum salt concentration of the nanoparticle medium that could be achieved was ~45 mM NaCl. Zeta-potential was measured with Malvern Zetasizer Nano ZS. Folded capillary cells were filled with nanoparticle solution at the concentration of 10 µg/ mL of miRNA[312]. The measurement was made in triplicates, at 25 ºC, pH 6.0 using the Smoluchowski approximation.

Chapter – III

Optimization of miRNA-polymer interaction and Physico-chemical and biological evaluation of poly(amidoamine)-microRNA polyplexes prepared by "Salt in Polymer" method

Nanoparticle Development – Stage I

- Optimization of pH and Salt

– "Salt in Polymer" method for Nanoparticle Preparation

3 Optimization of miRNA-polymer interaction; Physico-chemical and biological evaluation of poly(amidoamine)-microRNA polyplexes prepared by "Salt in Polymer" method

3.1 Introduction

The basic understanding of the nature of interactions between polymer and microRNAs (oligonucleotide with ~23 base-pairs) is critical to successfully formulate polyplexes that would be functional under *in vitro* and *in vivo* conditions. Hence the aim of this chapter was to define optimal conditions for miRNA nanoparticle formation using two sets of homopolymer (HP) and copolymers (CP - CP2k and CP5k). It includes an initial set of optimizations focusing on the effect of ionic concentration and pH on miRNA binding to the polymer. Followed by preparation of both two-component (HP-miRNA) and three-component (HP-CP-miRNA) polyplexes at different polymer repeating unit to RNA nucleotide ratios (RU/Nt) and HP RU to CP RU ratios (HP: CP). All these different polyplexes were characterized by gel-retardation assay and size measurements (DLS). Based on the results obtained from these physico-chemical characterizations, suitable formulations that satisfy defined selection criteria were selected for *in vitro* testing. The three major selection criteria for the selection of polyplexes are, (a) efficient miRNA incorporation (≥ 90% of miRNA complexation efficiency); (b) No or minimal free polymer in the miRNA-polyplexes to avoid excess free-polymer mediated cytotoxicity; and (c) Size of the polyplexes. Biological characterization included toxicity studies of free polymer on a brain tumour cell line, U87MG. The *in vitro* performance of microRNA-polyplexes were evaluated based on cellular uptake and gene knock-down efficiency.

3.2 Background

3.2.1 Polyplex Formation – Steps in Post Crosslinking

The key to form stable cross-linked miRNA-PAA nanoparticles with these PAA polymers depends on several factors. In general, the formation of the crosslinked polyplexes were assumed to occur by following the steps outlined below[245].

1. **Mixing** of nucleic acid (miRNA) and polymer mixture (PEGylated and non-PEGylated PAA) at a required RU/Nt ratio. RU/Nt denotes the mol to mol ratio of PAA Repeating Unit to RNA nucleotides [see 1.9.7, page: 38, for polymer RU structural details]. In a three component polyplex system, the RU is the sum of PAA RU from each polymer in the blend (HP-PAA-RU + CP-PAA-RU).
2. **Self-assembly:** Electrostatic attraction acts as glue between the polymer and microRNA, bringing several polymer strands and microRNA together. As the core of the polyplex becomes relatively hydrophobic and compact, the PEG tends to preferentially assemble at the surface of the nanostructure in the aqueous medium where it can be mobile. The PEG chains would limit the size of the complexes due to stearic hindrance and also prevent aggregation due to charge neutralization[296].
3. **Crosslinking, compaction and stabilization:** Active thiols from the copolymer would form di-sulphide bridges with other active thiols from co-polymer or thio-pyridine molecules from the homo-polymer which are in close proximity. This new crosslinking might result in compaction of the nano-structure, which intern might promote further crosslinking, compaction and stabilization.

As the nanoparticle formation is dependent on electrostatic interaction and thiol crosslinking, any physicochemical conditions [**Figure 3-1** (page: 71)] that influence these interactions would affect the size and stability of the final miRNA polyplexes.

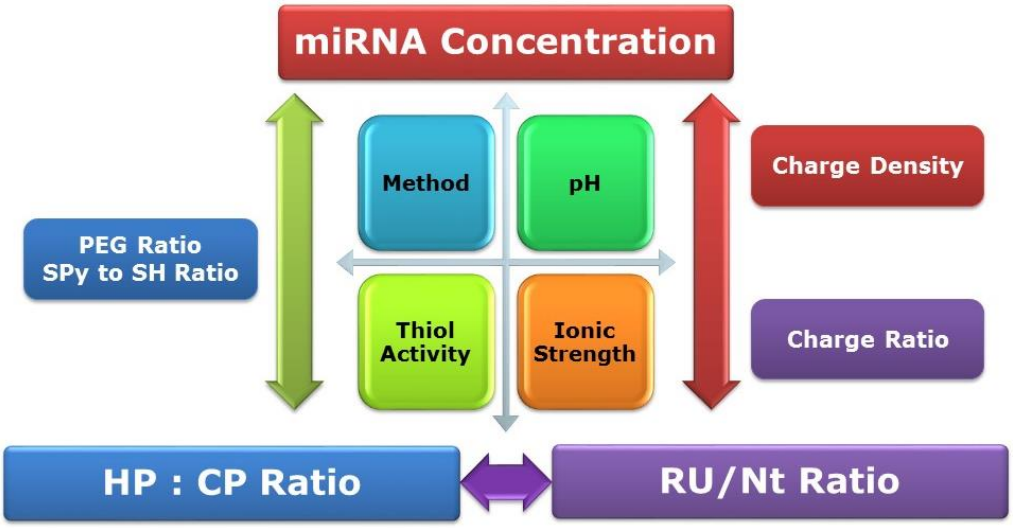

Figure 3-1: Critical factors in the preparation of crosslinked nanoparticle.

Various formulation strategies have been developed in our group and are summarized in the following section. (SPy – Thio-Pyridine).

3.2.2 Evolution of Formulation Methodology

Initially, the nanoparticles were prepared by mixing a single polymer with nucleic acid defined as two component system[296,297], 3.2.2.1, page: 71. As a later development, nanoparticles were prepared by mixing the plasmid DNA with a polymer blend consisting of PEGylated and non-PEGylated polymers, defined as three-component system which had several advantages like uniform size distribution, higher DNA condensation ability resulting in the formation of smaller, compact and stable nanoparticles and a quantitative incorporation of both polymer and nucleic acid components[296], **Figure 3-3**, page: 73. For both preparations, the polyplex formulation involves addition of one bulk of the polymer stock solution to the nucleic acid solution, followed by gentle mixing and incubation for 20 – 30 minutes for complexation.

3.2.2.1 Two Component Approach

pDNA polyplexes were prepared by addition of polymer stock dissolved in water to the pDNA in 0.1x PBS (14 mM NaCl equivalent), **Figure 3-2, A** (page: 72). Complexation and gene delivery was studied with homopolymers with different PAA backbones. The homopolymer NG30, p(DMEDA-MBA) showed efficient DNA condensing properties and transfection activity[297]. NG30 (M_w 21,500) was able to form small [150 d.nm at RU/Nt ratio 5:1 and 10:1] and stable

nanoparticles with pDNA [4.6, 6 and 7 kilo base-pairs] even in the presence of high salt concentrations, 1x PBS (150 mM NaCl). Although it was possible to form polyplexes in the physiological salt concentrations, 150 mM NaCl did affect polyplex condensation and stability. Hence, it is necessary to have low salt concentrations (< 150 mM) for stable polyplex formation.

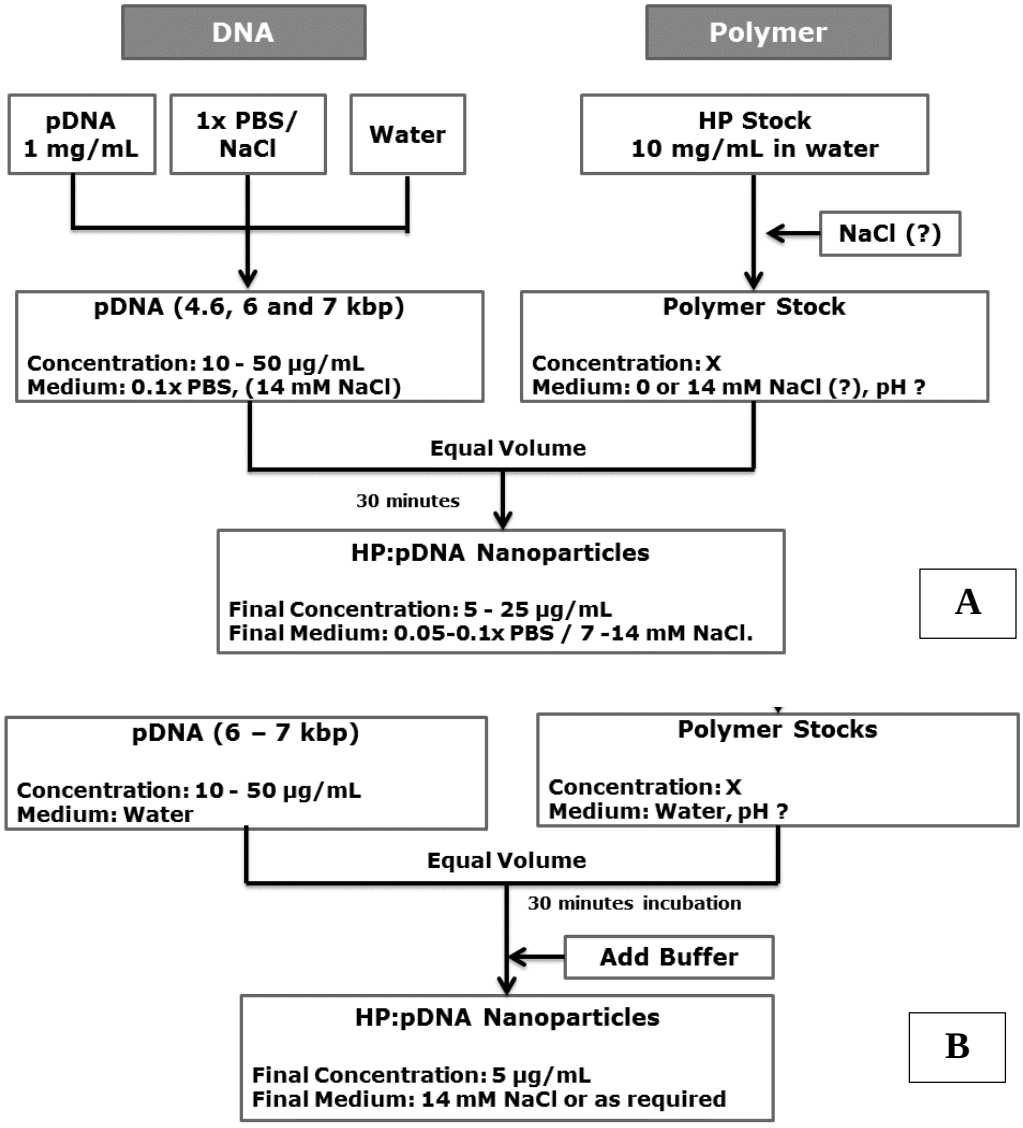

Figure 3-2: General method for polyplex formation.
(A) General[297]; (B) Alternative approach[297].

3.2.2.2 Rackstraw's three component approach

Multi-component systems involving PEGylated and non-PEGylated PAA for gene delivery was initially reported by Rackstraw *et al*[296]. Homopolymer NG49 (M_w 28,000), p(DMEDA-MBA), and tri-block-copolymer NG47, $PEG_{1900\ Da}$-$p(DMEDA\text{-}MBA)_{>10\ kDa}$-$PEG_{1900\ Da}$, were used for the delivery of plasmid DNA[296].

The polyplexes were formed by adding polymer blend (in water) in to the pDNA solution in 40 mM Tris-acetate, 1 mM EDTA (TAE, pH 7.4) or 1x PBS (140 mM NaCl, 10 mM phosphate, pH 7.4). At RU/Nt ratio 2:1, these polymers were able to form complexes around 200 nm by DLS, whereas at higher RU/Nt ratio 5:1 and 10:1, the size of the polyplexes was around 500 and 300 nm respectively[296].

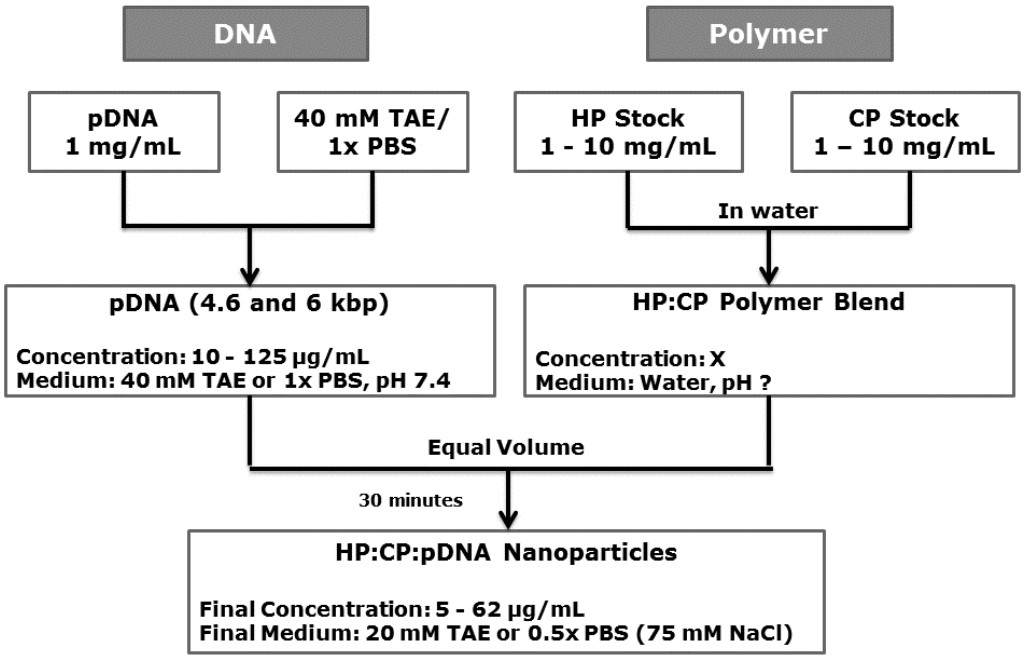

Figure 3-3: Rackstraw *et al.* multi-component polyplex formation method.

3.2.2.3 Aljaeid's and Danish's three component crosslinked NP formation

The crosslinkable PAA has been shown to self-assemble into stable nano-structures with plasmid DNA (5700 bp)[274,275], ODNs (79 and 21 bp)[275] and siRNA[275].

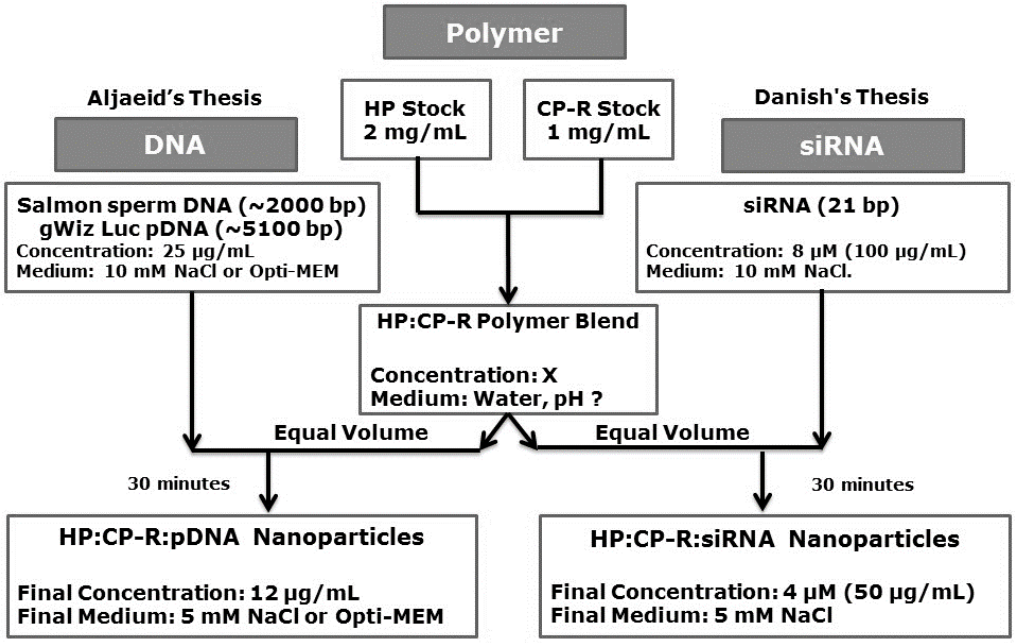

Figure 3-4: Aljaeid*'s* and Danish*'s* methods for polyplex preparation.

Homopolymers (PAA) with three different molecular weights (44 kDa, >10 kDa and 5-10 kDa) and copolymers (PEG-PAA-PEG) with varying length of PEG chains (655, 1700 and 4600 Da) were investigated in Aljaeid's thesis[274]. The size analysis of various crosslinked systems with salmon sperm DNA or pDNA in 5 mM NaCl produced 100 – 200 nm particles (by DLS) at low RU/Nt ratios 1.5:1 and 2:1[274,275]. The nanoparticles for cell treatment were directly prepared in Opti-MEM and showed transfection activity inversely proportional to the length of PEG chain (655, 1700, 4600 Da)[274]. Usually, the pDNA-PAA crosslinked complexes were prepared in low-salt medium and transferred to physiological medium for cell assays.

A comparative study involving the packing of different nucleic acids (pDNA, ODNs and siRNA) with the crosslinked PAA polymer system was investigated in Danish's thesis (2009-2013). Copolymer (PEG-PAA-PEG) with 4600 kDa PEG was used along with three different homopolymers (44 kDa, >10 kDa and

5-10 kDa)[275]. The central PAA block of CP was 6700 kDa with randomly distributed cystamine residues. These nanoparticle formation data at high salt concentrations indicate that the condensation process of PAA with 4000 – 6000 bp DNA in relatively favourable compared to 21 – 23 bp siRNA. Crosslinked siRNA nanoparticles were prepared in 5 mM NaCl and the resulting complexes were found to be stable under physiological salt concentration after complexation[275].

3.3 Materials and Methods

3.3.1 Polymer Reduction and Purification

Each polymer was dissolved in water (10 mg/mL), pH was adjusted to pH 7.4 and deoxygenated by passing nitrogen for 10 minutes. Freshly prepared DTT solution (5 – 15 molar polymer-thiol equivalent) was added to the polymer and stirred for 1 hour in dark, under nitrogen atmosphere at room temperature. After an hour, the pH of the reaction mixture was set to pH 4.0 by adding appropriate amounts of HCl [2M]. DTT and the by-products of the reduction reaction eliminated from the polymer solution through ultra-filtration against acidified deoxygenated water (pH 4.0) employing a 5 kDa MWCO filter. The final polymer solution obtained after 3 cycles of ultra-filtration was collected, snap-frozen in liquid nitrogen and freeze-dried for 48 hours using VirTis® Sentry 2.0 SP Scientific freeze-dryer. The polymer yield (mass recovered) was calculated using the following formula,

Yield = (Mass of polymer recovered after purification/ Theoretical yield) * 100

Formation of free thiols through the elimination of thio-pyridine or t-BOC after reduction and purification was confirmed by proton NMR and the quantification of free thiols was performed by Ellman's assay.

Percentage free thiol = (Actual free thiols / Theoretical Thiols) * 100

For more details on the procedure and calculations, please refer section 2.3 (page: 51).

3.3.2 Nuclear Magnetic Resonance

About 20 mg of the polymer was dissolved in 1 mL of D_2O immediately before performing proton NMR.

3.3.3 Electrophoretic mobility shift assay (EMSA)

Two component systems are complexes made by mixing a polymer, either PEGylated or non-PEGylated PAA, with the microRNA. The amount of miRNA was fixed and progressively increasing amounts of the polymer were added for complex formation. The complexes were loaded in to the wells which were cast in the middle of the gel. During electrophoresis, the negatively charged miRNA

migrates towards the anode side of the gel (downwards) while the positively charged species will migrate into the cathodic side of the gel (upwards).

In general, the free microRNA present in the complexes co-migrates at the same level as the control miRNA which is not mixed with any polymer (free miRNA). Any microRNA that is bound to the polymer becomes larger and less charged and migrates slowly in the gel. Hence, any mobility shifted fluorescence away from the free microRNA region can be considered as complexed miRNA. Different molecular weight soluble complexes appear in different locations on the gel. Soluble complexes with excess (polymer) positive charge migrate toward the cathode and vice versa. Complexes which are larger than the pore size of the gel and/or which are neutral appear in the well while tight interaction between polymer and microRNA prevents ethidium bromide from accessing the miRNA, hence disappearance of fluorescence.

3.3.4 Optimization of Formulation Method (miRNA polyplexes)

miRNA and siRNA are short nucleic acids (~23 bp) and hence tend to bind weakly with the cationic polymers compared to pDNA (>1000 bp). Determining optimal miRNA-PAA polymer binding conditions might help to form well-condensed complexes. The nucleic acid binding groups in the current PAA family of polymers are the tertiary amines (from DMEDA and cystamine, while the amide nitrogen (from the MBA) do not have a permanent charge and hence would have a negligible contribution to binding. As the PAA block is the sole cationic nucleic acid binding unit in these set of polymers, HP was used as a proxy for all the polymer used in this study including CP2k and CP5k.

The amount of miRNA used for complexation was kept constant (500 ng/well). To study the influence of one parameter (e.g. pH), only that parameter was varied while maintaining other parameters constant (salt concentration, polymer RU to RNA nucleotide ratio).

3.3.5 Buffering Capacity of HP

The buffering capacity of HP (2 mg/mL in 1 mM KCl) was studied by acid-base titration. The polymer was initially acidified to pH 3.0 followed by progressive addition of 0.1 M NaOH (10 – 20 µL). The pH was recorded at each step until the pH reached pH 11.

3.3.6 MicroRNA-PAA Polyplex Preparation

Optimized complexation buffer (2x) was prepared by diluting 1x PBS in water to a final concentration of 0.33 x (50 mM NaCl/KCl, 4 mM phosphate). The pH of the buffer was set to pH 6.0 using phosphoric acid and NaOH. The pH of the polymer solution was adjusted to pH 6.0 after dissolution in this 2x complexation buffer. The polymer blends were prepared by mixing appropriate amounts of HP and CP. Equal volume of polymer blend was mixed with equal volume of miRNA solution and incubated for 30 minutes to form complexes. These complexes were used for further physico-chemical and biological characterization.

3.3.7 MicroRNA polyplex - Selection criteria for *in vitro* testing

The three major criteria for the selection of polyplexes for *in vitro* testing include, (a) efficient miRNA incorporation (≥ 90% of miRNA encapsulation efficiency); (b) No or minimal free polymer in the formulation to avoid excess polymer mediated cytotoxicity; (c) Size of the polyplexes.

The amount of free miRNA and free polymer after complexation was determined from gel retardation assay. Size of the polyplexes were measured by DLS, Viscotek 802DLS.

3.3.8 Cytotoxicity Assay

The U87MG cells were seeded (10,000 cells/ well) and incubated overnight for attachment. The polymer solution (10 mg/mL) was prepared by dissolving the polymer in HBSS with Ca^{2+} and Mg^{2+}. Polymer solution was mixed either with medium with serum (EMEM complete medium) or without serum (OptiMEM, transfection medium). The cells were treated with different polymers (HP, HP-R, CP2k-R and CP5k-R) and at different concentrations (1, 10, 50, 100, 500 and 1000 µg/mL). The cells were exposed to polymer-containing-medium for 4

hours and then replaced by EMEM complete medium. The cells were further incubated for 48 hours before performing the MTS assay. The 48-hour incubation allows the evaluation of delayed toxicity of the polymer exhibited on cells. The MTS assay was performed following the manufactures protocol (Promega). The absorbance, at 492 nm and 750 nm, was recorded 90 minutes after adding MTS containing medium. The absorbance from 750 nm was subtracted from 492 nm $(A_{492\,nm} - A_{750\,nm})_{\,Sample}$. The blank absorbance (no cells, medium + MTS) was subtracted from all samples,

$(A_{492\,nm} - A_{750\,nm})_{\,Sample}$ - $(A_{492\,nm} - A_{750\,nm})_{\,Blank}$.

The percentage viability was determined by assuming that viability of untreated cells was 100 %. All experimental conditions were performed in triplicate. The percentage viability of the samples was determined using the following formula,

$$\left[\frac{(A_{570\,nm} - A_{690\,nm})_{Sample} - (A_{570\,nm} - A_{690\,nm})_{Blank}}{(A_{570\,nm} - A_{690\,nm})_{Untreated} - (A_{570\,nm} - A_{690\,nm})_{Blank}}\right] X\ 100\ (\%)$$

3.3.9 Nanoparticle Uptake Assay

U87MG cells were seeded (1000 cells/well) in a 96 well plate one day before the treatment. For 3D-spheroid culture, cells were seeded in a ultra-low attachment 96-well plates (2500 cells/well) in EMEM complete medium. The plates were centrifuges at 400 rpm and incubated for 3 days before treatment.

The PAA-miRNA nanoparticles were prepared using a Dy547-pre-labelled miRNA [Pierce DyLight™ 547 (Dy547) was conjugated to 5′-end of a miRNA. This pre-labelled miRNA-Dy547 was purchased directly from Dharmacon, miRIDIAN microRNA Mimic Transfection Control, Cat.no: CP-004500-01, for sequence information see **Table 2-1**, page: 48, (Excitation: 557 nm; Emission: 574nm)]. The cells were treated with these polyplexes in OptiMEM medium for 4 hours. Then the medium was replaced by medium containing Hoechst 33342 (~ 5 µg/mL) for 15 minutes and replaced with normal EMEM medium supplemented with serum. The fluorescence from live cells imaged using EVOS microscope using appropriate excitation settings and filters. The nuclear staining (Hoechst 33342) was imaged using a DAPI filter set (Excitation: 357/44,

Emission: 447/60) while the red fluorescence from DY547 was imaged using RFP channel (Excitation: 531/40, Emission: 593/40).

3.3.10 Luciferase Knockdown Assay

U87MG cells were stably transfected with luciferase gene containing one of the human 3′-UTRs [full length 3′-UTR of human BMI1 gene]. Hence, the luciferase expression can be specifically reduced by the introduction of miRNA-128 which is one of the miRNAs targeting 3′-UTR of BMI1.

These luciferase expressing cells were seeded (5000 cells/well) in a 96 well plate (white walled) and incubated overnight for attachment. The following day, the cells were treated with different PAA-miRNA formulations (10 µL) in Opti-MEM medium (90 µL). The miRNA concentrations used were 50, 250, 500 and 670 nM corresponding to 75, 375, 750 and 1000 ng of miRNA per well (100 µL). After 4 hours of nanoparticle exposure, the medium containing the complexes were replaced with complete medium (EMEM with 10 vol.% serum). The cells were further incubated for 60 – 72 hours before performing luciferase assay.

The amount of luciferase present in the cells after treatment was measured by adding DMEM medium without phenol-red, supplemented with serum (10 vol.%) and D-luciferin (0.15 mg/mL). The luminescence from live cells was recorded immediately after the addition of medium, using a FLUOstar Omega Microplate Reader (BMG LABTECH). The instrument was operated using top optics, focal length 15, gain 3600 and the luminescence was recorded using well scan mode (2x2 matrix).

Resazurin assay was performed on the same cells following the luciferase assay. The D-luciferin containing medium was replaced with DMEM medium without phenol-red, supplemented with serum (10 %) and resazurin (44 µM). The cells were incubated for about 2 hours and the fluorescence was recorded using the following settings, excitation: 544 nm, emission: 590 nm, end-point mode.

The background fluorescence of resazurin medium, measured from wells with no cells, was subtracted from the whole data set. The relative cell number (RCN) was determined for individual wells using the following equation,

Relative Cell Number, RCN

$$= \frac{\text{Fluorescence from each well}}{\text{Average fluorescence from untreated cells}} \text{ x } 100$$

As the fluorescence from untreated cells was assumed to be 100%, % RCN also represents "percentage viability".

The background luminescence from D-luciferin medium, from the well containing no cells, was subtracted from rest of the samples. Luminescence (ALU, arbitrary luminescence unit) from each well was divided by relative cell number (RCN) of the corresponding wells to obtain cell number corrected luminescence (ALU/RCN). This corrected luminescence was represented relative to the untreated cells, assuming 100 % luciferase expression in these cells.

$$\textbf{Relative luciferase expression}, \% = \frac{(\text{ALU/RCN})_{Treated}}{(\text{ALU/RCN})_{Untreated}} \text{ x } 100$$

More details on the data normalization procedure and its background development are provided in ***Appendix I: Development of Normalization Technique for Live Cell Luciferase Assay with High Throughput Compatibility, page: 214-237***.

3.4 Results

3.4.1 Polymer Reduction and NMR Analysis

Each of the polymers were reduced with DTT and purified by ultra-filtration. H^1 NMR spectra of the polymers before and after reduction was analysed. Typical proton NMR pattern for HP and CP are presented in **Figure 3-5** (page: 82). The NMR peaks corresponding to the thio-pyridine (9 – 6 ppm) was not detected after reduction of HP, **Figure 3-6** (page: 83). Similarly, the peaks corresponding to the thiol-protecting group, tertiary-Butyloxycarbonyl (t-BOC), disappeared from the NMR spectrum after reduction of CP2k [Figure 3-7 (page: 83)] and CP5k [**Figure 3-8** (page: 84)]. These results confirm that the DTT mediated reduction reaction was efficient in removing the protecting groups and activated the thiols for crosslinking. A slight shift in the NMR peaks corresponding to the polymer backbone was observed for HP(R), but not with other CP2k(R) or CP5k(R). It was speculated that the formation of disulphide crosslinked polymer chains (HPR-HPR) might be causing such observed shifts.

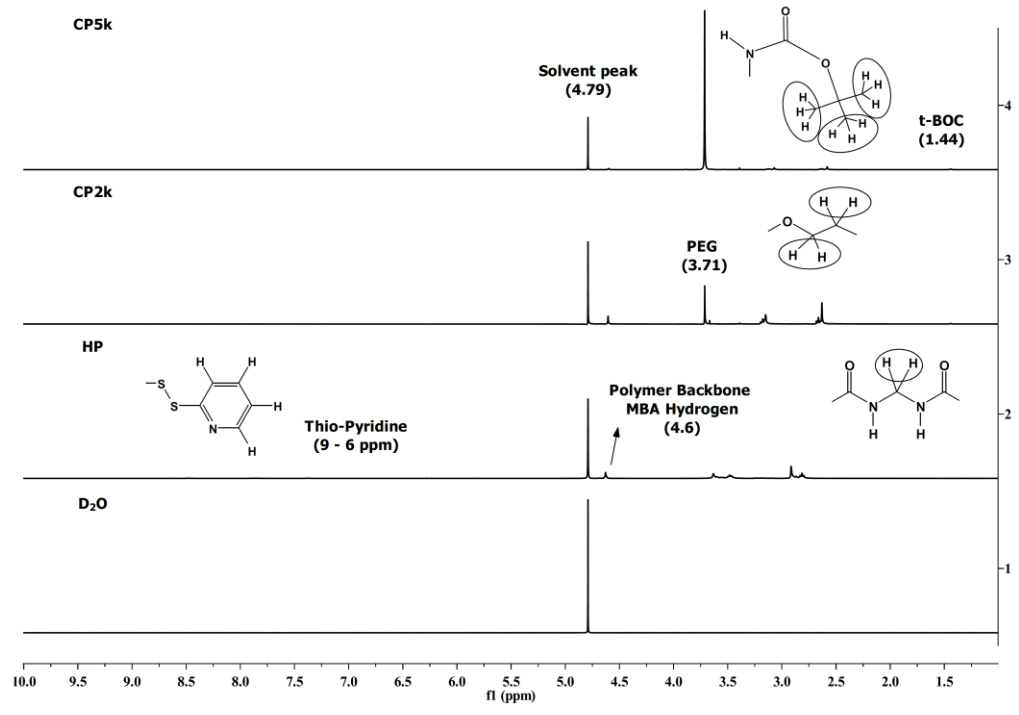

Figure 3-5: Typical proton-NMR of non-reduced polymers.
Deuterium oxide was used as the solvent. Major signalling regions of the polymer are presented along with their chemical shift in brackets.

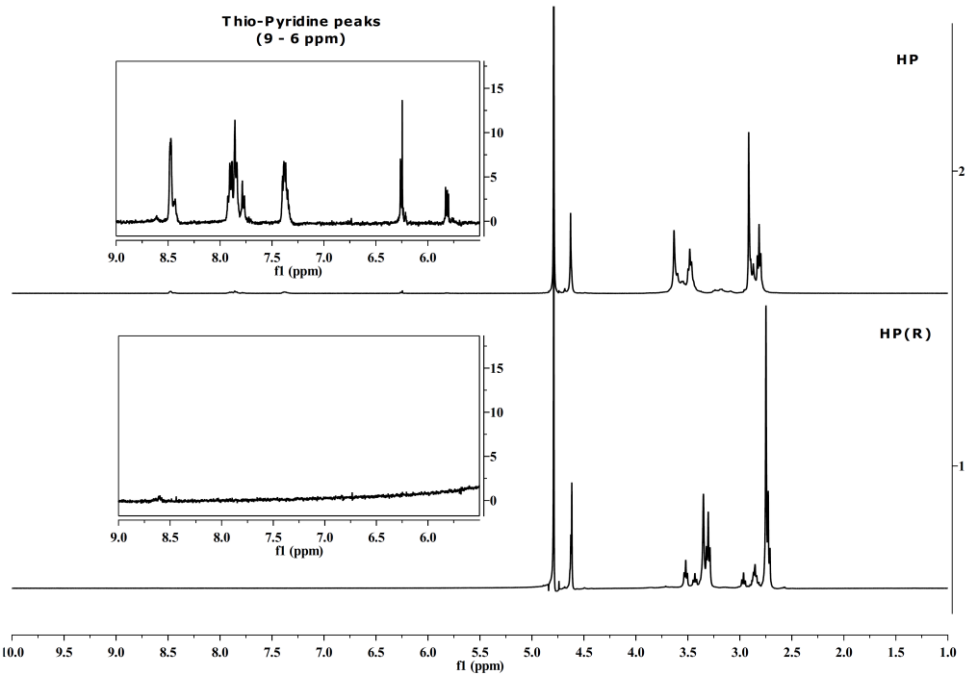

Figure 3-6: Proton NMR of homopolymer, HP and HP(R).

Proton NMR of HP before (top) and after reduction (bottom plot). The inserts in the plot shows the zoomed-in image of the peaks in the thio-pyridine (aromatic hydrogen) region (6 – 9 ppm)[315] indicating that the thio-pyridine group was not detected by NMR after reduction and purification.

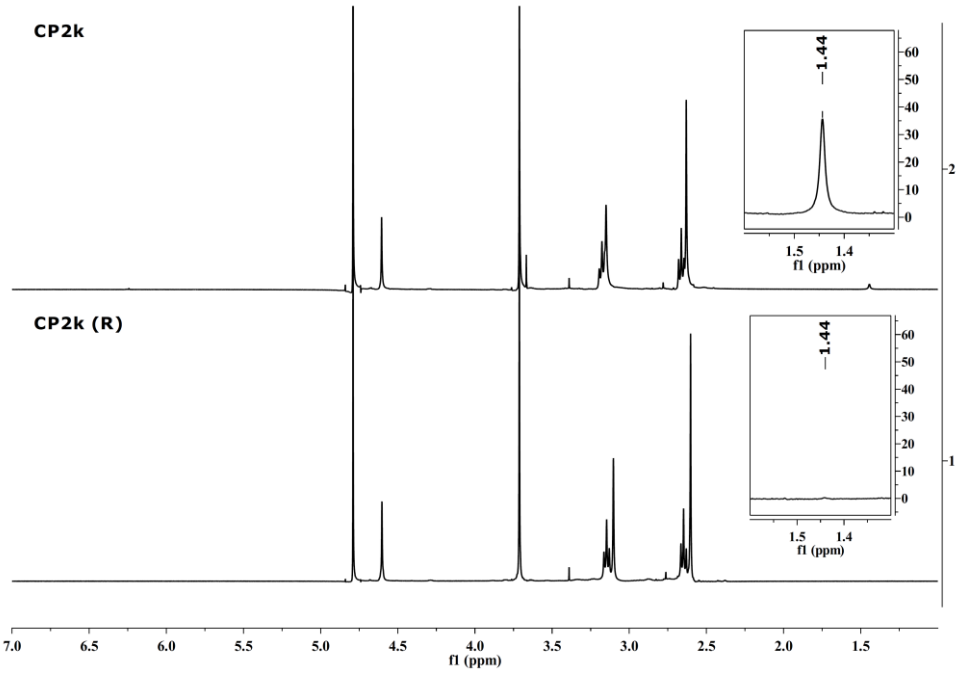

Figure 3-7: Proton NMR of copolymers, CP2k and CP2k(R).

Proton NMR of CP2k before (top) and after reduction (bottom plot). The insert represents the zoomed-in region (1.6 – 1.3 ppm) corresponding to the thiol-protecting group (t-BOC).

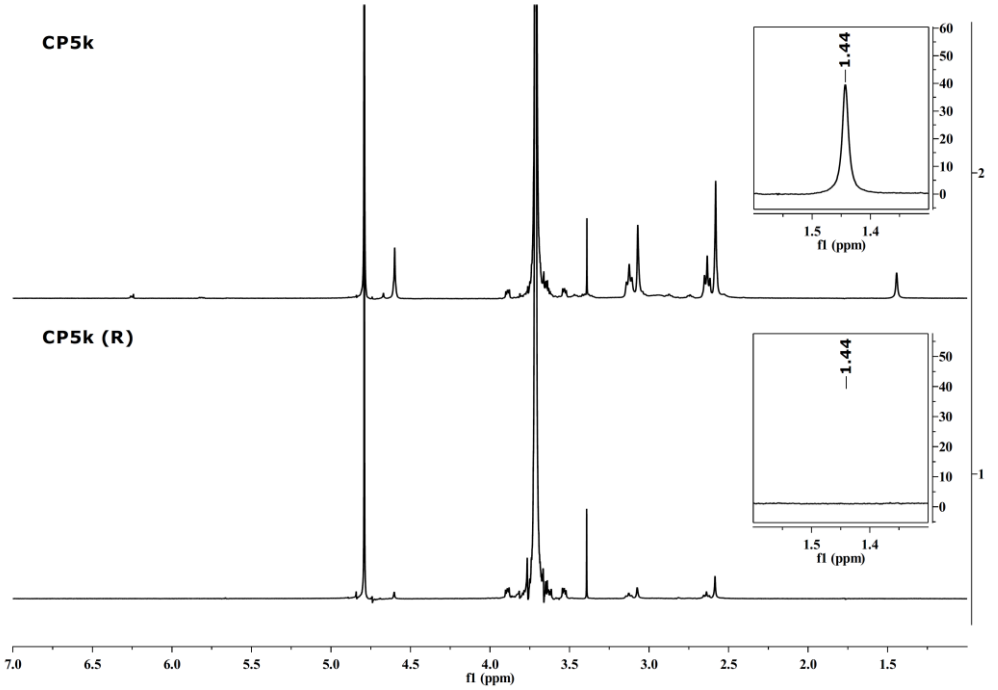

Figure 3-8: Proton NMR of copolymers, CP5k and CP5k(R).

Proton NMR of CP5k before (top) and after reduction (bottom plot). The insert represents the zoomed-in region (1.6 – 1.3 ppm) corresponding to the thiol-protecting group (t-BOC).

3.4.2 Yield of Reduced Polymers

The recovery of each polymer after reduction and purification was presented in the by percentage mass recovery and percentage free thiol in the **Table 3-1** (page: 84). Mass recovery was roughly above 50 % of the expected yield, while the thiol yield was variable depending on the polymer. Homopolymer (HP) showed highest thiol recovery (98 %) while the PEGylated copolymers showed moderate (34 % for CP2k) and poor thiol recovery (10 % for CP5k). This could be due to the long filtration time (6 – 8 hours) which might favour self-oxidation of thiols.

Table 3-1: Polymer yields after reduction and ultra-filtration.

Ultra-filtration	% Mass Recovery	% Thiol yield
HP (R)	53.18 ± 5.24 (N = 3)	98.16 (N = 1)
CP2k (R)	70.76 (N = 1)	34.10 ± 2.81 (N = 1)
CP5k (R)	50.45 ± 30.24 (N = 3)	9.61 ± 4.36 (N = 3)

3.4.3 "Salt in Polymer" Method

The interaction between polymer and miRNA can be improved by using optimal pH and salt concentrations during complex formation. The optimal conditions for miRNA polyplex formation was determined as 25 mM NaCl [**Figure 3-10** (page: 86)], pH 6.0 [**Figure 3-11** (page: 88)] and phosphate as the buffering agent [**Figure 3-12** (page: 89)].

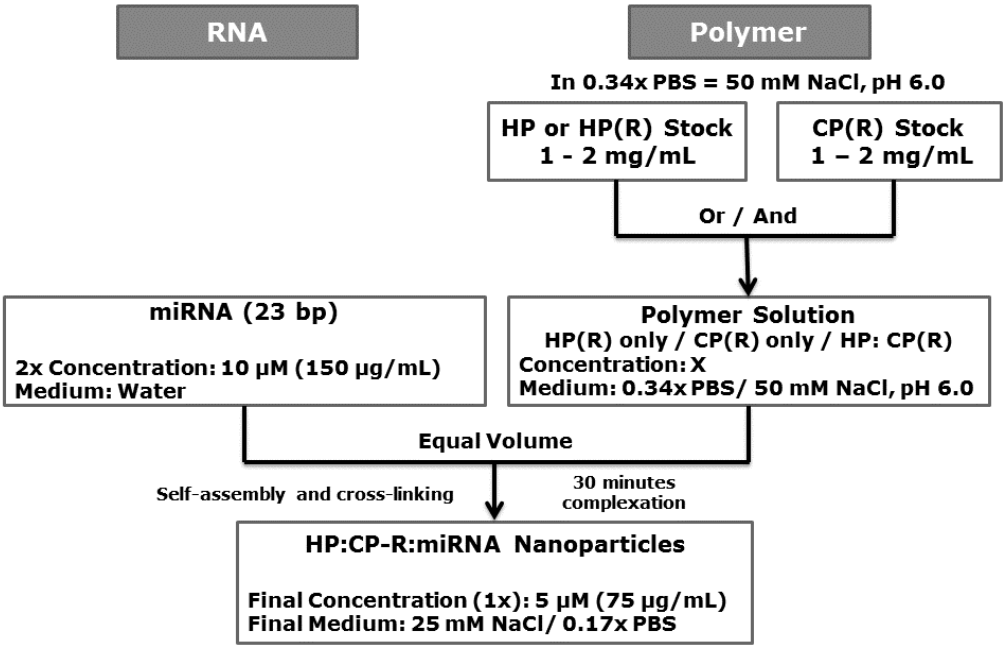

Figure 3-9: Polyplex preparation [Salt in polymer approach].

The polymer solution was prepared in 2x complexation buffer (0.34x, 50 mM PBS, pH 6.0) and miRNA (2x) in diluted with Milli-Q water. Both these solutions were mixed in equal proportions to obtain optimal complexation condition (1x) which would be ideal for polyplex formation.

Previously, Aljaeid[274] and Danish[275] used 5 mM NaCl during the complexation step for PAA polyplex formation. The ionic concentration used by them were adapted from the work reported on polyelectrolytes by Kabanov *et al*[316] but was not formally optimized for these set of PAA-polymers. The present optimization indicated that miRNA-PAA interaction was improved when using slightly higher ionic concentration (25 mM NaCl) for complexation and the pH was defined as pH 6.0.

3.4.3.1 Ionic Concentration and Polymer-miRNA interaction

The ionic concentration required for maximal miRNA-PAA binding at a fixed polymer RU to RNA nucleotides mol/mol ratio (RU/Nt - 1:1) was studied by varying the salt concertation from 0 mM to 600 mM, at pH 7.4. Briefly, the polymer solution was prepared and pH was set to pH 7.4. Appropriate amounts of salt solution were added to the miRNA solution and mixed with polymer. After a 30-minute incubation, the complexes containing 500 ng of miRNA were subjected to gel retardation assay, as described in **3.3.3** (page: 76).

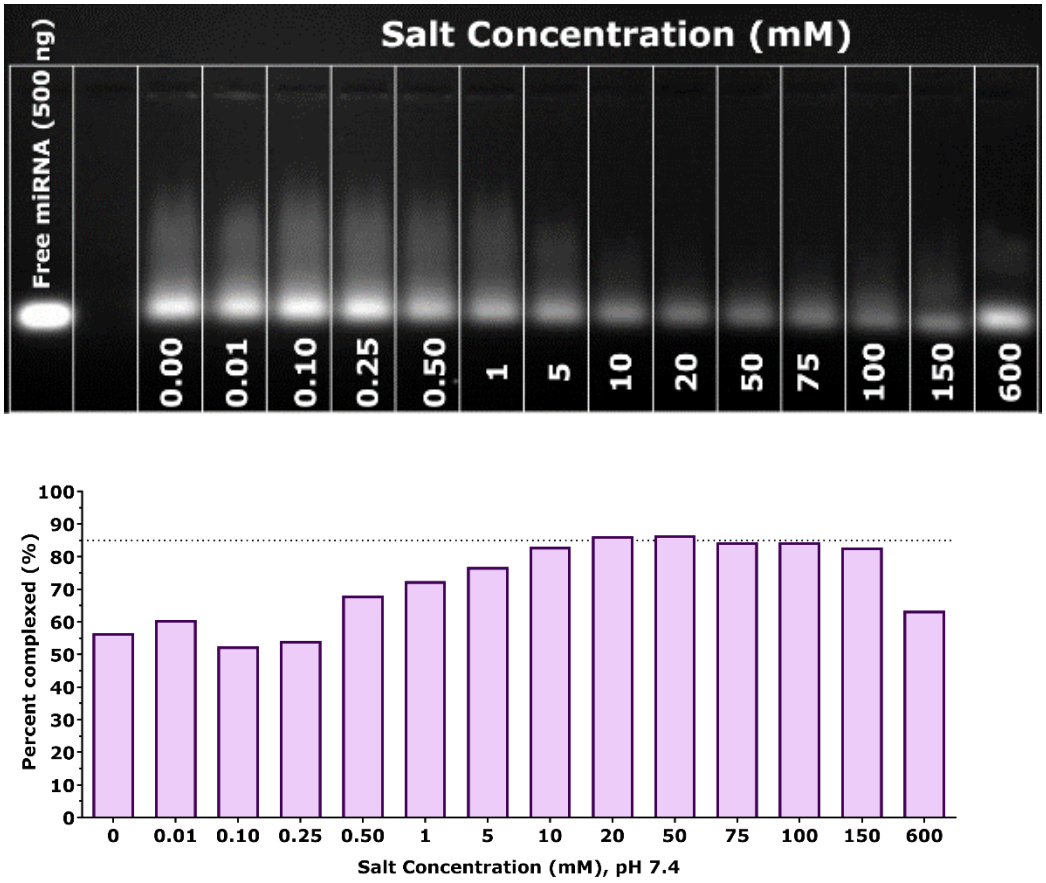

Figure 3-10: Effect of salt concentration on HP-miRNA interaction.
RU/Nt ratio 1:1; pH 7.4. **Top image** represents the fluorescence image of agarose gel while the **Bottom graph** represents the percentage of microRNA fluorescence diminished compared to the free microRNA (Lane 1 from left). Percentage complexed miRNA = 100 – Percentage of free miRNA in each sample. (N = 1, n = 1).

Polymer-miRNA interaction at low salt concentrations (0 – 1 mM NaCl) produced three different species as indicated by the gel [**Figure 3-10** (page: 86)], (a) free miRNA, (b) low molecular weight soluble complexes (intermediate

streaks), and (c) traces of large molecular weight negatively charged complexes (fluorescence in the wells). The intermediate streaks became fainter as the salt concentrations increased [1 to 20 mM NaCl] indicating the reduction of loose soluble complexes. Tight PAA-miRNA binding was observed between 5 and 150 mM NaCl, as indicated by the reduced fluorescence in those lanes due to exclusion of ethidium bromide from miRNA.

The percentage of miRNA complexed with the polymer increased from 56.6 % (0 mM, NaCl) to 76.9 % (5 mM) and 86.3 % (20 mM) in the presence of sodium chloride. A small amount of salt can improve the complex formation between oppositely charged polymers (here PAA and miRNA) by reducing the electrostatic interactions, which in turn favours easier polymer chain rearrangement and adapting flexible polymer conformations for optimal binding[317-319]. Maximum binding was observed between 20 – 50 mM salt concentrations. Hence, 25 mM NaCl was decided as a minimum salt concentration to be used for further complexation studies to obtain maximum and effective miRNA loading into the complexes.

3.4.3.2 Effect of pH on PAA-miRNA interaction

To find the optimal miRNA-PAA binding pH, the polymer was dissolved in 50 mM NaCl and set to required pH between 3.0 and 11.0. The complexes were formed by mixing the polymers with miRNA at a fixed RU/Nt ratio (1:1) and analysed by gel retardation assay, **Figure 3-11** (page: 88).

The maximum binding occurred between pH 6 – 7, **Figure 3-11** (page: 88). In the present polymer system, the crosslinking can occur through two different chemistries, thiol-thiol (SH ←→ SH) and thiol-dithiopyridine (SH → SSPy). Both these reactions can occur between pH 4 – 8, while the optimal pH for thiol-thiol oxidation is between pH 6.5 - 8.0 and pH 4.0 – 5.0 for the latter[320]. Hence, pH 6.0 was selected for further studies as it favoured maximal miRNA binding and expected to support both crosslinking chemistries.

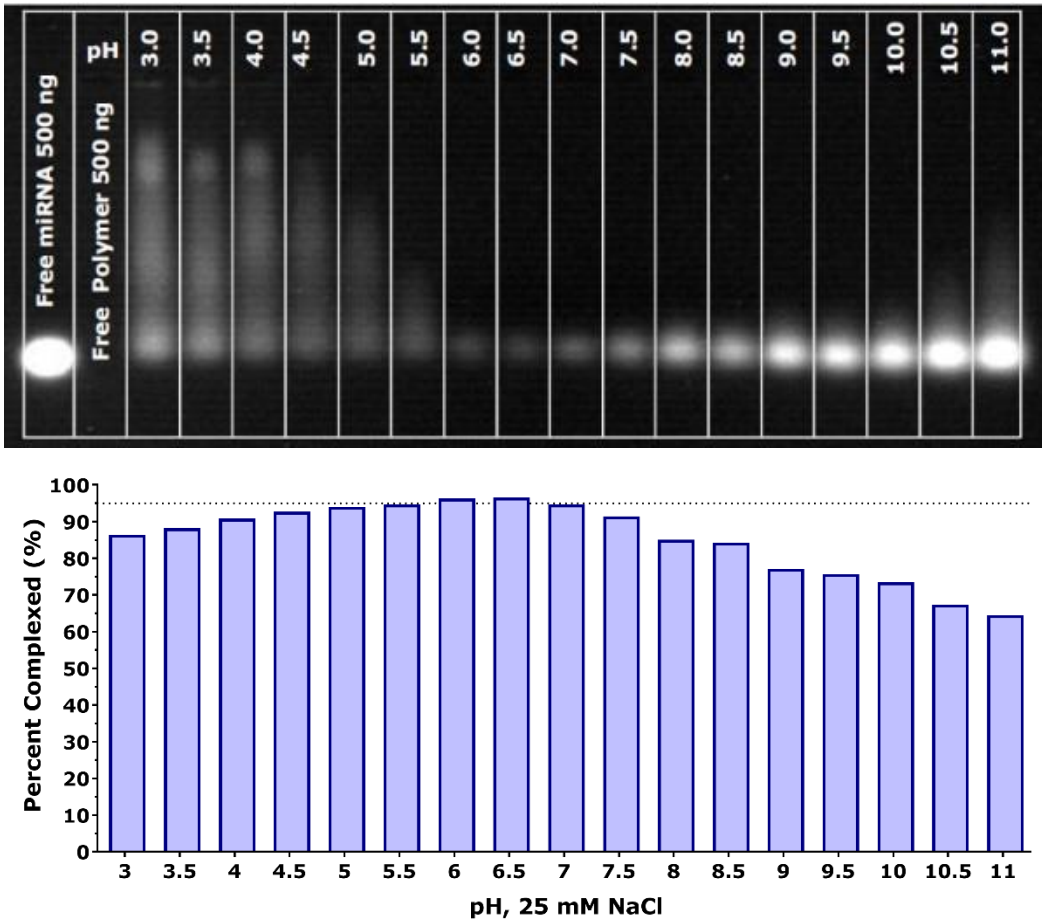

Figure 3-11: Effect of pH on PAA-miRNA binding.

Top image: Agarose gel image indicating microRNA fluorescence. **Bottom image:** The graph represents the percentage of fluorescence lost in each lane compared to free miRNA (100%). Percentage complexed miRNA = 100 – Percentage free miRNA in each sample. (N = 1, n = 1).

3.4.3.3 Selection of Optimal Buffering Agent

As pH seems to be a critical parameter which could not only influence ionic interaction between miR and PAA, but it can also affect cross-linking. Although the polycationic polymers intrinsically possess some buffering capacity, the complexes would be prepared in very dilute solutions of polymer, and hence using a buffering agent in the polymer solution was expected to be beneficial. To select a suitable buffering ion, five different buffering agents (Phosphate, Citrate, Carbonate, PIPES and MES) were chosen that had buffering capacities spanning between pH 6 and 7. Polymer was dissolved in each buffer (50 mM buffering ion, without NaCl) and the pH was adjusted to pH 6, 6.5 and 7. The

complexes were formed by mixing the polymer solution with miRNA at a fixed RU/Nt ratio (1:1) and the complexes were analysed on agarose gel.

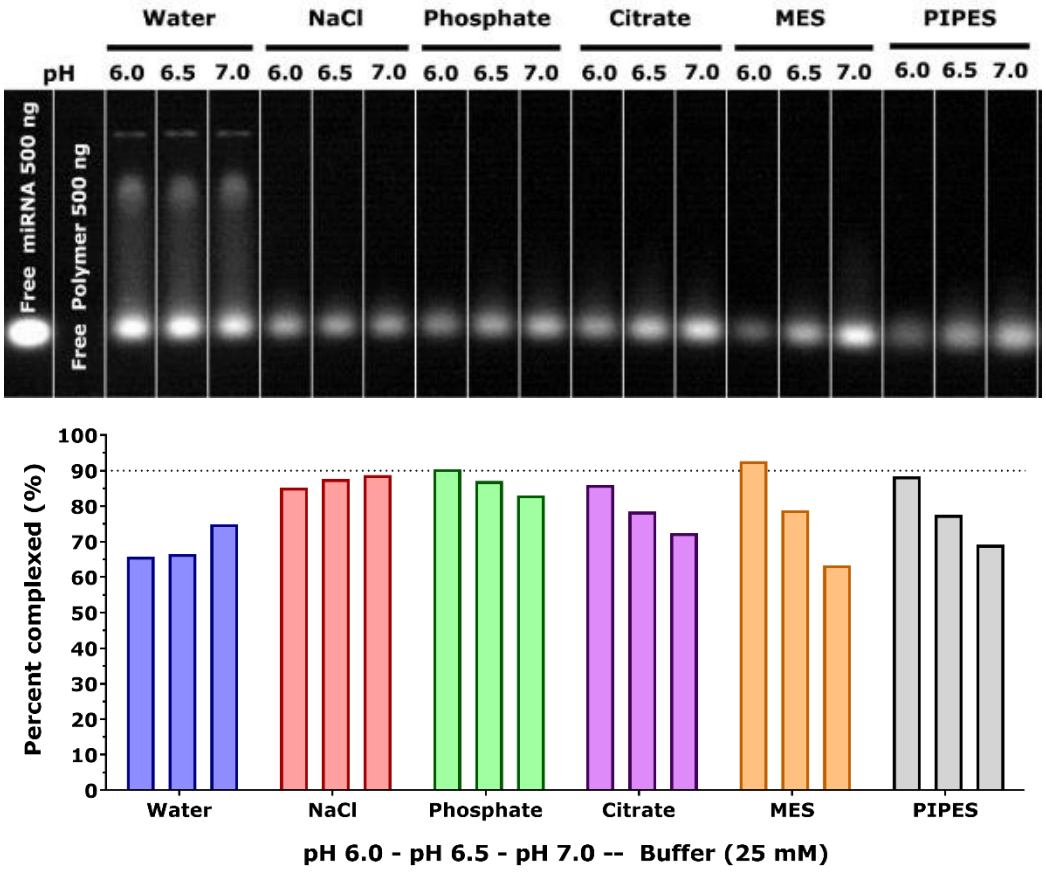

Figure 3-12: Buffering agents and PAA-miRNA interaction.
Percentage complexed miRNA = (100 – Percentage of free miRNA in each sample).

Phosphate buffer and NaCl provided better binding of polymer to the miRNA and minimal pH dependent variation compared to other buffering agents, **Figure 3-12**. Hence, a combination of NaCl and phosphate would be an appropriate choice for miRNA-PAA complexation.

Phosphate buffered saline (1x PBS) is a widely used physiological buffer containing NaCl (138 mM), KCl (1.8 mM) and phosphate (10 mM). Hence, low concentration PBS (0.165 x) corresponding to 25 mM NaCl could serve as an ideal PAA-miRNA complex preparation medium.

3.4.4 Buffering Range of HP

High buffering capacity polymers trapped in endosomes resist endosomal pH change[321]. This induces continuous inflow of H^+ ions (along with water molecules) in an effort to acidify the late-endosomal compartment resulting in osmotic swelling and rupture of late-endosome, which is commonly known as the proton-sponge effect[322]. High buffering capacity of PEI[321,322] and chitosan[323] between the physiological pH (pH 7.4) and late-endosomal pH (pH 5.5) is known to trigger endosomal escape by this mechanism yielding higher transfection efficiency[322]. Hence, the buffering capacity of HP was studied by acid-base titration, **Figure 3-13**, page: 90. The titration curve of HP indicated that the polymer had a very broad buffering range (pH 3.25 – pH 10.5) like PEI[321,323]. The pKa values for p(MBA-DMEDA) has been previously calculated as pKa_1 8.1, pKa_2 4.5[324,325].

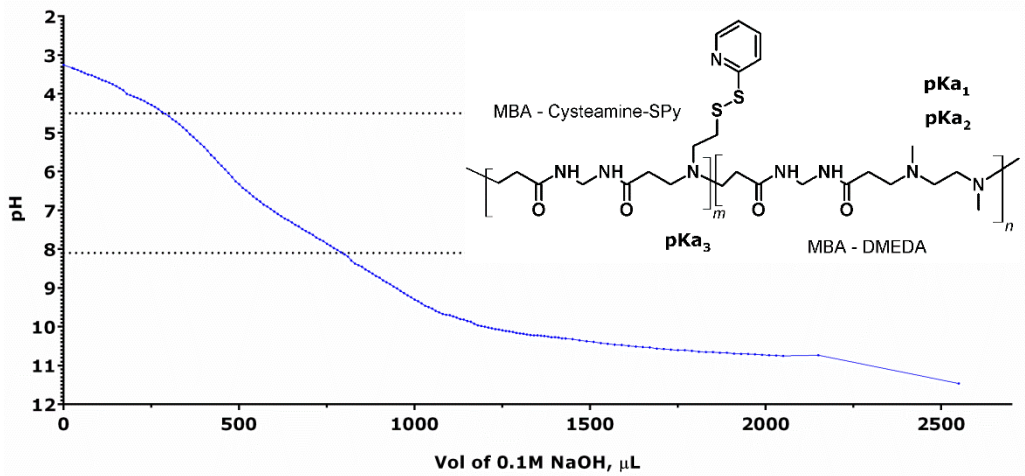

Figure 3-13: Titration Curve of HP in 1 mM KCl.

The horizontal lines represent previously calculated pKa value of p(DMEDA-MBA) polymer, NG30[324]. The insert image shows the structure of HP with possible ionisable tertiary amines[13]. (N = 1, n = 1).

3.4.5 Two component systems

In order to select suitable miRNA-PAA polyplexes, initially two-component complexes were prepared by mixing one polymer and miRNA at different RU/Nt ratios (Polymer Repeating Unit/ RNA Nucleotide, mol/mol ratio). Gel retardation assay provided two key information, a) percentage of miRNA complexed with the polymer and b) presence of free polymer. Subsequently, the size of the polyplexes were determined from DLS measurement.

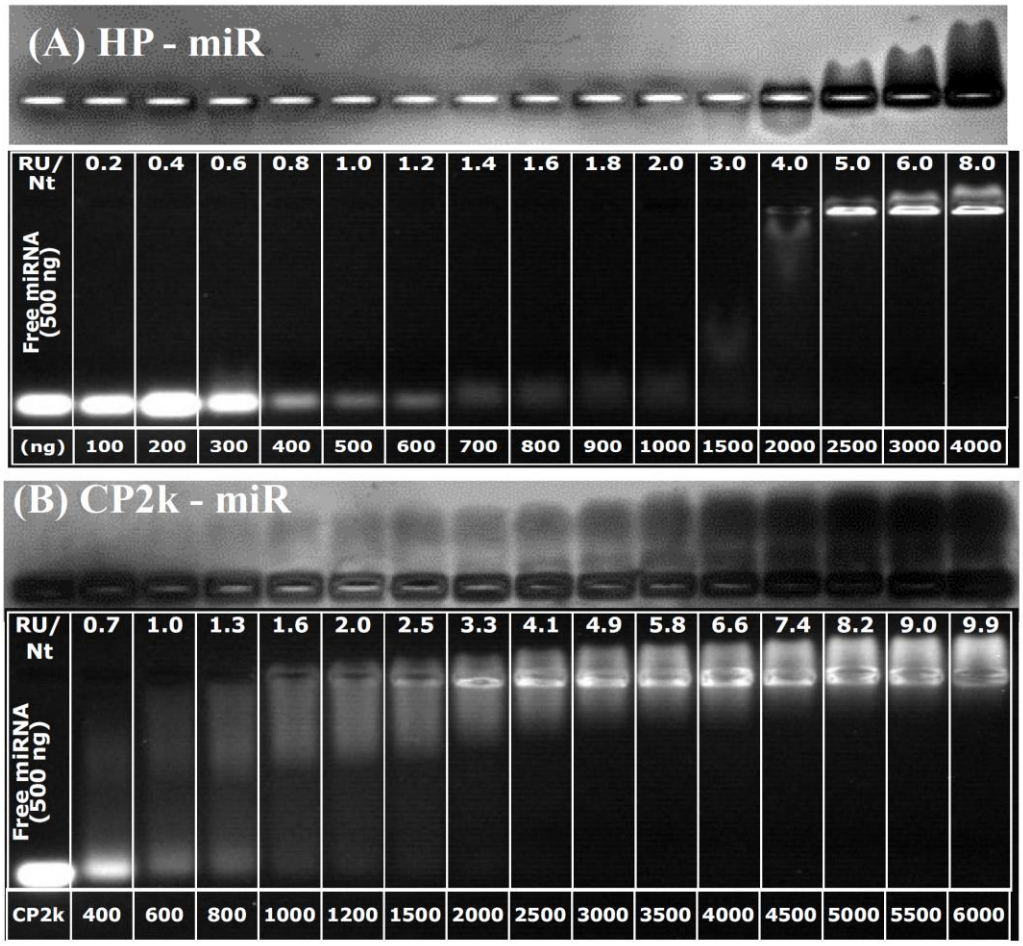

Figure 3-14: Agarose gel assay of HP-miR and CP2k-miR complexes.
(A) HP-miR; **(B)** CP2k-miR, two component complexes; In each image, the top panel represents coomassie blue staining for the polymer and the bottom panel represents the fluorescence image of ethidium bromide stained gel detecting the miRNA.

For non-PEGylated HP [**Figure 3-14, A** (page: 91)], and PEGylated CP2k [**Figure 3-14, B** (page: 91)], the complexation percentage was similar, **Figure 3-15 mol/ mol Ratio Plot (**page: 92**)**. Almost 90% of the microRNA was bound to these polymers at RU/Nt ratio 1:1, while complete complexation (~100%)

occurred at RU/Nt ratio 5:1. This indicated that the PEG chains (1700 Da x 2) on CP2k did not interfere with miRNA accessing the PAA chain (~14 kDa). When the mass ratios were compared, CP2k required relatively higher mass than HP for equivalent complexation because of the mass contribution from the PEG chains, **Figure 3-15, Summary Plot** (page: 92). The miRNA fluorescence pattern created was not similar to HP. CP2k-miRNA complexes produced a distinctive fluorescence immediately above and below the wells while this was not observed with HP. The length and intensity of the smear on the cathode side of the gel diminished with increasing RU/Nt ratio.

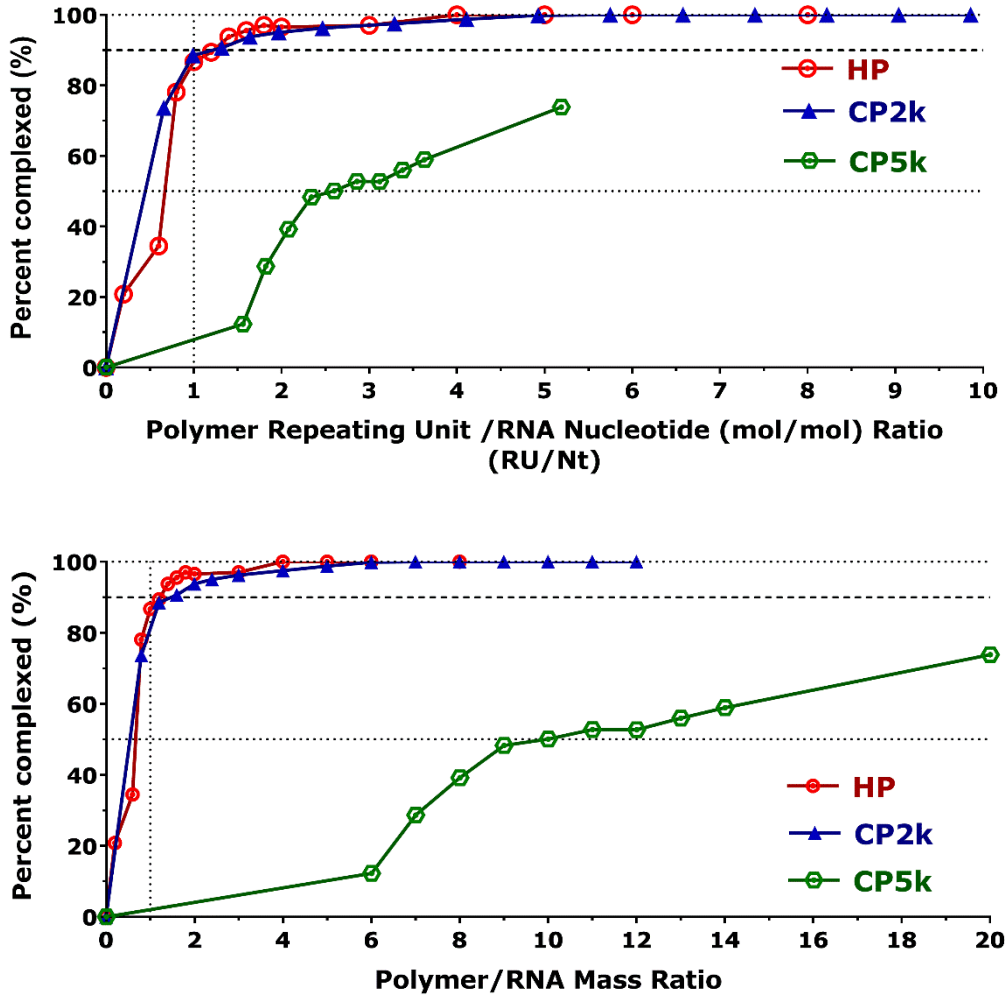

Figure 3-15: Percentage miRNA complexation with individual polymers.

Top Plot: Represented in (RU/Nt ratio) Polymer RU to RNA nucleotide (mol/mol) ratio. **Bottom plot:** Presented by Polymer to RNA mass ratio. Two component complexes of HP-miR, CP2k-miR and CP5k-miR complexes were prepared in 25 mM PBS, pH 6.0 (salt in polymer). (N = 1, n = 1).

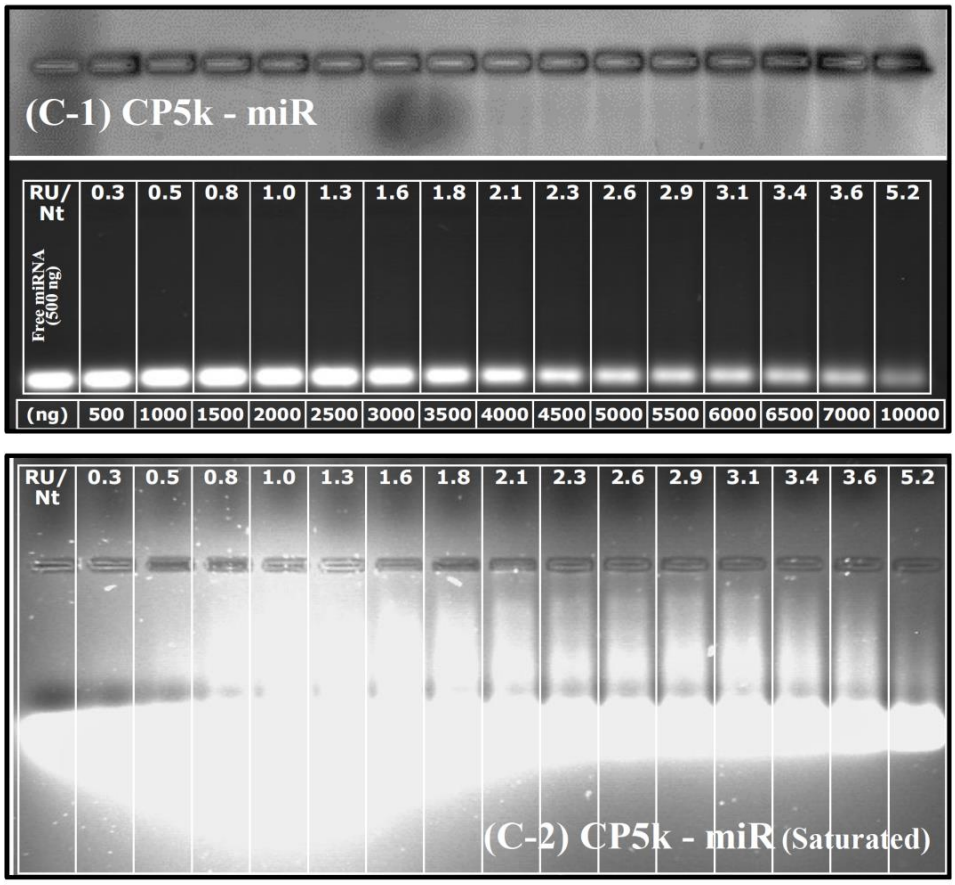

Figure 3-16: Agarose gel assay of CP5k-miRNA complexes.

C-1 - normal exposure; Top panel: Coomassie staining for the polymer detection; Bottom panel: Ethidium bromide staining for miRNA detection; intermediate complexes only visible when the gels were exposed for extended time, **C-2**.

For the PEGylated CP5k [Gel images in the **Figure 3-16** (page: 93), and Summary Plot in the **Figure 3-15** (page: 92)], only 75% of the miRNA was complexed at RU/Nt ratio 5:1 indicating poor miRNA binding due to the short PAA chain (3100 Da) of the polymer. Also, this experiment indicates that miRNA did not bind to the PEG chains which are 77% of this polymer. The image taken with longer exposure time revealed weaker binding indicated by the presence of loose soluble complexes distributed in between the free miRNA band and the wells, **Figure 3-15, C2** (page: 92). Coomassie staining did not stain the polymer efficiently also because of the short PAA chain.

Taken together, the gel images showed clear differences in the miRNA complexation behaviour among different polymers. Complete complexation (~100%) occurred around RU/Nt ratio 5:1 for HP and CP2k, but not for CP5k.

More than 90% of the miRNA was bound to the HP and CP2k at RU/Nt as low as 1:1 ratio.

3.4.5.1 HP(R)-miRNA Two-component Polyplexes

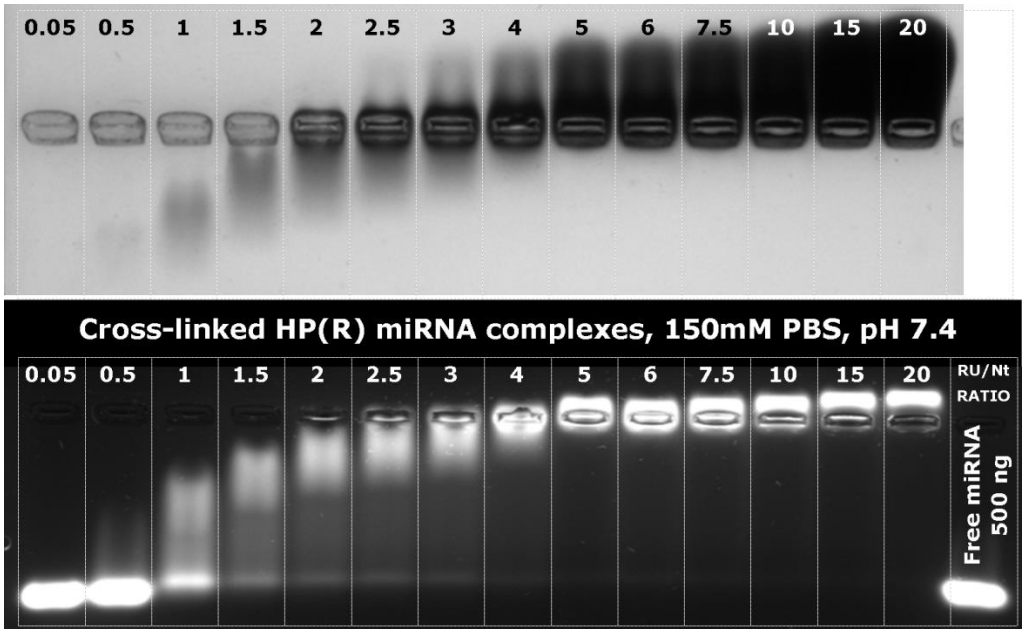

Figure 3-17: Agarose gel analysis of HP(R)-miRNA complexes.

Complex formation at 150 mM PBS, pH 7.4. Top: Coomassie staining; Bottom: Ethidium bromide staining (saturated image).

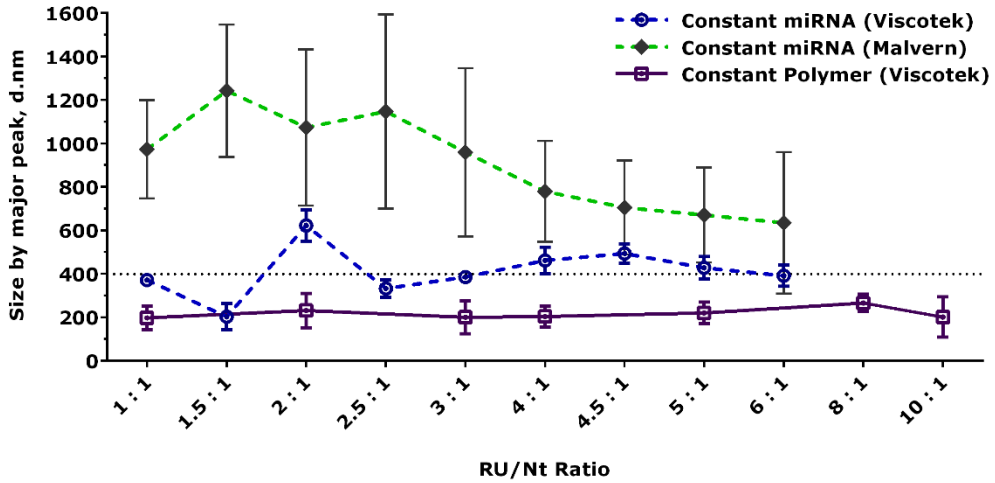

Figure 3-18: Size analysis of HP(R)-miRNA complexes (salt in polymer).

Constant miRNA concentration (final concentration - 2.5 µM, 38 µg/mL) and constant polymer (final concentration ~ 300 µg/mL). The graph represents size from the major peak. The error bar for "Malvern" represents Pdi width (overall sample size distribution), while the error bar from Viscotek represents standard deviation of individual peak (SD). N = 1, n = 3.

For two-component HP(R)-miRNA polyplexes, sufficient miRNA binding (> 90%) was achieved at RU/Nt ratio 1:1 or 1.5:1 depending on the complex-forming condition, optimal **[**data not shown, but similar to **Figure 3-14, a** (page: 91)] or physiological condition [**Figure 3-17** (page: 94)]. When the RU/Nt ratio was greater than 2:1, no differences in miRNA complexation was observed on gel when comparing optimal and physiological salt concentrations [25 mM NaCl, pH 6.0 versus 150 mM NaCl, pH 7.4]. Excess polymer started to appear after RU/Nt ratio 4: 1.

HP(R)-miRNA polyplexes were prepared at different RU/Nt ratios 1:1 to 10:1, either by fixing the initial miRNA concentration (5 µM or 76 µg/mL) or initial polymer concentration (~ 600 µg/mL). The final complexes were obtained by mixing equal volume of polymer and miRNA, hence the half concentrations of miRNA and polymer were half the initial concentrations. The size of these complexes were analysed by DLS, **Figure 3-18** (page: 94).

The samples prepared by fixing miRNA concentration were analysed by Malvern and Viscotek DLS instruments. Both the instruments produced very different size profiles for the same samples. The size data obtained from Viscotek was smaller than the size data obtained from Malvern. At all RU/Nt ratios, Viscotek reported hydrodynamic diameter was around 400 nm, while Malvern reported between 500 and 1200 nm. Due to practical difficulties (availability of ultra-low volume cuvette, 12 – 15 µL), all the other measurements in this chapter were performed only on Viscotek DLS instrument.

For the samples at RU/Nt ratio 1:1 to 3:1, the quality of size data obtained were not good due to low scattering indicating dilute sample concentrations. As the microRNA concentration was constant in all the samples, the increase in scattering at higher RU/Nt ratio must be due to increase in the polymer concentration. Good scattering was observed when polymer concentration was above 250 µg/mL (RU/Nt 4:1). This concentration is 25 times higher than the minimum sample concentration recommended (0.01 mg/mL) for 100 – 1000 nm particles, for DLS measurements[310]. This could be either due to the formation of loose complexes or these complexes inherently scatter less light.

When the final concentration of the polymer was kept constant around 300 µg/mL, sufficient scattering and good quality data was obtained for all the RU/Nt ratios tested (1:1 to 10:1). Hence, this indicates that the PAA-miRNA complexes require high polymer concentrations to obtain sufficient scattering by DLS. Surprisingly, the size of the polyplexes obtained were constant around 200 - 270 nm for all the RU/Nt ratios tested. Hence all the RU/Nt ratios from 1:1 to 10:1 were selected for *in vitro* testing. All the samples produced multiple minor peaks indicating polydispersity of the sample. The major peak represented more than 80% of the peak area in all cases. It was expected that more uniform mono-disperse formulations could be achieved by using a mixture of HP and CP.

3.4.6 Three Component PAA-miRNA Complexes

Three component complexes are formed by mixing a homopolymer (HP) and a PEGylated copolymer (CP) with a nucleic acid molecule. This kind of system permits varying the amount of PEG and thiol ratios by simply varying the HP:CP ratio.

3.4.6.1 HP – CP2k(R) Complexes

The polymer blends were prepared by mixing homopolymer [HP] and reduced-copolymer [CP2k(R)] in three different HP: CP ratios, 3:1, 1:1 and 1:3. HP: CP ratio is the mol/mol ratio of PAA RU. Once the polymer blends were prepared, they were added to miRNA in appropriate concentrations to obtain different polymer PAA RU to RNA nucleotide mol/mol ratio (RU/Nt).

The aim was to select conditions where there was maximum miRNA binding (>90 %) with minimum excess free polymer in the complexation mixture to minimize toxicity issues arising from free polymer.

Maximum complexation was seen for HP: CP ratio of 1:3 followed by 1:1 and 3:1. At all polymer blend ratios, greater than 90% complexation was observed above RU/Nt ratio of 3:1 and free polymer started to appear at this ratio.

It would be desirable to have a large number of PEG chains (HP: CP 1:3) on the surface of the nanoparticles to increase their stability while more PEG coverage might reduce the cellular uptake. Hence, to achieve nanoparticles with a lower surface PEG density, HP: CP ratio 1:1 or 3:1 could be used.

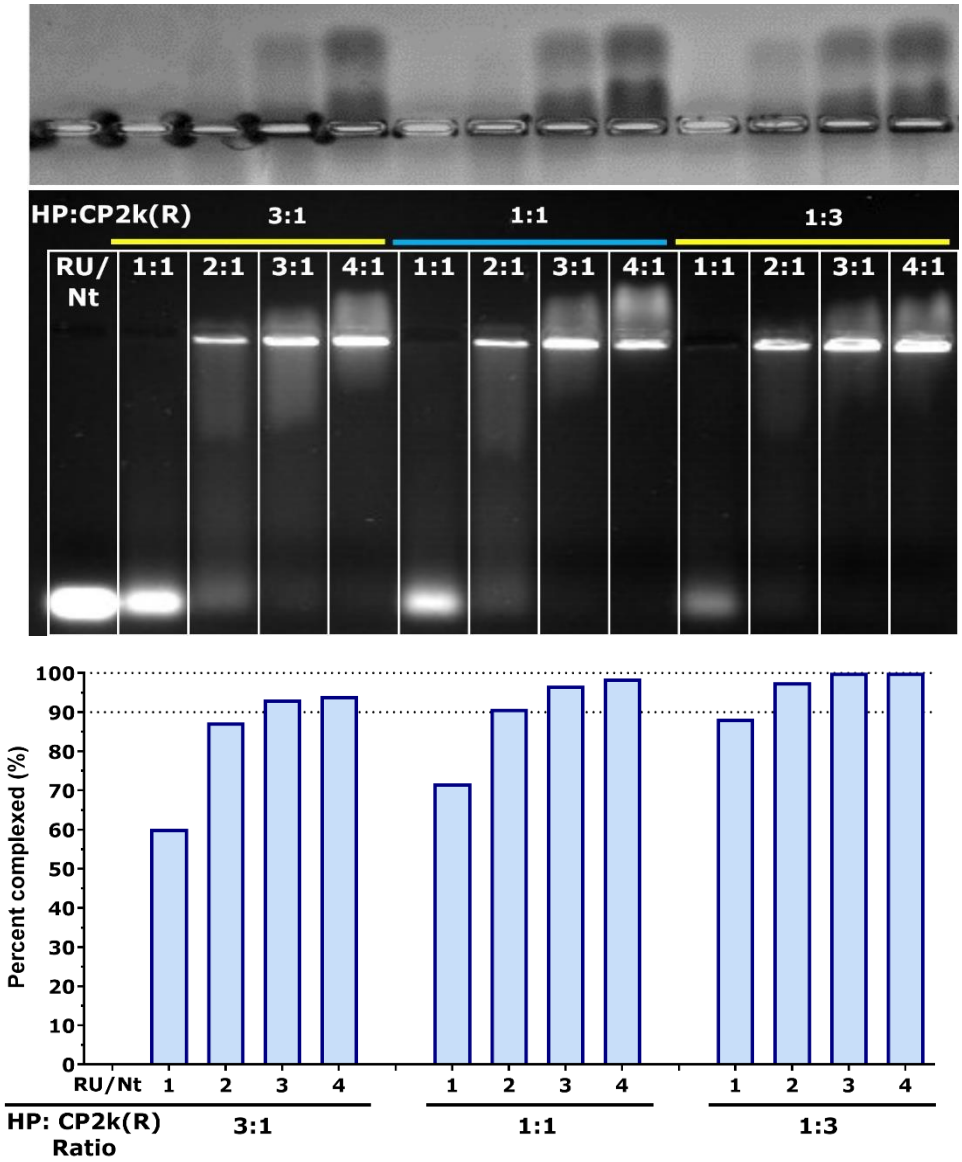

Figure 3-19: Agarose gel analysis of HP:CP2k(R):miRNA complexes.

Left: Agarose gel stained with coomassie blue (top) or ethidium bromide (bottom); **On right:** Summary plot representing percentage miRNA complexed under the tested conditions. (25 mM PBS, pH 6.0). N= 1, n = 1.

All the formulations produced multiple peaks indicating the polydisperse nature of the complexes. However, presence of one major peak around 200 nm was observed for all the formulations. Almost all other peaks represented smaller species (< 200 nm). All of these complexes were selected for *in vitro* testing, [For the summary of list of complexes, see supplementary data, **Table 3-5** (page: 120)].

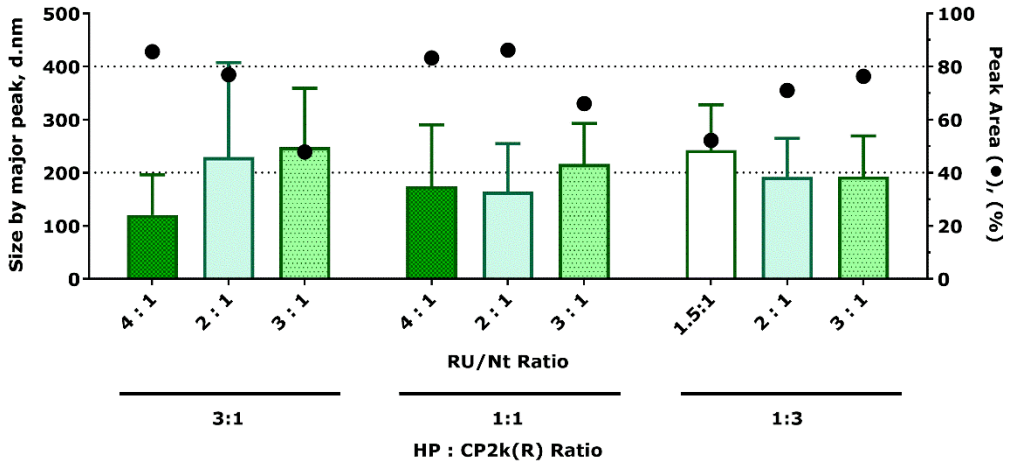

Figure 3-20: Size Analysis of HP:CP2k(R) polyplexes (salt in polymer).

HP: CP Ratio is presented on the X-axis. The size of the nanoparticles is represented by bar chart (Left-Y-axis); all the measurements produced more than one peak. The percentage of each peak is represented by dot plot along the Right-Y-axis. Different RU/Nt ratios were tested. The complexes were prepared and measured in 25 mM PBS, pH 6.0. Instrument: Viscotek DLS802. N = 1, n = 3.

3.4.6.2 HP – CP5k(R) – miRNA complexes

The polymer blends were prepared by mixing the homopolymer [HP] and reduced-copolymer [CP5k(R)] in three different HP: CP ratios, 3:1, 1:1 and 1:3. HP: CP ratio is the mol/mol ratio of PAA RU. Once the polymer blends were prepared, they were added to miRNA in appropriate concentrations to obtain different polymer PAA RU to RNA nucleotide mol/mol ratio (RU/Nt).

The complexation studies conducted between HP and CP5k(R) revealed the opposite behaviour to that of HP and CP2k(R). As the amount of PEGylated CP5k increased in the polymer blend to 1:3, the complexation with miRNA reduced probably due to the short PAA chain which is unable to complex efficiently with miRNA as observed previously with CP5k alone (**Figure 3-16**, page: 93).

When the size of the complexes was analysed by DLS, all formulations with RU/Nt ratio above 2: 1 produced good complexes indicated by the presence of one major peak (peak area > 98%). The size of the complexes was around 300 nm for most of the formulations, **Figure 3-22** (page: 100). All of these complexes were selected for *in vitro* testing, [For the summary of list of complexes, see supplementary data, **Table 3-6** (page: 120)].

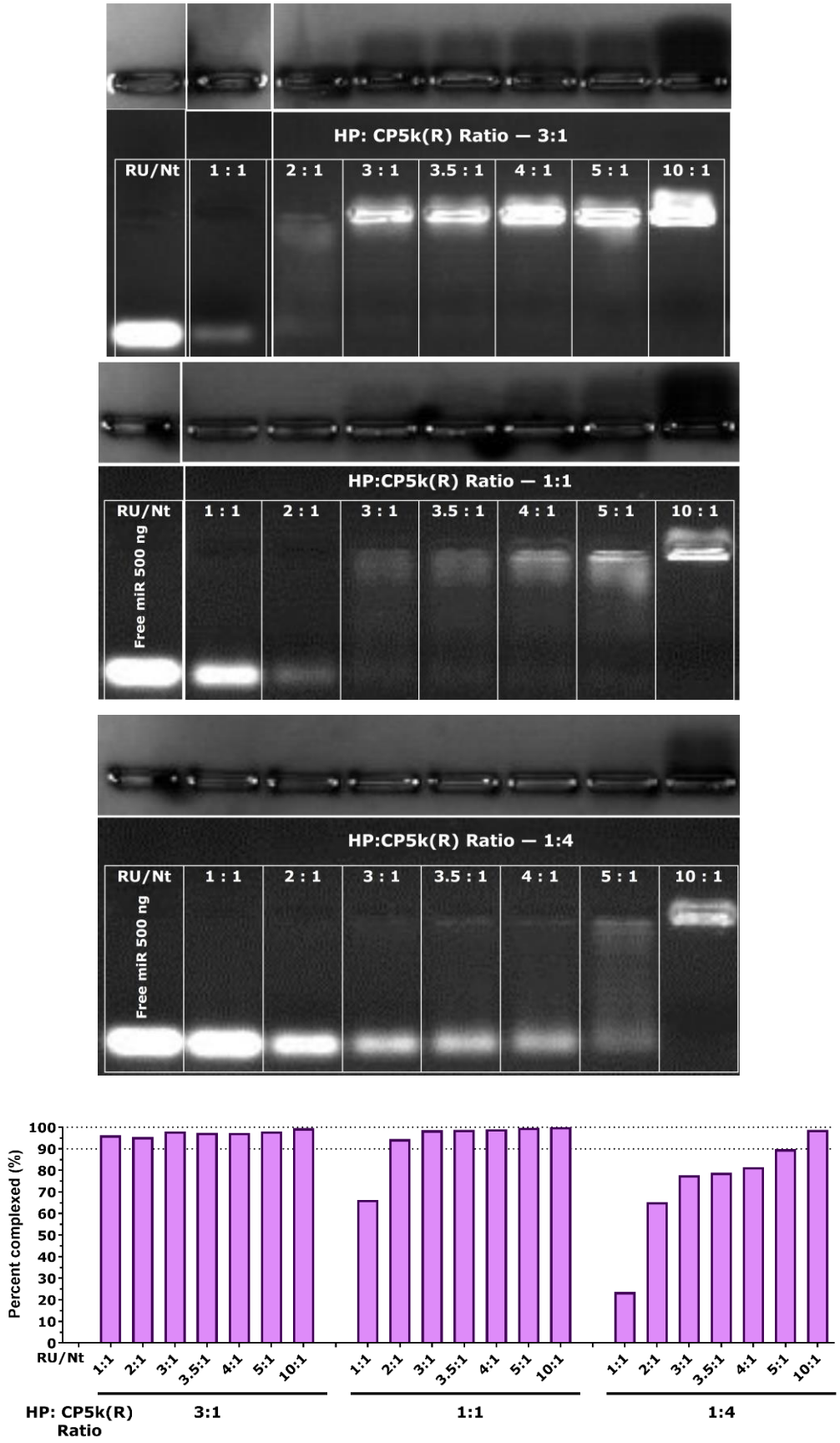

Figure 3-21: Agarose gel analysis of HP:CP5k(R):miRNA complexes.

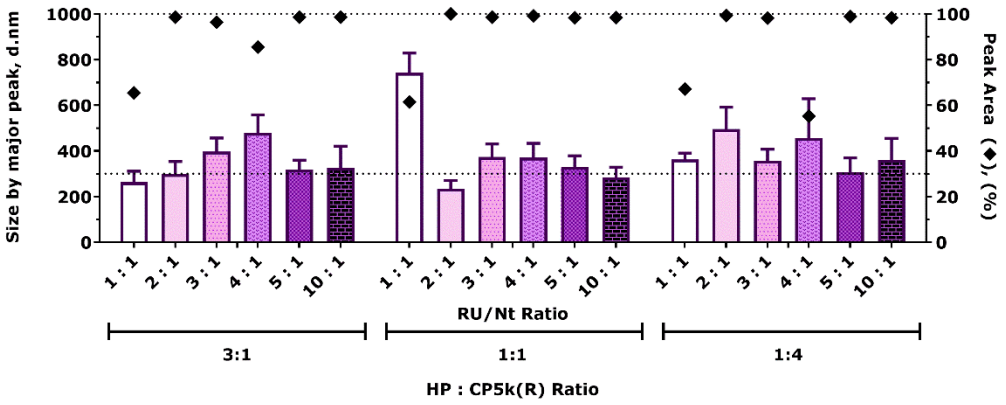

Figure 3-22: Size Analysis of HP: CP5k(R) complexes (salt in polymer).

HP: CP Ratio is presented on the X-axis. The size of the nanoparticles is represented by bar chart (Left-Y-axis); The percentage of each peak is represented by dot plot along the Right-Y-axis. Different RU/Nt ratios were tested. The complexes were prepared and measured in 25 mM PBS, pH 6.0. Instrument: Viscotek DLS802. N = 1, n = 3.

3.4.7 *In vitro* Uptake of miRNA Nanoparticles (2D vs 3D)

In the previous section, several combinations of homopolymer, copolymer, miRNA complexes were prepared. The ability of a delivery system to functionally deliver miRNA or siRNA to cells depends on several factors, like high cellular entry, sufficient endosomal escape and the ability of the complexes to release the nucleic acid from the polymer in the cytoplasm. In this section, the cellular uptake of few of the PAA-miRNA complexes were tested. The complexes were selected based on its ability to effectively complex miRNA (complexation efficiency > 90%); the complexes that have no or minimal free polymer; As the size of the complexes measured by DLS (Viscotek) did not vary across formulations except at very low RU/Nt ratios, representative nanoparticles that satisfied the above two conditions were selected for cellular uptake. Uptake was tested in both 2D- and 3D- cell culture models of U87MG cells. A fluorescent miRNA (miR-Dy547) was used for the preparation of these complexes. The cells were treated in the absence of serum (OptiMEM medium). The nucleus was stained with Hoechst 33342. The results from cellular uptake by 2D-cell culture is presented in **Figure 3-23** (page: 101) and 3D-cell culture is presented in **Figure 3-24** (page: 103).

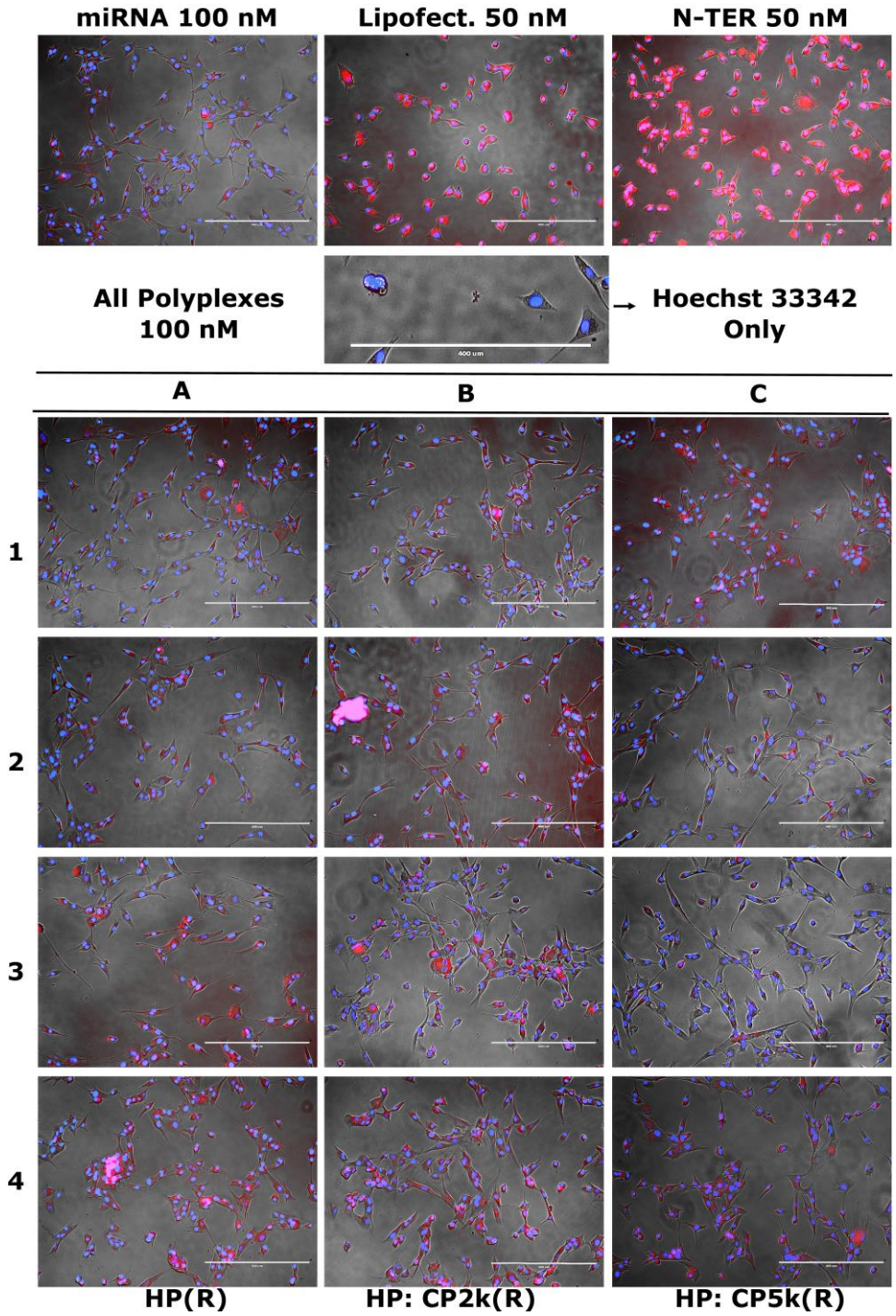

Figure 3-23: Uptake of polyplexes by U87MG cells in 2D cell culture.
Each image represents a bright field image of cells overlaid by blue fluorescence from Hoechst 33342 (Nucleus) and red fluorescence from miRNA labelled with Dy547. Images from **A1 to A4** represents crosslinked HP(R) complexes with RU/Nt in the following order 1.5:1, 3:1, 5:1, 10:1. **B1** and **B2** represents HP: CP2k(R) complexes (HP: CP ratio 3:1) with RU/Nt 2:1 and 4:1, while **B3** and **B4** represents HP: CP ratio 1:3 with RU/Nt 1:1 and 2:1. **C1** and **C2** represents HP: CP5k(R) complexes at HP: CP ratio 3:1 with RU/Nt 2:1 and 3:1, while **C3** and **C4** represents HP: CP ratio 1:1 with RU/Nt 2:1 and 3:1, respectively. Scale bar: 400 µm.

The uptake of crosslinked polyplexes loaded with fluorescent miRNA was tested on U87MG cells, **Figure 3-23** (page: 101). All the complexes were treated at 100 nM miRNA concentration while the positive controls, N-TER and Lipofectamine 2000, were treated at 50 nM as per the manufacturer' recommendations. Both the positive controls showed very high transfection efficiency of which peptide-based N-TER reagent had superior uptake over Lipofectamine (liposomes).

Free miRNA treated at 100 nM seemed to enter the cells on its own, which is consistent with several observations from literature. Although free siRNA and miRNA can enter the cells at low frequency, it is known that they are not functionally active as they are normally degraded, in the endolysosomes, before reaching the cytoplasm. Another reason for observed fluorescence inside the cells could be because of the passive cellular entry of free dye molecule that is released when miRNA is degraded outside the cells by endonucleases.

All the polyplexes [100 nM] showed moderate uptake compared to Lipofectamine and N-TER reagents (50 nM). Among the polyplexes tested, HP(R) with RU/Nt ratio 5:1 and 10:1 showed better uptake [**Figure 3-23** (page:101), **A3** and **A4]**, which is consistent with previous observations with non-crosslinked homopolymer [NG49] at the same RU/Nt ratios that showed higher DNA transfection efficiency[296]. All the tested HP: CP2k formulations (**B1 to B4**) seemed to be taken up by cells compared to only a few HP: CP5k formulations (**C1** and **C4**) which may be because of the large PEG chain reducing nanoparticle uptake. However, no noticeable differences could be seen among the better performing polyplexes.

In general, the fluorescence seemed to accumulate in clustered cells compared to individual cells [**Figure 3-23** – **A4, B2** and **B3** (page: 101)**]**. Hence, the uptake of polyplexes in 3D spheroid culture was also tested, **Figure 3-24** (page: 103). It was also previously known that cellular uptake of nanoparticles differs between 2D and 3D cell culture models depending on the cell population[326], nanoparticle type and its surface properties[326,327]. Dose dependant increase in miRNA fluorescence was observed in all the formulations tested. The cellular uptake was better in 3D cell culture compared to 2D cell culture, based on

fluorescence intensity. However, the observed fluorescence represents only the fluorescence from the surface of spheroids (maximum 20 µm deep[328], whereas the diameter of the spheroid was about 500 µm), while the ability of these nanoparticles to penetrate the interior of these spheroids was not investigated.

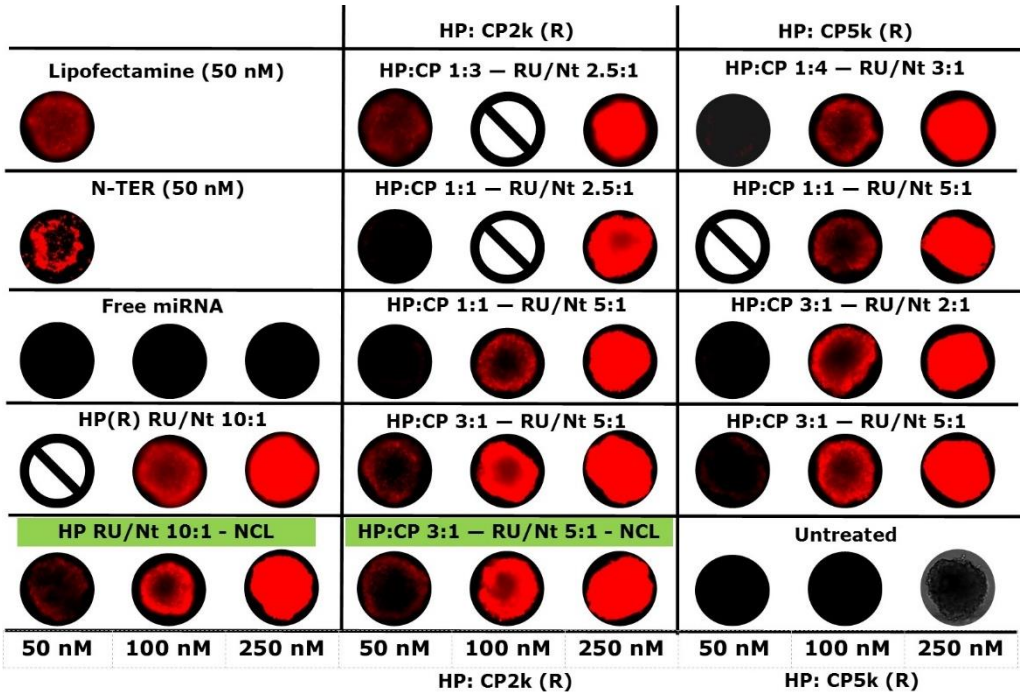

Figure 3-24: Uptake of polyplexes by U87MG cells in 3D cell culture.

The image of spheroids represents only the red epifluorescence from the Dy547 labelled miRNA. Black wells indicate no fluorescence in the red channel while the "slashed circle" indicates the loss of spheroid during sample preparation. The concentration of miRNA-polyplexes tested were 50, 100 and 250 nM as indicated below the image. The positive controls were tested only at 50 nM concentration. All the polyplexes tested were crosslinked, except those highlighted in green (NCL – non-crosslinked). Diameter of spheroids ~ 500 µm. HC represents HP: CP polymer RU (mol/mol) ratio, while RU/Nt represents Polymer RU to RNA nucleotide (mol/mol) ratio.

3.4.8 Delayed-toxicity of Free Polymers

Toxicity of free polymer was tested on U87MG cells, **Figure 3-25** (page: 104). In the presence of serum [10 %], none of the polymers reached its LD50 even at the highest concentration tested [1000 µg/mL]. In the absence of serum, most of the polymers only approached its LD50 at 1000 µg/mL polymer concentration. Typically, when treating the cells with miRNA polyplexes [50 – 500 nM, RU/Nt ratio 5:1], the concentration of polymer in medium would be in the range of 4 – 40 µg/mL and hence no or minimal toxicity could be expected from these polymers.

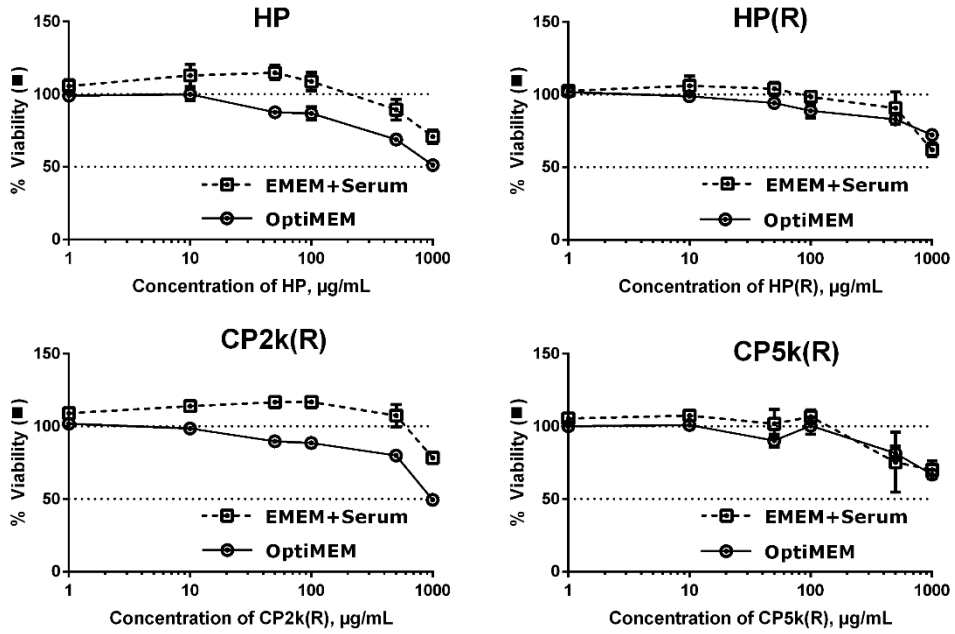

Figure 3-25: Toxicity of free polymers.

U87MG cells were exposed to different polymers for 4 hours either in the presence of serum (EMEM complete medium - dotted line) or absence of serum (OptiMEM – continuous line). The toxicity was measured by MTS assay which was performed 48 hours after polymer exposure, mimicking the transfection assay conditions. This assay measures the "delayed" toxicity of the polymer as the assay was performed 48-hours after the polymer treatment. Acute toxicity can be measured by performing the cytotoxicity assay right after the polymer treatment. (N = 1, n = 3).

3.4.9 Luciferase Knock-down Assay

The PAA-miRNA nanoparticles screened in the previous section were tested for the luciferase knockdown activity by varying the concentration from 50 nM to 690 nM. N-TER and Lipofectamine 2000® were used as positive controls. The optimal miRNA concentration recommended for cell treatment spans between 10 nM to 50 nM. miR-128 delivered using these commercial transfection reagents not only reduced luciferase expression but also induced cell death (~60%). Treatment with negative control miRNA (miR-NC) did not reduce luciferase expression, but showed noticeable toxicity (~75% viability).

None of the PAA complexes tested showed significant difference between miRNA-negative control (miR-NC) and miR-128 treatments, while the toxicity observed was minimal under lower miRNA concentrations as expected from assessing the delayed toxicity of free-polymers (section: 3.4.8, page: 104), [50 nM, **Figure 3-26** (page: 106) and 200 nM, **Figure 3-27** (page: 107)]. The details of statistical tests are provided in the supplementary data, **Table 3-7** (50 nM) (page: 121) and **Table 3-8** (200 nM) (page: 122).

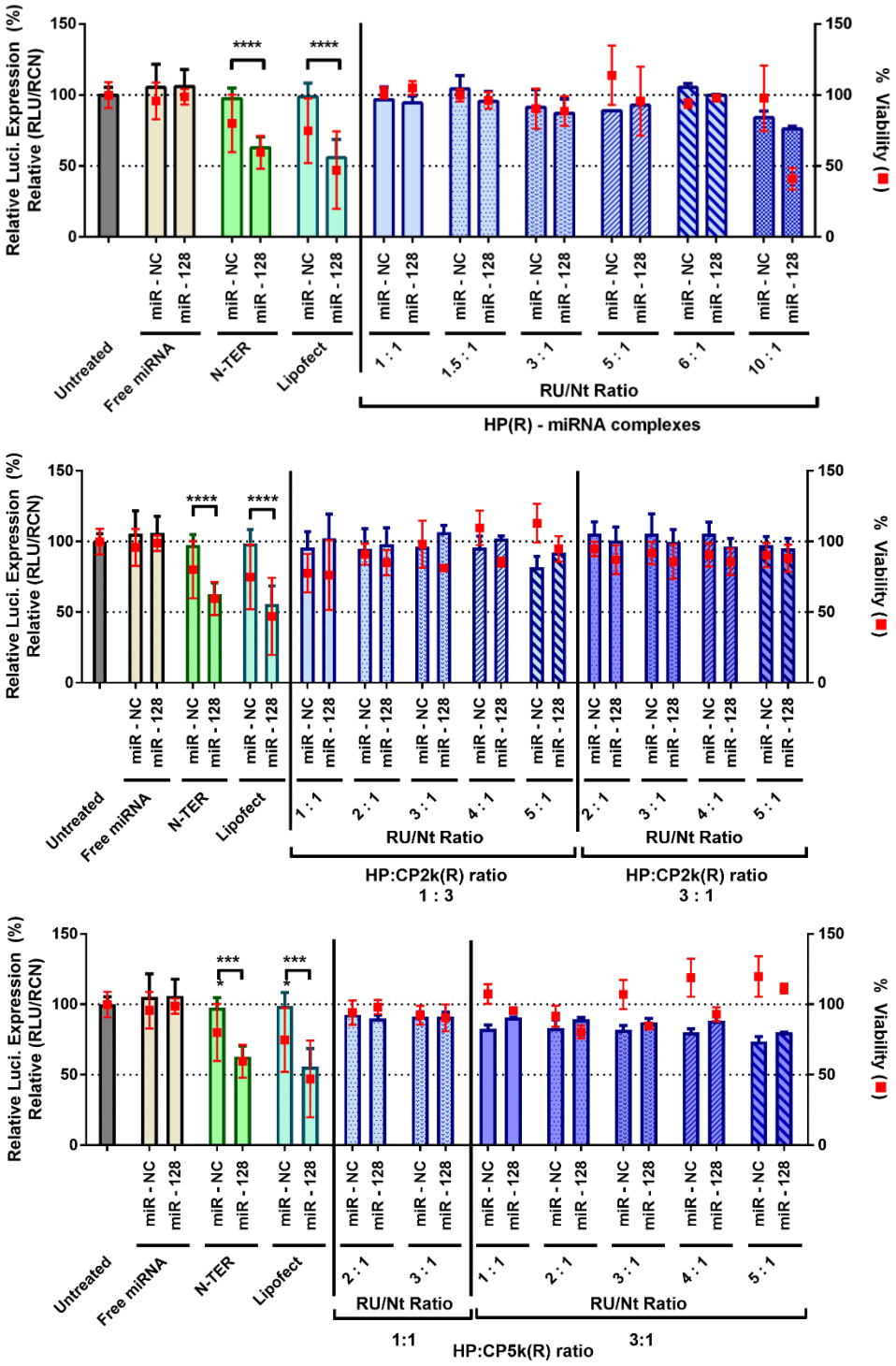

Figure 3-26: Luciferase assay of miRNA polyplexes (50 nM).

Treatment with HP(R)-miRNA complexes (**Top plot**); HP: CP2k(R) miRNA complexes (**Middle plot**); HP: CP5k(R) miRNA complexes (**Bottom**). The cell viability was represented as red squares, right Y-axis; while the relative luminescence was represented as bar chart (Left Y-axis). RLU – Relative Luminescence Unit. RCN – Relative cell number. Controls (Untreated, Free miRNA, N-TER and Lipofectamine) N: 4 - 8, n = 3; Test (Polyplexes) N = 1, n = 3 - 6. *** $P < 0.001$; **** $P < 0.0001$.

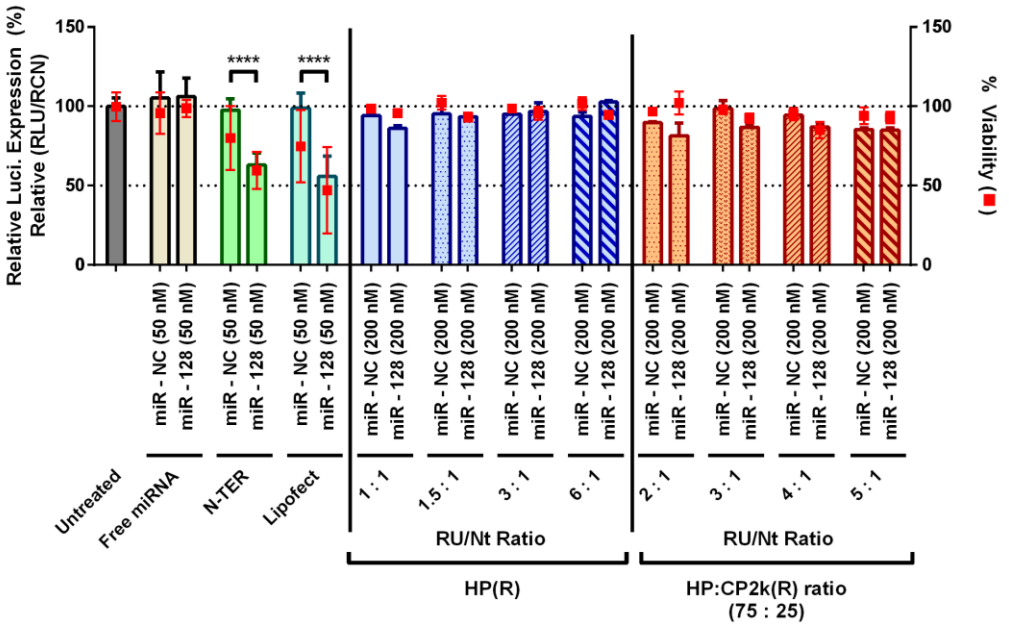

Figure 3-27: Luciferase of miRNA polyplexes (200 nM).

The cell viability was represented as red squares, plotted on right Y-axis; while the relative luminescence was represented as bar chart (Left Y-axis). The miRNA concentrations 50, 200 nM corresponds to ~ 75 and 300 ng of miRNA per well (100 µL). RLU – Relative Luminescence Unit. RCN – Relative cell number. Pooled data-analysis: Controls (Untreated, Free miRNA, N-TER and Lipofectamine) N = 4 - 8, n = 3; Test (Polyplexes) N = 1, n = 3 - 6. *** P < 0.001; **** P < 0.0001.

As there was no significant toxicity observed for most of the complexes treated at 50 and 200 µM miRNA concentrations, this amount was increased further to 250, 500 and 670 nM, **Figure 3-28** (page: 109). The complexes prepared at low RU/Nt ratio (up to 3: 1) were used for these experiments in order to avoid toxicity issues that could arise from free polymer present in the mixture, **Figure 3-17** (page: 94), **Figure 3-19** (page: 97), **Figure 3-21** (page:99) (for excess polymer).

Free-microRNA were able to enter the cells (2D) on their own at 100 nM (**Figure 3-23,** page:101), but they did not show any reduction in luciferase expression at any of the concentrations tested (50 to 670 nM) indicating that they were not functionally active after cellular entry when delivered without a nanocarrier, see Free miRNA in **Figure 3-26** (page: 106) and **Figure 3-28** (page: 109).

Small differences in luciferase expression were observed between miR-NC and miR-128 for many of the complexes at higher miRNA concentrations, but they were not statistically significant, **Table 3-9** (page: 122). A few of the complexes showed statistically significant differences, but only at very high miRNA concentration compared to N-TER and Lipofectamine (670 nM vs 50 nM).

It should be noted that the miRNA-treatment could reduce the luciferase expression only by 50% (maximum) even when using the well-optimized commercial transfection agents, N-TER and Lipofectamine. Hence, this luciferase assay might be less sensitive to identify moderately performing or sub-optimal delivery systems due to the small changes in luciferase expression after miRNA-complex treatment. As miRNAs can target multiple genes at the same time, the effective miRNA concentration that is available to target a single gene will depend on the relative abundance of other target genes co-expressed in the cell. In contrast, using siRNA against luciferase gene might effectively inhibit its expression due to the absence of other targets and hence might improve the sensitivity of the luciferase assay and in turn help to identify suitable miRNA delivery systems. As siRNA and miRNA are double stranded RNA molecules that are 21 – 23 base-pairs long, they can be used interchangeably to form complexes. Although the mismatches in the miRNA-mimics structure can contribute to small difference in the way these molecules are packaged, it could be assumed that these differences should not drastically affect the performance of the polyplexes.

Based on this idea, siRNA targeting the coding region of firefly luciferase (siR-Luc) was used. The siRNA loaded polyplexes were treated at 100 and 200 nM siRNA concentrations. One formulation representing each polymer set was chosen from 3D-uptake assay and tested for knock-down activity. Indeed, as expected, siRNA delivered by N-TER and Lipofectamine were able to knock-down luciferase gene more efficiently than miRNA, **Figure 3-29, page: 110**. However, none of the complexes tested show statistically significant difference between miR-NC vs siR-Luc treatments, **Table 3-10, page: 123**.

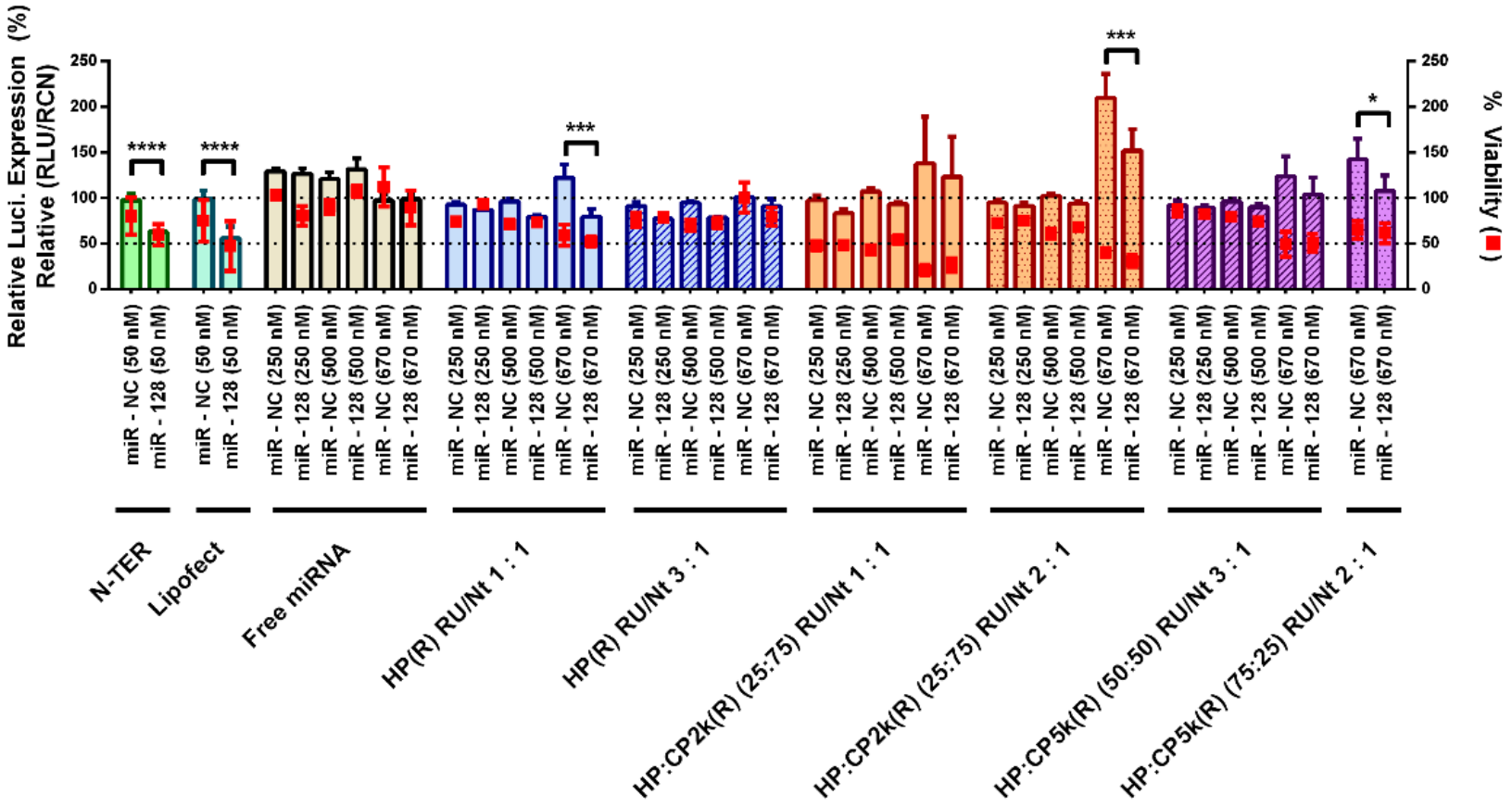

Figure 3-28: Luciferase assay of miRNA polyplexes (250 to 670 nM).

The miRNA concentrations 50, 250, 500 and 670 nM corresponds to ~ 75, 375, 750 and 1000 ng of miRNA per well (100 µL). Pooled data-analysis: Controls (N-TER, Lipofectamine and Free miRNA) N = 4 - 8, n = 3; Test (Polyplexes) N = 1 - 2, n = 3 - 6. *** P < 0.001; **** P < 0.0001.

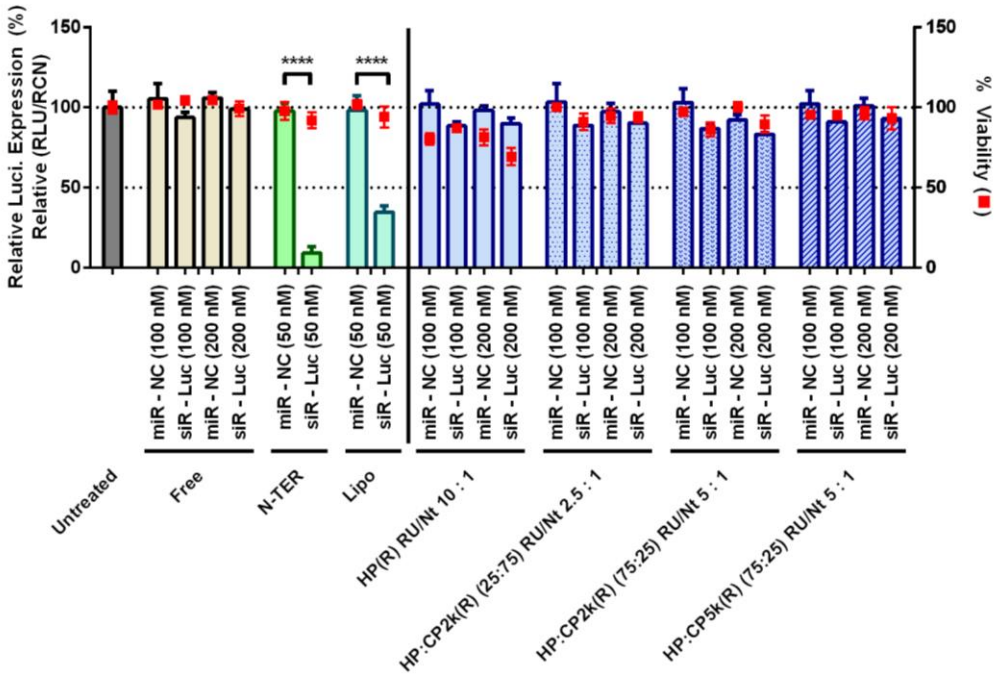

Figure 3-29: Luciferase assay for siRNA polyplexes (100 and 200 nM).

RLU – Relative Luminescence Unit. RCN – Relative cell number. Lipo refers to Lipofectamine 2000. Controls (N-TER, Lipofectamine and Free miRNA) N = 2, n = 3; Test (Polyplexes) N = 1, n = 3. *** $P < 0.001$; **** $P < 0.0001$.

3.5 Discussion

3.5.1 Effect of Salt and pH on PAA-miRNA interaction

Polyelectrolyte complexes [PEC] are formed by electrostatic interaction between oppositely charged polymers [e.g. cationic polymer and nucleic acid]. The nanoparticles are formed when the complex forming condition are ideal to stabilize the PECs in nano-dimensions. The critical deciding factors to obtain uniform nanoparticles with polyelectrolytes include concentration of polyelectrolytes, ratio of polyelectrolytes (stoichiometry)[329], concentration of surface stabilizing molecules, concentration of counter-ions and pH[329]. Mixing of high concentration polyelectrolytes which have high charge densities tends to form large aggregates[318]. At an ideal concentration, they can form complexes in nano-dimension. But, these nano-complexes can start to aggregate in the absence of a surface stabilizing mechanism. The nanoparticles avoid aggregation when their surface is stabilized by excess charge [e.g. excess polymer] or steric hindrance [e.g. PEG]. The pH of the complex forming solution decides the charge density of the polymers. At high charge densities, the charges on the polymer repel each other and hence the polymer assumes a more rigid (linear/rod-like) conformation[293,330,331]. While the repulsion of the charges is reduced by increasing the pH to basic condition or by screening the charges by addition of salt, the polymers attain a more flexible (coiled) conformation[293,319,331]. Under the right conditions of pH and salt, the oppositely charged polyelectrolytes can form tight complexes (particles)[319]. Usually, polymer-nucleic acid nanoparticle formation and most of the PECs[319] are favoured at low ionic concentrations. This can also reduce the formation of large aggregates by reducing the charge densities. However, higher salt concentrations (> 100 mM) can result in the formation of loose complexes due to high shielding effect of the salt[319].

For the current set of poly(amidoamine) polymers, at a fixed RU/Nt ratio (1:1), the maximum complexation was obtained at pH 6.0 and 20 - 50 mM NaCl. This indicated that this low ionic concentration enabled the polymer to adapt favourable conformations to complex maximum amount of miRNA[317-319].

3.5.2 Polymer Toxicity

The polymer toxicity assay was performed to resemble a typical transfection assay. The U87MG cells were treated with free polymer for 4 hours [with or without serum] and replaced with complete medium. The toxicity was measured 48 hours after the polymer exposure. This 48-hour incubation allows the evaluation of any delayed toxicity caused by the polymer on the cells, which will reflect the toxicity observed during the transfection assays. Performing a cytotoxicity assay immediately after the treatment with free polymer would provide information on acute toxicity of polymer. This information would be valuable for the comparison on the toxicity of different kinds of polymers. Such comparison of acute toxicity of poly(amidoamine) versus other standard cationic polymers have been previously reported and the results are discussed below.

The polymer toxicity only approached 50% toxicity at the highest concentration tested [1000 µg/mL] in the absence of serum [OptiMEM], while the polymer was even less toxic in the presence of serum [10 %].

Poly(ethylene imine) [PEI] is a synthetic polymer with high transfection efficiency and widely used for nucleic acid delivery. Kunath *et al.* compared the cytotoxicity of high [HMW-PEI, 48 kDa] and low [LMW-PEI, 5.4 kDa] molecular weight branched PEI on L929 mouse fibroblasts cells. The cells were incubated with the polymer for 3, 12 and 24 hours in serum supplemented medium [10 vol.% serum] and the cytotoxicity assay was performed immediately after this incubation. The concentration of polymer required to reduce the viability of cells by 50% [Half Maximal Inhibitory Concentration, IC_{50}] was less than 10 µg/mL for HMW-PEI for all the incubation times tested. For LMW-PEI, the IC_{50} was 80 µg/mL (for 24 hours of incubation), 170 µg/mL (12 hours) and greater than 1000 µg/mL (3 hours).

Hill *et al*. tested a non-crosslinkable homopolymer [$PAA_{21500Da}$, NG30] with a similar backbone to that used in the current project [MBA-DMEDA] on human liver cancer (HepG2) cell line[324]. The free polymer was treated for 48 hours in the presence of serum [10 vol.%] and the cytotoxicity assay was performed following this incubation[324]. The IC_{50} value was 400 µg/mL for NG30, which was similar to Poly-L-lysine [PLL, 22 kDa] [300 µg/mL][324]. Hill *et al.* also

reported higher erythrocyte membrane lytic activity with NG30 in the absence of serum and higher DNA transfection compared to all the different poly(amidoamine) backbones tested[324].

Rackstraw *et al.* tested non-crosslinkable poly(amidoamines) with similar backbone [MBA-DMEDA][296]. The HepG2 cells were treated overnight [probably 12 – 18 hours] with free-polymers in serum supplemented medium and cytotoxicity assay was performed immediately after this incubation[296]. The IC_{50} value was 160 µg/mL for the homopolymer [$PAA_{28200Da}$, NG49] and 275 µg/mL for the copolymer [PEG_{1900Da}–$PAA_{11410Da}$–PEG_{1900Da}, NG47][296]. The polymer-DNA complexes and equivalent amounts of free polymer were treated on the cells for 4 hours in serum free medium [OptiMEM] and replaced with serum containing media[296]. The toxicity was tested after overnight incubation. Free polymer was slightly more toxic than polymer-DNA complexes[296].

Danish *et al.* tested similar set of crosslinkable-polymers on A549 human lung cancer cell-line[275]. The cells were exposed to free-polymer or polymer-siRNA complex in DMEM with no serum for 24 hours and the cytotoxicity assay was performed immediately after the treatment[275]. Free polymer and polymer complexed with siRNA did not show any significant difference in toxicity profiles[275]. The EC_{50} [Half Maximal Effective Concentration, EC_{50}] was determined for HP as 255 µg/mL and a different PEGylated copolymer as 354 µg/mL [CP-05, PEG_{4600Da}-PAA_{6700Da}-PEG_{4600Da}][275].

Although, the IC_{50} values cannot be directly compared among these publications and the results obtained from the current work, due to the differences in the cell lines [HepG2[296,324], A549[275] versus U87MG used in the current work], duration of polymer exposure [48 hours with serum[324], 18 hours without serum[296], 24 hours without serum[275] versus 4 hours with and without serum in the current work] and variations in the molecular weight of poly(amidoamine) chains among these polymers [21 kDa[324], 28 kDa[296], 7 kDa[275] versus ~12kDa used in the current thesis], some general conclusions can be made about the toxicity behaviour of these PAA polymers. The poly(amidoamine) polymers are less toxic than PEI. The longer incubation of these set of PAA polymers results in increased toxicity. The polymers were less toxic in the presence of serum. The

PEGylated copolymers are usually less toxic than the non-PEGylated polymers. The free polymers were either slightly more toxic or the same as the polymer-nucleic acid complex.

3.5.3 Uptake and Transfection Efficiency

The cellular uptake of nanoparticles differs between 2D and 3D cell culture models depending on the cell population[326], nanoparticle type and its surface properties[326,327].

The uptake of nanoparticles in 3D was higher compared to 2D as observed by fluorescence microscopy. These results only indicate the uptake at the surface of the 3D-speroid culture. Flow-cytometry of disintegrated spheroids[327] or cryo-sectioning would be able to indicate the ability of the nanoparticles to penetrate the interior of the spheroids[326]. Meng *et al.* demonstrated enhanced uptake of poly(glycerol-adipate) nanoparticles in 3D-tumour spheroids compared to 2D culture [Human medulloblastoma cell line, DAOY][326]. However, non-cancerous primary cells showed lower uptake in 3D-culture compare to 2D-culture [mixed neonatal rat brain cells][326]. Similarly, Sims *et al.* showed enhanced uptake of PLGA nanoparticles by human cervical cancer (HeLa) cells compared to non-cancerous vaginal (VK2) cells[327]. However, PLGA nanoparticles showed enhanced uptake in 2D-culture compared to 3D[327]. Interestingly, PEGylated PLGA nanoparticles showed better penetration of 3D-spheroids compared to other surface modifications[327]. More details on the role of PEG in tissue penetration and cellular uptake is presented in the General Discussion, **6.2**, page: 199.

The general concentration of miRNA or siRNA for cell culture treatment is between 10 – 100 nM [0.15 – 1.5 µg/mL, when MW: 15000 g/mol]. None of the PAA-miRNA complexes tested showed any luciferase knockdown activity at any of the miRNA or siRNA concentrations tested [50 – 690 nM, 0.75 – 10 µg/mL].

3.6 Conclusion

The polymer reduction was performed using DTT and NMR data confirmed the complete removal of the projecting group and hence activation of the polymer. However, the Ellman's assay showed varying amount of thiol recovery depending on the polymer. HP showed almost 100 % recovery of free thiols while CP2k and CP5k showed medium (~ 35%) and low (~ 10%) thiol recovery after purification by ultra-filtration. Possibly, this could be due to the long purification time [6 – 8 hours] which can lead to self-crosslinking (disulphide bond formation) and thiol oxidation to sulfinic acid under acidic condition (< pH 4)[332].

The optimal miRNA-PAA complexation conditions were determined by agarose gel electrophoresis [Optimal salt: 25 mM NaCl, pH: 6.0, buffer: Phosphate]. These conditions were used in the preparation of polyplexes with miRNA and different polymers [HP, CP2k and CP5k] either individually or in different combinations. HP and CP2k with long PAA chain (> 10kDa PAA) showed efficient miRNA binding even at low RU/Nt ratio [~ 90% miRNA binding at RU/Nt ratio 1:1]. DLS measurements showed polydisperse complexes measuring around 200 – 300 nm in diameter.

MTS assay revealed that the free polymers were less toxic when treated in the presence of serum. Even in the absence of serum, most of the polymers only were able to reach its LD50 at the highest concentration tested [1000 µg/mL]. At a typical miRNA concentration [50 nM] required to treat the cells *in vitro*, the concentration of polymer required would be less than 40 µg/mL and hence low or no toxicity from these polymers could be expected.

The uptake assay, using fluorescently labelled miRNA, showed moderate cellular uptake compared to commercial transfection reagents, N-TER and Lipofectamine 2000.

Finally, the ability to deliver miRNA was tested using U87-Luc cells. Small differences between control-miRNA (miR-NC) and target miRNA (miR-128) were found, but only at very high concentrations [670 nM or 1 µg per 100 µL or 10 µg/mL]. At lower concentrations, luciferase assay revealed that none of the

complexes tested showed significant differences between miR-NC and miR-128 treatments indicating that these polyplexes were not capable of functionally delivering oligonucleotides under the tested conditions [HP: CP ratio, RU/Nt ratio and treatment concentrations]. As all the formulations failed to elucidate any gene-knockdown efficiency, it was reasoned that using miRNA made the assay less sensitive as the maximum luciferase knockdown achieved by miRNA (miR-128) treatment was around 50% even with the commercial transfection agent (N-TER, Sigma). Replacing miRNA with a luciferase targeting siRNA (siR-Luc) was expected to increase the assay sensitivity and hence identify PAA-siRNA formulations that were capable of delivering siRNA into cells. However, none of the formulations reported significant luciferase knockdown. This could be due to the low thiol yield obtained after ultra-filtration which might in turn be affecting the stability of the complexes under physiological conditions.

In the following chapter, alternative protocol for polymer purification was developed with shorter processing time and the nanoparticle formulation was optimized based on stability of nanoparticles in the physiological ionic condition.

3.7 Supplementary Data

3.7.1 Size Analysis of HPR-miRNA polyplexes (Viscotek - Malvern)

Table 3-2: Size analysis of HPR-miRNA complexes, Viscotek DLS.
Nanoparticle Solution: 25 mM PBS, pH 6.0; Concentration of polymer [HP(R)] was varied between 30 - 180 µg/mL; Final concentration of miRNA was kept constant, 38 µg/mL (~ 2.5 µM); (The same samples were analysed with Malvern NanoZS and the results are presented in the next table (**Table 3-3**).

UoN Visco	RU/Nt Ratio	Peak 1 d.nm	% (Pk1)	% RSD	Peak 2 d.nm	% (Pk2)	% RSD	Peak 3 d.nm	% (Pk3)	% RSD	Final polymer conc. (µg/mL)	Corr. fn
5/25	**1.0 : 1**	372 ± 12	86.4	3.2	9 ± 0.2	13.6	3.1				65	Bad
24/25	**1.5 : 1**	203 ± 60	99.2	28.8	46 ± 3	0.8	7.4				97.5	**Good**
4/25	**2.0 : 1**	623 ± 72	98.8	11.5	13 ± 0.6	1.2	4.7				130	Bad
4/25	**2.5 : 1**	333 ± 40	57.1	12.0	1266 ± 132	29.5	10.5	99 ± 7	12.1	6.9	162.5	Bad
9/26	**3.0 : 1**	386 ± 17	96.7	4.5	7 ± 0.2	3.3	3.4				195	Bad
17/25	**4.0 : 1**	462 ± 62	95.6	13.3	110 ± 8	3.2	7.3	23 ± 1	1.2	4.8	**260**	**Good**
21/25	**4.5 : 1**	494 ± 45	98.8	9.1	23 ± 1	1.2	1.8				292.5	**Good**
24/25	**5.0 : 1**	428 ± 52	89.3	12.2	14010 ± 2276	9.6	16.3	10 ± 1	1.1	3.3	325	**Good**
39/40	**6.0 : 1**	392 ± 50	99.3	12.6	16 ± 0.5	0.7	2.7				390	**Good**

Some results containing poor particle size distributions are presented in these tables, to enable comparison between results of different instruments and to aid further optimization. N = 1, n = 3.

Table 3-3: Size analysis of HPR-miRNA complexes, Malvern NanoZS.

For comparison, same sample from **Table 3-2** was analysed in parallel with Malvern instrument. Viscotek Vs Malvern. Final concentration of miR = 2.5 µM.

UoN ZS	HP(R) RU/ RNA RU (RU/Nt) Ratio	Z-Ave ± PdI width d.nm	PdI	Peak 1 d.nm	% Pk1	Peak 2 d.nm	% Pk2	Peak 3 d.nm	% Pk3	Final polymer concentration (µg/mL)	Quality Report
	1.0 : 1	1360 ± 825	0.416	974 ± 226	100					65	Bad
	1.5 : 1	1448 ± 926	0.394	1243 ± 305	100					97.5	Bad
	2.0 : 1	~~1185 ± 708~~	0.355	1074 ± 359	91.8	5208 ± 471	8.2			130	Bad
	2.5 : 1	~~1420 ± 840~~	0.417	1148 ± 447	98.7	5560	1.3			162.5	Bad
	3.0 : 1	~~788 ± 564~~	0.547	960 ± 387	90.5	7 ± 1	5.8	5215 ± 477	3.7	195	Bad
	4.0 : 1	~~841 ± 455~~	0.312	780 ± 232	98.2	5500 ± 203	1.8			**260**	**Good**
	4.5 : 1	~~753 ± 401~~	0.303	705 ± 217	94.5	5156 ± 501	5.5			292.5	**Good**
	5.0 : 1	627 ± 292	0.213	671 ± 219	100					325	**Good**
	6.0 : 1	490 ± 222	0.217	635 ± 326	100					390	**Good**

The Z-avg values were marked red and marked with a strikethrough when there were two or more peaks or when the Pdi was > 0.5 (see section:). The last column was indicated as "Good", when the Zetasizer Software indicated "Data meets quality criteria" in both "Size Quality Report" and "Expert Advise". 'Bad' was indicated when the data did not meet the quality criteria with one or more of the following indications, "Sample highly polydisperse", "High Cumulant Error", "In range figure is low" due to low sample concentration, etc., Poor particle size distributions are presented in these tables, to enable comparison between results of different instruments and to aid further optimization. N = 1, n = 3.

3.7.2 Size Analysis of HP(R)-miRNA polyplexes (Constant polymer)

Table 3-4: Size analysis of miRNA-HPR complexes, Viscotek 802DLS.

Nanoparticle Solution: 25 mM PBS, pH 6.0; Initial concentration of polymer (HP(R)) was fixed at 578 µg/mL; Final concentration of miRNA in the complex was between 312.5 - 31.25 µg/mL (~ 21 – 2.1 µM)

UoN Visco	RU/Nt Ratio	Peak 1 d.nm	% (Pk1)	% RSD_1	Peak 2 d.nm	% (Pk2)	% RSD_2	Peak 3 d.nm	% (Pk3)	% RSD_3	Corr. fn	Final miR Conc.		
												µg/mL	µM	
28/30	**1 : 1**	**198 ± 54**	83.8	27.4	2141 ± 522	8.6	24.4	6 ± 1	4.0	17.0	Good	313	**21**	
21/30	**2 : 1**	**232 ± 79**	83.6	33.8	46 ± 7	7.2	15.5	8 ± 1	4.6	11.8	Good ^{p}	156	**10**	
39/50	**3 : 1**	**200 ± 76**	83.8	36.4	2808 ± 570	8.7	20.3	11 ± 2	5.8	13.5	Good ^{pp}	104	**7**	
24/30	**4 : 1**	**204 ± 48**	79.7	23.9	48 ± 7	8.5	14.8	9 ± 1	6.3	11.0	Good ^{pppp}	78	**5**	
25/35	**5 : 1**	**220 ± 50**	74.5	22.5	46 ± 8	9.5	17.9	2816 ± 418	5.5	14.8	Good ^{pppp}	63	**4**	
20/20	**8 : 1**	**266 ± 40**	98.8	14.7	25 ± 1	1.2	4.9				Good	39	**3**	
17/20	**10 : 1**	**201 ± 93**	82.3	46.0	32 ± 6	6.2	17.6	9 ± 1	6.1	16.4	Good ^{p}	31	**2**	

First column represents the number of runs that were suitable for final calculation to the total number of runs recorded for each sample. The first column was marked in green when > 60 % of runs qualified as clean runs that were available for size calculation; in 'yellow' when 31 - 60 % of the runs qualified and white when less than 30% of the runs qualified as clean runs. The last column represents the correlation function and its quality. A good (green) sample represents that the data obtained had good quality correlation functions and majority or all of them correlated well with the selected clean runs. The number of superscript 'p' (^{p}) represents the number of extra peaks that were not tabulated. The size data were represented with the descending peak percentage. N = 1, n = 3.

3.7.3 Selection of HP: CP complexes - Summary Table

Table 3-5: Selected HP:CP2k(R) miRNA complexes for *in vitro* assay.

HP : CP2k	RU/Nt	miR BE (%)	Free Polymer	Size by Major Peak, d.nm	Selected for *in vitro* (Y/N)
3 : 1	**1**	**60.2**	**-**		**Y (Control)**
	2	87.3	**+**	**229 ± 178**	**Y**
	3	93.2	**+**	**248 ± 111**	**Y**
	4	94.0	**++**	**120 ± 75**	**Y**
1 : 1	**1**	71.8	**-**	**164 ± 90**	**Y (Control)**
	2	90.9	**+**	**216 ± 76**	**Y**
	3	96.7	**+**	**174 ± 115**	**Y**
	4	98.6	**++**	**192 ± 73**	**Y**
1 : 3	**1**	88.4	**-**	**192 ± 77**	**Y (Control)**
	2	97.6	**+**	**229 ± 178**	**Y**
	3	100.0	**+**	**248 ± 111**	**Y**
	4	100.0	**++**		**Y**

Table 3-6: Selected HP-CP5k(R):miRNA complexes for *in vitro* testing.

HP : CP5k	RU/Nt	miR Bind (%)	Free Polymer	Size by Major Peak, d.nm	Selected for *in vitro* (Y/N)
3 : 1	**1**	96.2	**-**	263 ± 48	Y
	2	95.5	**-**	298 ± 55	Y
	3	98.0	**+**	397 ± 59	Y
	4	97.4	**+**	478 ± 80	Y
	5	97.4	**+**	319 ± 40	Y
	10	98.1	**++++**	325 ± 95	N
1 : 1	**1**	66.3	**-**	742 ± 87	N
	2	94.5	**-**	234 ± 36	Y
	3	98.6	**+**	373 ± 58	Y
	4	98.8	**+**	370 ± 62	Y
	5	99.1	**+**	329 ± 49	Y
	10	99.8	**++++**	284 ± 44	N
1 : 4	**1**	23.6	**-**	363 ± 27	N
	2	65.3	**-**	495 ± 96	N
	3	77.7	**-**	357 ± 51	N
	4	78.9	**-**	456 ± 172	N
	5	81.5	**-**	308 ± 62	N
	10	89.8	**+**	360 ± 95	N

3.7.4 Luciferase Knock-down Assay – Statistical Analysis

Two-way ANOVA with multiple comparison was performed to evaluate the differences in luciferase expression of cells treated with PAA-miRNA complexes loaded either with miR-NC or miR-128. The luminescence of the cells treated with the same formulation loaded with either miR-NC or miR-128 were collected and analysed for statistical differences treated under the same conditions but loaded with different miRNA. Two-way ANOVA with multiple comparison (GraphPad Prism v6.07) was used for this analysis. The mean luminescence from each treatment was compared with every other treatment; only the relevant results were presented in Table 3-7 (page: 121, 50 nM miR-NP), Table 3-8 (page: 122, 200 nM miR-NP), Table **3-9** (page: 122, 250-670 nM miR-NP) and Table 3-10 (page: 123, 200 nM siR-NP).

Table 3-7: Statistical test, miRNA complex treatment (50 nM).

Treatment Condition (miR-NC Vs miR-128)	Mean Diff.	95% CI of diff.	Significant?	Summary
	Two-way ANOVA (Tukey's multiple comparisons test)			
Free miRNA	-0.7327	-8.373 to 6.908	No	ns
N-TER	**34.65**	**26.40 to 42.90**	**Yes**	****
Lipofectamine	**43.05**	**31.50 to 54.60**	**Yes**	****
HPR				
RU/Nt 1:1	2.318	-12.96 to 17.60	No	ns
RU/Nt 1.5:1	8.713	-8.932 to 26.36	No	ns
RU/Nt 3:1	4.28	-9.457 to 18.02	No	ns
RU/Nt 5:1	-4.018	-28.97 to 20.94	No	ns
RU/Nt 6:1	5.528	-19.43 to 30.48	No	ns
RU/Nt 10:1	7.881	-17.07 to 32.84	No	ns
HP:CP2k (R) 1:3				
RU/Nt 1:1	-6.891	-23.50 to 9.719	No	ns
RU/Nt 2:1	-3.104	-19.71 to 13.51	No	ns
RU/Nt 3:1	-10.46	-37.58 to 16.66	No	ns
RU/Nt 4:1	-6.451	-33.57 to 20.67	No	ns
RU/Nt 5:1	-10.09	-37.21 to 17.03	No	ns
HP:CP2k (R) 3:1				
RU/Nt 2:1	5.05	-14.13 to 24.23	No	ns
RU/Nt 3:1	6.061	-13.12 to 25.24	No	ns
RU/Nt 4:1	9.003	-10.18 to 28.18	No	ns
RU/Nt 5:1	2.311	-16.87 to 21.49	No	ns
HP CP5k (R) 1:1				
RU/Nt 2:1	2.748	-21.50 to 27.00	No	ns
RU/Nt 3:1	-0.0394	-14.89 to 14.81	No	ns
HP CP5k (R) 3:1				
RU/Nt 1:1	-7.908	-32.15 to 16.34	No	ns
RU/Nt 2:1	-6.094	-30.34 to 18.15	No	ns
RU/Nt 3:1	-5.504	-29.75 to 18.74	No	ns
RU/Nt 4:1	-8.338	-32.59 to 15.91	No	ns
RU/Nt 5:1	-6.584	-30.83 to 17.66	No	ns

Controls (Untreated, Free miRNA, N-TER and Lipofectamine) N: 4 - 8, n = 3; Test (Polyplexes) N = 1, n = 3 - 6. *** P < 0.001; **** P < 0.0001; ns = Not significant.

Table 3-8: Statistical test, miRNA-complex treatment (200 nM).

Treatment Condition (miR-NC Vs miR-128)	Mean Diff.	95% CI of diff.	Significant?	Summary
	Two-way ANOVA (Tukey's multiple comparisons test)			
HPR				
RU/Nt 1:1	8.099	-3.959 to 20.16	No	ns
RU/Nt 1.5:1	1.797	-10.26 to 13.86	No	ns
RU/Nt 3:1	-1.651	-13.71 to 10.41	No	ns
RU/Nt 6:1	-9.035	-21.09 to 3.024	No	ns
HP:CP2k (R) 3 : 1				
RU/Nt 2:1	8.244	-3.814 to 20.30	No	ns
RU/Nt 3:1	11.72	-0.3351 to 23.78	No	ns
RU/Nt 4:1	7.375	-4.683 to 19.43	No	ns
RU/Nt 5:1	0.2878	-11.77 to 12.35	No	ns

Controls (Untreated, Free miRNA, N-TER and Lipofectamine) N = 4 - 8, n = 3; Test (Polyplexes) N = 1, n = 3 – 6. *** P < 0.001; **** P < 0.0001; ns = Not significant.

Table 3-9: Statistical test, miRNA-complex treatment (250 - 670 nM).

Treatment Condition (miR-NC Vs miR-128)	Conc. (nM)	Mean Diff.	95% CI of diff.	Significant?	Summary
		Two-way ANOVA (Tukey's multiple comparisons test)			
Free miRNA	250	2.797	-43.61 to 49.21	No	ns
	500	-10.92	-57.33 to 35.49	No	ns
	670	-1.596	-43.96 to 40.77	No	ns
HPR					
RU/Nt 1:1	250	5.625	-40.79 to 52.04	No	ns
	500	16.91	-29.50 to 63.32	No	ns
	670	**42.75**	**11.46 to 74.04**	**Yes**	***
RU/Nt 3:1	250	14.14	-32.27 to 60.56	No	ns
	500	16.25	-30.16 to 62.66	No	ns
	670	10.06	-32.31 to 52.43	No	ns
HP:CP2k (R) 3:1					
RU/Nt 1:1	250	14.28	-32.14 to 60.69	No	ns
	500	14.01	-32.40 to 60.42	No	ns
	670	14.34	-16.95 to 45.63	No	ns
RU/Nt 2:1	250	3.546	-42.86 to 49.96	No	ns
	500	8.072	-38.34 to 54.48	No	ns
	670	**57.89**	**15.52 to 100.3**	**Yes**	***
HP:CP5k (R) 1:1					
RU/Nt 3:1	250	2.242	-44.17 to 48.65	No	ns
	500	6.345	-40.07 to 52.76	No	ns
	670	19.83	-11.46 to 51.12	No	ns
HP:CP5k (R) 3:1		Unpaired t test			
RU/Nt 2:1	**670**	**-34.52 ± 11.46**	**-60.05 to -8.989**	**p = 0.0131, Yes**	*

Controls (N-TER, Lipofectamine and Free miRNA) N = 4 - 8, n = 3; Test (Polyplexes) N = 1 - 2, n = 3 - 6. *** P < 0.001; **** P < 0.0001; ns = Not significant.

Table 3-10: Statistical test, siRNA-complex treatment (100 and 200 nM).

Treatment Condition (miR-NC Vs miR-128)	Conc. (nM)	Mean Diff.	95% CI of diff.	Significant?	Summary
		Two-way ANOVA (Tukey's multiple comparisons test)			
Free miRNA	100	11.65	-5.026 to 28.33	No	ns
	200	6.758	-9.917 to 23.43	No	ns
N-TER	50	**88.48**	**79.26 to 97.70**	**Yes**	****
Lipofectamine 2000	50	**63.67**	**54.44 to 72.89**	**Yes**	****
HPR					
RU/Nt 10 : 1	100	13.57	-3.106 to 30.25	No	ns
	200	7.97	-8.706 to 24.65	No	ns
HP:CP2k (R) 1:3					
RU/Nt 2.5 : 1	100	14.86	-1.817 to 31.53	No	ns
	200	7.071	-9.605 to 23.75	No	ns
HP:CP2k (R) 3:1					
RU/Nt 5 : 1	100	16.39	-0.2812 to 33.07	No	ns
	200	8.828	-7.848 to 25.50	No	ns
HP:CP5k (R) 3:1					
RU/Nt 5 : 1	100	11.07	-5.606 to 27.75	No	ns
	200	8.057	-8.619 to 24.73	No	ns

Controls (N-TER, Lipofectamine and Free miRNA) N = 2, n = 3; Test (Polyplexes) N = 1, n = 3. *** P < 0.001; **** P < 0.0001; ns = Not significant.

Chapter – IV

Optimization of polymer purification, Evaluation of various factors affecting the stability of poly(amidoamine)-microRNA polyplexes, Physico-chemical and biological evaluation of stable crosslinked nanoparticles prepared by "Salt-free complexation" method

Nanoparticle Development – Stage II

- Polymer purification by gel-filtration chromatography
- Stability based nanoparticle screening
– Salt-free complex formation

4 Improvements in the polymer purification, stability and biological activity of crosslinked poly(amidoamine)-microRNA nanoparticles - "Salt-free complexation" method

4.1 Introduction

Bioreducible nanoparticles produced in this work are formed by the thiol-crosslinking that occurs when the free thiols from copolymer [CP] reacts with the dithiopyridine of HP. Higher crosslinking could be expected when there are higher amounts of free thiol in CP. The free-thiols have the tendency to oxidize into disulphide bonds (self-oxidation). This decrease in free thiols can occur either during the purification process or storage. In order to increase the stability of these nanoparticles in the physiological conditions, it is important to preserve the free thiols until they are mixed with the nucleic acid to form crosslinked nanoparticles. The amounts of free thiol recovered by ultra-filtration protocol was only about 35% for CP2k and 10% for CP5k. The original ultra-filtration protocol had long filtration period (4 x 2 hours) which could lead to self-oxidation. It was speculated that a rapid purification protocol (~ 30 minutes) using a desalting PD-10 column might yield higher free thiols in the polymer.

Hence, the first section of this chapter is about the method development for polymer purification using PD-10 column. The second section studied the stability of polyplexes using the copolymer prepared from PD-10 column. The third part studied the crosslinking behaviours of the polymers [HP and CP2k(R)]. Based on the results obtained, improvements were made in the method for nanoparticle preparation. The nanoparticle formulation was optimized to obtain physiologically stable miRNA-PAA crosslinked nanoparticles. Finally, these nanoparticles were tested for their *in vitro* uptake behaviour and transfection efficiency on U87MG and U87MG-Luc cells respectively. In order to study different parameters and to reduce the number of experimental variables, this chapter was focused only on HP-CP2k(R) miRNA nanoparticle system.

4.2 Methods

4.2.1 Polymer Purification: Method Development (PD-10 column)

Background: PD-10 is a size exclusion column packed with Sephadex™ G-25 medium generally used for desalting applications [Cat. No. GE17-0851-01; Packed bed dimension: 1.45 x 5.0 cm; Bed-volume: 8.3 ml]. The Sephadex G25 column consists of micron-sized (85 to 260 µm) porous beads. The larger molecules (M_r >5000 Da) will be excluded from entering the pores of the beads and hence elutes first, while the smaller molecules (< 1000 Da) enter the pores in the beads and hence takes longer time to elute out of the column. The size of 1,4-Dithiothreitol (DTT, MW: 154.25 g/mol) and polyamidoamine (PAA) polymers (M_w >10000 Da) respect the separation criteria for the PD-10 column and hence theoretically possible to separate DTT from the polymer solution.

Priming the column: The PD-10 column is normally supplied in an aqueous solution of Kathon™ CG/ICP Biocide (Cosmetic Grade/ In-Container Preservative, 0.15%). This storage solution was eliminated from the column by passing at-least 25 mL of ultrapure water (milli-Q). Then the column was equilibrated by passing at least 25 mL of elution solution [0.1 mM HCl = acidified water, pH 4.0] as recommended by the manufacturer.

CP2k Elution Profile: CP2k was dissolved in acidified water (10, 15, 20 mg/mL). The polymer solution (2.5 mL) was allowed to pass through the column and the flow-through was collected in a pre-weighed glass-vial. The elution of polymer was performed by the addition 6 mL elution buffer (0.5 mL x 12 times) and the eluates were collected in pre-weighed microfuge tubes. All the samples were freeze-dried for 20 hours using Steris Lyovac™ GT2 (**G**efrier**t**rockner, German expression for freeze dryer).

DTT Elution Profile: DTT was prepared in elution solution at different concentrations [1, 1.5, 2.5, 5 and 10 mg/mL or ~ 6.5, 10, 16, 32 and 65 mM]. DTT solution [2.5 mL] was added into the column and the flow-through was collected in 0.5 mL fractions. After DTT-solution has completely entered the column, the elution buffer was added in 0.5 mL fractions for 10 times (0.5 mL x 10 times) and then 1 mL fractions were collected 20 times (1 mL x 20 times).

The presence of DTT in each fraction of the eluate was determined by Ellman's assay. Briefly, 100 µL from each fraction was mixed with 20 µL of the Ellman's reagent and 1 mL of Ellman's assay buffer [for composition of reagents see Chapter 2, Section: **2.2**, page: 50]. 200 µL of the above solution was transferred in a 96 well plate with clear flat bottom. The absorbance at 412 nm was recorded.

Polymer Reduction and PD-10 Column Purification: The polymer [CP2k, 120 mg, 35.6 mmol thiol RU] was dissolved in water (9 mL), pH was adjusted to 7.4 with NaOH (2M) and freshly prepared DTT solution [15 mg/mL, 97 mmol] was added (1 mL). The mol to mol ratio of DTT to CP2k's t-Boc bearing RU was ~2.7 :1. The reduction reaction was carried out at room temperature for 1 hour in the dark, followed by setting the pH to 3.5 - 4.0 with hydrochloric acid (2M). The sample [2.5 mL containing CP2k (12 mg/mL) and DTT (1.5 mg/mL)] was loaded on to an equilibrated column and the flow-through was discarded. Elution buffer (3.5 mL) was added to the column and the eluate was collected in a pre-weighed glass-vial, snap-frozen in liquid nitrogen and freeze-dried for 20 hours as described previously. The elution can be performed by gravity protocol instead of centrifugation (1000g, 2 min) to reduce the chance of DTT elution and to facilitate reutilization of the PD-10 columns.

Column Regeneration and Storage: Following polymer elution, the column was regenerated by passing elution buffer (at least 25 mL) followed by ultrapure water (Milli-Q, at least 25 mL). The column was equilibrated with ethanol [20 vol.%] for long-term storage (room temperature). The PD-10 column was reused several times for polymer purification.

Yield Calculation: The final yield of the activated polymer from the starting materials can be determined using following equation,

Percentage recovery by mass,

$$\textbf{Yield}, (\%) = \frac{\textbf{Final amount of polymer recovered}}{\textbf{Theoretical yield of polymer}} \textbf{x 100}$$

Theoretical yield for different polyamidoamine polymers are presented in the following table, **Table 4-1**, page: 127.

Table 4-1: Theoretical yield of polymer (100 %, by mass).
The table represents the theoretical maximum of polymer that can be recovered when 100 mg of polymer is used for DTT reduction. Theoretical Yield of the Polymer = Initial mass of polymer (g) – Mass of leaving group (g).

Polymer	100 % Theoretical yield (mg/ 100 mg)
HP	93.93
CP2k	94.78
CP5k	96.66

The percentage yield of the polymer in terms of free thiol can be calculated as follows,

$$\textbf{Percentage free thiol recovery} = \left(\frac{\textbf{Actual concentration of thiols measured by Ellman's Assay } (\mu M)}{\textbf{Theoretical thiol concentration of the polymer } (\mu M)}\right) \textbf{X 100}$$

Table 4-2: Theoretical thiol concentration (100 %) of different polymers.

Polymer	Polymer Concentration (mg/mL)	Theoretical Thiol Concentration (µM)
HP	1	586
CP2k	2	694
CP5k	4	997

4.2.2 Size Analysis by Dynamic Light Scattering (DLS)

The particle size was measured by Malvern Nano S. About 12 - 20 µL of the sample was transferred to an ultra-low volume DLS quartz cuvette (Hellma-105.251.005-QS). Water was selected as the dispersant and sample viscosity was considered same as dispersant. Temperature was set to 25˚ C. ZEN 2112 was selected as the quartz cuvette model. The measurement angle was set to 173˚ backscatter (NIBS default) mode. Measurement duration was set to "Automatic" and each sample was measured in triplicate.

4.2.3 Electron Microscopy (Transmission and Scanning)

The miRNA-PAA nanoparticles were prepared either in water or NaCl salt solution. Use of phosphate was avoided in the nanoparticle preparations as it is known to precipitate Uranyl acetate. This nanoparticle formation solution was allowed to stand for 30 minutes and 10 µL of the sample was drop cast on a 3.05 mm TEM copper grid coated with Formvar (poly-vinyl formal), 200 mesh (TAAB Laboratories Equipment Ltd). The sample was allowed to air dry overnight before imaging with FEI Tecnai 12 Biotwin TEM (Nottingham) or JEM1400, JEOL (Angers). For Scanning electron microscopy (SEM), the nanoparticle solution was deposited over aluminium surface and allowed to air dry overnight. The following day, the sample was sputter coated with gold and imaging was done on EVO LS10, ZEISS Scanning electron microscope.

4.2.4 Flowcytometry

Preparation of Nanoparticles with Fluorescent miRNA: The optimized formulation, HP: CP2k(R) 1:1 RU/Nt 5:1, was used for the preparation of nanoparticles with fluorescently-labelled microRNA (miR-Cy3). The microRNA was purchased as a cyanine 3 (Cy3) dye covalently linked with at its 3′-passenger strand [see Chapter II, Materials section]. The size of the nanoparticle was measured by DLS and found to be around 150 nm and Pdi < 0.2. The PAA-miRNA nanoparticles (2500 nM, miRNA concentration) were diluted in OptiMEM medium to required concentrations.

N-TER nanoparticles (Sigma) were used a positive control. The N-TER nanoparticles were prepared by following the manufacturer's protocol. Briefly, the N-TER-peptide solution was diluted in water [8 µL N-TER + 42 µL water]. The fluorescent miRNA was diluted in siRNA dilution buffer supplied by the manufacturer [13 µL, 5µM miR-Cy3 + 37 µL siRNA dilution buffer]. The diluted miRNA was then added to the diluted N-TER solution, mixed and incubated at room temperature for 20 minutes [650 nM miRNA containing N-TER nanoparticles]. Finally, the N-TER nanoparticles were diluted to 50 nM with OptiMEM medium and added to the cells.

Cell culture and Sample Collection: The U87MG cells were seeded in a 24 well plate (40000 cells/well) and incubated overnight for attachment. The cell culture medium was replaced by nanoparticles [NP] in OptiMEM medium. Free miRNA and N-TER-miRNA nanoparticles were used as controls. To study the effect of concentration of miRNA on nanoparticle uptake, the cells were treated with nanoparticles at different concentrations [50, 250 and 500 nM] for 6 hours. The medium with nanoparticles was replaced by medium containing Hoechst 33342 (5 µg/mL) and incubated for 15 minutes. Finally, the medium was removed, washed twice with PBS (1x) and the cells were collected by trypsinization. The cells were pelleted and resuspended in ice cold FACS buffer (100 µL, PBS, 10% serum and 0.1% sodium azide) followed by addition of ice cold formaldehyde (100 µL, 4% paraformaldehyde dissolved in PBS, pH 7.4).

Data Collection and Analysis: The cell samples were analysed by MACSQuant® Analyzer 10 (Miltenyi Biotec) using the following instrument settings: flow rate was set to low; voltage for forward scatter (FSC, 212 V), side scatter (SSC, 260V); voltage for fluorescence channels, violet-blue (V1, 260 V), blue (B2, 350 V). The fluorescence from Hoechst 33342 was collected from channel V1 (Excitation: 405 nm; Emission: 450/50 nm) and Cy3 fluorescence was collected from channel B2 (Ex.: 488 nm; Em.: 585/40 nm). Fluorescence compensation and data analysis was performed with FlowJo software v10.1.

4.2.5 Confocal Imaging

The U87MG cells were seeded in a Lab-Tek® Chamber Slide™ (Nunc, 177402) at 10000 cells/well (200 µL). After overnight incubation, the cells were treated with nanoparticles loaded with fluorescent miRNA (miR-Cy3) in OptiMEM medium. After 4 hours of treatment, the nanoparticle containing medium was replaced with nuclear and lysosomal labelling medium [EMEM complete medium supplemented with serum (10 vol.%), sodium pyruvate (1 mM), non-essential aminoacids (1x), Hoechst 33342 (5 µg/mL) + LysoTracker Green DND-26 (100 nM)]. The cells were incubated for 30 minutes for nuclear and lysosomal labelling, followed by washing twice with HBSS [Hank's Balanced Salt Solution, containing Ca^{2+} and Mg^{2+} ions]. The cells were fixed in formaldehyde solution [4% paraformaldehyde buffered in PBS, pH 7.4] for 15

minutes. The mounting medium was added on the slide, cover-slip was sealed around the edges and imaged using Leica TCS SP08 Confocal Laser Scanning Microscope. The Cy3 was excited at 561 nm to obtain better fluorescence yield and to avoid simultaneous excitation of LysoTracker dye. The LASER power settings for the instrument were optimized initially with the cells treated with N-TER-miRNA complexes [50 nM] and the same settings were used for all other treatments to enable comparison of fluorescence intensity across different treatments.

4.2.6 Luciferase Assay

The U87-Luc cells were seeded (5000 cells/well) the night before the nanoparticle treatment in EMEM complete medium which is supplemented with Non-essential amino acids (1 vol.%), sodium pyruvate (1 mM), bovine growth serum (10 vol.%). The cells were treated in OptiMEM medium for 4 hours. The medium containing nanoparticles was replaced with EMEM complete medium. The luciferase assay was carried-out between 48 and 60 hours. Initially, EMEM complete medium with no phenol-red was supplemented with D-luciferin substrate (0.15 mg/mL) was added to the cells and the luminescence was recorded by a Clariostar plate-reader. The D-luciferin medium was replaced with resazurin supplemented medium (44 µM). The cells were incubated for 40 minutes and the fluorescence was recorded by a plate reader (Excitation: 544 nm; Emission: 590 nm).

More details on the data normalization procedure and its background development are provided in ***Appendix I: Development of Normalization Technique for Live Cell Luciferase Assay with High Throughput Compatibility, page: 214-237***.

4.3 Results

4.3.1 PD-10 Column Purification – Method Development

The standard PD-10 desalting protocol recommends loading the column with 2.5 mL of the sample [e.g. bovine serum albumin - BSA, 1 mg/mL, dissolved in NaCl (up to 1M)] and recovering the larger molecule [BSA, M_w 66.5 kDa] in 3.5 mL of water (95% recovery), while the impurity [NaCl, M_w 58.44 g/mol] elutes after this volume, hence achieving >99% of elimination of the impurity [salt]. For the purification of polymer from DTT, if the polymer is used at the same concentration as BSA (1 mg/mL), the maximum expected yield would be 2.5 mg of polymer for one PD-10 column, which is too low a quantity of polymer and not economical. In order to obtain higher polymer yield and maximum elimination of DTT, the elution profiles of polymer and DTT should not overlap each other. Hence, it is important to know the elution profiles of polymer and DTT at different concentrations to determine the optimal polymer and DTT concentrations that can be safely used with PD-10 column.

The presence of DTT can be detected even at low concentrations using Ellman's reagent. However, if a mixture of polymer and DTT is used, it will not be possible to precisely quantify the amount of polymer and DTT in each elution fraction as both the species have free thiols and react with Ellman's reagent (DTNB). Hence, the elution behaviour of DTT and the non-reduced polymer (CP2k) were investigated independently. The amount of CP2k eluted in each fraction (0.5 mL) was deduced by measuring the weight of the polymer after freeze drying (**Figure 4-1,** page: 132), while the elution of DTT was deduced by performing Ellman's assay on each fraction (**Figure 4-2,** page: 132). Finally, the results from both the experiments were plotted in the same graph (**Figure 4-3,** page: 133) to reflect the possible elution profiles of CP2k and DTT as it might occur while purifying CP2k(R) from DTT. The elution profiles also indicated that the polymer and DTT eluted completely from the PD-10 column after addition of 6 mL and 14 mL of water respectively. This prompted the possibility of reusing the PD-10 column for several purification cycles.

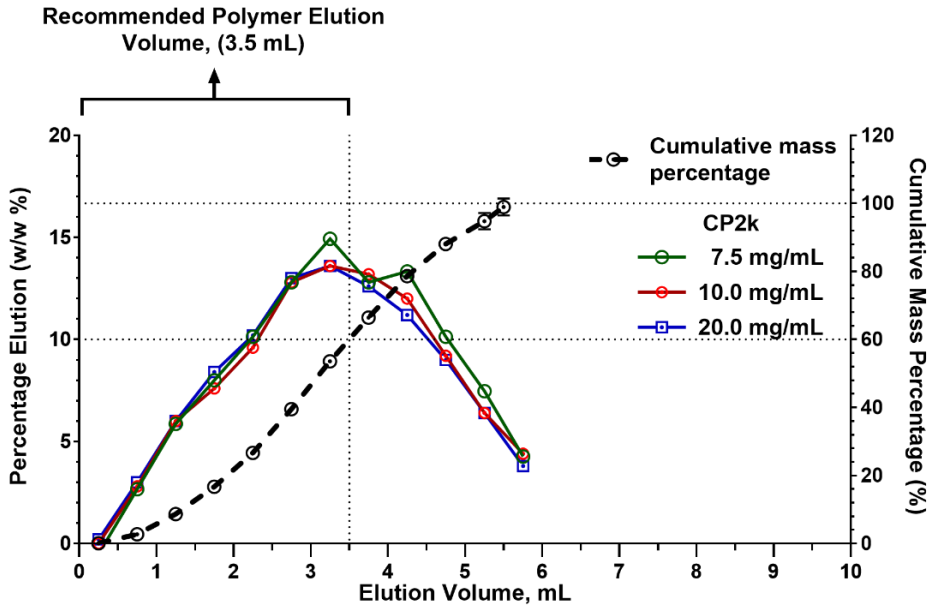

Figure 4-1: Elution profile of CP2k (PD-10 column).

CP2k was loaded on to PD-10 columns at different concentrations (2.5 mL of 7.5, 10 and 20 mg/mL). On the left Y-axis, the percentage of eluted polymer was calculated with respect to the total polymer loaded (18.75, 25 or 50 mg). The mean of cumulative polymer elution was plotted on the right Y-axis (discontinuous black line). N = 1, n = 1.

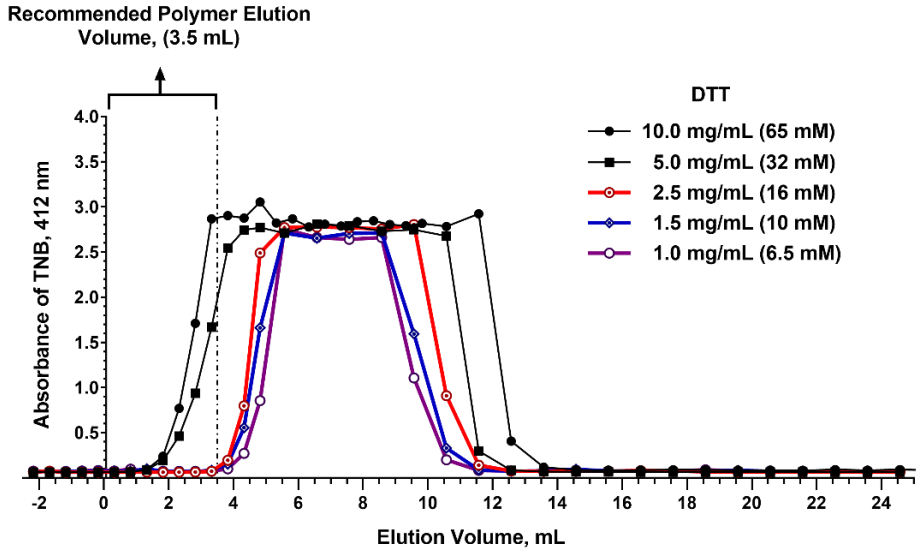

Figure 4-2: Elution profile of DTT (PD-10 column).

DTT was loaded on to PD-10 columns at different concentrations (2.5 mL of 1, 1.5, 2.5, 5 and 10 mg/mL). The eluate was collected in 0.5 mL fractions and Ellman's assay was performed on each fraction. The reaction between DTT and Ellman's reagent [$DTNB^{2-}$, 5,5′-Dithiobis(2-nitrobenzoic acid)] produces a coloured product [TNB, 2-nitro-5-thiobenzoate] which was measured at 412 nm. N = 1, n = 1.

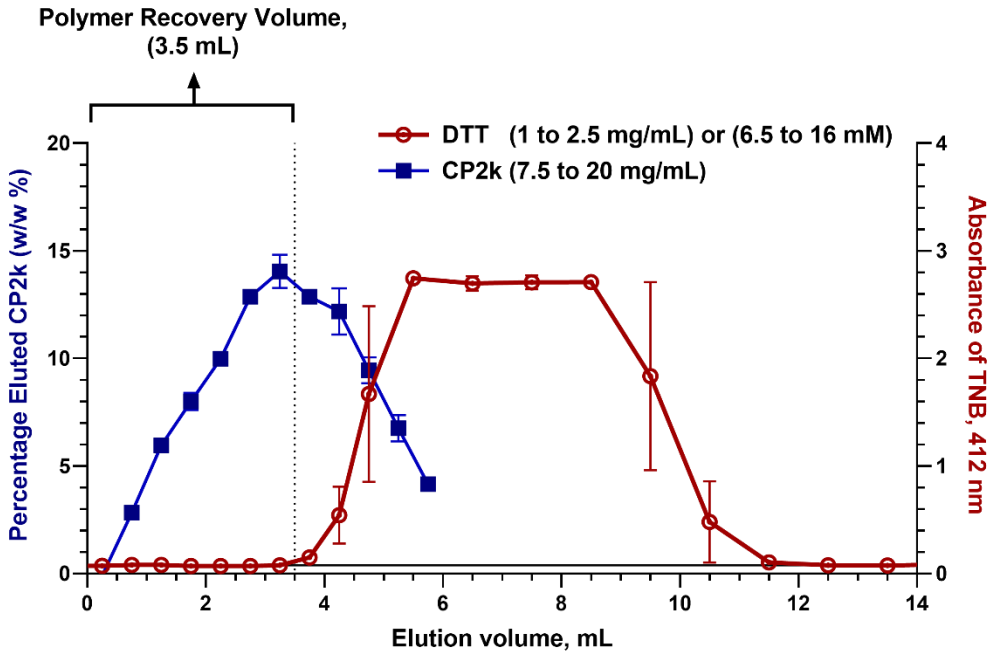

Figure 4-3: Combined elution profile of CP2k and DTT (PD-10 column).
This graph represents the mean of three different elution profiles of CP2k (7.5, 10 and 20 mg/mL) and DTT (1, 1.5 and 2.5 mM). The background absorbance of Ellman's reagent is represented by a continuous black line (Absorbance at 412 nm = 0.077). N = 3, n = 1.

The recommended volume for PD-10 column purification is 3.5 mL as it is normally expected that the larger molecules (>5000 Da) elute in this volume while the smaller molecular weight impurities (<1000 Da) elute after this volume. As the polymer concentrations tested were higher than the recommended (> 1 mg/mL), the elution of CP2k continued even after this recommended elution volume, **Figure 4-1,** page: 132. The cumulative percentage of polymer eluted indicate that only 60% of CP2k can be recovered with 3.5 mL of elution irrespective of the polymer concentrations tested (7.5, 10 and 20 mg/mL). Complete elution (~100%) of CP2k occurred at 6 mL of elution volume.

At the lower concentration of DTT (≤ 2.5 mg/mL or 16 mM) the elution started just after 3.5 mL, while at higher concentrations (5 and 10 mg/mL) the elution of DTT started at 1.5 mL. The amount of polymer that can be recovered at 1.5 mL would be less than 20% (see cumulative elution curve, **Figure 4-1,** page: 132), hence DTT concentrations higher than 2.5 mg/mL cannot be used for

efficient polymer recovery. During the reduction reaction between the polymer (CP2k or CP5k) and DTT (**Figure 4-4,** page: 135), one mole of DTT creates one mole of free thiol in the polymer while releasing one mole of the thiol-protecting group, [t-Boc-SH, mono-Boc (t-butoxycarbonylamino) ethyl mercaptan]. DTT is usually used in excess, compared to the amount of thiol repeating units present on the polymer, to achieve higher efficiency at the reduction reaction. It should be noted that the purification step should eliminate both excess DTT and the by-products of the reduction reaction. In order to theoretically determine the maximum amount of polymer and DTT that can be used for PD-10 column purification, the following assumptions were made: (a) The elution profile of all the impurities were assumed to be similar, hence the total amount of impurities in the purification mixture should not exceed the concentration of 16 mM; (b) The minimum ratio between DTT to polymer thiol repeating units (mol/mol ratio) was assumed as 1.5: 1. Accordingly, it was theoretically calculated that the maximum amount of DTT and polymer concentrations that would yield high polymer recovery and complete elimination of impurities would be 1.5 mg/mL DTT with 16 mg/mL CP2k.

Using the same assumption, the maximum amount of DTT and polymer concentrations were predicted for other two polymers, **Table 4-3,** page: 134.

Table 4-3: Maximum polymer concentration for PD-10 purification.
DTT to polymer ratio was fixed to 1.5:1. The maximum amount of DTT that can be used was calculated as 1.5 mg/mL. The maximum amount of polymer that can be used while the total impurity concentration was ≈16 mM was calculated and listed. The impurities consist of DTT and thiol protecting groups.

Name of the Polymer	Maximum concentration of polymer, mg/mL
CP2k	16
CP5k	30
HP	10

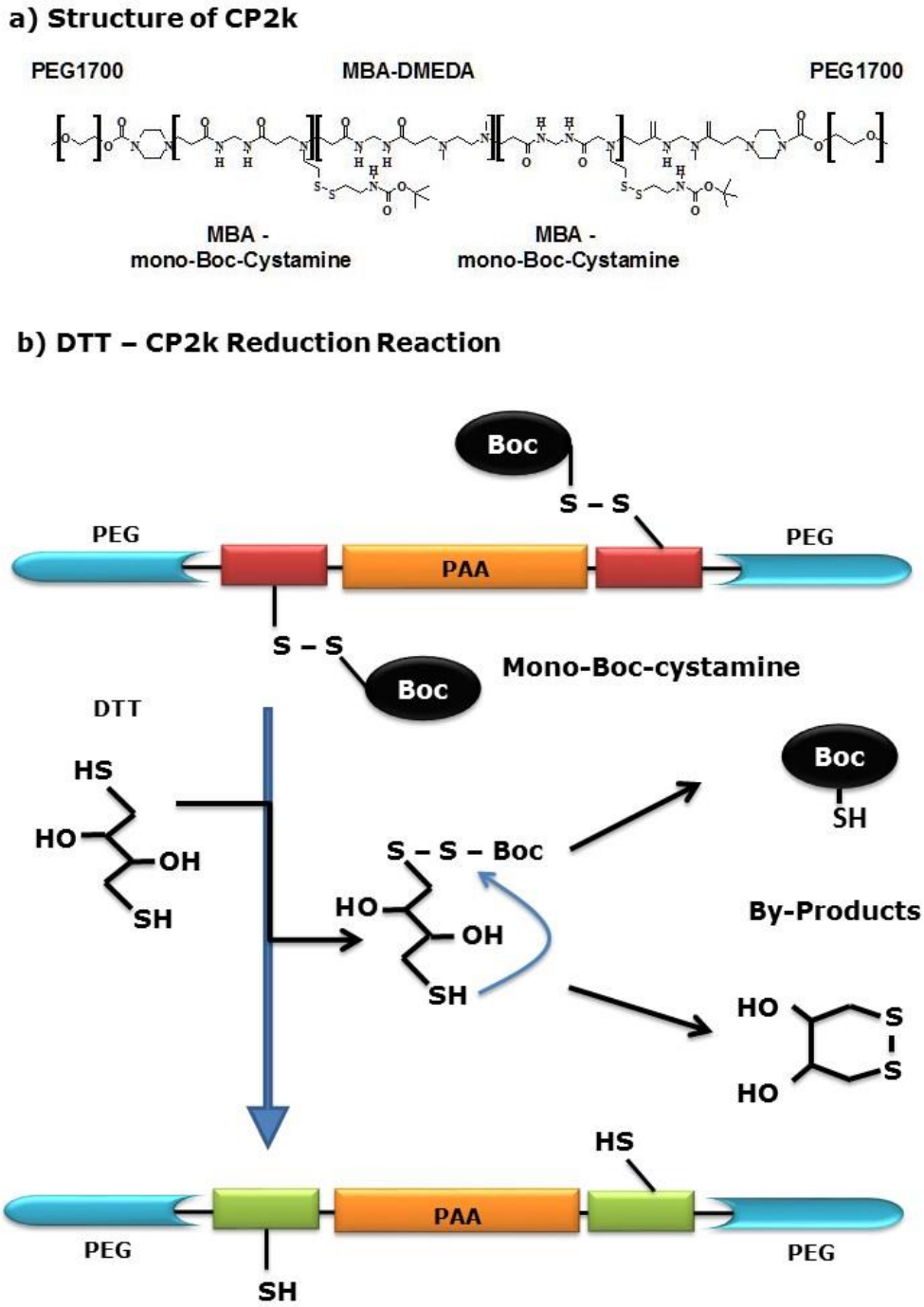

Figure 4-4: Reduction reaction between CP2k and DTT.

Top panel 'a' shows the chemical structure of CP2k(non-reduced); the bottom panel 'b' shows the schematic representation of the reduction reaction between DTT and CP2k. The by-products of this reaction are cyclic-DTT and the thiol protecting group, Boc-SH [mono-Boc (t-butoxycarbonylamino) ethyl mercaptan].

Polymer Yield: Following reduction with DTT, CP2k was purified with the PD-10 column. The eluate from PD-10 column was collected, freeze-dried and the yield was measured. The purification was also performed by dialysis using a 6000-8000 Da MWCO [molecular weight cut-off] dialysis membrane. The dialysis was performed for 30 hours against 5L of distilled water. The water was changed 6 times. The polymer yield and free thiol yield were calculated after freeze-drying. The results were compared with the yield from the original ultra-filtration protocol. The ultra-filtration step consisting of 4 cycles of 250 mL acidified water was performed using a 5000 Da MWCO filter.

Table 4-4: Comparison of different modes of copolymer purification.

CP2k	**PD-10 Column**	**Ultra-filtration**	**Dialysis**
Purification Time	20 minutes	8 hours	30 hours
Polymer Yield	49.2 ± 10.1% (N = 29)	50% (N = 1)	35.5% (N = 1)
Free Thiol - Yield	49.9 ± 7.3 (N = 4)	35% (N = 1)	0% (N = 1)
CP5k	**PD-10 Column**	**Ultra-filtration**	**Dialysis**
Polymer Yield	83.2 ± 4.5 (N = 2)	50.45 ± 30.24 (N = 3)	Not performed
Free Thiol - Yield	27.3 ± 2.8 (N = 4)	9.61 ± 4.36 (N = 3)	Not performed

4.3.2 Gel Retardation Assay - HP: CP2k Complexes

This chapter is focused only with the preparation of HP-CP2k-miRNA complexes. In the previous chapter, HP: CP2k complexes were investigated at different HP: CP ratios [3:1, 1:1, 1:3] and PAA RU to miRNA Nt ratios [RU/Nt = 1:1, 2:1, 3:1, 4:1 and 5:1]. These complexes were investigated for their complexation efficiency with miRNA, size of the complexes and *in vitro* performance. In this chapter, these complexes were investigated on the basis of their stability in physiological ionic concentration (150 mM NaCl) and *in vitro* performance.

The complexes were either prepared in optimal [25 mM PBS, pH 6.0] or physiological ionic concentration [150 mM, 1x PBS, pH 7.4]. These complexes were loaded on to an agarose gel. No prominent differences in binding behaviour

were found between both conditions on the gel. Only the gel images for complexes prepared under physiological condition are presented, **Figure 4-5,** page: 137. Almost complete complexation was seen for the RU/Nt ratio ≥ 2.5:1 for both the complexes HP: CP ratio 3:1 and 1:1, and at two different salt concentrations (25 mM and 150 mM). It could be anticipated that the agarose gel assay may not distinguish between crosslinked and non-crosslinked complexes, especially for high RU/Nt ratios, as the major interaction between miRNA and polymer is via electrostatic interaction.

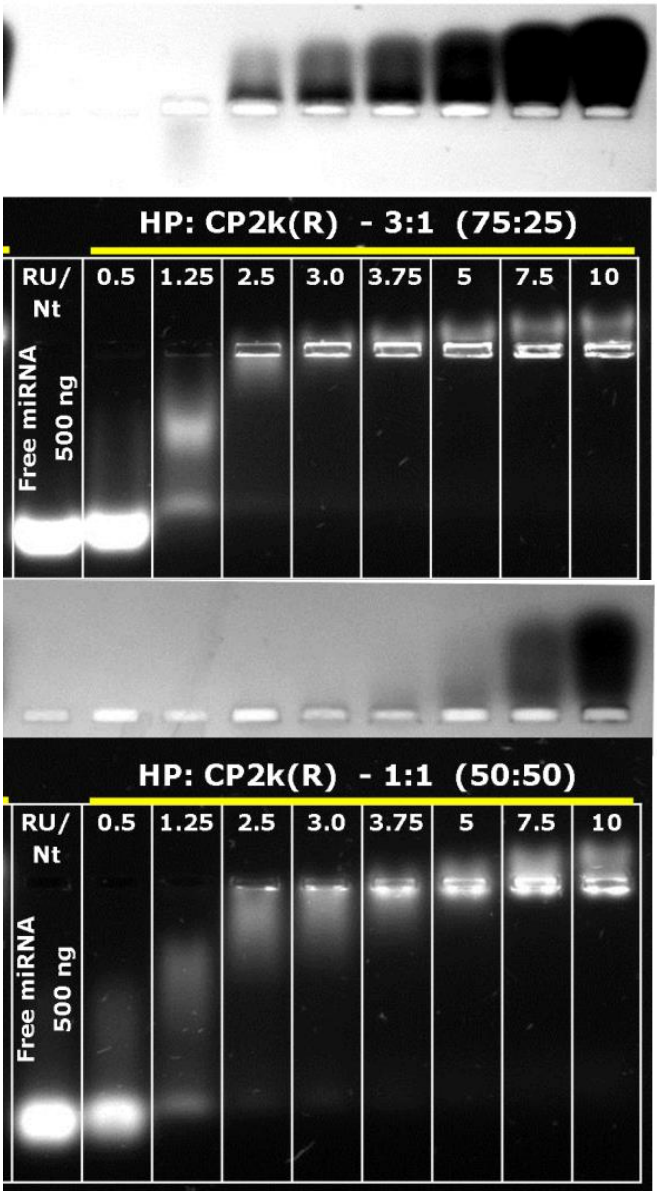

Figure 4-5: Gel retardation assay, HP: CP2k(R) miRNA complexes.

Top Image: HP: CP Ratio 3:1; Bottom Image: HP: CP Ratio 1:1. Complexes were prepared in 150 mM PBS, pH 7.4; Each image represents the same gel stained either by coomassie blue (top white part) or ethidium bromide (bottom black part).

4.3.3 Size Analysis

The PAA-miRNA polyplexes were analysed by Dynamic Light Scattering (DLS) using Malvern NanoS instrument (University of Angers) which is different from the Viscotek DLS802 (University of Nottingham).

4.3.4 Effect of miRNA concentration on size of the polyplexes

Initially, non-crosslinked HP: CP2k complex at a fixed HP: CP ratio (3:1) and RU/Nt ratio (5:1) was prepared by mixing equal volume of polymer blend and miRNA at different concentrations, **Figure 4-6,** page: 138. The complexes were prepared in 25 mM PBS, pH 6.0.

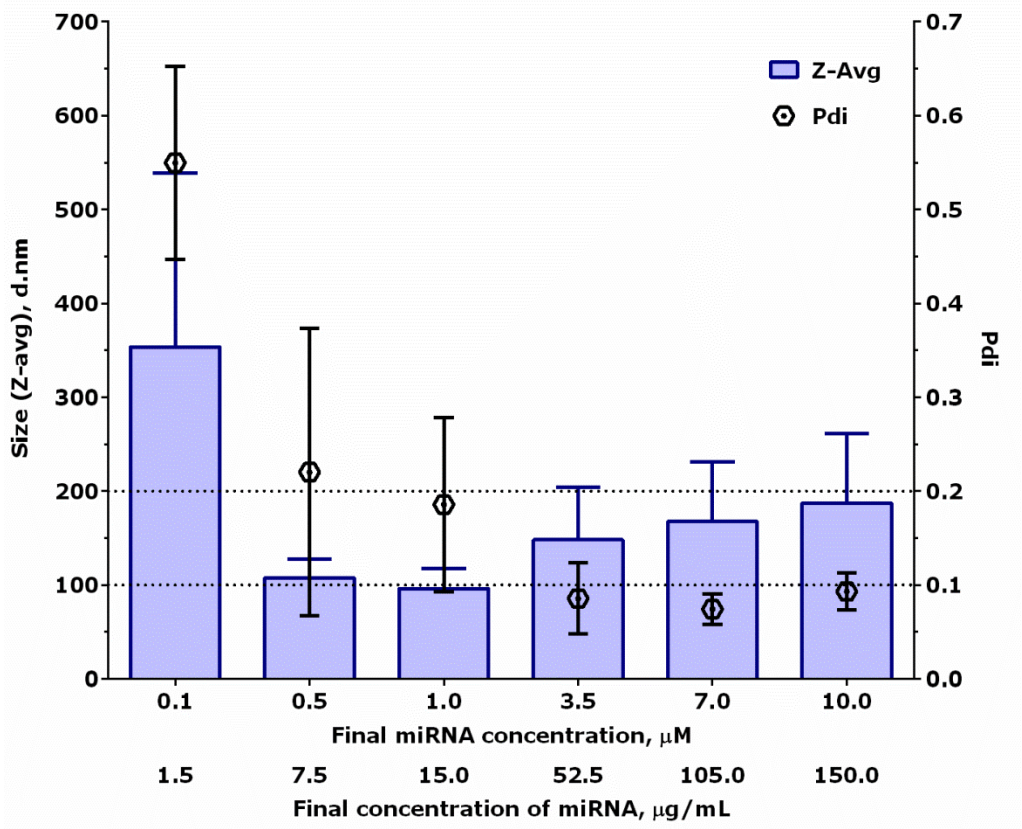

Figure 4-6: Influence of miRNA concentration on particle size.
miRNA concentration versus size of non-crosslinked HP: CP2k polyplexes in 25 mM PBS. HP: CP Ratio 3:1; RU/Nt Ratio 5:1; 25 mM PBS, pH 6.0; X-axis represents final miRNA concentration of polyplexes. Pdi < 0.1 monodisperse particle size distribution, Pdi > 0.4 means presence of multiple peaks. The error bars represent the width of the size-peak hence indicating the size distribution. (N = 3, n = 3).

The polydispersity index (Pdi) of the polyplexes reduced as the concentration of microRNA increased, indicating efficient complex formation. Best complexation (small monodisperse nanoparticles: size < 200 nm, Pdi < 0.2) was obtained between 3.5 and 10 µM (50 – 150 µg/mL) concentrations of miRNA. This concentration was similar to the miRNA concentration used for other polymeric nanoparticle preparations, while higher than the peptide- (N-TER) and lipid- based (Lipofectamine) commercial reagents, see **Table 4-5,** page: 139. It was known from two-component polyplex systems that the concentration of polymer-nucleic acid mixture was not only important for achieving sufficient scattering on DLS, but it also had control over size.

Table 4-5: Comparison of different nanoparticle formation media.

Optimized miRNA concentration and nanoparticle formation media among different nanoparticle systems. £ - Composition not defined; # - The molecular weight of siRNA and miRNA was assumed as 13300 and 15000 g/mol, respectively, for calculating the concentration in µg/mL. * - Initial concentration of nanoparticle formation solution (NFS) in which either the nucleic acid or polymer or both were prepared before mixing them together.

Nanoparticle / Nucleic acid	**Initial conc. of miRNA, µM (µg/mL)**	**Initial NFS* Medium Composition**
N-TER Peptide, Sigma[333] (miRNA/ siRNA)	0.650 (9.75) #	siRNA Dilution Buffer £
Lipofectamine RNAiMAX[334], Invitrogen (miRNA/ siRNA)	0.100 (1.50) #	Opti-MEM
Lipid Nanoparticles (LNP) assembled in microfluidic device[190] (siRNA)	20 – 40 (300 - 600) #	siRNA in 25 mM acetate buffer, pH 4.0 + Lipid in ethanol
***In vivo*-jetPEI®, Polyplus (miRNA)[335]**	25 (375) #	5% Glucose
Chitosan[336] (miRNA)	2.5 (37.5) #	Acidified water
PAA – p(DMEDA-MBA) (pDNA – 6 and 7 kbps)[297]	10 µg/mL	1X PBS (150 mM NaCl); 1/10 PBS (14 mM NaCl); 5% Glucose
PAA – p(DMEDA-MBA) (pDNA – 6 and 7 kbps)[296]	10 - 125 µg/mL	40 mM TAE, pH 7.4 1x PBS pH 7.4
PAA – HP10k: CP05[275] (siRNA, OligoDNA)	7.0 µM (100 µg/mL) #	5 mM NaCl

4.3.4.1 miRNA concentration versus HP:CP ratio

To test the effect of miRNA concentration and HP: CP ratio for thiol crosslinked nanoparticles, RU/Nt ratio was fixed at 5:1, while different HP: CP ratios (3:1, 2:1, 1:1, 1:3) and two different microRNA concentrations (5 µM and 7µM) were tested, **Figure 4-7**, page: 140. HP-CP polymer blends were prepared in 50 mM PBS, pH 6.0 and mixed with equal volume of microRNA solution (10 µM and 14 µM miRNA in water). Hence, the final concentration of miRNA during complex formation was 5 µM and 7 µM, while the salt concentration corresponds to 25 mM of PBS (0.33x PBS). All the complexes obtained were monodisperse with a narrow size distribution (Pdi ≤ 0.1). All the HP: CP ratios tested produced nanoparticles smaller than 200 nm, except 1:3. The size of thiol-crosslinked complexes formed at 5 µM miRNA concentration produced slightly smaller nanoparticles compared to 7 µM, so 5 µM was chosen for further experiments.

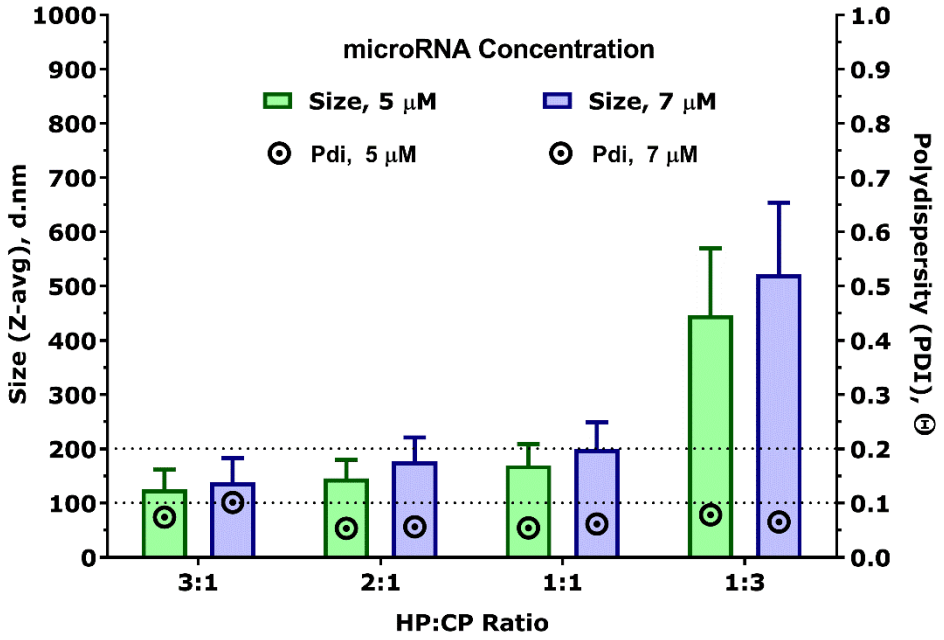

Figure 4-7: microRNA concentration and HP:CP ratio on particle size.

Comparison of miRNA concentrations (5 µM and 7 µm) on the size of thiol crosslinked HP: CP2k(R) polyplexes at different HP: CP ratio, in 25 mM PBS, pH 6.0; RU/Nt Ratio fixed at 5:1. The error bars represent the width of the size-peak hence indicating the size distribution. (N = 1, n = 3).

4.3.5 Stability Analysis

All the complexes formed in 25 mM NaCl (low salt concentration) produced small, mono-disperse nanoparticles. These nanoparticles were tested for their stability in ionic (e.g.150 mM NaCl) and non-ionic (e.g. Glucose, Sucrose) isotonic solutions.

4.3.5.1 HP: CP Ratio Vs Stability of Polyplexes

The stability of the complexes prepared at different HP to CP ratios were studied at a fixed RU/Nt ratio (5:1) and miRNA concentration (5 µM).

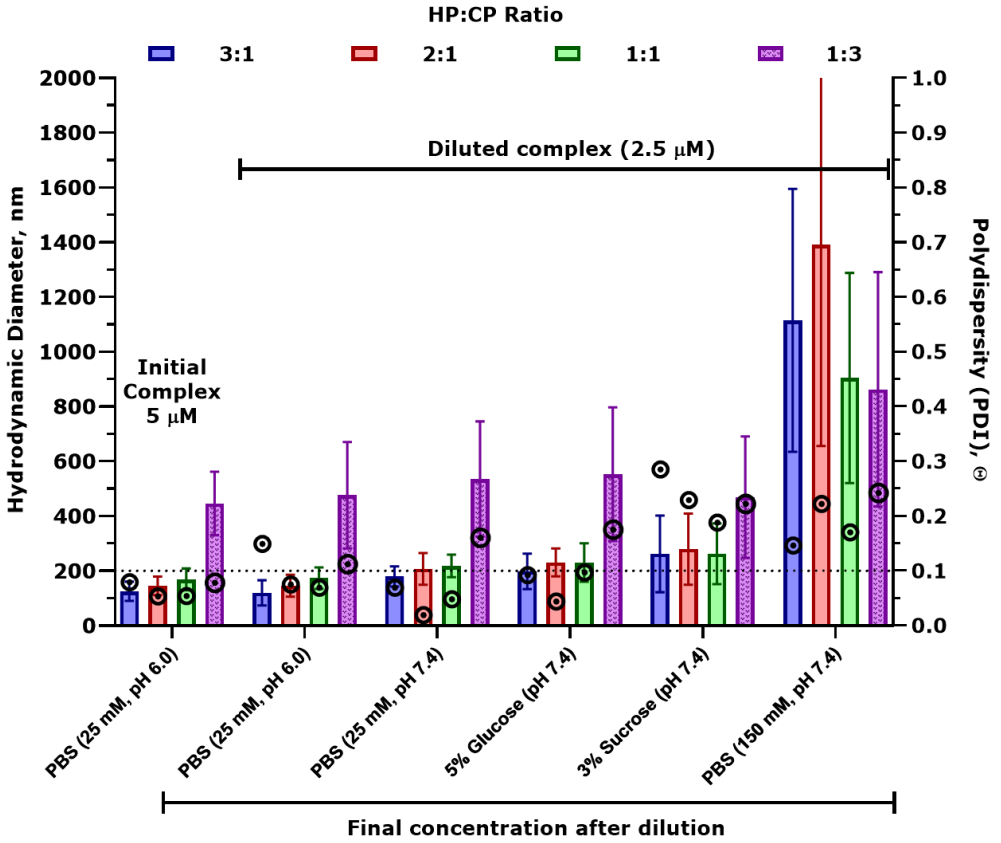

Figure 4-8: Stability of HP: CP2k(R) complexes, (salt in polymer).
All the complexes were prepared at a constant RU/Nt ratio 5:1. The initial complex (5 µM, miRNA concentration) was prepared by mixing equal volumes of polymer blend (in 50 mM PBS) and miRNA (10 µM, in water). The initial complex was then diluted with equal volume of 1x or 2x diluent to achieve the indicated conditions. 5% glucose and 3% sucrose were prepared in 25 mM PBS, pH 7.4. (N = 1, n = 3).

All the initial complexes (5 µM, in 25 mM PBS, pH 6.0) were monodisperse (Pdi < 0.1). The size of the complexes did not change upon dilution (1/2) with a

medium same as the nanoparticle solution [PBS (25 mM, pH 6.0)]. However, when diluted with PBS (25 mM) at pH 7.4, a slight increase in size was observed for all the complexes indicating that change in pH can influence the size of these PAA-miRNA complexes, probably due to looser binding between miRNA and polymer. The pH of the medium determines the charge density and conformation of the polymer by controlling the percentage of protonated amines[337] which in turn increases or decreases the adhesive forces between polymer and nucleic acid[337]. Dilution with low-ionic solutions like glucose [5% glucose in 25 mM PBS, pH 7.4] or sucrose [3% sucrose in 25 mM PBS, pH 7.4] resulted in a slight increase in the complex size, whereas dilution with full strength PBS [150 mM, pH 7.4] showed 4- to 6- fold increase in its size. The increase in size was inversely proportional to the amount of CP2k in the mixture. This increase in size of polyplexes can be explained by combining polyelectrolyte theory (PEC)[317] and salt-induced aggregation phenomenon.

Salt-induced aggregation: High salt concentrations can induce formation of large aggregates. This salt-induced aggregation is a well-known phenomenon in colloidal systems[338], proteins[339] and charged non-polyelectrolyte nanoparticles[340,341]. Physiological to high salt concentrations [150 mM[340] – 855 mM[341], NaCl] neutralise the excess negative-charge (repulsive force) at the surface of citrate coated gold nanoparticles and caused aggregation. This type of aggregation can be prevented by steric stabilization [e.g. addition of PEG at the surface of nanoparticles][342]. As the HP: CP2k(R)-miRNA polyplexes have PEG at their surface, salt-induced aggregation alone is not able to explain the increase in size of nanoparticles after the exposure of physiological concentrations of salt.

Polyelectrolytes and Salt: Polyplexes are formed by the interaction between oppositely charged polyelectrolytes. Presence of salt (counter-ions) would compete with the interaction between anionic [e.g. miRNA, siRNA or plasmid DNA] and cationic [e.g. PEI (polyethylenimine), PAA (polyamidoamine)] polyelectrolytes[317]. When there is high concentration of one of the polyelectrolytes and there are no or very few counter-ions, the polyplexes formed would be less compact due to the repulsive force between the un-neutralized charges[317]. When there is right amount of counter-ions in the system,

they would allow rearrangement of the polyelectrolytes resulting is tighter and more compact polyplexes[317]. If counter-ions are present in sufficient high quantities (excess salt), they compete effectively with polyelectrolyte interactions resulting in the destabilization and disassembly of polyplexes into smaller polyelectrolytes[317]. The extent of disassembly might depend on the strength of interaction between the polyelectrolytes and concentration of salt.

When the crosslinked complexes were subjected to excess salt concentration, the competition from counter-ions might destabilize miRNA-polymer interactions hence affecting the structure and compactness of the polyplexes while the complete disassembly of the individual polymer chains would not occur due to the presence of disulphide bridges. If there are sufficiently high number of disulphide bridges, then it might create a thiol-crosslinked polymer-skeleton/cage-like structure preserving the existing structure of polyplexes from deformation induced by salt. But, when there is insufficient or very few disulphide bridges, the excess salt would destabilize the miRNA-polymer interaction resulting in loose, large complexes (salt mediated swelling or salt sponge effect). The PEG at the surface of such loose complexes may not have sufficient steric hindrance to prevent salt-induced aggregation. Hence, these sterically unstable loose complexes would aggregate resulting in larger particles consisting of a PAA-miRNA core and PEG shell. This aggregation might continue until the surface-PEG gains sufficient steric hindrance to prevent further aggregation.

Alternatively, the physiological salt concentration might disrupt the nano-assemblies creating loose PAA-miRNA complexes. Usually these destabilized complexes scatter much less light, indicated by the attenuation factor during DLS measurement. Although this salt concentration might be strong enough to disrupt the compactness and structure of nano-assemblies, it might not necessarily release miRNA from the polymer. Hence, the increase in size of all the complexes in 150 mM PBS might be attributed to insufficient thiol-crosslinking resulting in the salt-sponge effect and subsequent aggregation[247] or simple nano-disassembly. Therefore, increasing the amount of thiol-crosslinking might help improve the stability of these polyplexes.

4.3.6 Salt induced crosslinking

The effect of salt-induced aggregation on polyplexes, discussed above, can also be applied to polymers themselves. Aggregation of polymer would increase the rate of inter-molecular crosslinking of thiol containing polymers. Hence, the kinetics of self-oxidation of free thiols of CP2k(reduced) was determined in the presence and absence of salt (50 mM PBS, pH 6.0), by Ellman's assay. L-cysteine standard curve is presented in the supplementary data, **Figure 4-30,** page: 168. The amount of free thiols decreased over time, **Figure 4-10,** page: 144. The concentration of free thiol decreased faster in the presence of salt (half-life time of free thiols in PBS, $t_{1/2,\ PBS,\ 50\ mM} \approx 4h$) compared to the same polymer in water ($t_{1/2,\ water} \approx 6.5h$). This confirmed that the salt is able to reduce the repulsive force between the cationic PAA chains and hence bringing the polymer chains closer together which in turn increases the chances of self-oxidation. This self-oxidation could occur by both intra- and inter-molecular crosslinking, **Figure 4-9**, page: 144. As the polymer was in dilute solution (2 mg/mL), inter-molecular collusions might be less frequent and hence the majority of crosslinking could be happening by intra-molecular mode. Further investigation is needed to confirm this speculation.

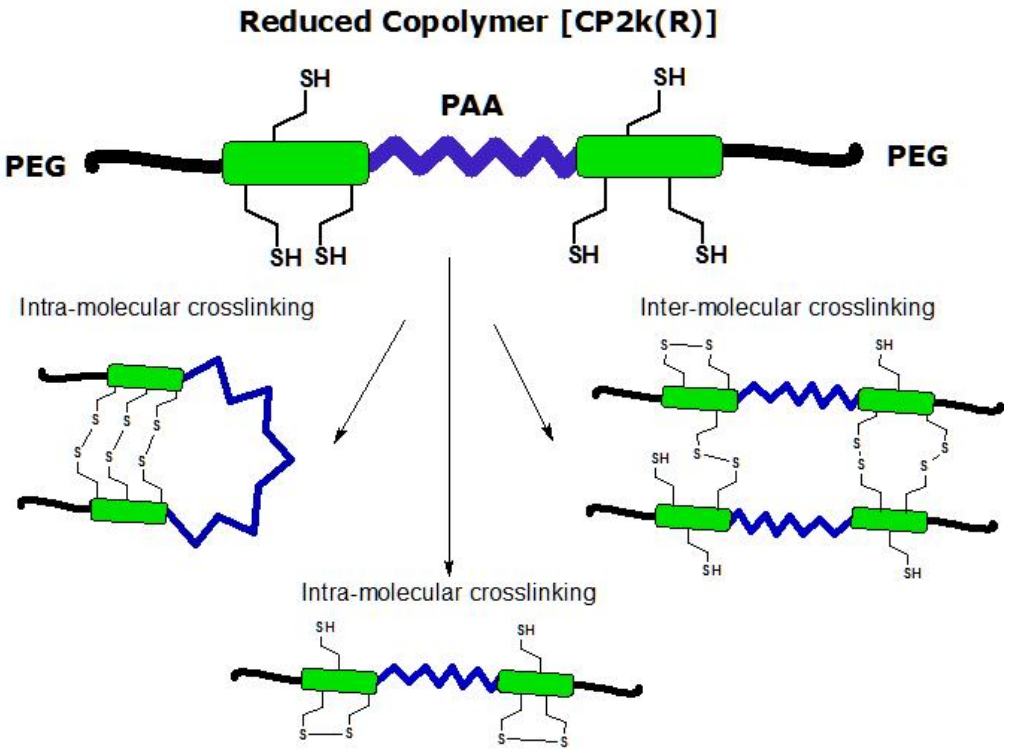

Figure 4-9 Different modes of copolymer self-oxidation [CP2k(R)].

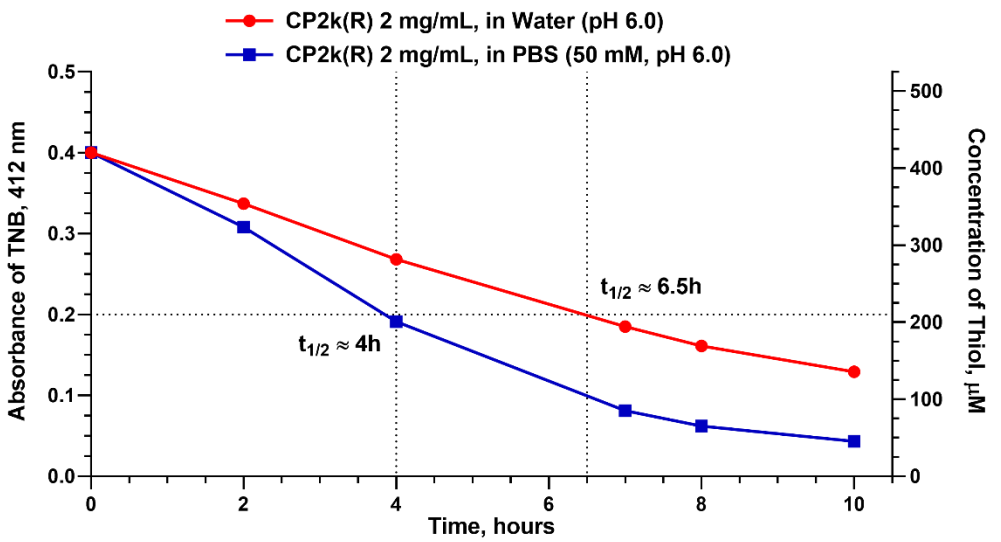

Figure 4-10: Salt induces self-oxidation kinetics of copolymer.

The concentration of thiol was periodically measured by Ellman's assay. The concentration of CP2k(R) was 2 mg/mL. (N = 1, n = 1).

For the preparation of polyplexes, the initial step is the preparation of polymer blends containing HP and CP. Similar to the previous observation with self-oxidation of CP2k(R), the presence of salt in this mixture would reduce the repulsive force between HP and CP, and hence enhance thiol-crosslinking process even before the addition of nucleic acid (miRNA), (for thiol-thiopyridine crosslinking reaction, see **Figure 4-11,** page: 145).

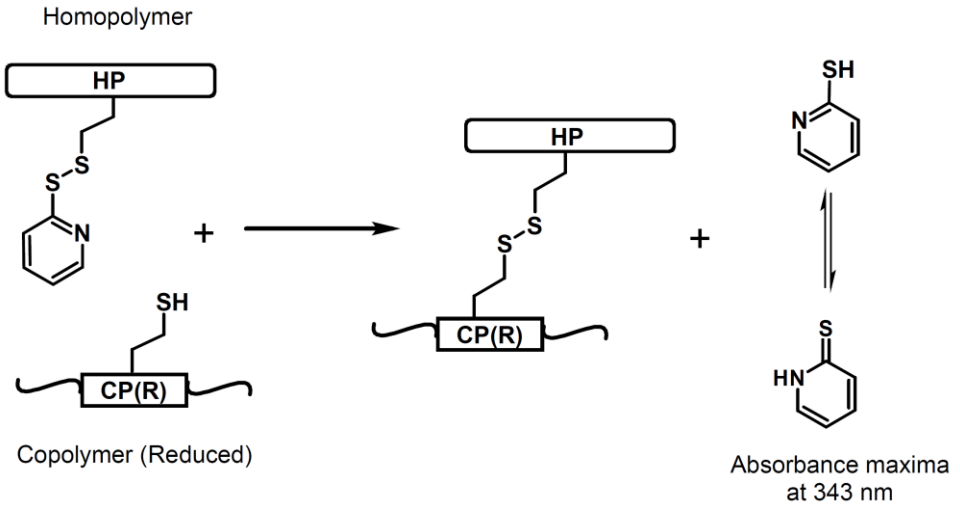

Figure 4-11: HP-CP thiol-crosslinking and release of thiopyridine.

The release of thiopyridine (tautomeric form - thiopyridone) can be monitored at 343 nm[343]. HP and CP are cationic homo- and co-polymers. CP(R) represents the reduced form of CP which contains free thiols.

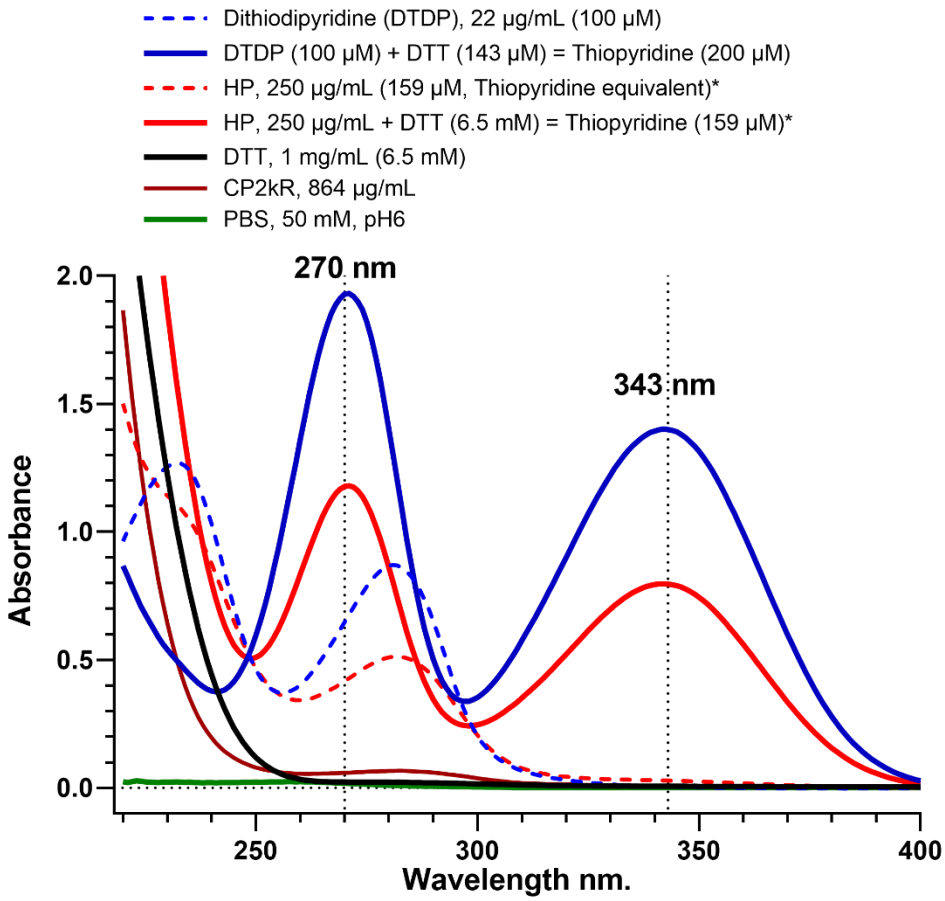

Figure 4-12: Absorption spectra for polymers and buffers (220 – 400 nm). Homopolymer (HP) and 2,2′-dithiodipyridine (DTDP) do not absorb light at 343 nm (dotted lines), while addition of DTT results in the release of thiopyridine which has a specific absorbance peak at 343 nm (continuous lines). * theoretical thiopyridine concentration. (N = 1, n = 1).

The characteristic absorption maxima of 2-thiopyridine is at 343nm[343]. Absorbance spectra of homopolymer (HP), copolymer [CP2k(R)], Phosphate buffered saline (PBS), 2,2′-Dithiodipyridine (DTDP), Dithiothreitol (DTT), HP+DTT and DTDP+DTT are presented in **Figure 4-12,** page: 145. None of the molecules or buffers tested showed an absorption peak at this wavelength (343 nm). However, the DTDP + DTT and HP + DTT mixtures showed the characteristic absorption peak at 343 nm, indicating the release of 2-thiopyridine. Hence, the crosslinking reaction between HP and CP2k(R) which would release 2-thiopyridine can be spectrophotometrically followed at 343 nm.

To test influence of salt in triggering the crosslinking reaction even before the addition of miRNA was tested using a polymer blend [HP-CP2k(R) 1:1, RU/Nt

10:1 equivalent] that was either prepared in the presence of salt [25 mM or 50 mM PBS, pH 6.0] or absence of salt [water, pH 6.0]. Equal amount of HP (in 50 mM PBS, pH 6.0) was used as a control. The absorbance at 343 nm was recorded, after mixing HP and CP2k(R), for two hours (between 5 – 125 minutes) to monitor HP-CP crosslinking (thiopyridine release), **Figure 4-13,** page: 146.

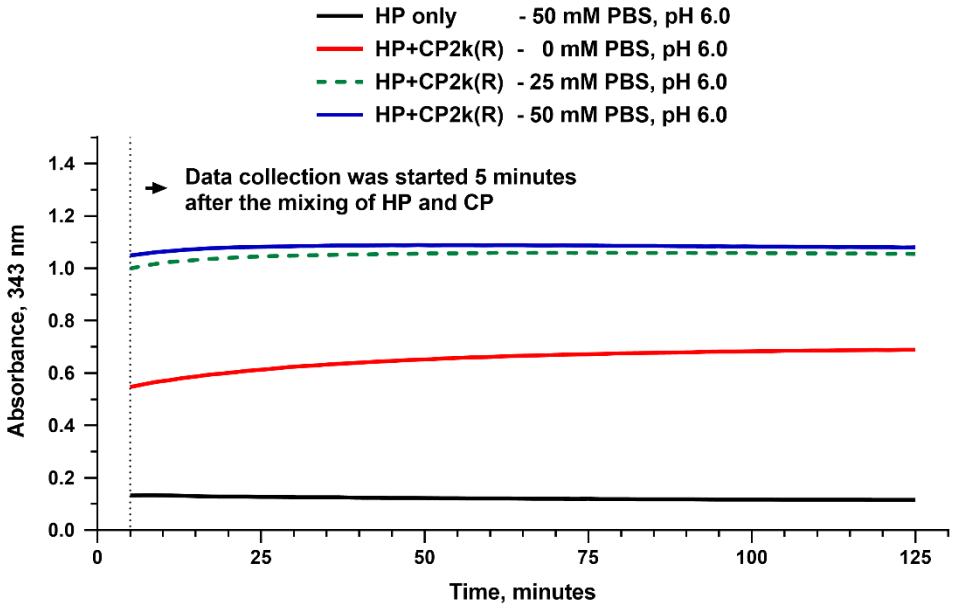

Figure 4-13: Kinetics of HP-CP crosslinking (120 minutes, no miRNA).
HP (0.75 mg/mL, pH 6.0) was mixed with CP2k(R) (0.8636 mg/mL, pH 6.0) which corresponds to HP: CP PAA repeating unit ratio of 1:1 and RU/Nt ratio of 10:1 (equivalent). Water was used as blank. (N = 1, n = 1).

The crosslinking between HP and CP2k(R) would release the HP's thiol-protecting group, 2-thiopyridine. The 2-thiopyridine was rapidly released in the first few minutes of mixing the polymers (HP and CP2k-R), indicating that the thiol-thiopyridine crosslinking reaction happens both in the presence and absence of salt, **Figure 4-11,** page: 145. However, the amount of crosslinking was half that when the polymer-blend was prepared in water (pH 6.0) compared to the polymer mixture prepared in PBS (50 mM or 25 mM, pH 6.0). The thiopyridine release reached its plateau within 30 minutes, for both the conditions. The polymer-mixture in water did not reach the same level of thiopyridine release as the polymer mixture in PBS, even after 2 hours of incubation. This again assures that salt improves polymer-polymer interaction,

probably by reducing the repulsive forces between the cationic chains and hence increasing the HP-CP crosslinking even in the absence of microRNA.

To re-confirm that the addition of salt improves HP-CP crosslinking, the HP: CP mixture was prepared either in the presence or absence of salt as described above. The thiopyridine release was monitored for initial 10 minutes. The HP-CP crosslinking was allowed to reach its plateau by incubating for another 15 minutes (data was not collected during this time) and then salt was added to the HP-CP blend which was already prepared in water and the thiopyridine release was monitored thereafter, **Figure 4-14,** page: 147. For the polymer-blend newly supplemented with salt, the thiopyridine release curve started at the same absorbance (Abs_{343nm} = 0.47) value and followed the thiopyridine release profile similar to the polymer-blend that was initially prepared in salt. It is known from the previous observation that the polymer-blend prepared in water would not reach the same amount crosslinking as the polymer-blend prepared in salt even after two hours of incubation. The immediate increase in thiopyridine absorbance triggered by the addition of salt confirms salt-induced crosslinking. It should be noted that the thiol-thiol crosslinking is a slow reaction (occurs in hours' scale) while the thiol-thiopyridine reaction is rapid (occurring in minutes' scale). Taken together, the presence of salt in the polymer mixture is detrimental to the free thiols, as they would enhance crosslinking even before the addition of nucleic acid. When the complexes are prepared in this pre-crosslinked polymer mixture, those complexes would only have a limited amount of free thiols to crosslink after the complex formation and hence would not be able to maintain its structural-integrity so easily upon exposure to physiological salt concentrations. Hence, when preparing the polyplexes, the polymers should be blended immediately before adding it to the nucleic acid and the blends should be prepared in water (in the absence of any salt). These measures would preserve free thiols to enable crosslinking after the formation of polyplexes, which would ultimately would result in the formation of stable nanoparticles. Although there would be some spontaneous crosslinking even when the polymer-blends are prepared in water, it should be noted that these polymer-blends would still contain crosslinkable thiols as indicated by the ability to release thiopyridine

upon addition of salt after the initial spontaneous crosslinking, **Figure 4-14,** page: 147.

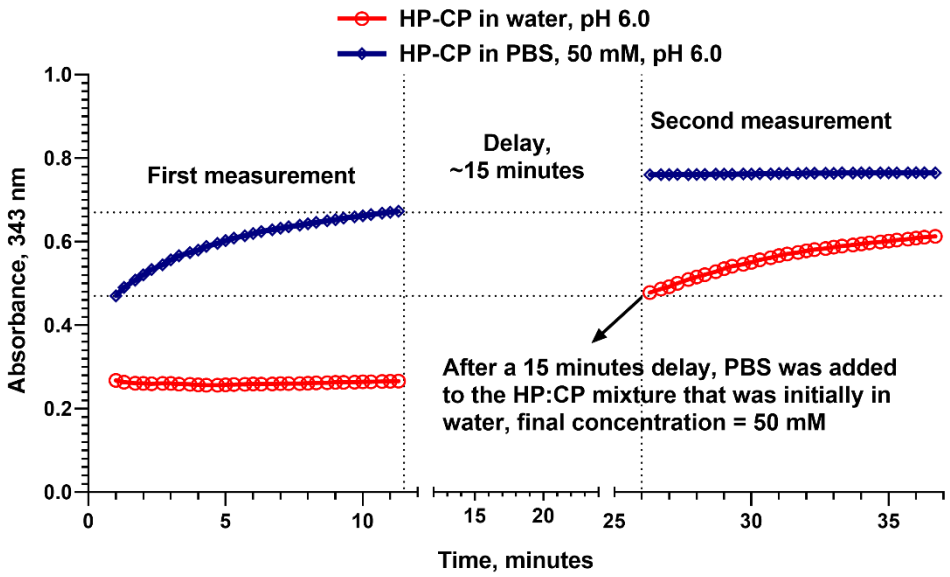

Figure 4-14: Kinetics of HP-CP crosslinking (40 minutes, no miRNA). Thiopyridine release was measured for 15 minutes in the presence and absence of salt (50 mM PBS, pH 6.0). After a 15 minutes of delay, 33 µL of PBS (10x, 1500 mM) was added to 1 mL of the HP-CP mixture. N = 1, n = 1.

Altogether, these salt-induced crosslinking explains the reasons for the instability of polyplexes (in physiological salt concentration) prepared in the previous section as the polymer-blends were prepared in the presence of salt (PBS, 50 mM, pH 6.0) (**Figure 4-8,** page: 141). Also, it provides deeper understanding of the crosslinking process which in turn enables the modification of the nanoparticle preparation protocol to obtain stable nanoparticles. In the following section, the nanoparticles were prepared in water (absence of salt).

4.3.7 Nanoparticles are stable when prepared in water

PAA-miRNA nanoparticles at a fixed HP: CP ratio [3:1] were prepared in the absence of salt (0 mM NaCl, water, pH 6.0). The RU/Nt ratio was varied (1.25, 2.5, 4.0, 5.0, 6.0). After 30 minutes of condensation and crosslinking, an aliquot of nanoparticle was diluted (1/2) by mixing either with equal volume of 300 mM NaCl (green bars) or 2x PBS, pH 7.4 (orange bars). The size of the complexes was studied before and after dilution, NaCl (150 mM) or PBS (1x), **Figure 4-15,** page: 149.

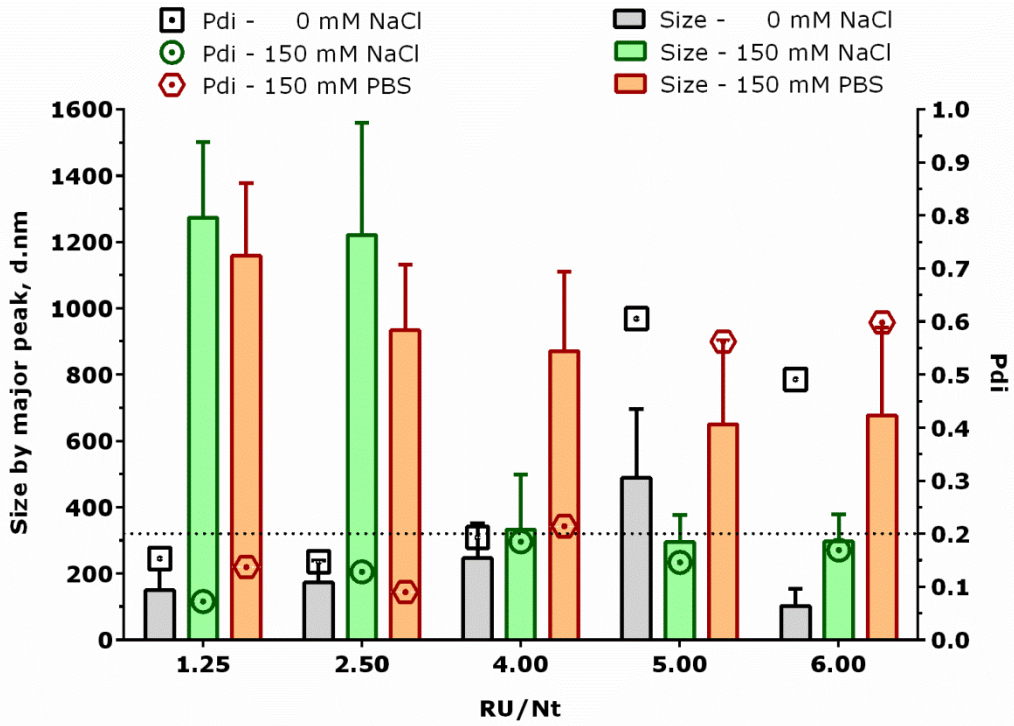

Figure 4-15: Improved stability of PAA-miRNA polyplexes (salt-free).

HP: CP Ratio 3:1; initial complex preparation in water, pH 6.0; The error bars represent the width of the size peak hence indicating the size distribution. (N = 1, n = 3).

Effect of Phosphate on Stability of Complexes: The complexes prepared in the absence of salt produced stable complexes when diluted with NaCl (150 mM), while the size and polydispersity of the complexes increased in PBS (1x, pH 7.4). This increase in size induced by PBS (1x) could be because of the competitive binding of phosphate ions with the polymer creating loose complexes that might lead to aggregation as discussed in the previous section (see polyelectrolytes and salt, **section 4.3.5.1,** page: 141).

The negatively charged phosphate group from miRNA backbone interacts with the positive charged polymer to form polyplexes. Full strength PBS (1x) contains 138 mM NaCl, 2 mM KCl and 10 mM Phosphate. The concentration of miRNA in each of the complexes tested was 2.5 µM (46 nucleotides) which corresponds to 115 µM of phosphate ions from microRNA backbone. The concentration of phosphate ion from 1x PBS is 10 mM (10,000 µM). Due to the chemical similarities, phosphate ions from PBS might be competing with phosphate ions from miRNA more potently than the chloride ions from NaCl. This competition might be disrupting the miRNA-PAA interactions resulting in the increase in nanoparticle size.

Further improvements in the amount of thiol crosslinking might be able to counteract the phosphate induced destabilization effect. This can be achieved by increasing the amount of CP in the polymer mixture, ie. by using HP: CP ratio to 2:1 or 1:1, instead of 3:1. The HP: CP ratio and the corresponding thiopyridine to thiol ratio (SPy: SH ratio).

Stable Nanoparticles in Saline Solution (150 mM NaCl): The size analysis of the complexes formed in water produced monodisperse small nanoparticles (Pdi < 0.2 and size ~ 200 nm) from RU/Nt ratio 1.25:1 to 4:1. At higher RU/Nt ratios they produced polydisperse particles (Pdi > 0.2, multiple peaks). However, when these complexes were mixed with 300 mM NaCl (equal volume) to obtain physiological salt concentrations, RU/Nt 4:1, 5:1 and 6:1 yielded monodisperse small nanoparticles, whereas the size and pdi of the lower RU/Nt ratio did not produce stable particles. Hence, the final size of the nanoparticles under physiological condition could not be directly inferred from the complexes formed at 0 mM NaCl. This prompted that the size of all the PAA-miRNA polyplexes prepared must be studied under physiological ionic concentrations (150 mM NaCl) to closely resemble the nanoparticle size in the actual condition it would be used, cell culture media or body fluids.

4.3.8 Salt-Free Formulation Method

Presence of salt in the polymer blends leads to crosslinking of HP and CP and hence affects the stability of the resulting PAA-miRNA complexes. Based on this finding, the salt (PBS, 25 mM) was removed from the complex formation step. However, following 30 minutes of incubation to allow crosslinking, the complexes were mixed with equal volume of 2x physiological salt solution (300 mM NaCl), **Figure 4-16,** page: 150. The polyplexes present in the physiological ionic concentration is then subjected to physicochemical characterization and *in vitro* analysis. The size of the complexes measured in low (25 mM) or no (0 mM) salt concentration does not always reflect the actual size of the complexes in physiological ionic concentration. Hence, it is necessary to test the size of all complexes in physiological salt concentration to ensure the size and stability of complexes before they can be used for *in vitro* or *in vivo* analysis. This step would not only produce stable nanoparticles, but also enable spotting the presence of one of the several factor that would affect the stability of the polyplexes in physiological medium. Those factors include degradation or poor quality of nucleic acid, sub-optimal polymer to nucleic acid ratio (RU/Nt ratio), insufficient thiol-crosslinking due to self-oxidation of free thiols from activated copolymer [CP2k(R)], presence of traces of DTT etc.,

Table 4-6: Composition of polymer-blends for nanoparticle preparation.

Formulation	Volume of		
	HP 1 mg/mL, pH 6	**CP2k (R)** 2 mg/mL, pH 6	**Water**
	µL	**µL**	**µL**
HC2r75 RUN5 HP: CP2k(R) ratio 3:1 (75:25) RU/Nt Ratio 5:1	**225.0**	**43.2**	**132.0**
HC2r50 RUN5 HP: CP2k(R) ratio 1:1 (50:50) RU/Nt Ratio 5:1	**150.0**	**86.4**	**163.7**

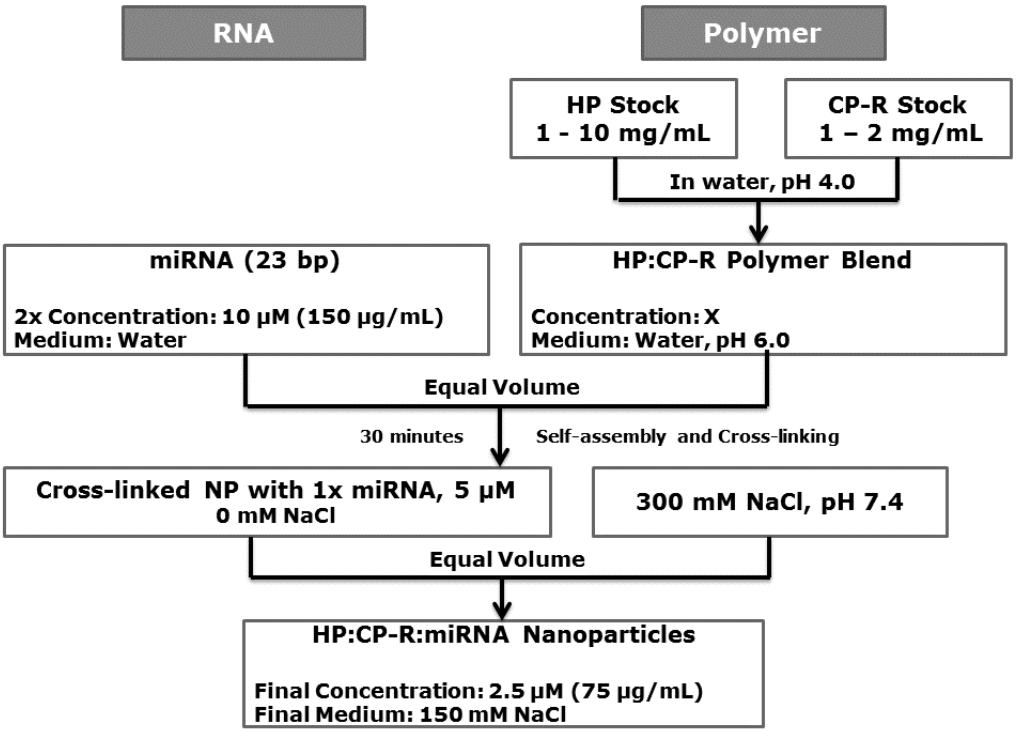

Figure 4-16: Salt-free nanoparticle preparation procedure.
Combining salt-free complex formation and stability check in physiological saline (NaCl, 150 mM). The total preparation time is around 1 to 2 hours.

Improved Nanoparticle Preparation: Initially the polymers were dissolved individually in acidified water (pH 4.0) and just before use their pH was set to pH 6.0. The polymer solutions were freshly prepared each time before use. The reduced polymer [CP2k(R)] was used within 2 hours of dissolution to make use of maximum free thiols. The self-oxidation kinetics of CP2k (R) in water at pH 4.0 and 6.0 measured by Ellman's assay is presented in the supplementary data, **Figure 4-32,** page: 171. The required volume (e.g. 20 µL) of microRNA or siRNA solution [10 µM, in water] was transferred to a micro-centrifuge tube [2 mL]. The concentration of nucleic acid used was always 10 µM, unless otherwise specified. The polymer-blend was prepared according to the composition presented in the **Table 4-6,** page: 152. Equal volume of polymer blend (e.g. 20 µL) was added to the microRNA solution and gently mixed. The mixture was then incubated for 30 minutes at room temperature. Finally, equal volume of (e.g. 40 µL) of 2x NaCl solution (300 mM) was added. This final nanoparticle solution contained 2.5 µM microRNA and 150 mM NaCl, **Figure 4-16,** page: 150.

4.3.9 Optimization of Nanoparticle Formulation

As all the previous complexes were prepared in polymer-blends containing PBS (50 mM PBS, pH6.0), the RU/Nt ratio (**Figure 4-17,** page: 153) and microRNA concentrations (**Figure 4-18,** page: 155) were re-optimized for salt-free complexation. The complexes were prepared in water and the size was measured after increasing the ionic concentration of nanoparticle solution to physiological levels. The size and polydispersity of complexes were compared between two different HP: CP ratios, 3:1 or 1:1.

HP: CP ratio 3:1 produced stable miRNA-nanoparticles (Size ~300 nm; Pdi < 0.2) from RU/Nt ratio of 4:1 to 6:1. Based on this result, HP: CP ratio 1:1 were prepared between RU/Nt 3:1 to 6:1. The size of the nanoparticles gradually decreased as the polymer to RNA repeating unit ratio was increased. The smallest nanoparticle produced was around 150 nm (Pdi ~ 0.2) at RU/Nt ratio 5:1, **Figure 4-17** (page: 153). To know whether increase in RU/Nt ratio would further reduce the size of the nanoparticles, two different RU/Nt ratios (5:1 and 6:1) were tested along with the optimization of miRNA concentration, **Figure 4-18** (page: 155).

The size of the complexes produced by RU/Nt ratio 6:1 was the same size as those produced by 5:1. Also, at RU/Nt ratio 6:1, varying the microRNA concentration during the complexation step affected the polydispersity (Pdi), **Figure 4-18** (page: 155). At polymer to microRNA repeating unit ratio 5:1, the size and Pdi remained almost constant irrespective of the microRNA concentration. This indicated the polymer to RNA repeating ratio was optimal at 5:1.

Taken together, one nanoparticle formulation was selected from these optimizations, HP: CP2k(R) 1:1 RU/Nt 5:1. Among different PAA-miRNA formulations, only this nanoparticle would be tested in the further sections, hence it would be referred as NP (nanoparticle) for simplicity.

4.3.9.1 Optimization of RU/Nt Ratio

The nanoparticles were prepared following the protocol depicted in **Figure 4-16** (page: 150).

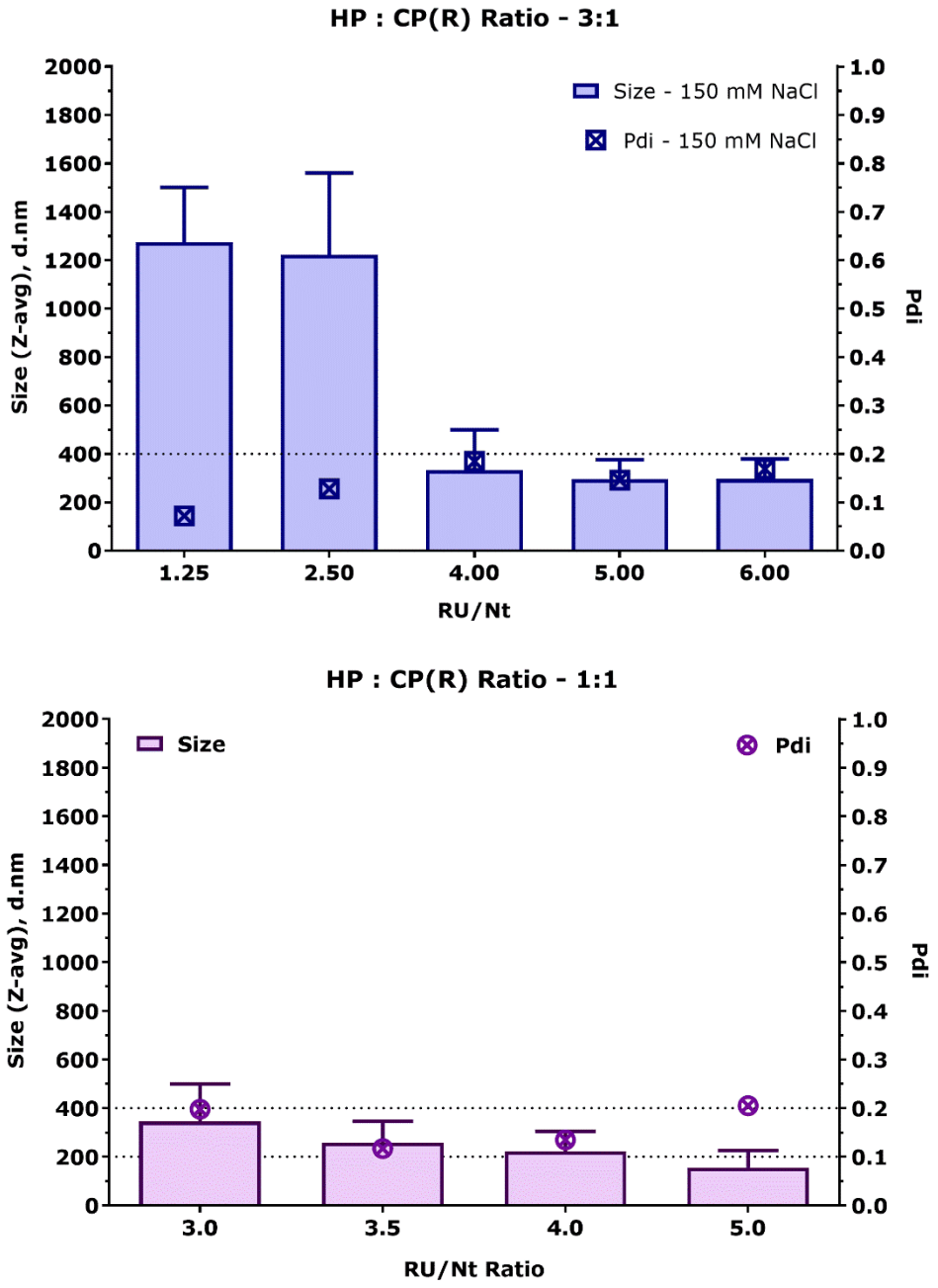

Figure 4-17: Optimization of RU/Nt Ratio for salt-free complexation.

The graph represents the size of the complexes in 150 mM NaCl. The error bars represent the width of the size peak (Pdi width) indicating the size distribution range. HP: CP ratio – **3:1** (Top Plot); **1:1** (Bottom Plot). N = 1, n = 3.

4.3.9.2 Optimization of microRNA Concentration

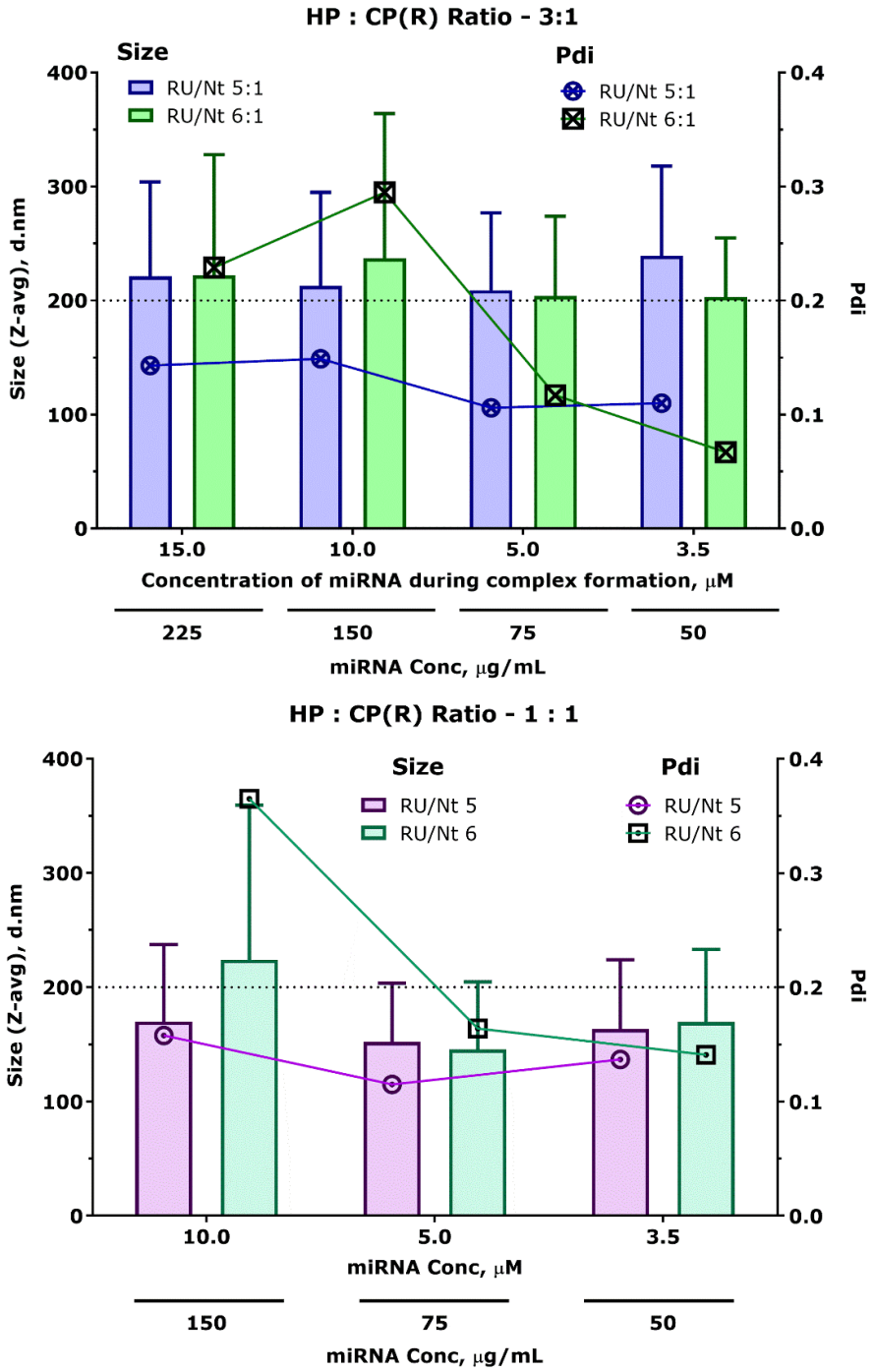

Figure 4-18 Optimization of miR-concentration for salt-free complexation.

The complexes were prepared in water, salt-free condition. The graph represents the size of the complexes in 150 mM NaCl. The error bars represent the width of the size peak (Pdi width) indicating the size distribution range. HP: CP ratio 3:1 (**Top Plot**); 1:1 (**Bottom Plot**). (N = 1; n = 3).

4.3.10 Physicochemical Characterization of Stable Nanoparticles

Stable PAA-miRNA nanoparticles were produced by the following formulation, HP: CP2k(R) 1:1 RU/Nt 5:1, when the complex formation was carried-out in the water (salt-free condition). These nanoparticles were characterized for size distribution [**Table 4-7**], zeta-potential [**Table 4-7**] and morphology [Transmission electron microscopy (TEM) - uranyl acetate stained nanoparticles on page: 158, **Figure 4-19**; unstained nanoparticles on page: 159, **Figure 4-20**; and Scanning electron microscopy (SEM) images on page: 160, **Figure 4-21**]. For TEM sample preparation, the 2.5 µM PAA-miRNA complexes were directly used without further dilution. It was easier to obtain images with TEM when the nanoparticles were imaged without any staining while obtaining highest contrast. As the final nanoparticles were actually in 150 mM NaCl solution, the high amount of salt could be preferably associated with the nanoparticles while drying and hence absorb the electrons efficiently creating the staining effect. However, when the samples were stained with Uranyl acetate (1 wt.% in water, best data shown) or Phospho-tungstic acid (1 wt.% in water, data not shown), or Ruthenium red (1 wt.% in water, data not shown) the quality of the images obtained were poor and the whole surface was usually dark. This maybe because of the high concentration of the nanoparticles in the sample [2.5 µM miRNA concentration]. Further dilutions [1/10 or 1/100] was expected to improve the quality of the images obtained by TEM when using the contrast staining agents.

Table 4-7: Size and zeta-potential measurements.

HP: CP2k(R) 1:1 RU/Nt 5:1	**Size, nm**	**Measurement Condition**
Z.average, nm	167 ± 54	150 mM NaCl. ~ pH 6 (N = 6, n = 3)
Polydispersity Index, Pdi	0.125 ± 0.027	
	Zeta Potential, mV	**Measurement Condition**
Zeta-Potential	- 0.01948 ± 3.705	45 mM NaCl*, pH 6.25 (N = 2, n = 3)

* - The initial nanoparticle solutions contained 2.5 µM (~ 38 µg/mL) miRNA in ~ 150 mM NaCl solution. The nanoparticle solution must contain at least 10 µg/mL of miRNA to obtain sufficient scattering signal. Due to this requirement, the minimum salt concentration of the nanoparticle medium that could be achieved was ~45 mM NaCl. More details in section: 2.7.2, page: 68.

4.3.10.1 Transmission Electron Microscopy (TEM)

Transmission electron microscopy images showed almost spherical particles on both unstained and stained samples.

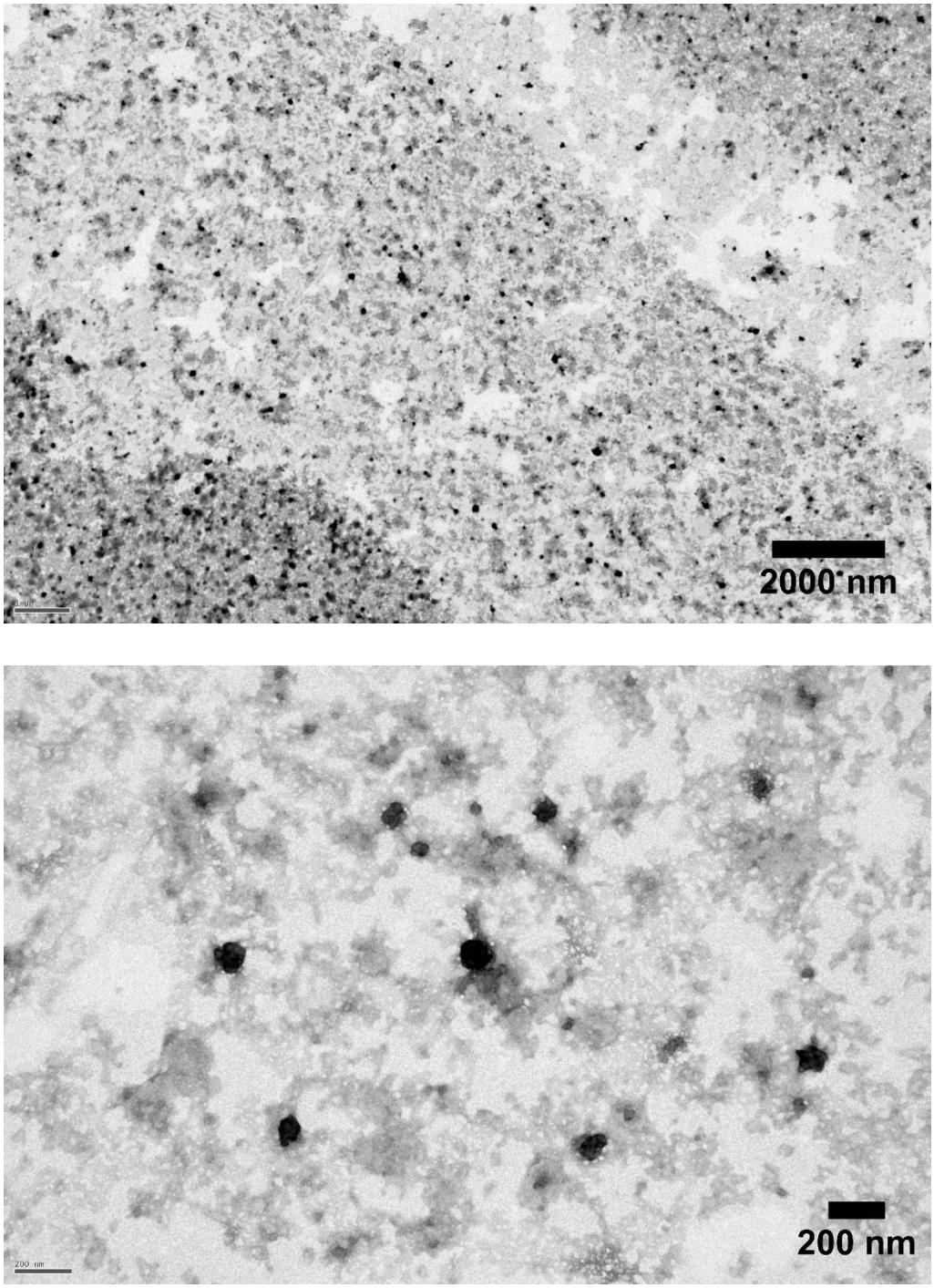

Figure 4-19: TEM images of nanoparticles, uranyl acetate staining.
PAA-miRNA nanoparticles [HP: CP2k(R) 1:1 RU/Nt 5:1 in 150 mM NaCl] were stained with uranyl acetate (1 wt.%).

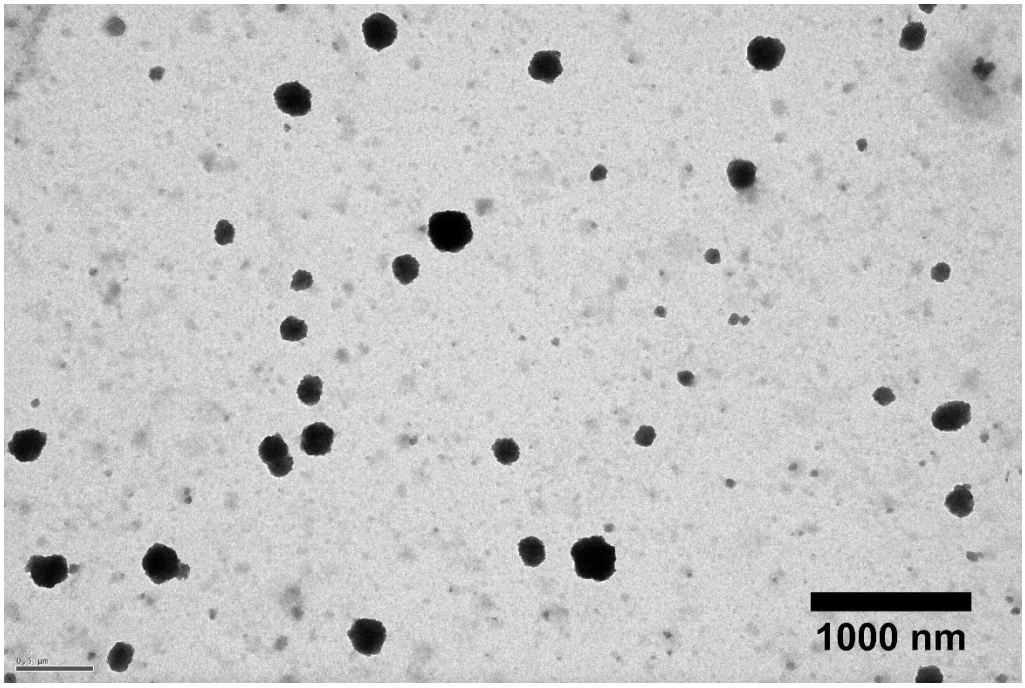

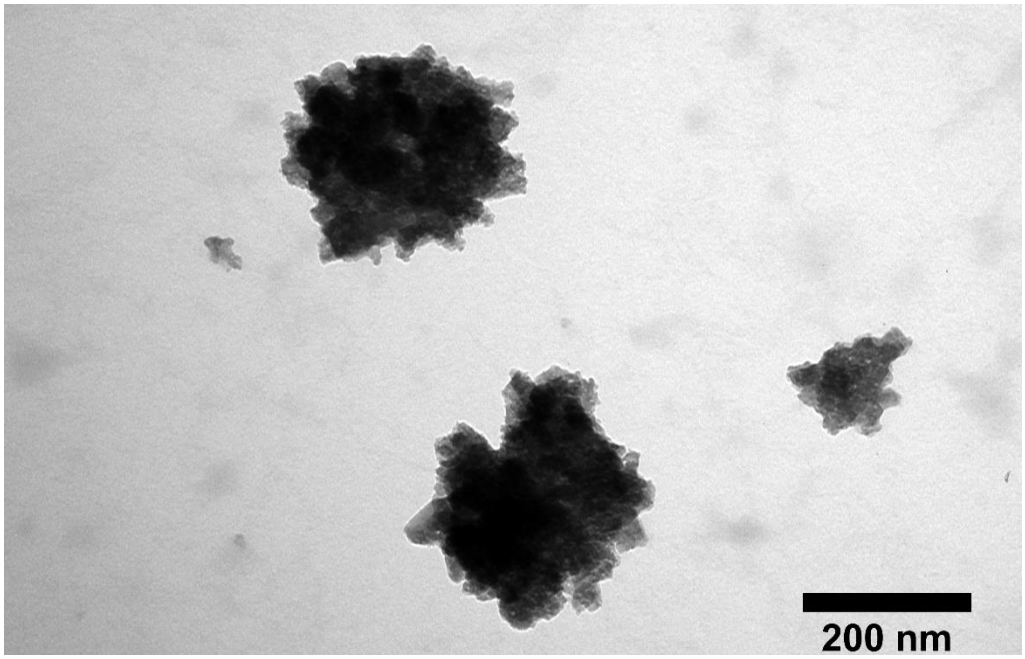

Figure 4-20: TEM images of unstained nanoparticles.

PAA-miRNA nanoparticles [HP: CP2k(R) 1:1 RU/Nt 5:1 in 150 mM NaCl] were imaged without staining.

4.3.10.2 Scanning Electron Microscopy (SEM)

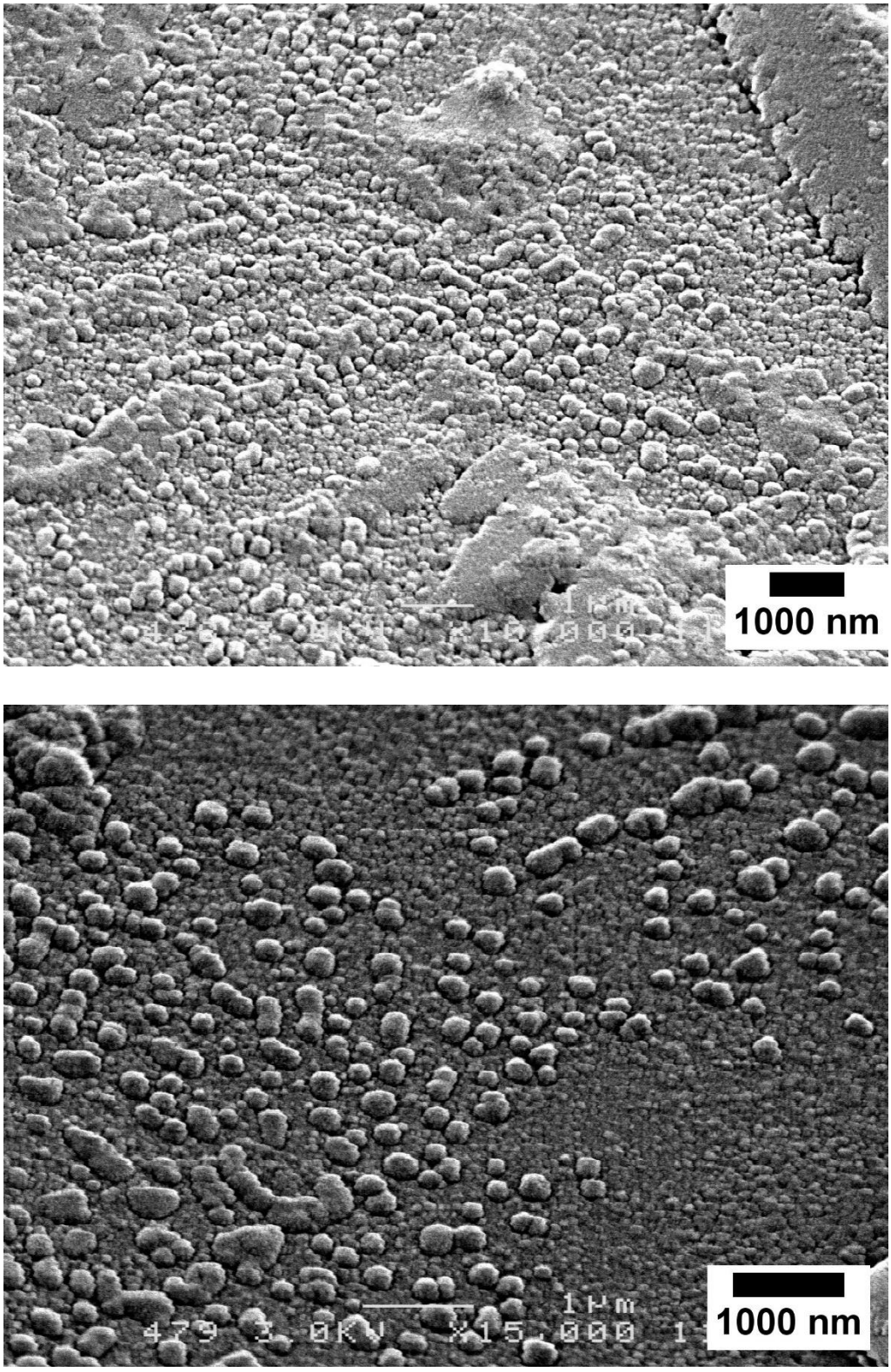

Figure 4-21: SEM images of nanoparticles.

PAA-miRNA nanoparticles [HP: CP2k(R) 1:1 RU/Nt 5:1 in 150 mM NaCl] were coated with gold vapour and imaged at 10000x (top) or 15000x magnification (bottom).

4.3.11 *In vitro* Testing

For the miRNA delivery system to be functional, it should be able to enter the cell and release miRNA in the cytosol in sufficient amounts. Hence, the optimized nanoparticle [HP: CP2k(R) 1:1 RU/Nt 5:1] was quantitatively tested for its ability to enter the cell by flow cytometry and visualized by confocal imaging. Finally, these nanoparticles were tested on U87-Luc cells to study the functional gene-silencing activity.

4.3.11.1 Uptake Assay by Flow-cytometry

Initially, the U87MG cells were treated with different concentrations of PAA-miRNA nanoparticles [HP: CP2k(R) 1:1 RU/Nt 5:1] carrying fluorescent miRNA [Treatment - 6 hours; Concentrations – 50, 250 and 500 nM]. Commercial N-TER nanoparticles was used as a positive control and treated as per the recommendations from the manufacturer (4 hours, 50 nM). The cells were collected following the treatments and analysed by flow cytometry, **Figure 4-22** [page: 156], **Figure 4-23** [page: 163]. Dose dependant uptake was observed for both PAA-miRNA nanoparticles and free microRNA. Percentage double positive cells [$Cy3^+$, Hoechst 33342^+] represent the percentage of cells that have taken up the nanoparticles, while the geometric-mean fluorescence intensity (GMI) represents the relative amount of Cy3 fluorescence from the transfected population. **Note:** It should be noted that the GMI should be given a higher weighting than the percentage positive cells. The percentage double positive cells were calculated using a random value of fluorescence close to the maximum fluorescence observed for non-treated cells. All the cells that have more fluorescence than the user-defined limit was considered to be positive for Cy3 fluorescence. However, under all the tested conditions, the whole population appeared to have shifted. This indicates that 100% of the cells have taken up the fluorophore (Free miR-Cy3 or N-TER-miR-Cy3 or NP-miR-Cy3). Hence, the percentage of double-positive cells calculated here is a relative percentage of positive cells with respect to an arbitrary limit (represented by the dotted-line on the histograms) and not the exact amount of cell population.

The maximum uptake was observed at 500 nM for PAA-miRNA nanoparticles. The relative amount of miRNA transfected was different, indicated by the geo-

mean fluorescence intensity [$Cy3^+$ population], **Figure 4-23** [page: 163]. The amount of fluorescence emitted by cells treated with N-TER (50 nM, GMI = 42.5) was ~10-fold higher than the PAA-miRNA nanoparticle treatment (500 nM, GMI = 5.86), indicating moderate uptake of PAA-miRNA nanoparticles.

The uptake of nanoparticle (500 nM) was studied as a function of treatment time (2, 4, 8, 12 hours), **Figure 4-24** [page: 163] **and Figure 4-25** [page: 164]. The Cy3 positive cells represent the transfected population. N-TER nanoparticle showed excellent cellular uptake with only 2 hours of incubation (~98% Cy3 positive cells). However, the geometric-mean fluorescence increased as a function of time and saturated after 8 hours of treatment, **Figure 4-25**.

For PAA-miRNA nanoparticles, the trend in Cy3 positive cells increased from 77% (2h), 78% (4h), 83% (8h) and 93% (12h). The increase in geo-mean fluorescence (GMI) was as follows, 4.7 (2h), 5.2 (4h), 5.8 (8h) and 7.0 (12h). The cells treated with PAA-miRNA nanoparticles with prolonged incubation time, more than 4 hours, showed drastic changes in the morphology, but not the same was observed for free miRNA or N-TER treatments (data not shown). The cell recovery was also poor partly due to nanoparticle toxicity and strong attachment of cells to the surface of the cell culture plates. Comparing 4 hours and 8 hours of nanoparticle treatments, there was only a small increase in percentage positive cells (78% to 83%) and amount of Cy3 fluorescence (5.2 to 5.8). So, it was decided to treat the cells only for 4 hours for standard transfection experiments. The cells treated for 12 hours with PAA-miRNA nanoparticles [500 nM, 12 hours, GMI = 7.0] did not quite reach the same geo-mean fluorescence as that of N-TER nanoparticles [50 nM, 4 hours, GMI = 42.5]. At 4 hours, the uptake was twice the amount compared to free miRNA, [5.2 (nanoparticles) Vs 2.7 (free miRNA)]. At 12 hours, the amount of Cy3 fluorescence was comparable between PAA-miRNA nanoparticles and free miRNA [7.0 (nanoparticle) vs 5.6 (free miRNA)].

For free miRNA, the uptake was clearly time dependant. The percentage positive cells increased gradually with time [7% (2 hours) to 95% (12 hours)]. However, the amount of miRNA-Cy3 taken up by the cells was low [2.6 (2 hours) to 5.6 (12 hours)] compared to N-TER-(miRNA-Cy3) nanoparticles.

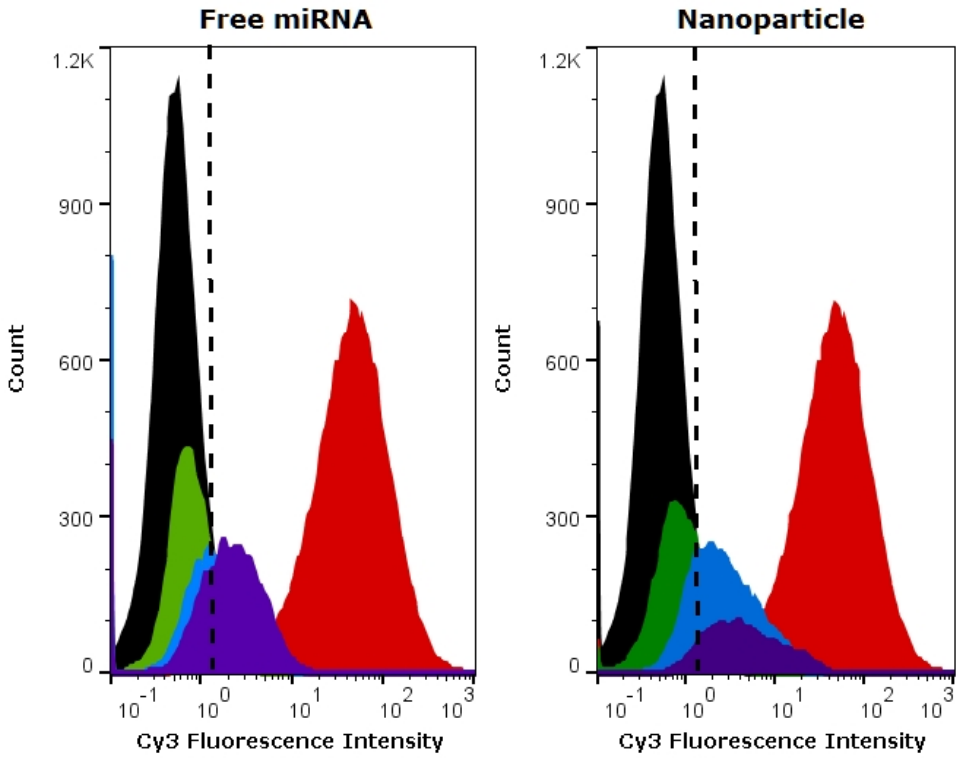

Figure 4-22: miRNA concentration versus cellular uptake (Histogram).

Colour coding: Untreated cells (**Black**); N-TER-50 nM (**Red**); 50 nM (**Green**); 250 nM (**Blue**); 500 nM (**Violet**). The X-axis represents the fluorescence intensity produced of Cy3 (Hoechst 33342 fluorescence compensated data). The cell population right-side to the dotted line was considered as Cy3-positive cells, indicating cellular uptake. The Y-axis represents the cell count. (N = 1, n = 3).

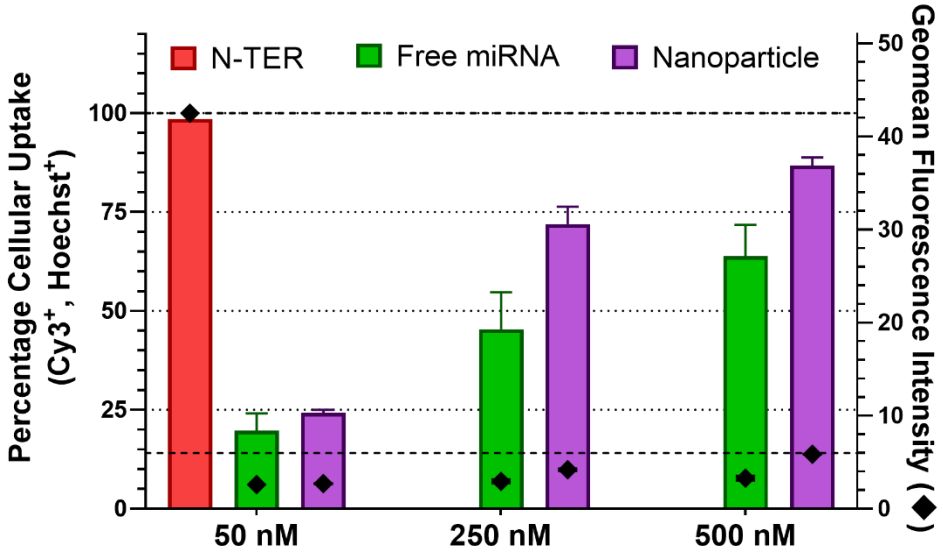

Figure 4-23: miRNA concentration versus cellular uptake (Bar Chart).

Cell line: U87MG. The percentage of double positive cells ($Cy3^+$, Hoechst 33342^+) is presented as bar chart (Left Y axis), while the geo-mean Cy3 fluorescence intensity is plotted on the Right Y axis (Black diamond). (N = 1, n = 3).

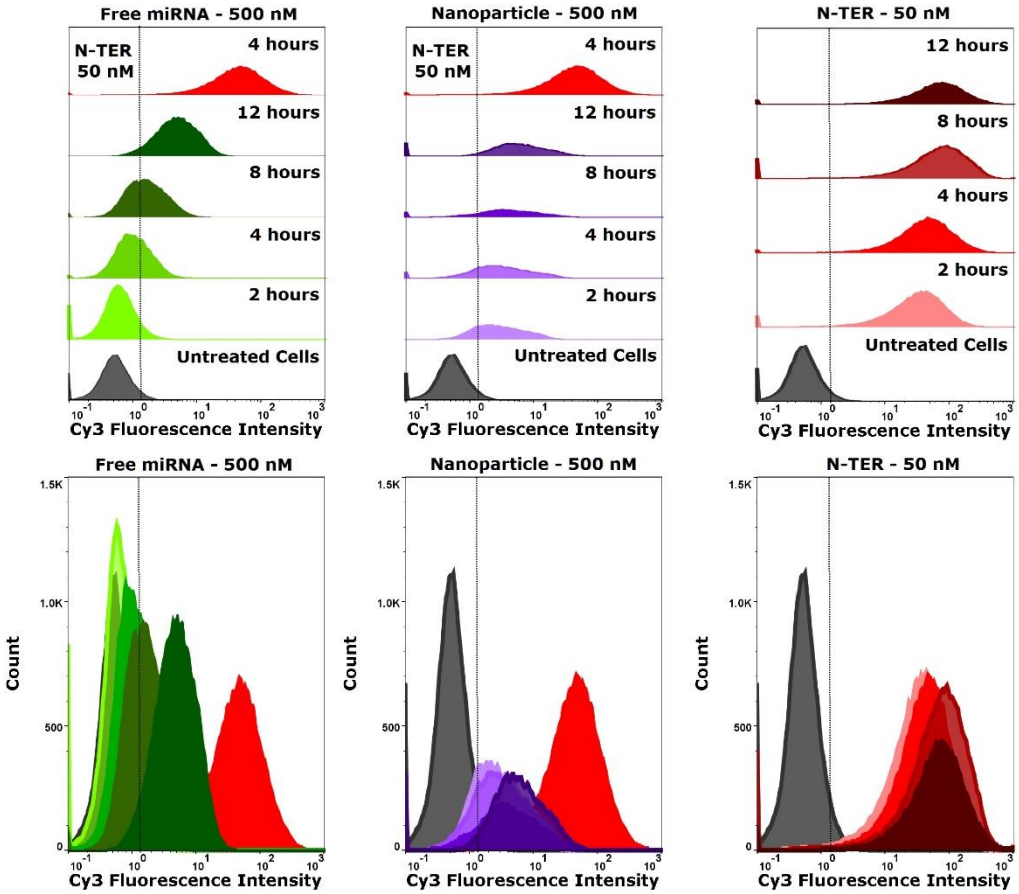

Figure 4-24: Treatment time versus cellular uptake (Histogram).

Top: Stacked view; Bottom: Overlay view. The X-axis represents Cy3 fluorescence intensity (Hoechst 33342 compensated data). The cell population right-side to the dotted line was considered as Cy3-positive cells. The Y-axis represents cell count. N = 1, n = 3.

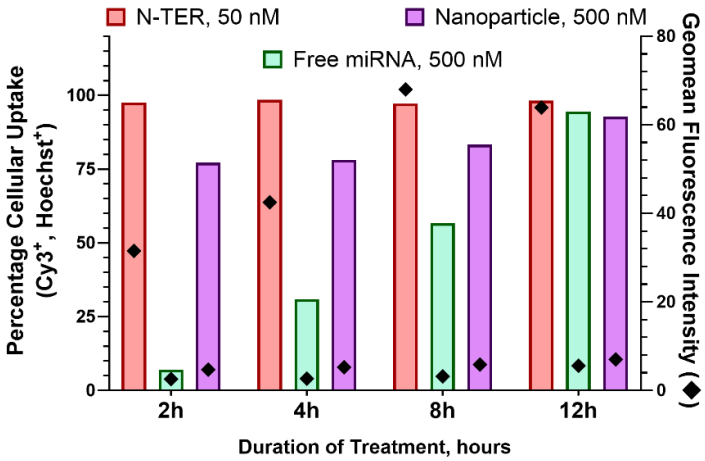

Figure 4-25: Treatment time versus cellular uptake (Bar Chart).

The percentage of double positive cells ($Cy3^+$, Hoechst 33342^+) is presented as bar chart (Left Y axis), while the geo-mean Cy3 fluorescence intensity is plotted on the Right Y axis (Black diamond). (N = 1, n = 3).

4.3.11.2 Uptake Assay – LASER Scanning Confocal Microscopy

Fluorescent miRNA (miR-Cy3) was used for the preparation of miRNA-nanoparticles. The U87MG cells were treated with N-TER (Sigma) (**Figure 4-26,** page: 165) or PAA-miR nanoparticles [HP: CP2k(R) 1:1 RU/Nt 5:1] (**Figure 4-27,** page: 165). Free miR-Cy3 was used as the control (**Figure 4-28,** page: 166). N-TER nanoparticles (50 nM) had very high uptake compared to PAA miRNA nanoparticles (500 nM). All the red fluorescence (miR-Cy3) was localized in the perinuclear area, (nucleus in blue). PAA-miR nanoparticle uptake was dose dependant and relatively better than free miRNA uptake at 4 hours. Confocal imaging correlated well with the flow-cytometry data. The 3D image showed fluorescence from all the sections of the cytoplasm (Z-direction). This indicated that the nanoparticles were internalized.

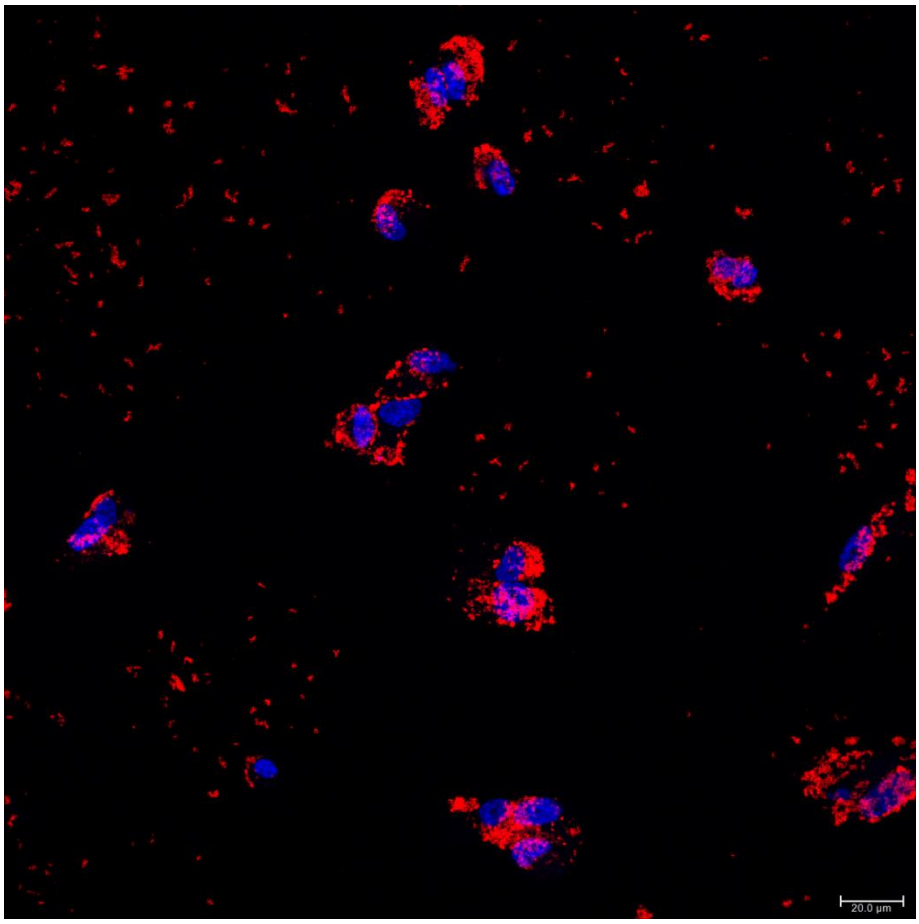

Figure 4-26: Confocal imaging of cellular uptake, N-TER nanoparticles.
Cell line: U87MG. Nucleus is stained by Hoechst 33342 (Blue) and microRNA covalently linked with Cy3 is seen by red fluorescence. Concentration of nanoparticles: 50 nM (miRNA-Cy3); Incubation time: 4 hours. Scale bar: 20 µm.

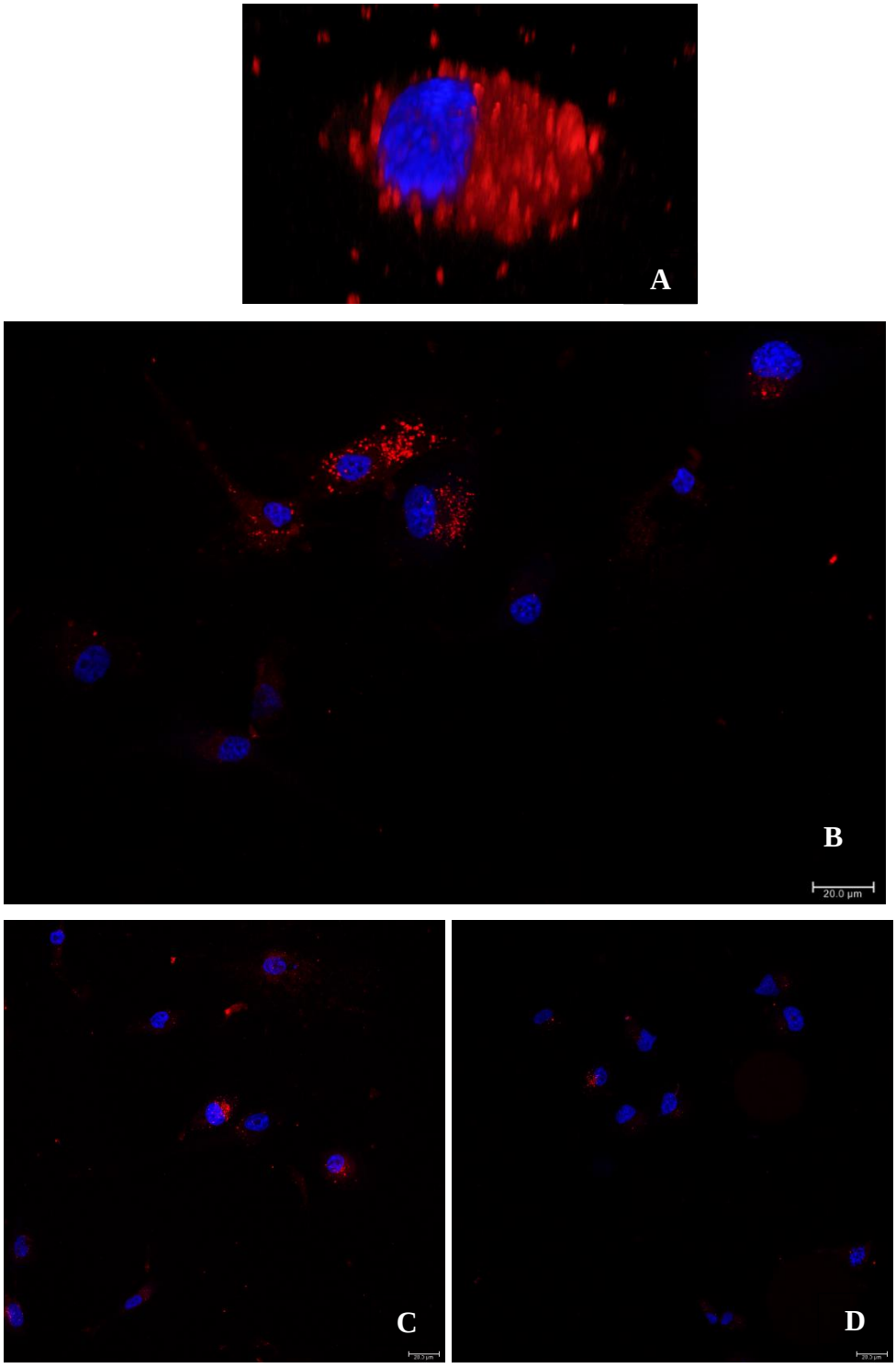

Figure 4-27: Confocal imaging of cellular uptake, PAA nanoparticles.
Cell line: U87MG. PAA-miRNA formulation: HP: CP2k(R) 1:1 RU/Nt 5:1. Nucleus was stained by Hoechst 33342 (Blue) and the nanoparticle was formed with fluorescent miR-Cy3 (Red). Concentration of nanoparticles (miR-Cy3): (A) 500 nM, 3D image, brightness increased – not for comparison; (B) 500 nM (2D); (C) 250 nM (2D); and (D) 100 nM (2D); Incubation time: 4 hours; Scale bar: 20 µm.

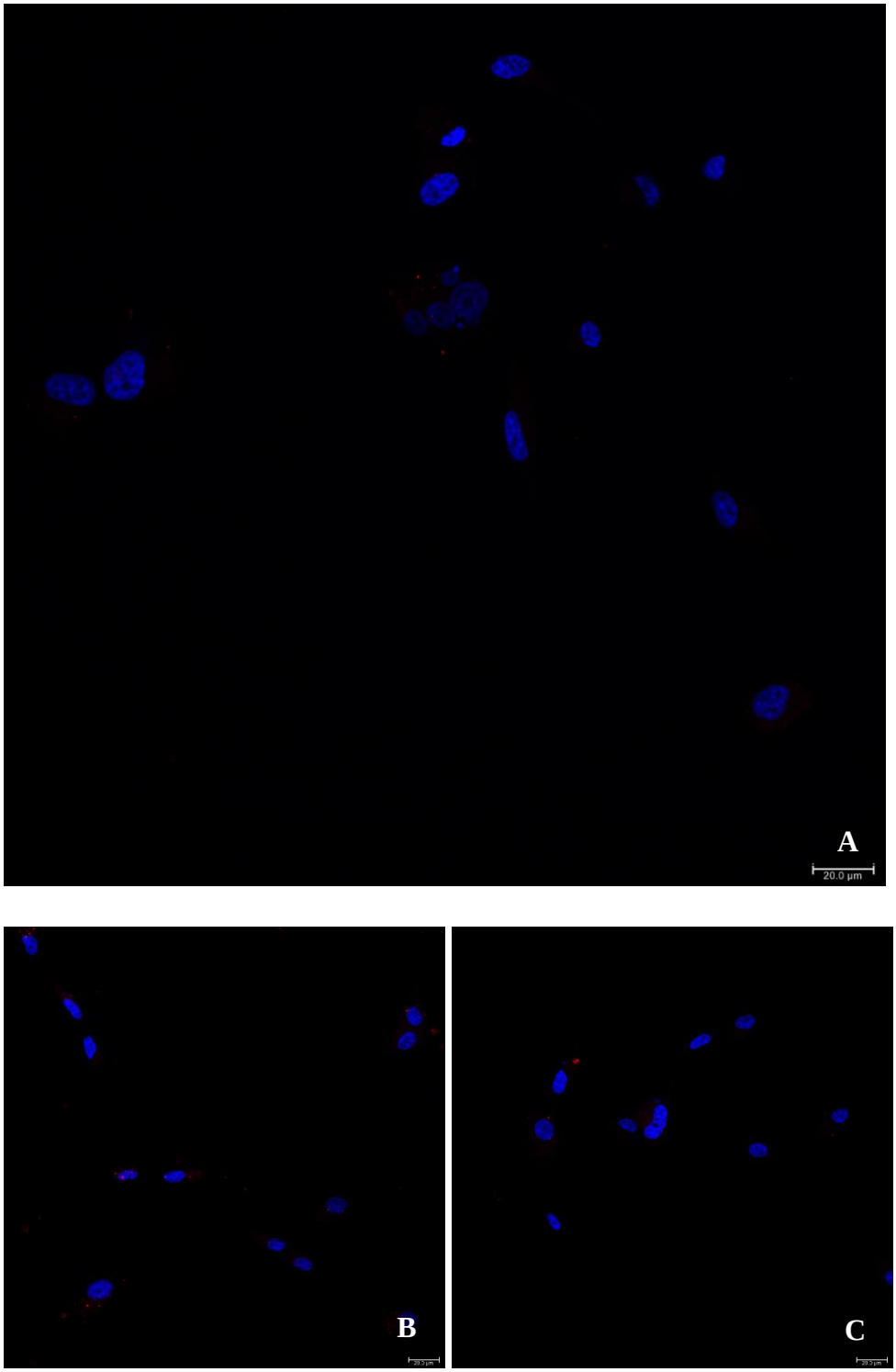

Figure 4-28: Confocal imaging of cellular uptake, free-miRNA.
Cell line: U87MG. Nucleus was stained by Hoechst 33342 (Blue) and the nanoparticle was formed with fluorescent miRNA-Cy3 (Red). Concentration of free miRNA: (A) 500 nM; (B) 250 nM; and (C) 100 nM; Incubation time: 4 hours; Scale bar: 20 µm.

4.3.11.3 Luciferase knock-down assay

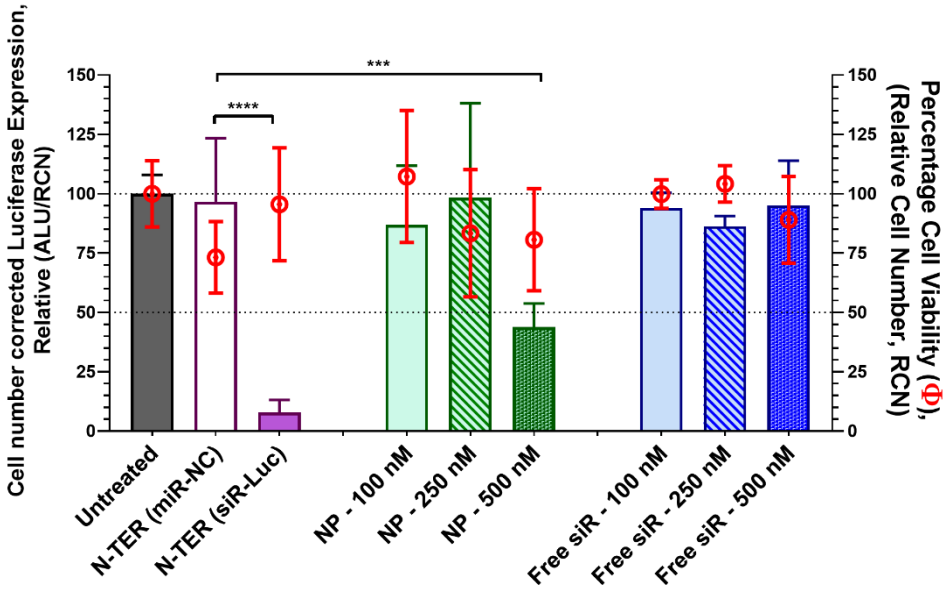

Figure 4-29: Luciferase assay, Stage - II.

Comparison of functional effect of siRNA-Luc loaded either in polyamidoamine [NP = HP: CP2k(R) 50:50 RU/Nt 5:1] or N-TER (Sigma) nanoparticles. The cell viability is represented as red circles plotted on right Y-axis; while the relative luminescence was represented as bar chart (Left Y-axis). The miRNA concentrations 100, 250 and 500 nM corresponds to ~ 150, 375 and 750 ng of miRNA per well (100 µL). ALU – Arbitrary Luminescence Unit. RCN – Relative cell number. Statistical significance obtained from Tukey's multiple comparisons test (One-way ANOVA), $p < 0.0001$ (****); $p \leq 0.001$ (***). (N = 3, n = 3).

The positive control used in this, N-TER commercial nanoparticles (50 nM), were able to downregulate luciferase by more than 90% (Percentage knockdown = 100 – Percentage luciferase expression; Luciferase expression = 7.7 ± 5%). The siR-Luc loaded PAA nanoparticles (500 nM) were able to significantly down-regulate the expression of luciferase by 45 – 55% (Luciferase expression = 44 ± 9%). The moderate amount of gene knock-down even at very high concentrations of the nanoparticle can be attributed to the poor uptake of these nanoparticles by U87MG cells. None of the free siRNA-Luc treatments produced any knock-down, hence confirming the fact that naked siRNA delivery does not cause any functional effect on cells[164]. This is due to poor cellular uptake and lack of the ability of naked siRNA molecules to reach cytoplasm after endocytosis. This reaffirms the need of a delivery vector for siRNA or microRNA molecules.

4.4 Discussion

Gel-filtration Chromatography: The PD-10 protocol was adapted for the purification of the polymer, following the reduction reaction to get rid of DTT and other by-products. This alternative polymer purification procedure is faster compared to the existing original protocol. Due to fast recovery of the polymer from PD-10 column, this approach increases the free thiol yield. The polymer recovery was around 50% due to overlapping of the DTT and polymer peaks. Higher recovery could be achieved by increasing the resolution of separation between polymer and DTT, that can be achieved by using a larger column[344].

Nanoparticle Uptake and Functional Activity of Nanoparticle: This topic is discussed in detail in the General Discussion Section, **6.2**, page: 199.

Uptake of Naked miR-Cy3 and Functional Activity of siR-Luc: The uptake assay indicated that the naked miR-Cy3 was able to enter the cells at low quantity indicated by the increase in Cy3 fluorescence. At four hours of incubation, the miR-Cy3 uptake was one third of the uptake compared to PAA-miRNA nanoparticles. However, when the luciferase knock-down efficiency was compared for naked-siR-Luc [500 nM, 4 hours incubation] and equivalent PAA-siR-Luc nanoparticles, the naked siRNA did not show any activity. This confirms that the cellular uptake pathway of naked-siRNA or miRNA is non-productive, i.e. the miRNA entering the cells would be degraded inside the cells by the lysosomes[164]. Delivering miRNA using nano-particulate system may use a productive cellular uptake pathway and avoiding endo-lysosomal degradation or the endosomal escape mechanism might facilitate the release of some miRNA into the cytoplasm[164].

Also, as the incubation time was increased to 8 and 12 hours, the uptake of naked-miR-Cy3 gradually increased and was the same level as the PAA-miRNA nanoparticles. One reason for this gradual increase could be because of the degradation of the miR-Cy3 in the cell-culture medium due the nucleases secreted[345] by the cells on prolonged incubation and the increase in Cy3-fluorescence might be just because of the free-Cy3 dye generated by the degradation of miR-Cy3[164].

4.5 Conclusion

An alternative method of polymer purification was developed using PD-10 columns. When compared to the ultra-filtration protocol, there was no improvement in the percentage polymer yield by mass (49% Vs 50%), but the thiol yield was improved from 35% to 50%.

The stability analysis of nanoparticles provided the hint that presence of salt in the polymer blend interfered with the stability of the polyplexes. The stability of the nanoparticle depends on the disulphide bonds that are formed after the formation mixing PAA and miRNA. Further investigation on the crosslinking behaviour provided deeper understanding of the crosslinking process. Kinetic study on thiol-crosslinking was conducted with copolymer alone or in combination with homopolymer, in the presence and absence of salt. Salt enhanced the CP2k(R) self-oxidation process [half-life of thiols was 6.5 hours (in water, pH 6) versus 4 hours (in 50 mM PBS, pH 6)]. The presence of salt also promoted instantaneous HP-CP crosslinking (pre-crosslinking) even before the addition of nucleic acid and hence affected its stability in physiological medium. Based on this observation, removal of salt during the preparation of HP-CP blend (PAA) and during the formation of PAA-miRNA nanoparticles created post-crosslinked complexes that were stable under physiological conditions. One of the best stable formulations was chosen and its *in vitro* knockdown behaviour was studied.

The uptake assay showed that the tested formulation had a moderate uptake behaviour compared to N-TER. The nanoparticle concentration (500 nM, miRNA) and treatment timing (4 hours) was deduced from the uptake analysis. The luciferase assay showed that the tested PAA-siRNA-Luc formulation (500 nM) showed ~50% of knock-down activity compared to more than 90% knock-down achieved by N-TER (50 nM). This indicated that PAA-miRNA formulation was able to act functionally at higher concentrations. However, the cellular uptake being the limiting-factor. Ligand tagging of the nanoparticles would result in better uptake and might improve the knock-down efficiency of the nanoparticles. This ligand-tagging approach was explored in the next chapter.

4.6 Supplementary Data

4.6.1 Ellman's assay – Standard Curve

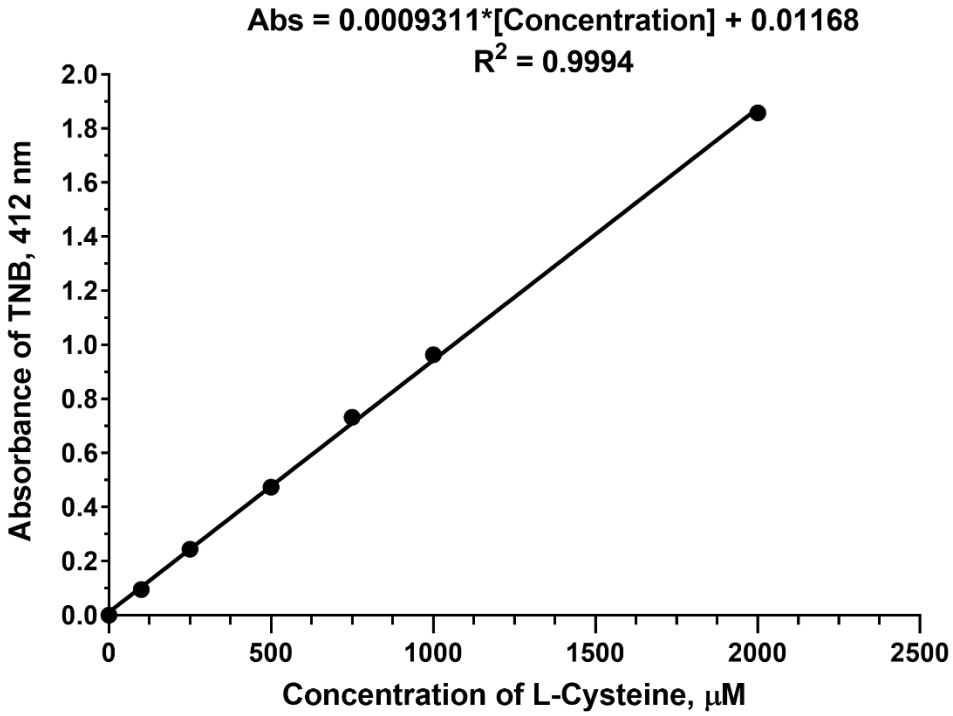

Figure 4-30: L-Cysteine Standard Curve, (Spectrophotometer).

Ellman's Assay, UV-Visible Spectrophotometer. Pathlength of cuvette = 1cm. (N = 1)

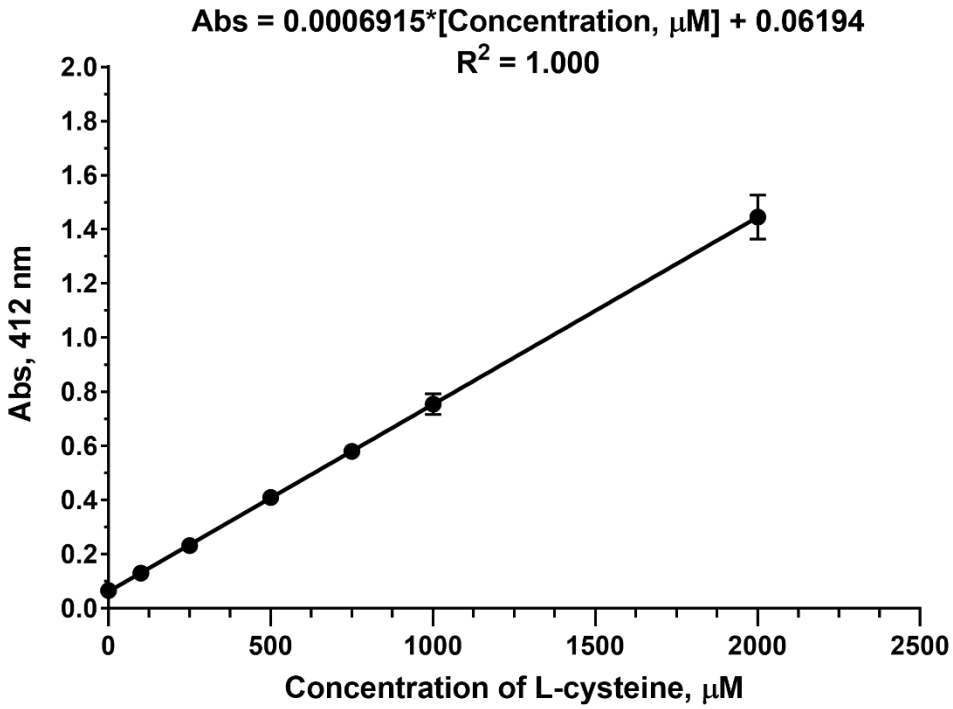

Figure 4-31: L-Cysteine Standard Curve (Micro-plate reader).

Ellman's Assay on micro-plate reader (200 μL). (N = 3).

4.6.2 Kinetics of self-oxidation of CP2k(R): Effect of pH

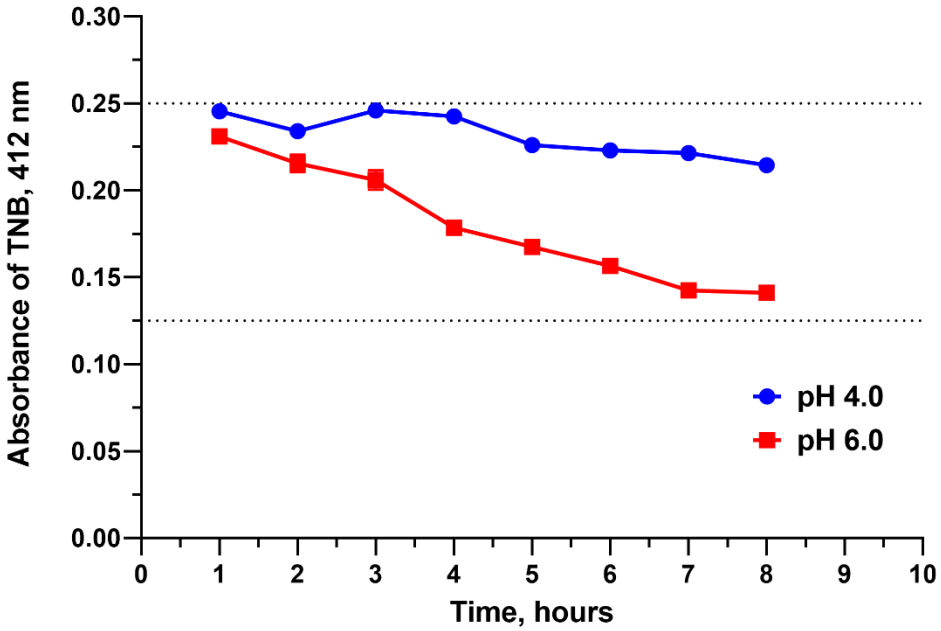

Figure 4-32: Effect of pH on self-oxidation of copolymer.

The polymer was dissolved in water and pH was adjusted later. The absorbance measurements were performed on a microplate reader. (N = 1, n = 2)

4.6.3 Kinetics of thiopyridine release – Tabular Representation

Table 4-8: Kinetics of thiopyridine release.

The concentration of 2-thiopyridine was calculated using the molar absorbtivity[343], $\varepsilon_{343\ nm} = 8080\ M^{-1}\ cm^{-1}$. The actual concentration of thiopyridine in HP (0.75 mg/mL) was calculated as 296 µM.

	Concentration of thiopyridine released, µM (Percentage thiopyridine released)		
	after 5 minutes	**after 125 minutes**	**Between 5 and 125 minutes**
HP only, 50 mM PBS, pH 6.0	0.00	0.00	0.00
HP + CP2k(R) in water **0 mM PBS**, pH 6.0	51.27 (19.3 %)	70.99 (26.8 %)	19.72 (7.5 %)
HP + CP2k(R) **25 mM PBS**, pH 6.0	107.19 (40.4 %)	116.27 (43.9 %)	9.08 (3.5 %)
HP + CP2k(R) **50 mM PBS**, pH 6.0	113.47 (42.8 %)	119.41 (45.1 %)	5.94 (2.3 %)

4.6.4 Statistical Analysis – One-way ANOVA (Luciferase Assay)

Table 4-9: Tukey's multiple comparisons test (Luciferase assay, stage II).
NP refers to polyamidoamine nanoparticles [HP: CP2k(R) 50:50 RU/Nt 5:1].

N-TER (miR-NC) vs X (siR-Luc)	Mean Diff.	95% CI of diff.	Significant ?	Summary	Adjusted P Value
N-TER, 50 nM	-88.81	-127.8 to -49.85	**Yes**	********	**<0.0001**
NP, 100 nM	9.681	-29.28 to 48.65	No	ns	0.9962
NP, 250 nM	-1.679	-40.64 to 37.28	No	ns	>0.9999
NP, 500 nM	52.74	16.47 to 89.01	**Yes**	*******	**0.0006**
Free siRNA, 100 nM	2.64	-36.32 to 41.6	No	ns	>0.9999
Free siRNA 250 nM	10.29	-28.68 to 49.25	No	ns	0.9943
Free siRNA 500 nM	1.528	-35.44 to 38.49	No	ns	>0.9999

Chapter – V

Preparation of stable crosslinked nanoparticles using "Salt in RNA" procedure and Development of *in-situ* ligand grafting method

Nanoparticle Development – Stage III

- Salt in the RNA for Nanoparticle Preparation
- Ligand Conjugation

5 Formulation of stable crosslinked nanoparticles by "Salt in RNA" method and Development of *in-situ* ligand grafting technique

5.1 Introduction

The PAA-miRNA interaction was found to be optimal when the complexes were formed in the presence of salt (20 – 50 mM, Chapter IV). But the presence of buffered salt (25 – 50 mM, PBS) in the polymer mixture induced HP-CP crosslinking prior to the addition of miRNA. As this pre-HP-CP crosslinking affected the amount of crosslinking that could occur after the formation of PAA-miRNA complexes, this in-turn affected the stability of the complexes in physiological salt concentrations (150 mM). Hence, the polymer-blends (HP-CP) and polymer-miRNA complexes were prepared in water (absence of salt). This salt-free complex formation method was able to produce nanoparticles that were stable under physiological salt concentrations.

In this chapter, the beneficial properties of salt will be used to produce stable PAA-miRNA nanoparticles. As presence of salt can favour optimal polymer-miRNA interaction and accelerate crosslinking reaction, the PAA-miRNA complexes would be prepared by adding the salt with the miRNA instead of in the polymer-blend. As the previous chapter only focused on HP: CP2k(R) complexes, this new nanoparticle preparation method will be used for optimizing of both HP: CP2k(R)- and HP: CP5k(R)- miRNA complexes.

The uptake studies in the previous chapter (4.3.11.1, page: 161) indicated that the PAA-miRNA nanoparticles showed moderate uptake only at very high concentrations of miRNA (500 nM) and poor uptake in the widely used miRNA concentration, 50 nM. When the uptake of PAA-miRNA (500 nM) was compared with a commercially available nanoparticle (N-TER, 50 nM), the uptake intensity was ~10 times lower for PAA-miRNA complexes (Geometric-

mean Florescence Intensity, 5.2 Vs 42.5). But, the knock-down efficiency was only a half that of N-TER nanoparticles, (Luciferase knock-down efficiency, 50% Vs 93%). This indicates that the PAA-miRNA nanoparticles were able to have comparable functional activity even with moderate cellular uptake. Hence, increasing the cellular uptake should further improve the knock-down efficiency and performance of PAA-miRNA nanoparticles.

The uptake of PAA-miRNA nanoparticles could theoretically be improved either by reducing the amount of PEG or grafting a ligand at the surface of the nanoparticles. The PEG can be reduced by increasing the amount of homopolymer (HP) in the HP:CP mixture while maintaining sufficient crosslinking to stabilize the nanoparticles in the physiological salt concentration. Alternatively, stable crosslinked non-PEGylated nanoparticles made from different combinations of homopolymer [HP: HP(R)- or HP(R)-miRNA] should improve the cellular uptake and functional activity *in vitro* and possibly these nanoparticles could be better suited for *in vivo* loco-regional delivery. Both these approaches to produce stable nanoparticles were explored in the first part of this chapter. In the second part, the preparation of ligand conjugated nanoparticles was explored.

5.2 Methods

5.2.1 Preparation of miRNA-polyplexes – Salt in nucleic acid

microRNA (10 µM) was prepared in 50 mM NaCl, by mixing miRNA (20 µM) and 4x complexation buffer (100 mM, NaCl). The individual polymers were dissolved in water (pH 4.0) and the polymer-blend was prepared by mixing homopolymer (HP) and reduced copolymer [CP(R)] in water. The polymer blend was added to the microRNA solution (10 µM) and mixed gently. This polymer-miRNA complex formation step would contain optimal concentration of NaCl (25 mM) and miRNA (5 µM). After 30 minutes of incubation, an equal volume of 300 mM NaCl was added to the PAA-miRNA complex. The final complexes contained 2.5 µM of miRNA and 162 mM NaCl, **Figure 5-1**.

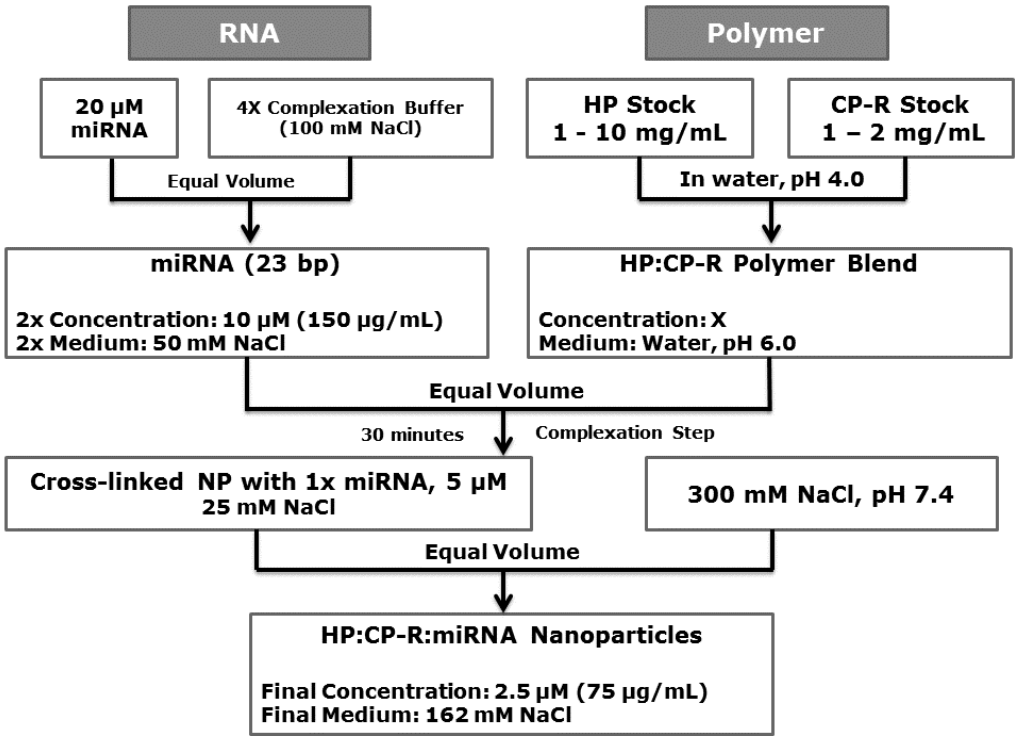

Figure 5-1: Nanoparticle Preparation Method – III (Salt in nucleic acid).

5.2.2 Size Analysis – Dynamic Light Scattering

The PAA-miRNA complexes (2.5 µM, 17 – 20 µL) were used directly for DLS analysis (Malvern Nano S) without further dilution. The size analysis was performed in triplicate using standard settings, as described in the previous chapter, **4.2.2**, page:127.

5.2.3 HP: CP ratio (Total RU versus Thiol RU ratio)

The disulphide crosslinking between the polymers can occur by two modes of thiol chemistry, (i) free thiols reacting with di-thio-pyridine (SH – SSPy) and (ii) free thiols crosslinking with free thiols (SH – SH). The amount of crosslinking influences the stability and *in vitro* behaviour of the complexes. In order to appreciate this relationship, it would be useful to know the theoretical amounts thiol-bearing groups (SPy and SH) at various ratios of HP and CP.

The amount of polymer required to form complexes with miRNA was calculated assuming the following conditions: Initial concentration of miRNA (23 bp): 10 µM; RU/Nt 5:1 ratio. The amount of thiol-bearing groups on HP (SPy) and CP (SH) in a given amount of polymer was calculated using the following equations,

$$\textbf{Amount of thio-pyridine bearing residues in HP (mol)} = \frac{\textbf{Amount of polymer (g) x } \left(\frac{\textbf{Percentage of disulphide RU}}{\textbf{100}}\right)}{\textbf{MW of PAA Thiol RU before reduction } \left(\frac{\textbf{g}}{\textbf{mol}}\right)}$$

$$\textbf{Amount of thiol bearing residues in CP (mol)} = \frac{\textbf{Amount of polymer (g) x } \left(\frac{\textbf{Percentage of PAA}}{\textbf{100}}\right) \textbf{ x} \left(\frac{\textbf{Percentage of disulphide RU}}{\textbf{100}}\right)}{\textbf{MW of PAA Thiol RU after reduction } \left(\frac{\textbf{g}}{\textbf{mol}}\right)}$$

when, (Amount of SPy – Amount of SH) ≥ 0,

$$\% \text{ available SPy} = \frac{(Amount\ of\ SPy - Amount\ of\ SH)}{(Amount\ of\ SPy)}\ x\ 100$$

when, (Amount of SPy – Amount of SH) < 0,

$$\% \text{ available SH} = \frac{-(Amount\ of\ SPy - Amount\ of\ SH)}{(Amount\ of\ SH)}\ x\ 100$$

The calculated values are presented in the **Table 5-2** [page: 181] and **Table 5-4** [page: 182]

5.2.4 Preparation of *in-situ* Biotin-Grafted Nanoparticles

Biotin grafting was performed using the thiol-maleimide chemistry while the nanoparticle stabilization was based on thiol-thiol crosslinking among the inter-polymer chains (HP-CP). The polymer-blend was prepared by mixing reduced homopolymer [HP(R)] and reduced copolymer [CP(R)]. The microRNA solution was prepared in salt [10 µM miRNA, 50 mM NaCl]. The polymer blend was added to the miRNA solution, mixed gently and incubated for one hour. Biotin maleimide stock solution was freshly prepared in acetic acid [3000 µM (1.3545 mg/mL) in 7M acetic acid]. Diluted biotin-maleimide [300 µM in 0.7M acetic acid] was added to the PAA-miRNA complex and mixed gently. The biotin-maleimide was allowed to react for an hour with the free thiols from the PAA-miRNA complex. Alternatively, the incubation time can be extended longer [~12 hours] to facilitate higher grafting and crosslinking. Following this incubation, NaCl was added to bring the ionic concentration to physiological levels, **Figure 5-2 [page: 179]**.

Finally, the pH of the nanoparticle solution was neutralized by the addition of sodium hydroxide solution [concentration of NaOH lower than the concentration of acetic acid present in biotin maleimide solution; volume of NaOH added was the same as the amount of biotin maleimide solution added to the PAA-miRNA complex]. Alternatively, this pH neutralization step was carried out after diluting the nanoparticles with cell culture medium.

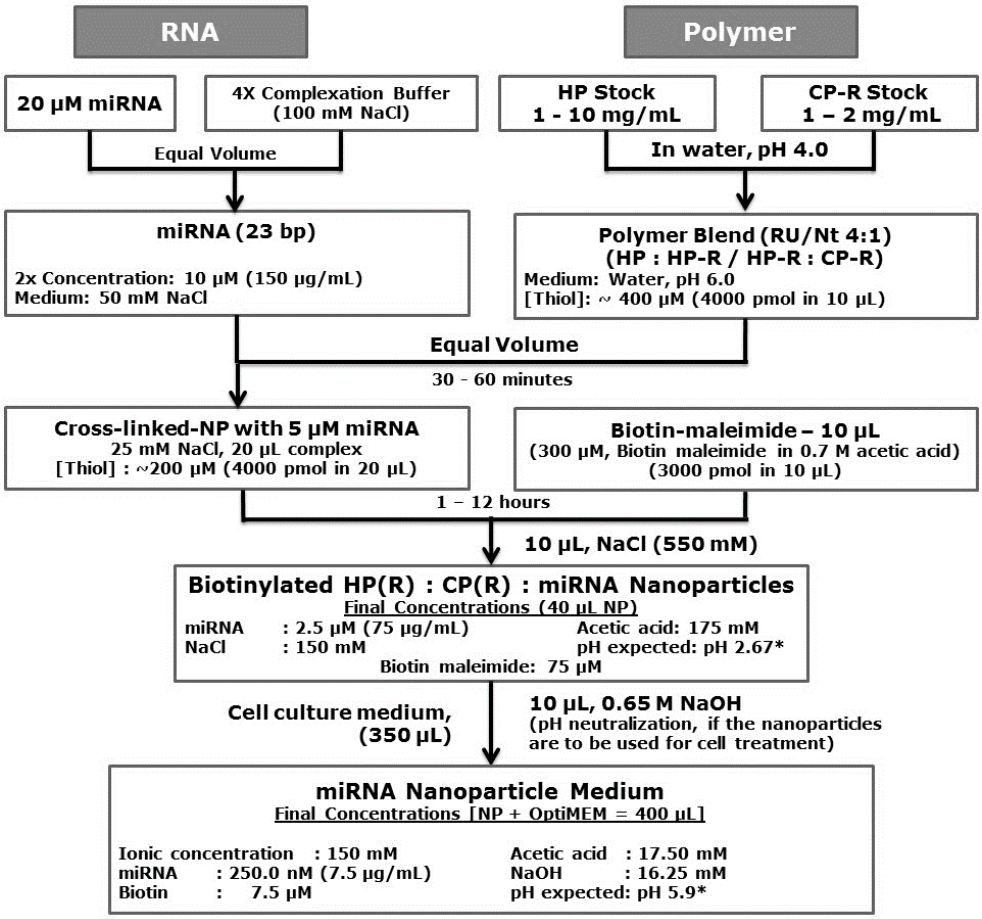

Figure 5-2: *In-situ* biotin-grafting protocol for nanocomplexes.
[Biotin Maleimide - HP(R): CP2k(R) – miRNA complexes]. * - pH was theoretically calculated using online pH solver (http://www.webqc.org/phsolver.php).

5.2.5 Nanoparticle Uptake Assay (flowcytometry)

The U87MG cells were seeded on a 24 well plate [40000 cells/well]. After overnight incubation, the cells were treated with nanoparticles for 6 hours in OptiMEM medium. Following incubation, the nanoparticle medium was replaced by Hoechst 33342 containing medium (5 µg/mL) and incubated for 15 minutes for nuclear staining. The medium was removed after 15 minutes of incubation, the cells were washed twice with PBS (1x, pH 7.4). The cells were collected by trypsinization and resuspended in ice cold FACS buffer [100 µL, PBS, 10% serum and 0.1% sodium azide] followed by addition of ice cold formaldehyde [100 µL, 4% paraformaldehyde dissolved in PBS, pH 7.4]. The cells were analysed by MACSQuant® Analyzer 10 (Miltenyi Biotec) using the settings described in previous chapter (4.2.4, page: 128).

5.3 Results

5.3.1 Optimization of PAA-miRNA Nanoparticles: Salt in RNA

Initially, presence of salt in the complexation mixture resulted in polyplexes with poor stability and hence the complexation was carried out in the absence of salt which consistently yielded more stable nanoparticle formulations. However, in this section, the complexes were prepared in the presence of salt which was added to the nucleic acid (miRNA) instead of the polymer blend. This was expected to facilitate optimal PAA-miRNA complex formation and increase the crosslinking effectiveness. The formation of stable crosslinked complexes were tested for both HP:CP2k(R) and HP:CP5k(R) polymer-blends and the results are presented in **Figure 5-3** [page: 181] and **Figure 5-4** [page: 182], respectively. The thiopyridine to thiol (SPy:SH) ratio for different HP:CP ratios are presented in **Table 5-2** [page: 181] and **Table 5-4** [page: 182].

HP: CP2k(R) – miRNA nanoparticles: Most of the nano-complexes formed in the presence of salt (25 mM NaCl, pH 6.0) were stable at physiological salt concentrations, **Figure 5-3** [page: 181]. All the HP:CP ratios tested formed stable nanoparticles when the RU/Nt ratio was 4:1 or above. At RU/NT ratio 4:1, the size and Pdi were minimum (size ≤ 200 nm; Pdi < 0.2) among all other RU/Nt ratios tested, **Table 5-1** [page: 176]. At RU/Nt ratio 2.5:1, stable nanoparticles were obtained only for HP:CP ratios 3:1, 2:1 and 1:1, while the size of the nanoparticles were between 200 and 300 nm (Pdi < 0.2).

HP: CP5k(R) – miRNA nanoparticles: Similar to the HP:CP2k(R) complexes, HP:CP5k(R) complexes were stable under physiological salt concentrations when the RU/Nt ratio was 4:1 or higher, **Figure 5-4** [page: 182]. In contrast, the RU/Nt ratio of 2.5:1 did not produce any stable nanoparticles. The best complexes with the smallest size and Pdi are presented in **Table 5-3** [page: 181].

Taken together, the salt in RNA approach is able to produce nanoparticles that are stable under physiological salt concentration. This indicated that homopolymer (HP) and reduced copolymer [CP(R)] were able to crosslink sufficiently after the addition of miRNA in the presence of salt (25 mM NaCl).

5.3.1.1 HP: CP2k(R) – miRNA nanoparticles (Salt in RNA)

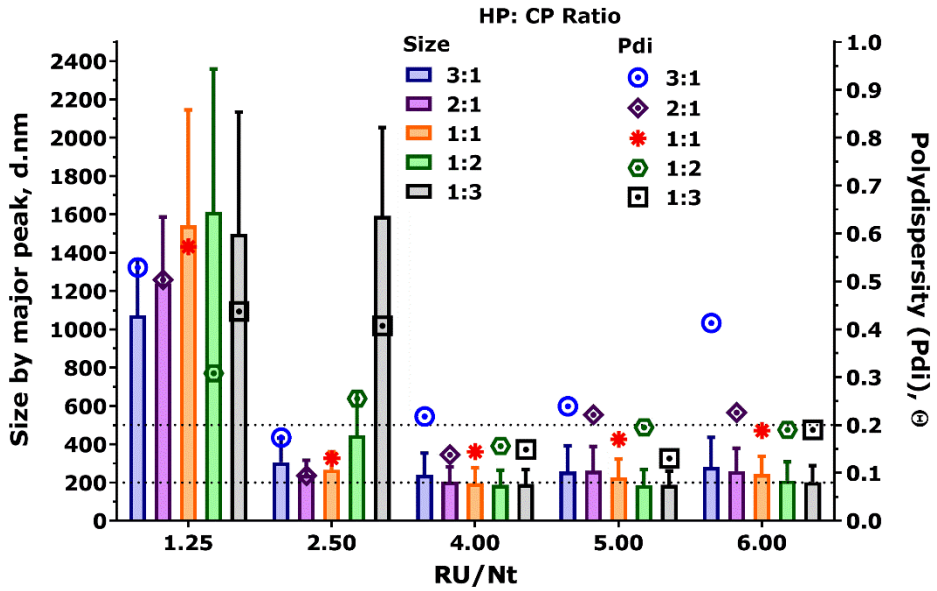

Figure 5-3: HP:CP2k(R)-miRNA complexes (Salt in RNA).

Complex formation in 25 mM NaCl, pH 6.0, Salt in RNA approach. The graph represents the size of the nanoparticles in 150 mM NaCl [Bar chart]. The error bars represent the width of the size peak indicating the size distribution range. The Pdi is represented as dot plot. (N = 1, n = 3).

Table 5-1: Size distribution of HP-CP2k(R) complexes at RU/Nt 4:1.

HP: CP2k(R) Ratio	Z-Avg d.nm	PdI width d.nm	PdI	Major Peak d.nm	SD d.nm	% Pk
3 : 1	195.8	91.48	0.218	238.9	113.9	99.3
2 : 1	**178.7**	**66.50**	**0.138**	**204.3**	**76.37**	**100**
1 : 1	167.6	63.59	0.144	196.8	79.79	99.9
1 : 2	163.6	64.55	0.156	188.2	75.56	100
1 : 3	168.6	65.06	0.149	191.7	75.72	100

Table 5-2: Thiol ratio for HP – CP2k polymer blends.

When the percentage of free thiol is in excess than the amount of SPy RU of HP, it might crosslink among themselves and was represented in 'red'.

HP RU: CP RU Ratio		HP (µg/µL)	CP2k(R) (µg/µL)	HP-SPy : CP-SH Ratio	
(mol/mol)	(mol/mol) %			(mol/mol)	% available SPy or SH
3: 1	75: 25	1.124700	0.431879	5.5 : 1	82 (SPy)
2: 1	66: 34	0.989736	0.587355	3.6 : 1	72 (SPy)
1: 1	50: 50	0.749800	0.863758	1.8 : 1	44 (SPy)
1 : 2	34: 66	0.509864	1.140160	0.95 : 1	**5 (SH)**
1 : 3	25: 75	0.374900	1.295637	0.61 : 1	**39 (SH)**

5.3.1.2 HP: CP5k(R) – miRNA nanoparticles (Salt in RNA)

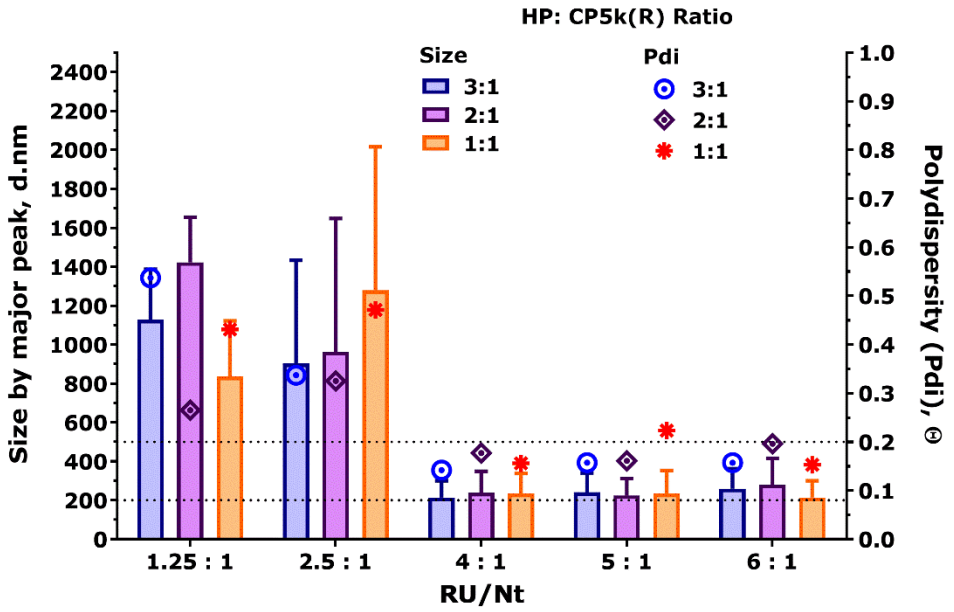

Figure 5-4: RU/Nt ratio vs size of HP: CP5k complexes (Salt in RNA).
Optimization of HP: CP5k(R) complex formation in 25 mM NaCl, pH 6.0. The graph represents the size of the nanoparticles in 150 mM NaCl. The error bars represent the width of the size peak indicating the size distribution. (N = 1, n = 3).

Table 5-3: HP: CP5k(R) -miRNA nanoparticles with smaller size and Pdi.

HP: CP5k Ratio	RU/Nt	Z-Avg d.nm	PdI width d.nm	PdI	Major Peak d.nm	SD d.nm	% Pk
3:1	4 : 1	184.7	69.7	0.142	215	86.21	100
2:1	5 : 1	197	78.94	0.161	225.4	87.07	99.5
1:1	6 : 1	182.7	71.45	0.153	214.7	86.63	100

Table 5-4: Thiol ratio for HP – CP5k polymer blends.
When the percentage of free thiol is in excess to the amount of SPy RU of HP, it was represented in 'red' to indicate that these thiols might crosslink among themselves.

HP RU: CP RU Ratio		HP (µg/µL)	CP5k(R) (µg/µL)	HP-SPy : CP-SH Ratio	
(mol/mol)	(mol/mol) %			(mol/mol)	% available SPy or SH
3: 1	75: 25	1.124700	1.612405	1.96 : 1	49 (SPy)
2: 1	66: 34	0.989736	2.192871	1.27 : 1	21 (SPy)
1: 1	50: 50	0.749800	3.224810	0.65 : 1	**35 (SH)**
1: 2	34: 66	0.509864	4.256749	0.34 : 1	**66 (SH)**
1: 3	25: 75	0.374900	4.837215	0.22 : 1	**78 (SH)**

5.3.2 *In-situ* Ligand Grafting

The functional activity of the PAA-miRNA nanoparticles not only depends on how good the complexation is, but also the characteristics of nano-bio interfaces and the nature of interaction of nanoparticle surface and the cells. The previous uptake experiments show poor or no uptake of nanoparticles at typical microRNA concentration (50 nM) and the uptake was improved only moderately by using very high concentrations of microRNA (500 mM) or increasing the time of incubation (6 – 12 hours). To improve the uptake of nanoparticles the surface of the nanoparticles can be modified by ligand grafting.

5.3.2.1 Ligand Grafting Strategies

Ligand grafting on the polymer can be performed either before mixing with miRNA (pre-grafting) or after the formation of the nanoparticles (post-grafting[346,347]). The polymer has thiol bearing residues which can be used for ligand grafting. The two possible thiol chemistries are, (a) grafting a ligand with free thiol to the thio-pyridine bearing homopolymer (HP); (b) grafting a maleimide bearing ligand on a thiol bearing polymer, **Figure 5-5, a, b** [page: 184].

Maleimide – thiol conjugation chemistry has several advantages. The maleimides are highly reactive with thiols, hence quickly produce very high yields of thiol-maleimide adducts. This highly efficient reaction eliminates the need for the use of excess ligands. Also, this reaction does not produce any by-products hence would not require further purification. The thiol-maleimide linkage (S – C) is quite stable[253], but still reversible through thiol exchange reactions which are 10 times slower than disulphide cleavage (S – S)[241]. Different ligands can be easily conjugated to commercially available bi-functional maleimide reagents through the classical carboxyl-amine chemistry. Moreover, several thiol-maleimide antibody-drug conjugates (ADC) have been approved by Food and Drugs Administrations (FDA) for clinical applications[348].

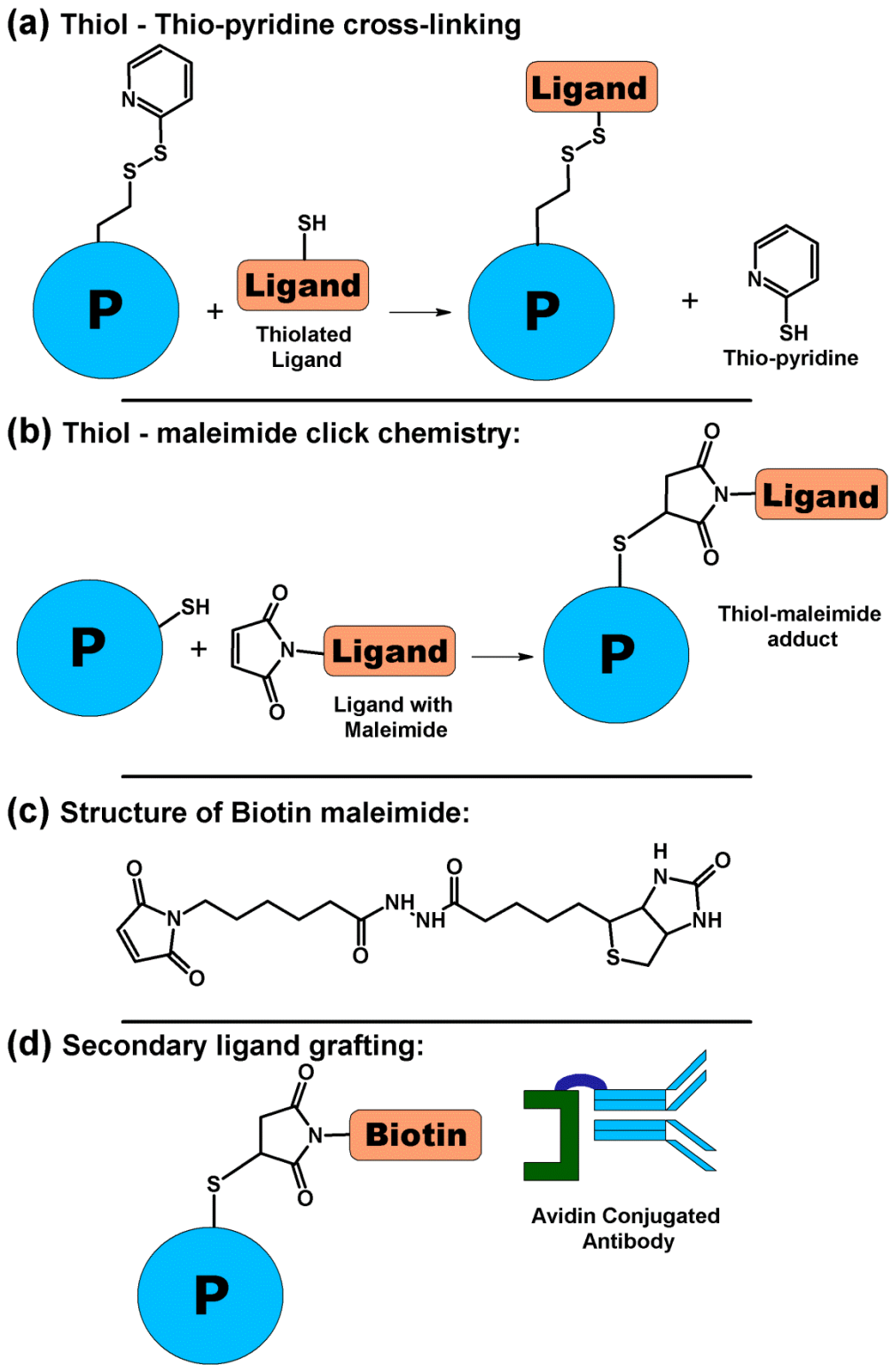

Figure 5-5: Ligand grafting strategies.

The blue circle (P) represents either the polymer or the nanoparticle.

5.3.2.2 Biotin-maleimide as a Ligand

Biotin (vitamin H) receptors are expressed by most mammalian cells, and particularly are over-expressed by cancer cells so can be used to enhance uptake[349] into cancer cells. In this work biotin was used as the ligand, but, biotin conjugated nanoparticles can be easily conjugated with commercially available streptavidin tagged antibody or peptide molecules for targeted delivery, **Figure 5-5, d** [page: 184]. Hence, new one-pot protocol [**Figure 5-2**, page:179] was developed for the preparation of biotin conjugated miRNA nanoparticles using biotin maleimide, **Figure 5-5, b, c** [page: 184].

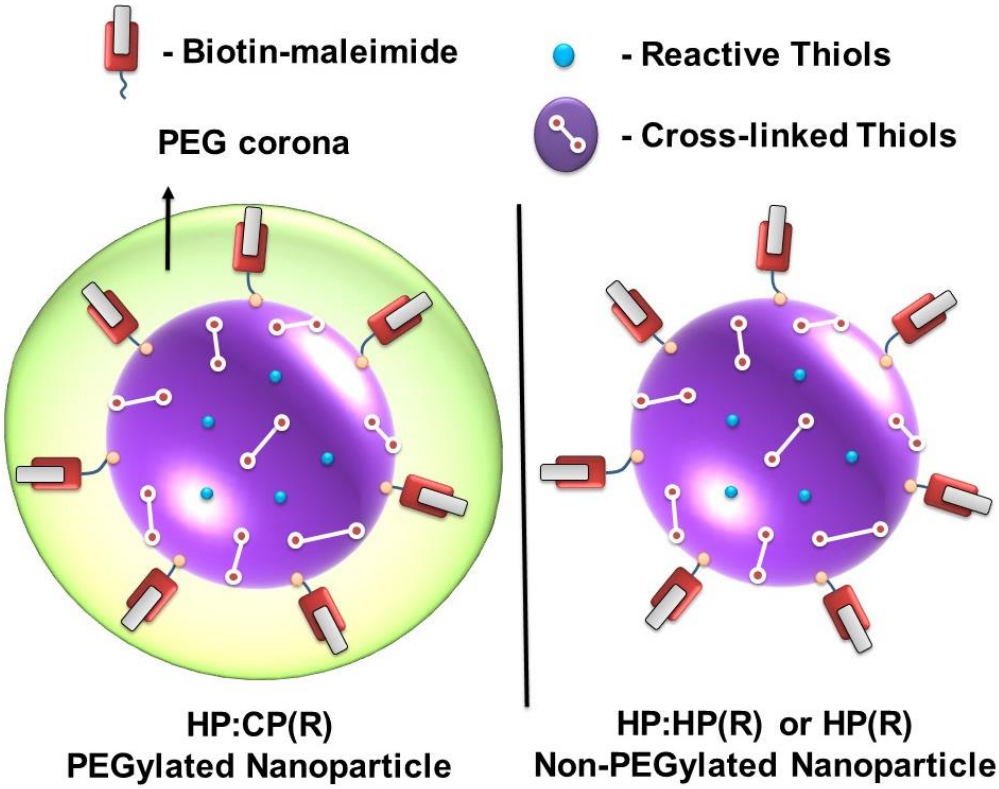

Figure 5-6: Schematic of a biotin-grafted PAA-miRNA nanoparticle.

The basic concept of biotinylated nanoparticle preparation was to use thiol-thiol chemistry for inter-polymer crosslinking, instead of thiol-thiopyridine chemistry, while part of the thiols from the polymer would be involved in the biotin-conjugation by thiol-maleimide chemistry.

Accordingly, two different types of biotinylated nanoparticles were prepared, HP(R): CP2k(R) and HP:HP(R). It was decided that 75% of the free thiols from the polymers would be used for ligand grafting, while the remaining 25% would contribute to the nanoparticle stabilization.

5.3.2.3 Biotinylated - HP(R): CP2k(R) – miRNA Nanoparticles

The polymer repeating unit to miRNA nucleotide ratio (RU/Nt) was fixed as 4:1. The HP(R):CP(R) polymer-blends were prepared at different ratios, between 3:1 to 1:3, as indicated in **Figure 5-7** (X-axis) [page: 187]. miRNA solution was prepared [10 µM miRNA in 50 mM NaCl]. Polymer-blend (PAA, 10µL) was added to the miRNA solution (10 µL), mixed gently and incubated for 30 minutes. The PAA-miRNA complex was divided in two equal parts. Biotin maleimide [5 µL, 300 µM biotin maleimide in 0.7M acetic acid] was added to one part of the PAA-miRNA complex (10 µL) while the other part was not functionalised with ligand. After 30 minutes of incubation, 300 mM NaCl (10 µL) was added to both the PAA-miRNA complexes. The size was measured by DLS (Malvern Nano S).

The results indicated that those complexes which were incubated with biotin-maleimide formed stable nanoparticles, while the non-biotinylated HP(R):CP2k(R) complexes were not stable at physiological salt concentration, **Figure 5-7** [page: 187]. This indicated that insufficient thiol-thiol crosslinking was formed between HP(R) and CP2k(R) when there was no biotin maleimide. As thiol-thiol crosslinking is a slow reaction (half-life ~ 4.5 to 6 hours), the HP(R):CP(R) complexes were allowed to crosslink overnight (~18 hours) before the addition of 300 mM NaCl. Even this extended crosslinking time did not yield stable nanoparticles (data not shown). It was suspected that there might be traces of DTT remaining after the purification of polymers. Presence of DTT can reduce the stabilizing thiol-thiol bonds and hence reduce the stability of the PAA-miRNA complexes in physiological salt concentration. The percentage free thiols from CP2k(R) after reduction was ~50% of the theoretical amount, indicating that the CP2k(R) did not contain any traces of DTT. However, the thiol percentage determined for HP(R) was 148% of the theoretical thiol concentration. This excess could be because of the presence of DTT after PD-10 purification. This explained why the HP(R): CP(R) complexes were not stable even after extended incubation time. However, when biotin maleimide was added to the PAA-miRNA complex, they were able to form stable nanoparticles even in the presence of DTT. This could be because that some of

the biotin maleimide added to the PAA-miRNA complex would have reacted with excess DTT and hence neutralizing its destabilizing effect.

One of the formulation was selected for further investigation, HP(R):CP2k(R) 2:1 RU/Nt 4:1, as this formulation produced nanoparticles around 200 nm with Pdi < 0.2.

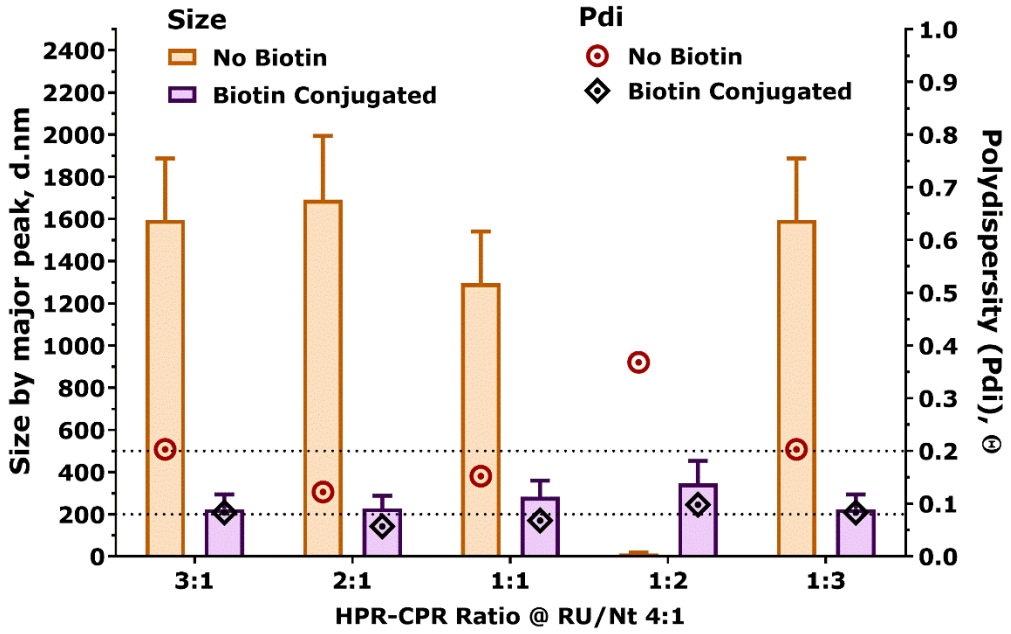

Figure 5-7: Biotin-conjugated HP(R):CP2k(R) miRNA complexes.

HP(R): CP2k(R) complex formation in NaCl (25 mM), pH 6.0, Maleimide: SH (~ 0.75: 1)*. The graph represents the size of the nanoparticles in 130 mM NaCl. The error bars represent the width of the size peak indicating the size distribution range. * Polymer-miRNA complex (10 µL, 5 µM) + biotin maleimide (5 µL, 300 µM) + NaCl (10 µL, 300 mM). (N = 1, n = 3).

A similar attempt to produce biotinylated HP(R):CP5k(R) miRNA nanoparticles did not produce stable nanoparticles (data not shown). It was reasoned that the short PAA segment of CP5k [5kDa PEG – 3kDa PAA – 5kDa PEG] did not crosslink sufficiently even when there was biotin maleimide added to the PAA-miRNA mixture. Also, the presence of large PEG chains was expected to shield the biotin from cellular recognition, hence this axis [Biotinylated - HP(R): CP5k(R) – miRNA complex] was not further investigated.

5.3.2.4 Biotinylated - HP: HPR – miRNA complexes

The HP:HP(R) polymer blends were prepared at three different HP:HP(R) ratios, 1:1, 1:2 and 0:1. HP:HP(R) ratio 0:1 represents the HP(R) nanoparticles formed only with reduced homopolymer [100% HP(R)]. The polymer to miRNA repeating unit ratio (RU/Nt) was varied from 4:1 to 10:1 as indicated in **Figure 5-8** (X-axis). Initially polymer-blends were added to miRNA solution [10 µM miRNA in 50 mM NaCl], mixed gently and incubated for 1 hour. The biotin maleimide was added to one part of the PAA-miRNA mixture, while the other part was not grafted with ligand. After about an hour of incubation, 300 mM NaCl was added to all the complexes and the size was measured by DLS, **Figure 5-8**.

Stable nanoparticles [200 – 300 nm, Pdi ~ 0.2] were produced when the HP:HP(R) ratio was 1:1 or 1:2, at all RU/Nt ratios and both in the presence and absence of biotin maleimide. For pure HP(R) [100% HP(R)], small stable complexes were obtained at RU/Nt ratio 7.5:1 with biotin.

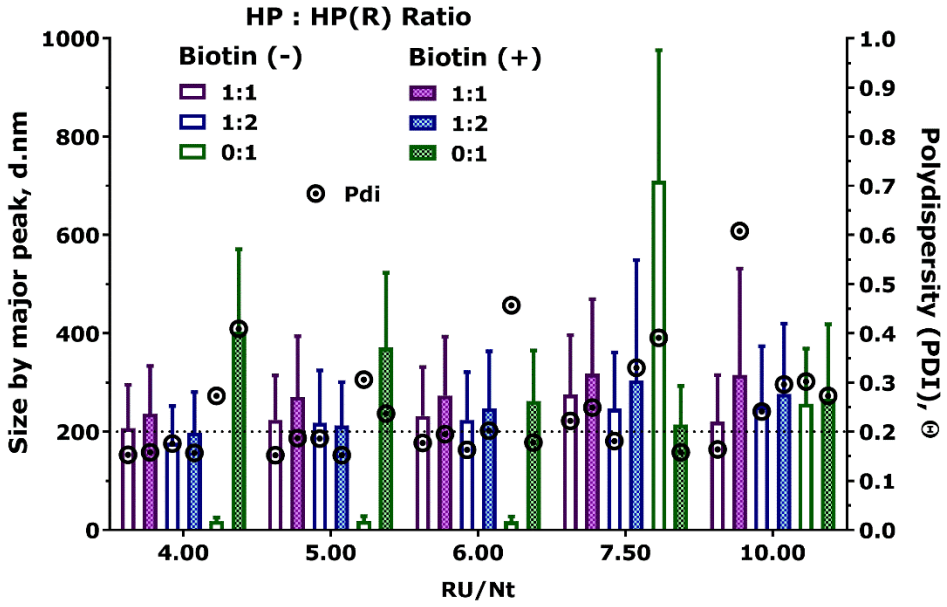

Figure 5-8: Biotin conjugated HP:HP(R) miRNA complexes.

HP:HP(R) complexes were prepared in NaCl (25 mM), pH 6.0, Maleimide: SH (~ 0.75: 1)*. The bar-chart represents the size of the nanoparticles in 130 mM NaCl. The error bars represent the width of the size peak indicating the size distribution range. The polydispersity (Pdi) is represented by dotted-circles (Right Y axis). * Polymer-miRNA complex (10 µL, 5 µM) + biotin maleimide (5 µL, 300 µM) + NaCl (10 µL, 300 mM). (N = 1, n = 3).

5.3.3 Nanoparticle Uptake Assay

U87MG cells were treated with biotinylated [**HHR-Biotin** = Biotin maleimide - HP:HPR 1:2 RU/Nt 4:1, size = 318 nm, Pdi = 0.234] and non-biotinylated [**HC2k** = HP:CP2k(R) 2:1 RU/Nt 4:1, size = 150 nm, Pdi = 0.175; **HC5k** = HP:CP5k(R) 2:1 RU/Nt 5:1, 200 nm, Pdi = 0.106] nanoparticles. All the nanoparticles were prepared with fluorescently labelled miRNA (miR-Cy3). The cells were treated at 250 nM concentration in OptiMEM medium for 6 hours. The cells were stained with Hoechst 33342 nuclear staining dye. The results from flow cytometry data clearly indicated that the biotinylated nanoparticles showed enhanced uptake compared to non-biotinylated nanoparticles, [Geometric-mean Fluorescence Intensity (GFI), 6.3 Vs ~ 2.6 - 3.0] **Figure 5-9** [pg.no.:190] and **Figure 5-10** [pg.no.: 190]. However, the uptake of biotinylated nanoparticles was under-performing when compared to the commercial nanoparticles (N-TER) (GFI, 6.3 Vs 40). Also, reducing the size of the biotinylated nanoparticles may improve cellular uptake. It should be noted that the biotinylated nanoparticles did not have any PEG at its surface as they were prepared from two different forms of homopolymer. The HP: HP(R) complexes prepared without biotin maleimide did not form stable complexes and hence not tested. Also, the biotinylated nanoparticles prepared with different batches of HP(R) were not stable, due to the presence of DTT. Hence, further investigation is needed for the complete purification of homopolymer (HP), optimization of biotinylated nanoparticle preparation and its biological characterization.

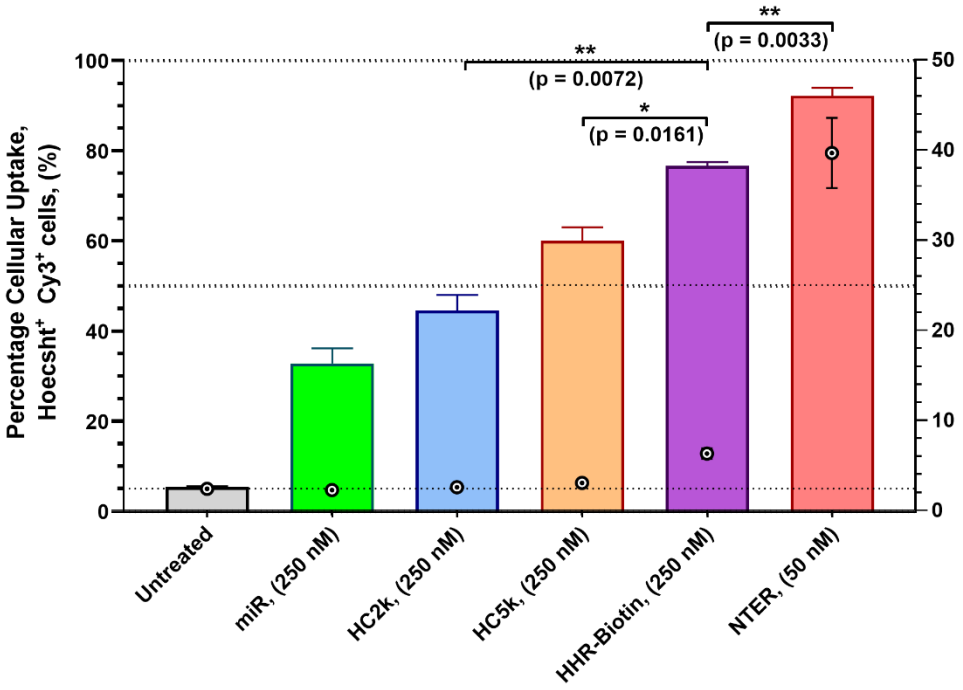

Figure 5-9: Uptake of biotin-conjugated nanoparticle (Bar chart).

Nanoparticle uptake assay by flow cytometry. The left-Y-axis represents percentage double positive cells, while the right-Y-axis represents the geometric-mean fluorescence. The statistical analysis was based on two-tailed paired-t-test on geometric-mean fluorescence intensity (GFI). (N = 1, n = 3).

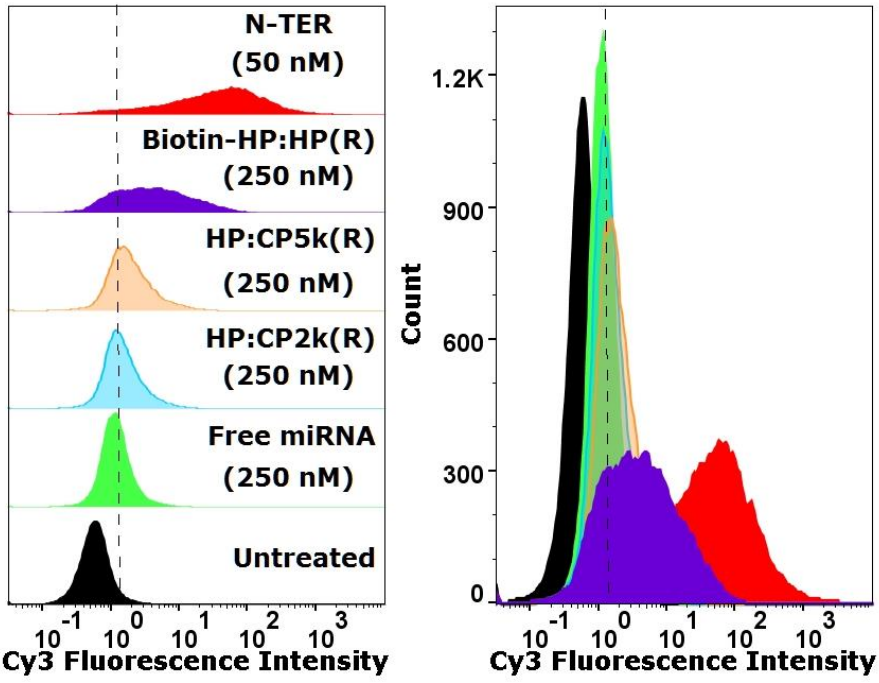

Figure 5-10: Biotin-conjugated nanoparticle uptake (Histogram).

Left: Stacked view; **Right:** Overlaid view (Colour codes same as left image). The cell population right-side to the dotted line was considered as Cy3-positive cells. N = 1, n = 3.

5.4 Discussion

5.4.1 Cellular uptake

As biotin receptors are expressed on all cells, biotin acts as a non-specific target ligand that would enhance cellular uptake. The results from the uptake assay suggest that the biotin-grafting on the PAA-miRNA nanoparticles improved cellular uptake. However, the amount of uptake was still not as high as the commercial peptide nanoparticles (N-TER).

Biotinylated hydroxpropylmethacrylic acid (HPMA) polymers showed several-fold enhanced uptake compared to non-targeted polymers in many of the cancer cell lines tested[349]. Biotin conjugated poly(amidoamine) dendrimers (PAMAM) showed improved uptake in both the cell lines tested, ovarian cancer [OVCAR-3] and human embryonic kidney cells [HEK-293][350]. Addition of biotin to PLGA nanoparticle also improved its uptake in a human hepatic carcinoma cell line (SMMC-7721), [Percentage NP positive cells, ~20% for PLGA-NP; ~40% for Biotin-PLGA-NP][351].

Percentage of ligand grafting can also affect the uptake and functional activity of nanoparticles. Bioreducible polyamidoamine (PAA) polymers were conjugated with cholesterol to improve its uptake. It was observed that moderate degree of cholesterol conjugation (57%) resulted in increased uptake and maximal gene knockdown, while lower (14%, 29%) or very high degree (87%) of cholesterol conjugation produced suboptimal siRNA-mediated gene knock-down efficiency[352].

5.4.2 Problems and Solutions on Reproducibility

The HP:HP(R) or HP(R):CP2k(R) complexes prepared without biotin maleimide did not form stable complexes. This instability was possibly due to the presence of traces of DTT in the purified HP(R). The purified HP(R) showed 140 – 170% of thiol activity to the theoretical expectation. This varying amount of DTT contamination in the HP(R) resulted in the variation in the stability of the biotinylated PAA-miRNA complexes prepared with HP(R) [e.g. HP(R):CP(R) and HP:HP(R) complexes]. Addition of biotin maleimide produced complexes with varying size and stability. The reproducibility of these

complexes were thought to be affected by the presence of varying amounts of DTT in the purified HP(R) solution.

As there was no problem in the purification of CP2k(R) and CP5k(R) by PD-10 column, a new method has to be developed for HP(R) purification. The formation of stable complexes primarily depends on thiol-thiol post-crosslinking occurring among the polymer chains after mixing the polymer-nucleic acid solutions. Hence, the polymer solution used for the formation of complexes must be completely free from any reducing agents. DTT can be replaced by TCEP [Tris(2-carboxyethy1)phosphine] which is a more potent reducing agent[353] and hence lowering the amount of reducing agent required for the reaction. This would facilitate complete elimination of reducing agents when using the standard PD-10 columns. Alternatively, a larger desalting column or an ultra-filtration spin column could be used for an effective elimination of the reducing agent from the polymer, HP(R).

The crosslinking reaction between HP(R) and CP(R) can also be affected by the amount of biotin maleimide. A higher concentration of biotin maleimide would react with more thiols for ligand grafting and fewer thiols would be available for stabilizing crosslinking. The other factor that can be a concern is the presence of high concentration of acetic acid (175 mM, pH 2.67) during the complex formation step. The acidic pH can reduce the thiol-thiol crosslinking reaction and possibly thiol-maleimide reaction. The high concentration acetate ion might also interfere with the complex formation between polymer and miRNA. Hence, biotin-maleimide could be dissolved in an alternative solvent like dimethyl sulfoxide (DMSO), which can solve the issues with pH and accelerate the thiol-thiol crosslinking by acting as an oxidising agent[264]. Alternatively, the biotinylation can be uncoupled from the nanoparticle preparation step by conjugating the biotin to the polymer at various degrees. This biotin-grafted polymer can be purified from acetic acid and other impurities, before they are used for nanoparticle preparation.

One of the ways to achieve effective biotinylation of the polymer is by replacing DTT with TCEP which is a non-sulfhydryl reducing agent and hence less reactive with maleimides. For example, equi-molar TCEP to maleimide would

only inactivate 30 – 40% of the maleimide (at pH 6.0), whereas thiol-containing reducing agents can inactivate more than 80% of the maleimides under similar conditions[354]. In order to allow effective thiol-maleimide (polymer-biotin) conjugation, at least a partial elimination of TCEP would be required[355], where as a complete elimination is required for DTT. Hence, TCEP would be a good choice of reducing agent for the preparation of biotin-grafted-polymer.

In situ ligand grafting can also be achieved using a thiolated ligand which can directly attach to the surface of crosslinked nanoparticles [HP:CP(R)] that were prepared through thiopyridine-thiol (SPy:SH) chemistry. When the amount of thiopyridine from HP is higher than the thiols from CP, then the remaining thiopyridine can be used for conjugating a ligand reversibly, (see **Table 5-2**, page: 181 and **Table 5-4**, page: 182 for the SPy:SH ratio). Like thiol-maleimide reaction, the thiol-thiopyridine conjugation is also a fast reaction, hence highly efficient ligand grafting can be achieved by both the methods.

5.5 Conclusions

In the previous chapter, the nanoparticles were mixed in water, with salt added later to help finalise crosslinking. Presence of salt in the polymer-blend was found to be detrimental for the stability of the complexes as the polymer-blends prepared in the salt solutions resulted in the instantaneous HP: CP crosslinking and this drastically affected the stability in physiological ionic concentrations. In this chapter, it was shown that the addition of salt in the miRNA solution did not affect the stability of the nanoparticles formed. This improvement in the miRNA nanoparticle preparation takes advantage of salt. Taken together, it is possible to prepare stable nanoparticles both in the presence and absence of salt, while the presence of salt in the miRNA solution can have added advantages like optimal PAA-miRNA interaction and increased stability due to enhanced thiol-thiopyridine crosslinking.

In the second part of this chapter, in situ ligand grafting protocol was developed for PAA-miRNA complexes. Biotin-maleimide was used as a ligand for improving the cellular uptake. Biotin can not only act as an uptake enhancing ligand, but also enable attachment of secondary target-specific ligands or

antibodies via biotin-avidin interaction. In order to conjugate biotin maleimide at the surface of PAA-miRNA nanoparticles, it was essential to have free thiols are the surface of these nanoparticles. The classical method involves the mixing of thiopyridine protected homopolymer [HP] with thiol-bearing reduced copolymer [CP(R)]. This type of complexation [HP-CP(R)] would yield nanoparticles that have thiopyridine groups at the surface. These nanoparticles would be ideal for the attachment of thiol-bearing ligands. As the present ligand contains a maleimide group, it was decided to use a new strategy where the PAA-miRNA complexes would be formed with thiol bearing reduced-homopolymer [HP(R)] and copolymer [CP(R)]. Such a complex would have excess thiol at its surface enabling the conjugation of biotin-maleimide via thiol-maleimide chemistry. The new protocol was initially able to produce stable biotinylated nanoparticles. Biotinylated non-PEGylated nanoparticles showed enhanced uptake compared to non-biotinylated nanoparticles. This preliminary data suggests that biotin (or other ligand) grafted PAA-miRNA nanoparticles could display enhanced cellular uptake and possibly higher gene-silencing ability compared to non-targeted PAA-miRNA nanoparticles.

However, there was a problem with the reproducibility of these biotin conjugated nanoparticles due to the issues faced with the incomplete purification of homopolymer [HP(R)] after reduction. Traces of DTT was detected in most of the purified batches of reduced homopolymer [HP(R)] but none was detected with the purification of reduced copolymer [CP(R)]. Presence of DTT in the formulation did not allow the formation of stabilizing disulphide bonds, leading to formation of unstable nanoparticles. Due to the problems with reproducibility, extensive further in vitro testing was not performed.

Alternative methods have to be developed for HP(R) purification which would allow complete elimination of DTT. This would allow the preparation of stable and reproducible biotin-grafted PAA-miRNA nanoparticles. Due to time limitations, this troubleshooting was not performed in this work. However, this last section serves as a proof-of-concept for thiol-maleimide mediated ligand conjugation and enhanced cellular uptake for these kind of poly(amidoamine) nanoparticles.

Chapter – VI

General Discussion, Future Perspectives and Conclusions

6 General Discussion and Conclusion

The main aim of the thesis was to develop stable thiol crosslinked poly(amidoamine)-miRNA (PAA-miRNA) nanoparticles that can be used for the treatment of brain tumours using a loco-regional route of administration.

The major part of the thesis was focused on the development of methods for the production of stable crosslinked nanoparticles. An alternative polymer purification protocol was optimized using PD-10 columns for maximum polymer recovery and DTT elimination. Polymer crosslinking kinetics were investigated under different conditions (salt and pH) which provided deeper understanding of the behaviour of these crosslinkable poly(amidoamine) polymers. This was key for troubleshooting the issues related to nanoparticle stability and method improvement. Two different nanoparticle preparation methods were investigated, salt free complex formation (Chapter IV) and salt in RNA (Chapter V). Both these methods were able to produce stable crosslinked nanoparticles. The details for the method optimization are discussed in the section 6.1.

The moderate cellular uptake of the PAA-miRNA nanoparticles was identified as the reason for low knock-down efficiency even at high concentrations of PAA-miRNA nanoparticles (Chapter IV). Hence, the final part of the work was focused on the development of ligand-conjugated nanoparticles to improve the cellular uptake (Chapter V). The possibility of biotin-maleimide conjugation on thiol-bearing nanoparticle surface was investigated. Flow-cytometry data showed significant improvement in cellular uptake of biotin-conjugated nanoparticles compared to untargeted nanoparticles. This initial observation indicated that the ligand-targeted PAA-miRNA nanoparticles can improve cellular uptake. Further investigation is required to optimize homopolymer purification and new modes of ligand conjugation to obtain better cellular uptake and increase gene-knockdown efficiency.

A simple and accurate luciferase normalization technique that reports both the luciferase expression and cell viability in the same sample was also developed

(6.4.1). This assay is an important development as a screening platform for miRNA/siRNA delivery systems.

6.1 Method Development - Nanoparticle Preparation

The three component PAA-miRNA polyplexes are formed by mixing a non-PEGylated cationic homopolymer (HP, PAA), a PEGylated cationic copolymer (CP, PEG-PAA-PEG) and polyanion (miRNA or siRNA or plasmid DNA). The thiol group (SH) from the reduced copolymer [CP(R)] reacts with the thiopyridine (SPy) from the homopolymer (HP) to form disulphide bonds. These disulphide bridges formed after the PAA-miRNA complex formation prevents disassembly of the nanostructure and hence provides stability to the nanoparticles in physiological medium.

The first step in the PAA-miRNA nanoparticle preparation is the activation and purification of the copolymer. The thiol groups from copolymer are initially protected with t-BOC during polymer synthesis. Hence, CP must be activated with a reducing agent [e.g. DTT] and purified from the by-products of the reaction. The original protocol for the purification of DTT from the reduced polymer [CP(R)] was performed by ultra-filtration. The thiol recovery obtained from this method [35% thiol recovery for CP2k(R) and 10% for CP5k(R), [Chapter III])] was only moderate when using 4 cycles of filtration, **Table 3-1** (**page: 84**). This low thiol recovery was attributed to the long filtration time (8 hours) during which oxidation can take place. Hence, a PD-10 column purification (30 minutes) protocol was adopted and optimized for the purification of PAA-copolymers. This protocol improved the thiol recovery to 50% for CP2k(R) and 27% for CP5k(R), [Chapter IV]. The inability to obtain 100% free thiols can be because of the inevitable thiol crosslinking that can occur during the freeze-drying process[356].

The second step in the preparation of nanoparticles is the mixing of homo and copolymer to prepare a polymer-blend [HP:CP(R) mixture]. This polymer blend is then mixed with an equal volume of miRNA or siRNA solution to obtain thiol-crosslinked nanoparticles. In order to obtain maximum miRNA incorporation

into the nanoparticle, it was expected that the nanoparticle preparation medium should be at optimal pH and ionic concentration.

The role of nanoparticle preparation medium is to facilitate optimal nanoparticle formation and resulting nanoparticle properties. In general, polymeric-miRNA nanoparticles are prepared in specific medium (low or non-ionic conditions) depending on the nature of polymer and its interaction between the nanoparticle forming components. Chitosan nanoparticles are prepared routinely in acidic medium to facilitate chitosan solubility. Chitosan (1 mg/mL) is dissolved either in acetic acid (2% or 350 mM)[357], acetate buffer (300 mM, pH 5.5)[203] or acidified water[336]. Polyamidoamine dendrimers are complexed with siRNA in water[358]. Commercial linear-polyethylenimine based nanoparticles [*in vivo*-jetPEI®, Polyplus-Transfection] are prepared in 5 wt.% glucose[335].

Previously, in our group, the PAA-nucleic acid nanoparticles were routinely prepared in 15 mM PBS (0.10 x)[297] or 5 mM NaCl[275]. The later concentration was adapted from a work reported on DNA-polyelectrolytes by Kabanov *et al*[316].

Hence, the first part of Chapter III focused on the systematic PAA-miRNA binding assay to obtain the optimal ionic concentration and pH for these set of poly(amidoamine) polymers. The optimal salt concentrations and pH required for the maximal PAA-miRNA interaction was determined by gel-retardation assay as 20 - 50 mM NaCl and pH 6.0. Presence of phosphate ion as a buffering agent did not interfere the PAA-miRNA interaction as observed by agarose gel electrophoresis. Hence, the complex forming condition was defined as 25 mM PBS (0.17x), pH 6.0.

However, preparation of polymer-blends in this optimized medium failed to produce stable nanoparticles. No differences were observed on the agarose gel analysis when the complexes were prepared in 25 mM PBS or 150 mM PBS. The DLS analysis measured the presence of small nanoparticles (150 – 300 nm, Chapter III and IV) when tested under low ionic concentration (25 mM PBS), but the size of the complexes increased in physiological medium (> 1000 nm, Chapter IV). These results indicated that the PAA-miRNA nanoparticles were behaving like non-crosslinked nanoparticles indicating some defects in the

crosslinking process. Similar aggregation behaviour has been reported for chitosan nanoparticles[359], non-crosslinked peptide-DNA nanoparticles[242], polyamine-DNA nanoparticles[247] etc.,. The crosslinking of these nanoparticles after complex formation conferred stability of these nanoparticles in physiological salt solutions by preventing the dissociation of polyelectrolyte complexes under physiological conditions[242,244,247].

Further investigations identified the spontaneous salt-induced crosslinking between homo and copolymers in the polymer-blends. This thiol-thiopyridine reaction was instantaneous and increased by the presence of salt, even before the addition of miRNA. Absence of salt during complex formation (Chapter IV) or addition of optimal amount of salt with nucleic acid (Chapter V) were able to produce stable nanoparticles in physiological medium. These experiments not only demonstrated the importance of post-crosslinking and its role in nanoparticle stabilization under physiological conditions, but also indicates the nanoparticle preparation method can affect the fate of the final nanoparticles.

6.1.1 Advantages of Salt in RNA (Double strand stability)

In Chapter V, the microRNA solution was prepared by mixing equal volume of miRNA (20 µM) and NaCl solution (100 mM) to obtain a working miRNA solution containing 10 µM miRNA in 50 mM NaCl. The presence of salt with the nucleic acid solution is known to screen the repulsive negative charges from the phosphate backbone and improve the stability of the double stranded RNA (dsRNA)[360,361]. This screening effect also makes the RNA molecule more flexible and compact, which not only can help in the formation of compact nanoparticles, but also preserve the functions of miRNA until delivery. Divalent ions (e.g. Mg^{2+}) are known to be more effective nucleic acid stabilizing agents compared to monovalent (e.g. Na^{+}) ions, i.e., 3 mM Mg^{2+} ≡ 50 mM Na^{+}[360]. Hence, divalent metal ions could be used for future nanoparticle formulations.

6.1.2 Advantages of Post-Crosslinking PAA-miRNA System

The PAA-miRNA systems take advantage of bioreducible disulphide crosslinking for nanoparticle stabilization. This disulphide stabilization of the nanostructure also allows maximum miRNA incorporation with minimum amount of polymer, hence these nanoparticle preparations have much less free

polymer or miRNA. The miRNA loading capacity of the PAA-miRNA formulation that was tested for *in vitro* assay was about 15 wt.% [HP: CP2k(R) 1:1 RU/Nt 5:1, or polymer to miRNA mass ratio 5.4:1]. The amount of thiol crosslinking required for stabilizing a DNA-polyplex is lower than the amount required for low-molecular weight siRNA/miRNA-polyplex[269]. The amount of thiol crosslinking and the amount of PEG at the surface of nanoparticles can be controlled by simply varying the homopolymer to copolymer ratio (HP:CP). This allows easy tailoring of the system for different nucleic acids. Thiol crosslinked nanoparticles are redox-responsive and hence release the cargo only in a highly reductive environment. L-Cysteine and Glutathione (GSH) are the major molecules in the body that are capable of reducing disulphide bonds[362]. The plasma and extracellular compartments contain relatively low concentrations of reducing agents [8 - 11 µM L-Cysteine and 4 - 8 µM Glutathione + other reducing agents], while the intracellular compartments contain very high concentrations of glutathione [1-11 mM][362]. This highly reducing intra-cellular environment is expected to facilitate selective delivery of cargo from the disulphide crosslinked nanoparticles. Taken together, physiological stability, selective intracellular release and minimum free components make these nanoparticles ideal for *in vitro* and *in vivo* applications.

6.2 Cellular Uptake and Role of PEG

The success of a miRNA delivery system depends on cellular entry and subsequent release of microRNA at the site of action (cytoplasm). Nanoparticles prepared with fluorescently labelled miRNA (miR-Cy3) were used to study the uptake of different PAA-miRNA nanoparticles.

In chapter V, the uptake behaviour of one PAA-miRNA formulation [HP: CP2k(R) 1:1 RU/Nt 5:1] was extensively tested on U87MG cells. The cellular uptake experiments showed poor to moderate cellular uptake of crosslinked PAA-miRNA nanoparticles (50, 250 and 500 nM) compared to the commercial peptide based N-TER reagent (50 nM). Even at the highest concentration tested (500 nM, 4 hours), the uptake was one tenth that of the N-TER transfection agent (50 nM, 4 hours). Longer incubation time (8 and 12 hours) did not improve

cellular uptake but had a negative effect on the morphology of the cells, probably due to membrane disruptive behaviour and cell death.

The poor uptake of the PAA-miRNA nanoparticles can be attributed to the poor interaction between nanoparticle and cellular surface. Aljaeid *et al.* demonstrated that the transfection efficiency of crosslinked PAA-DNA nanoparticles was inversely related to the length of the copolymer's PEG chains (655 > 1700 > 4600 Da)[274].

6.2.1 PEG and Reduced Cellular Uptake

The surface characteristics and the nature of PEG chains[363] (length, density[364] and conformation[364]) influence cell-surface interaction and hence affect uptake. Lower cellular uptake was observed when the nanoparticles had high PEG density with lower mobility[364]. Similarly, longer PEG chains (5 kDa < 2 kDa) and higher density of PEG (2 PEG molecules/nm^2 < 1 PEG molecule/nm^2) on gold nanoparticle surface reduced cellular uptake[365]. The highest uptake was observed for non-PEGylated gold nanoparticles[365].

The nanoparticle surface with no PEG or low density PEG allows the adsorption of proteins [e.g. serum albumin, fibrinogen][366]. This protein corona increases the cellular interaction by acting like a non-specific ligand and enhances *in vitro* cellular uptake[220]. Presence of high density and high molecular weight PEG reduces protein adsorption and shields the nanoparticle surface from directly interacting with the cell surface, which leads to lower cellular uptake compared to non-PEGylated nanoparticles[220,363,366].

6.2.2 PEG and Reduced Endosomal Escape

Presence of PEG at the nanoparticle surface not only affects the uptake, but also has been reported to affect the endosomal escape.

For liposomal DNA delivery systems, the main mode of endosomal escape is by membrane fusion[367]. Presence of PEG at the surface of liposomes interfere with the membrane fusion and hence prevented the endosomal escape of these lipoplexes[367].

For polymeric nanoparticles, the main mode of endosomal escape is by proton-sponge effect. The primary amines on the cationic polymer backbone exhibit a buffering reaction during endosomal acidification which subsequently leads to the osmotic swelling and rupture of endosomes which releases the polyplexes into the cytoplasm. PEGylation of PEI-DNA nanoparticles did not reduce the cellular uptake but drastically affected the endosomal escape[368]. The nanoparticle PEGylation was performed by reacting primary amines on nanoparticle surface with methoxy-PEG_{5000}-succinimidyl propionate[368]. The authors suggested that this reaction affecting the primary amines may have impaired the proton-sponge effect of PEI[368]. The same work also tested another cationic polymer, β-cyclodextrin-containing polymer (βCDP)[368]. These βCDP-DNA nanoparticles were grafted with PEG-adamantine, where the adamantine forms an inclusion complex with cyclodextrin[368]. This mode of PEGylation did not alter the amine groups. Hence, the reduction in transfection efficiency was attributed to the low cellular uptake of PEGylated-βCDP-DNA nanoparticles[368]. The authors also observed that PEGylated nanoparticles were small, discreet and smooth-edged. They suggested that such smooth particles would cause less physical damage to the endosomal compartment which can in turn diminish endosomal escape[368].

Taken together, PEG at the surface of polyamidoamine nanoparticles used in this study, did not alter the existing primary amines and hence it could be concluded that the use of PEGylated copolymer in the PAA-miRNA formulation may not altering the endosomal escape mechanism. Also, it should be noted that, if PEGylation is performed at the surface of homopolymer-miRNA complex using a thiol or maleimide chemistry, this will not affect the endosomal behaviour of these nanoparticles. But, PEGylation would affect the *in vitro* cellular uptake and hence impede with functional activity.

6.2.3 Importance of PEG and *in vivo* delivery

PEG is important for storage, stability and *in vivo* tissue penetration. The need for PEG in the effective bio-distribution of PEGylated nanoparticles has been extensively studied for systemic delivery which aims at prolonging circulation time by avoiding non-specific uptake by phagocytic cells.

The presence of PEG shields the surface charge of the nanoparticles and reduce the adsorption of proteins like opsonins thereby delaying the clearance by reticulo-endothelial system (RES)[220]. Hence, PEGylation is desirable for systemic *in vivo* delivery of nanoparticles. Longer circulation time ensures increased accumulation of nanoparticles in the tumour site[220]. The optimal molecular weight of PEG was determined as 2000 – 5000 Da for poly(lactic acid) (PLA) nanoparticles[220,363]. The optimal PEG density to avoid adsorption of serum proteins was found to be between 0.5 – 5 wt.% for PLA nanoparticles[363]. Above 5 wt.%, there was no improvement in the nanoparticle behaviour on protein interaction[363]. PEG2000 is widely used for different nanoparticle preparations[369]. The optimal amount of PEG2000 density was determined as 5 – 10 mol% when using ligand-targeted lipid nanoparticles[369]. More than 10 mol% PEG substantially interfered with the ligand-receptor interaction[369].

The nanoparticles ability to avoid protein adsorption ultimately depends on the density of PEG chains. Higher molecular weight PEG chains require relatively lower PEG attachment density for total coverage of the nanoparticle surface[370]. Hence, it is possible to achieve the same amount of stealth property when using a low molecular weight PEG chain at higher density[370]. PEG exists in mushroom or brush-like conformation depending on the density and molecular weight. At lower PEG density, when there is no steric interference from the adjacent PEG chains, the PEG exists in a relaxed mushroom confirmation. As the PEG density increases, the mushroom-form progressively transitions to a brush-like confirmation. At high PEG densities, the brush conformation of PEG is less mobile and hence efficiently shields the nanoparticle surface from protein adsorption[370].

6.2.4 Role of PEG in local delivery

As the ultimate aim of this work is to develop miRNA nanoparticle for loco-regional delivery, the role of PEG in local delivery is addressed in this section. Presence of dense PEG layer on the nanoparticle surface have shown to be advantageous in loco-regional brain and trans-mucosal delivery[371].

Dense grafting of PEG (2 – 40 kDa) at the nanoparticle surface reduces mucus-nanoparticle-surface interaction and muco-adhesion of PEG chains. This facilitates rapid muco-penetration of PEGylated nanoparticles[371,372]. This property has been exploited in the nanoparticle mediated drug and gene delivery across several mucosal barriers including ocular, nasal, pulmonary, gastrointestinal, colorectal[372] and cervico-vaginal mucosa[371].

Apart from stealth properties, PEG was also used to increase the solubility of hydrophobic polymer-gels [Oncogel, paclitaxel loaded PLGA-PEG-PLGA] or as a temperature sensitive liquefying agent in Paclimer microspheres [paclitaxel-loaded (10% wt./wt.) polyphosphoester particles][373].

6.2.5 Role of PEG in brain delivery

Dense PEG coating facilitates rapid penetration of nanoparticles through the brain tissue, while uncoated nanoparticles become entrapped in the extra-cellular matrix (ECM) of the brain[371,374]. The pores in brain ECM (~25%) can allow the diffusion of nanoparticles ≥ 100 nm[371]. As more than 75% of the pores are less than 100 nm, smaller nanoparticles (< 100 nm) with dense PEG coating would have higher chance of brain penetration. Densely PEGylated Paclitaxel-loaded PLGA nanoparticles (70 nm) showed enhanced diffusion and drug-distribution in rat brain[374]. Similarly, PEGylated poly(β-amino ester) nanoparticles[375] (50 nm) and highly PEGylated polyethylenimine (PEI/PEI-PEG) nanoparticles[376] (43 nm) were able to successfully deliver DNA in the brain following convection-enhanced delivery (CED)[371].

In the case of PAA-miRNA nanoparticles, as the *in vitro* cellular uptake seems to be compromised due to the presence of PEG, the uptake can be enhanced by preparing nanoparticles with lower PEG density or no PEG on its surface. But the reduction or elimination of PEG might lead to confinement of the nanoparticles at the site of injection. This might be interesting for intra-tumoral injections to achieve high concentration of miRNA delivery at the tumour site and to reduce nanoparticle toxicity in other regions of brain. If extensive diffusion is required along with high cellular uptake, then the nanoparticle surface can be attached with ligands (specific or non-specific). Also, copolymers with shorter PEG chains (e.g. 600 Da) can be used.

6.3 Targeted Delivery

Targeted delivery is the use of cellular uptake enhancing ligand, where the ligand is supposed to be selective for certain types of cells [e.g. cancer cells]. Biotin (Vitamin B7) is an essential micronutrient that is not produced by human cells. The uptake of biotin is facilitated by Sodium Dependent Multivitamin Transporter (SMVT) or SLC5A6 (Solute Carrier Family 5 member 6). The biotin-transporter is expressed by a wide-range of cells while over-expressed by several cancer cells. Enhanced cellular uptake was observed in biotin-conjugated drugs and nanoparticles in human cervical (HeLa)[377], ovarian (OVCAR-3, SKOV-3)[378] and breast cancer cell lines (T47D)[379] when they were compared with non-cancerous cell lines[380,381]. Although U87MG cells are known to express SLC5A6 gene at RNA level (24 TPM, Transcripts per Kilobase Million; TPM = 1 is the threshold for protein expression according to the Human Protein Atlas, http://www.proteinatlas.org/ENSG00000138074-SLC5A6/cell#human), biotin-mediated targeting of U87MG cells has not been explored before. It could be speculated that biotin can either act as a targeting agent or a non-specific uptake enhancer depending on the relative expression of the receptor on the tumour and normal brain tissue. Also, biotin-avidin conjugation can be used for the attachment of a specific secondary ligand imparting the targeting capability. In the last chapter of the thesis (Chapter V), biotinylated nanoparticles were prepared by thiol-maleimide chemistry and tested on U87MG cells. The *in vitro* uptake was improved by the addition of biotin ligand as indicated by the geometric-mean fluorescence intensity (GFI) between the biotinylated and non-biotinylated nanoparticles, 6.3 Vs 2.6 ($p = 0.0072$). Further optimization is needed for the preparation of reproducible, stable biotinylated PAA-miRNA nanoparticles. But, this preliminary result suggests that the uptake of PAA-miRNA nanoparticles can be improved by ligand targeting. This might also increase the gene-knockdown efficiency.

In this work, biotin was directly attached to the surface of nanoparticles (post-complexation). This approach can be advantageous when using a non-PEGylated nanoparticles which consists of homopolymer alone [e.g. HP:HPR or HP(R)100%]. When the biotinylation is performed on the surface of

PEGylated nanoparticles [HP: CP(R)], the receptor targeting might be hindered by the depth of the PEG layer which can hide the ligand and the steric properties of the PEG layer which can make it difficult for the NP to approach cell surfaces.

Klibanov *et al.* reported that the biotin-streptavidin interaction was abolished when the biotinylated liposome was grafted with PEG5000 even at very low PEG density (0.72 mol%, mushroom conformation[369])[382]. It was claimed that PEG5000 created a steric barrier between the liposomal surface and external environment, similar to the PEG stealth effect preventing the binding of serum proteins on cellular surface[382]. Salvati *et al.* reported that even the protein corona forming at the surface of the nanoparticles can have similar shielding effect on the surface functionalized ligands[383]. The accessibility of biotin grafted on to the nanoparticle surface can be tested by the streptavidin-mediated nanoparticle aggregation assay by simple turbidity measurement[382].

Alternatively, the ligand can be grafted with a PEG linker (Biotin-PEG2000-Maleimide/SH). The ligand at the distal end of PEG chain might enable easier access of biotin to the cell surface receptors and hence improve uptake.

Parkhouse *et al.* had tested this strategy by attaching a RGD containing peptide to the distal end of PEG chains of the PAA copolymer (RGD-PEG-PAA-PEG-RGD)[384]. RGD peptide grafting was performed either before or after the complex formation. Grafting the ligand post-complexation produced smaller and discreet nanoparticles. The non-crosslinked DNA-copolymer complexes showed slightly higher uptake, but with no improvements in the luciferase expression[384]. These results suggest that the uptake can be improved by attaching the ligand at the distal end of the PEG chains.

The ratio between the biotinylated-PEG and non-biotinylated PEG in a nanoparticle can affect the cellular uptake, (1) Ligand-receptor interaction could be inhibited by the shielding effect of PEG as described by Hak *et al*[369]; (2) At high density PEG grafting, less mobile brush confirmation might reduce the shielding effect of PEG on the ligand grafted at the distal end of PEG; (3) Higher ligand density would increase the cellular uptake when the ligands are accessible

by the receptor as described by Moradi *et al*[385]. The effect of PEG and nature of ligand grafting on expected cellular uptake is presented **Figure 6-1** (page: 206).

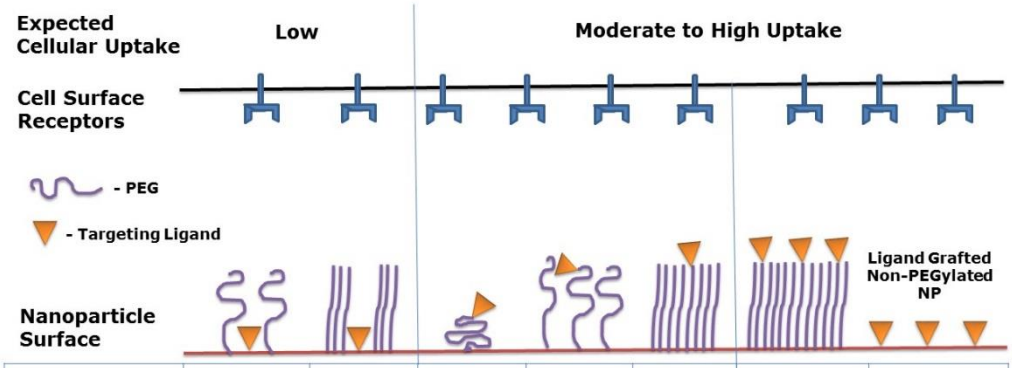

PEG Density	Low/Medium	High	Low	Medium	High	High	No PEG
PEG conformation	Mushroom	Brush	Mushroom		Brush	Brush	No PEG
Ligand Density	Low/ Medium/ High		Low	Low	Low	High	High
Ligand Position	NP surface		Distal end of PEG				NP surface

Figure 6-1: Factors affecting cellular uptake.
Effect of PEG density and nature of ligand grafting on cellular uptake.

Hak *et al*. reported that high PEG density reduces ligand targeting ability[369]. They showed that using PEG at low density (5 – 10 mol%) was able to achieve higher targeting efficiency[369]. At higher PEG densities the uptake was reduced significantly for both targeted and non-targeted nanoparticles. This inverse correlation between PEG density and uptake could be applicable only for the specific experimental set-up they had used. They studied lipid nanoparticles grafted with varying density of DSPE-PEG2000 [5 - 50 mol%] where 2.5 mol% was replaced with DSPE-PEG2000-Maleimide conjugated with a targeting ligand [cyclic RGD with activated thiol]. This study suggested that the higher density of PEG (>10 mol%) affected the ligand-receptor interaction by PEG's shielding effect on the ligand. However, if higher density of ligands (> 2.5 mol%) were used, the density of PEG would not have affected the uptake of targeted lipid nanoparticles. It is known that increasing ligand density can not only increase cellular uptake but also affects the mode of endocytosis[385]. Hence, increasing biotin grafting can improve cellular uptake of PAA-miRNA nanoparticles.

DSPE-PEG2000 = 1,2-distearoyl-sn-glycero-3-phosphoethanolamine-N-[methoxy(polyethyleneglycol)-2000]; **RGD** = L-arginine, glycine, and L-aspartic acid.

6.4 Functional Activity of Nanoparticles

Uptake of nanoparticles must be followed by the release of miRNA into the cytoplasm to have the gene-silencing activity (functional effect). The luciferase knock-down efficiency indicates the functional activity of the nanoparticles. In order to evaluate the efficiency of nucleic acid delivery of the crosslinked nanoparticles, siRNA-Luc was used instead of miRNA-128. The reason for using siRNA instead of miRNA for gene-knock down assay is discussed in the following section (6.5, page: 210).

6.4.1 Luciferase Assay and New Normalization Technique

The identification of a successful miRNA delivery system depends on the nanoparticle screening assay. Hence, a sensitive luciferase reporter assay and normalization technique was developed (Annexure I) using live cells. The new normalization technique was based on relative cell number calculated from resazurin (ALU/RCN). This can be used as an alternative to traditional protein based luminescence normalization (ALU/mg of protein). This technique is robust, sensitive, cost-effective, and quick to process multiple samples.

Although this technique was tested for a Luciferase-OFF system, it can also be used as a normalization technique for luciferase-ON systems. Luciferase-ON systems have a bacterial repressor controlling the transcriptional activity of the luciferase gene. The siRNA or miRNA targeting sequence is introduced on the 3′-UTR of the repressor gene. Hence, in the presence of targeted siRNA/ miRNA, the down-regulation of the repressor gene rescues the luciferase expression[386].

For dual-luciferase reporter systems, several variations of cost-effective luciferase assay buffers have been developed (for lysis method) which measures luminescence from two different luminescence enzymes, Firefly and *Renilla* luciferase [$RLU_{Firefly}$ / $RLU_{\textit{Renilla}}$][387,388]. For single luciferase reporter systems, normalization with total protein ($ALU_{Firefly}$/ mg of protein)[387] is the most widely used technique, although many other alternatives have been reported, like normalization with biological response ($ALU_{Firefly}$ / Concentration of interferon)[389], ratio of response between target and non-target siRNAs ($RLU_{Target\text{-}siR}$ / $RLU_{Non\text{-}target\text{-}siR}$)$_{Firefly}$[390], ratio of the amount of secreted luciferase

before and after treatment ($RLU_{0\text{-}15\ hours\ after\ treatment}$ / $RLU_{0\text{-}6\ hours\ before\ treatment}$)[391] etc.,. Due to the low sensitivity of the protein assay, it is important to have high cell number to obtain detectable amount of protein in the cell lysate and hence necessitate to be performed in larger assay formats (6 or 24 well plate). These large assay formats also limit the number of samples and replicates that can be performed. Also, the preparation of the cell lysate is a laborious and time-consuming process that are not convenient to be performed for medium and high-throughput formats. Due to these limitations, protein-based normalization is less suited for 96-well plate applications. If they are used in 96-well format, and when there are very few of cells due to low density seeding or nanoparticle toxicity, the sensitivity of protein detection is diminished and hence might report false positive gene-knockdown due to insufficient compensation. A similar disadvantage of protein based data normalization has been reported in the Promega's technical note to emphasize the importance of using dual-luciferase assays[392]. Tran *et la. (2015)* reported the NF-κB activity normalized to cell viability measured by Cell Tracker Green[393]. The new luciferase normalization technique developed in this work with resazurin is similar to the NF-κB normalization reported by Tran *et al*.

6.4.2 Knock-down efficiency of Nanoparticles

The PAA-siRNA-Luc nanoparticles [HP: CP2k(R) 50:50 RU/Nt 5:1] were able to knock-down luciferase expression by 50% only at high concentration of siRNA (500 nM), whereas the commercial reagent N-TER was able to knock-down more than 90% of luciferase at the optimal concentration (50 nM). The PAA-siRNA complex was slightly more toxic than N-TER nanoparticles (81 ± 18 vs 97 ± 15, $p = 0.1002$, not significantly different).

Commercial transfection reagents that are optimized for *in vitro* siRNA delivery generally work in the concentration range of 10 – 50 nM siRNA concentration [e.g. Peptide based N-TER (Sigma), Liposome based Lipofectamine® RNAiMAX (Life Technologies), Polymer based INTERFERin®-HTS (Polyplus Transfection)].

Polyethylenimine (PEI) is a synthetic cationic polymer used as a gold standard for DNA transfection. Although all forms of PEI are able to form complexes

with siRNA, it has been reported that only certain forms of PEI are capable of efficiently delivering siRNA [e.g. linear 22 kDa jetPEI® (Polyplus-Transfection), branched 10 kDa PEI obtained from gel-filtration chromatography of 25kDa PEI[394]. These two unmodified forms of PEI have relatively low toxicity and exhibit a working range of 50 - 100 nM. Several chemical modifications have been made on PEI to increase the efficacy and reduce toxicity. For example, pyridylthiourea-grafted polyethylenimine was effective at 10 nM siRNA concentration due to the enhanced buffering capacity and hydrophobic nature of the pyridylthiourea-group[395]. Similarly, imidazole-grafted-PEI showed slightly better knock-down efficiency than commercial transfection reagent (50 – 100 nM siRNA concentrations)[396]. Imidazole-grafting increased the endosomal escape and partially converted primary and secondary amines to secondary and tertiary amines, hence reducing the toxicity[396]. Chitosan-siRNA nanoparticles also work in the similar range of siRNA concentration (50 – 125 nM)[397].

Hence, it can be generalized that the siRNA concentration widely used in literature is between 10 – 150 nM. The PAA-miRNA nanoparticles require 500 nM to show some gene-knockdown activity. This requirement for high siRNA concentration is due to the moderate *in vitro* uptake of nanoparticles. Improvements in cellular uptake might enhance the knockdown efficiency of these PAA-miRNA nanoparticles. As the 3D-cellular uptake assay showed better uptake compared to 2D-cell culture, it is possible that these crosslinked PAA-miRNA nanoparticles have better cellular uptake and transfection efficiency in an *in vivo* settings without further modification, but this requires experimental validation.

Improvements in the Formulation: The major limitation of the current nanoparticle system is the poor *in vitro* uptake and subsequent low transfection efficiency. The *in vitro* cellular uptake and *in vivo* cancer cell targeting can be enhanced by the use of targeting ligand on the nanoparticle surface. The choice of the ligand would depend on the targeting organ and cell type. Another major hurdle for most of the nucleic acid delivery systems is the endosomal escape[195,398] and subsequent release of RNAi molecules in the cytoplasm. The

endosomal escape can be increased by incorporating few imidazole repeating units (e.g. Histidine) to enhance buffering capacity and proton-sponge effect of the polymers[396,398]. In order to enhance the release of the nucleic acid cargo the polymer-backbone can be modified to have acid-liable or bioreducible intra-molecular bonds[241,279].

6.5 MicroRNA or siRNA – Which is Better?

MicroRNAs are naturally occurring transcription-regulating RNAi molecules (~23-nucleotides). They recognise 3′-UTR of target gene's mRNA by complementary strand base-paring (6 – 8 seed-sequence). Due to the short sequence required for target recognition, a single microRNA is able to target multiple genes.

The screening of new miRNA delivery systems is usually performed with a luciferase expressing cell. The 3′-UTR of the luciferase gene is modified to carry a miRNA-targeting sequence. Under this condition, the down-regulation of the luciferase gene is diluted by the presence of competing endogenous target genes for the transfected miRNA[167]. This reduces the sensitivity of the luciferase knockdown assay. When the sensitivity of the assay is low, it is possible to not identify some formulations that may work well upon optimization. Also, therapeutic miRNAs inhibit tumour growth or even cause cell death. It would be difficult to isolate the cytotoxicity of the therapeutic miRNA from the cytotoxic effects of the delivery system without careful experimental design and proper controls.

In order to increase the sensitivity of the luciferase knockdown assay, siRNA could be used instead of miRNA. As the siRNA can be designed to target only the luciferase gene and with minimal off target effects, the siRNA-mediated luciferase knockdown would be more potent and this will increase the sensitivity of the screening assay. As siRNA and miRNA are chemically identical, the formulation optimized using an siRNA should also be able to complex with a miRNA and exhibit biological activity. Hence, siRNA makes a better option for the screening step of different delivery systems.

miRNAs are able to inhibit a network of genes involved in related function and this property makes it an attractive option for cancer therapy. Inhibiting a single gene with siRNA is synonymous to using a small molecule drug targeted against a single gene product. It might be a good strategy for targeting cancers which depend on one survival protein like BCR-ABL (exceptional cases)[70]. In general, cancer is a disease involving multiple gene aberrations and several resistance factors. The chances of building resistance against a siRNA is much higher compared to multi-targeted miRNA due to redundancy in biological pathways, cellular adaptation and changes in micro-environment. Cancer cells can also develop resistance to miRNAs by highly expressing miRNA-sequestering miRNA sponges [competitive endogenous RNA (ceRNA)[167]]. However, in order to achieve discernible miRNA-inhibition, the decoy-target sites from ceRNAs must be at least the same concentration as the total mRNA-3′-UTR target sites[167]. Usually, the cellular mRNA pool is several fold-larger than the concentration of ceRNAs[167]. Hence, ceRNAs can only affect the miRNAs that have low cellular abundance. If the nanoparticle delivery system is able to deliver miRNAs in high abundance, ceRNAs would be a less of a problem.

6.6 Conclusion - Clinical and Future Perspectives

PAA-siRNA/miRNA nanoparticles have great advantage to develop into efficient nucleic acid delivery systems due to the presence of thiol in the polymeric backbone. These thiols allow crosslinking between the polymeric chains which increased nanoparticle stability in physiological medium, which in turn would allow these nanoparticles to survive under harsh *in vivo* conditions which is lacking in the non-crosslinked systems. The bioreducible properties should allow the selective release of nucleic acid in the intracellular environment (cytoplasm) and hence be useful for *in vivo* siRNA or miRNA delivery. The thiols also allow easy modification and attachment of several functionalities on the nanoparticle surface [e.g. PEG chains and Ligands]. These modifications can be performed either before or after the formation of nanoparticles. Addition of an appropriate ligand can improve the *in vitro* uptake and *in vivo* targeting. The endosomal escape can be enhanced by the inclusion of imidazole containing repeating units in the polymer backbone[396,398]. Alternatively, use of lysosomally detachable PEG[367] or membrane disrupting peptides[399] may also enhance endosomal escape. Use of biodegradable PEG alternatives [e.g. Glycosylation[400] or Peptide-grafting[401]] might improve the biocompatibility and biodegradability of these nanoparticles. Inclusion of bioreducible intra-molecular bonds might improve the release of the cargo in the cytoplasm following endosomal escape[275]. Due to the disulphide mediated nanoparticle stabilization, the components self-assemble into nanoparticles with little excess free polymer or nucleic acid. The miRNA or siRNA loading into the nanoparticles is also high (~15 wt.% for RU/Nt ratio 5:1). It is also possible to load these nanoparticles with different forms of nucleic acids like plasmid DNA, oligonucleotides[245], locked nucleic acids etc. It is also easy to vary the amount of PEG at the surface of nanoparticles by simply varying the homopolymer to copolymer ratio. High density PEG would allow the nanoparticles to easily penetrate brain tissue and mucosal barriers[371,374]. PEG also inhibits aggregation of nanoparticles when in contact with serum proteins. Thiolated-chemotherapeutic drugs[402] can also be co-delivered along with the nucleic acids. The reducing property of thiols on these polymers can be used to synthesize metallic nanoparticles [e.g. gold nanoparticles][403,404]. The resulting metallic nanoparticles would be stabilized

and coated[405] with these polymers and hence can be used as a hybrid-delivery system[406] for nucleic acid and drugs[202]. Also, the PAA-miRNA nanoparticles can be delivered like an implant with bio-degradable PLGA capsules for sustained release of the nanoparticles [2 – 5 months][231].

Taken together, PAA-miRNA nanoparticles have the potential to become versatile nucleic acid and drug delivery system with possible clinical translation.

Appendix – I

Development of Normalization Technique for Live Cell Luciferase Reporter Assay with High Throughput Compatibility

7 Appendix I: Development of Normalization Technique for Live Cell Luciferase Assay with High Throughput Compatibility

7.1 Introduction

Luciferase assay serves as a valuable tool for multiple applications including evaluation of transfection efficiency of siRNA/ miRNA loaded nanoparticles. Though the measurement of luciferase activity has become a simple, efficient and quick process, the correct interpretation of the data depends on the use of suitable normalization technique, as the reduction in luciferase signal can occur either due to successful RNAi delivery or cytotoxicity of the nanoparticles. Several different normalization techniques have been proposed for transfection assays. The most commonly used normalization techniques include traditional protein based luciferase assay (RLU/ mg of protein) or the more recent dual-luciferase reporter assays ($RLU_{Firefly}$ / $RLU_{Renilla}$). Although protein estimation from cell lysates is suitable for experiments with small numbers of samples, it is a laborious and expensive technique not suitable for high-throughput applications or experiments involving large numbers of samples. Dual-luciferase reporter (DLR) assays are HTS compatible, but they do not provide any solution for cell assays using a stably transfected single luciferase reporter system. Relative cell number (RCN) can be used as a suitable alternative for total protein or secondary reference reporter luminescence (DLR). RCN can not only act as a robust normalization tool, but also provides valuable information about the cytotoxicity of the tested formulations. In this chapter, we explore the usability and devise standard calculation methods for resazurin based normalization of luminescence (RLU/RCN) with a special focus on luciferase gene silencing.

7.1.1 Reporter Gene Assays

Reporter gene assays were developed to study the activity of promotors[407], monitoring transcriptional response, transfection efficiency and many more parameters. The reporter genes are unique enzymes [Chloramphenicol Acetyl Transferase[407], β-Galactosidase[408], β-Lactamase[409], Alkaline Phosphatase, Aequorin, Luciferases[409]] or other proteins [Green Fluorescent Proteins[409,410]] that can be easily detectable with no or minimal interference from endogenous gene products[407,411]. Due to very high sensitivity, broad linearity, non-destructive mode of detection, increasing availability of detectors and glow-type luminescence, firefly luciferase reporters have widely been used for several *in vitro* and *in vivo* applications[409,412]. Moreover, the half-life of wild-type firefly-luciferase is short (2 – 3.68 hours[413,414]) compared to eGFP (26 hours[415]) which results in quick responsiveness to treatments and hence luciferase reporters are preferred over GFP reporters in gene induction and silencing studies[412,416]. The luciferase reporters can be broadly classified as single or dual luciferase reporters based on the number of luciferase genes encoded, while they can also be classified based on the mode of action as 'ON' and 'OFF' systems. In the presence of a specific RNAi molecule, 'ON' systems express high levels of luciferase, whereas 'OFF' systems switch OFF (reduce) constitutive luciferase gene expression. This chapter will focus on normalization techniques for cells stably expressing a single luciferase gene modified to respond to a specific RNAi molecule ('OFF' systems). However, the same principles might apply to 'ON' systems as well.

7.1.2 Quantification of Bioluminescence

Luciferases are enzymes that produce light (bioluminescence) in the presence of its substrate and co-factors. The light produced can either be of a flash emission or glow emission type. Flash emissions are very bright but only last for few seconds, while the glow emission emit luminescence for a prolonged period of time. Firefly luciferase (FLuc or Luc) is a glow type enzyme that can produce detectable luminescence for more than two hours both *in vivo* and *in vitro*[413] under appropriate conditions. FLuc converts its D-luciferin substrate into an energetically excited oxy-luciferin in the presence of ATP, oxygen and Mg^{2+} ions. Oxy-luciferin decays to produce green light (~ 530 nm)[409,417].

The bioluminescence can be quantified using ultra-sensitive photomultiplier tubes (e.g. Plate Readers) or CCD imaging cameras (e.g. *In vivo* imaging systems, IVIS). The luciferase assay can be performed in one of two formats, lysis or live cell format. IVIS system is versatile for the quantification of bioluminescence from both lysis and live cell methods. Modern plate readers with luminescence detectors offer end-point and well scan modes of detection (e.g. BMG Labtech: CLARIOstar, FLUOstar). End-point mode collects the luminescence signal either from centre of the well (one spot) or a few spots around the centre (orbital averaging). This mode is suitable for the measurement of homogeneous samples obtained by a lysis method. Well scan mode, similar to bioluminescence imaging, measures the light from the whole area of the well and it is especially suitable for non-homogeneously distributed live cell bioluminescence measurements.

7.1.3 Factors Influencing Luciferase Signal

Transfection, in a broader sense, is the process of delivering external nucleic acid cargoes [pDNA, ODNs, siRNA, miRNA, LNA, mRNA etc.,] into cells. In the screening of plasmid DNA delivery systems, transfection efficiency is measured as the increase in luciferase signal (luminescence). The amount of luminescence produced is directly proportional to the number of cells that express the delivered luciferase gene. Hence, by knowing the total number of cells alive and total luminescence, we can compare the transfection efficiency of different nanoparticles as theoretically described in 7.1.6, page: 220. As the number of cells is directly proportional to the amount of protein obtained from the cell lysate, amount of protein was traditionally used as a proxy for the cell number for data normalization.

In case of RNAi delivery, the transfection efficiency is measured as the decrease in luminescence signal from the cells that constantly express the luciferase gene. As the luminescence is directly proportional to the number of cells, cellular responses like cell proliferation and cell death can affect the amount of luminescence produced along with the knockdown activity of the transfected RNAi molecule, **Table 7-1**, page: 217. Hence, to obtain meaningful interpretations from the luminescence signal, it is important separate these events from one another through data normalization[392].

Table 7-1: Factor affecting the luminescence signal.

A comparative chart between pDNA and RNAi delivery.

Delivery →	**pDNA**	**siRNA or miRNA**
Nature of Cell Line	Cells without luciferase gene	Cells constantly expressing luciferase gene
Successful delivery =	Increase in Luminescence	Decrease in Luminescence
Possible factors that could increase luminescence	**Transfection efficiency of delivery system**	Increase in proliferation from siRNA[418] or miRNA[419,420] treatment
		miRNA mediated gene up-regulation[421]
		Variation in seeding density (pipetting error)
Possible factors that could decrease luminescence	Cytotoxicity from delivery system	Unexpected activation or suppression of reporter gene expression
		Transfection efficiency of delivery system + Knock-down efficiency of RNAi molecule
		Cytotoxicity of delivery system
		Decrease in proliferation from siRNA[422] or miRNA[423] treatment

7.1.4 Data Normalization in Transfection Assays

Data normalization is a powerful technique to obtain more detailed and accurate interpretations by cancelling out several disturbances occurring in an assay system[392]. This would require multiple or sequential normalization to extract the useful information from the assay[392]. Selection of inappropriate or less sensitive normalization technique can drastically affect the interpretations. This has been emphasised by several researchers and led to the development of various normalization techniques for luciferase assay, which include but are not limited to the following techniques.

Dual reporter assays are the widely used normalization technique for transient transfection assays but can also be used in stable expression systems. The test reporter signal, usually Firefly luciferase, is normalized against a reference reporter like β-galactosidase[424], *Renilla* luciferase[387,409] or eGFP[425-427] ($RLU_{Firefly}$ / $Response_{Ref.gene}$).

The importance of sequential data normalization was demonstrated by Campos-Melo *et al.* who used three step data normalization to decipher the gene-upregulation activity of miRNA which were not identified by normal data normalization technique[421]. The work aimed to isolate the effect of exogenous miRNA on the expression of firefly luciferase gene 3′-UTR bearing the miRNA binding sequence. The first step in normalization was made to get rid of differences in transfection efficiency and cell number, TransNorm (TN) = ($RLU_{Firefly}$ / $RLU_{Renilla}$). The second normalization was to cancel out the effect of endogenous miRNA on the firefly luciferase expression, EndoNorm (EN) = $(TN)^{\text{with miR mimics transfection}}$ / $(TN)^{\text{with no transfection}}$. The final normalization was to eliminate the effect of miRNA on the coding region to obtain the specific effect of miRNA on the 3′-UTR, ($EN_{\mathbf{Luc + 3'\text{-}UTR}}$ / $EN_{\mathbf{Luc}}$). EN_{Luc} is from the cells that have a luciferase reporter without the 3′-UTR specific to the miRNA.

Single reporter assays are widely used with stably transfected luciferase expressing cells due to simplicity and the several pitfalls associated with DLR assays, see 7.1.5. Most widely employed normalization is with total protein (RLU/ mg of protein)[387] (see 7.1.6) which corresponds to the number of cells. Similarly, fluorescence from nucleus ($RLU_{Firefly}$ / $RFU_{Genomic\ DNA}$) has also been employed to increase the sensitivity that is lacking with absorbance based protein estimation. To achieve greater sensitivity, *Renilla luciferase* was delivered as protein nanoparticles ($RLU_{Firefly\ from\ pDNA}$ / $RLU_{\textit{Renilla}\ from\ protein\ delivery}$)[408]. This method would be expensive and cannot be used to compare the data across cell lines, as the cell lines differ in their nanoparticle endocytic ability[428]. To overcome the endocytosis problem, the amount of plasmid transfected was determined by slot blot hybridization technique and used for normalization (RLU/ pg of plasmid DNA)[428]. This technique is laborious and uses autoradiography for detection of plasmid. Another method of single

luciferase gene normalization was performed by measuring a biological treatment in response to a treatment ($RLU_{Firefly}$ / Concentration of interferon)[389].

The luminescence from the supernatant collected before and after treatment was used for data normalization in a study that used a secreted form of luciferase ($RLU_{0\text{-}15\ hours\ after\ treatment}$ / $RLU_{0\text{-}6\ hours\ before\ treatment}$)[391].

A simple approach that can normalize the toxic effects of a nanoparticle delivery system is by treating the cells with a targeting siRNA and a non-targeting siRNA. The luminescence from the latter can be used to normalize the data ($RLU_{Target\ siR}$ / $RLU_{Non\text{-}target\ siR}$)$_{Firefly}$[390]. However, this technique cannot be applied if the target miRNA and control miRNA have different effects on the cell number, like RNAi sequence specific toxicity or proliferative effect.

Most of the normalization techniques are based on the direct or indirect representation of the cell number. For example, amount of protein, amount of *Renilla* luciferase expression in dual reporter assay, quantification of DNA content and cell viability using Cell Tracker Green[393], all these represent relative cell number and have been used for data normalization.

7.1.5 Dual Luciferase Reporter (DLR) Assay

Dual reporter assays were initially developed to normalize the differences in transient transfection efficiencies between experiments. It used two different reporter genes either in two different plasmids or within the same plasmid. One of the reporter genes would be modified to respond to certain molecules like miRNA or siRNA, while the other reporter gene expression is expected to be constant during the course of the experiment and hence would be used as an internal reference for normalization, ($RLU_{Test\ Reporter}$ / $RLU_{Reference\ Reporter}$)[425]. This technique is widely used as a screening and evaluation tool for novel DNA and RNA transfection reagents due to its increased sensitivity and accuracy[392].

However, there are some pit-falls associated with the use of two reporter systems. Expression of one reporter gene can be inhibited by the presence of the second plasmid in a dose dependent way due to the competition in the transcription factor binding[392,429]. To increase the sensitivity of the assay system, it is usually expected to have higher luminescence signal from the test reporter

(usually, Firefly luciferase) and a lower but conveniently detectable signal from the reference reporter (*Renilla* luciferase). This is usually achieved by transfecting the plasmids at different ratios. To obtain the required ratio of reporter expression, the ratio of plasmid required for transfection has to be empirically determined for each cell line and experimental set up[392,428]. Use of a single plasmid expressing two different reporters under two different promotors[430] could be a more convenient and accurate method compared to co-transfection protocol[421]. Careful choice of promotors and the effect of treatment on their transcription activity needs to be evaluated to avoid possible misinterpretations, especially when the treatment involves small molecule drugs[392,427,431-435]. The size of pDNA is also known to inversely affect the transfection efficiency[436] and transcriptional activity of the reporter gene[437].

Apart from biological factors, dual luciferase assays with transient transfection can be very expensive both from the cost of transfection reagent and commercial dual luciferase assay reagent[388]. Transient transfection of pDNA is generally associated with some levels of toxicity, while the co-transfection of RNAi molecules posse added toxicity on the treated cells. In certain cases, protein quantification cannot be performed with dual reporter assay due to incompatibility of protein assay reagent and dual luciferase lysis buffer[387].

7.1.6 Data Normalization with Total Protein

In case of plasmid DNA transfection, the untransformed cells do not have the reporter gene and hence do not show any luciferase activity (0 ALU @ 0% transfection). The percentage of cells that were transformed with luciferase gene cannot be determined as the amount of luminescence for 100% transformed cells cannot be predicted. However, when comparing the transfection efficiency of different nanoparticles for the same cell line, higher transfection efficiency yields higher luminescence in a linear fashion. The best performing nanoparticle formulations are normally chosen based on luminescence data normalized to amount of protein (RLU/ mg of protein) and the information about toxicity. Higher toxicity results in lower number of cell and hence lower amount of protein in the cell lysate.

To illustrate the process of normalization with protein. Taking a hypothetical condition where we have seeded 100 cells and treated them with 5 different pDNA-nanoparticles (A, B, C, D, E). Let us assume that the transfection efficiencies of all the nanoparticles are the same (40 %), but differ in the toxicity profile where A is non-toxic and E is highly toxic. If we assume that the un-transfected cells show no background luminescence and the amount of protein present in 100 cells equals 2.5 mg. Assuming that the sensitivity and linearity of the protein assay is 100%, we would be able to estimate the correct amount of protein in each sample. Also, we consider that successfully transfected cells would produce a signal of 1000 ALU/ cell.

Initial number of cells seeded = 100

Transfection efficiency, TE = 40 %

Table 7-2: Theoretical normalization of reporter gene expression.

Luminescence normalization with total protein and relative cell number (RCN).

NP	Toxicity TOX (%)	Cell Number (CN) or Number of Surviving cells, 100 – TOX = CN	Relative Cell Number RCN	Number of Luciferase positive cells CN x TE	Expected Luminescence CN x TE x 1000 ALU	Expected Total Protein 0.025 x CN mg	Normalized ALU (Arbitrary Luminescence Unit)	
							ALU/mg	ALU/ RCN
A	0	100	1.0	40	40,000	2.5	16,000	40,000
B	20	80	0.8	32	32,000	2.0	16,000	40,000
C	40	60	0.6	24	24,000	1.5	16,000	40,000
D	60	40	0.4	16	16,000	1.0	16,000	40,000
E	80	20	0.2	8	8,000	0.5	16,000	40,000

As luminescence produced from cells are known to be highly linear with cell number and the background (noise) is very low, hence the only deciding factor for accurate normalization depends on the sensitivity and accuracy of the protein estimation. Among the protein estimation techniques available, BCA (Bicinchoninic acid) and Bradford assay are widely used because of the ease and high sensitivity[438]. Similar results can be obtained by performing the normalization with relative cell number (RCN), **Table 7-2**, page: 227. RCN can be obtained using one of the many reagents used in cell viability measurements, MTT, MTS, Alamar blue (resazurin), lactate dehydrogenase, ATP, Cell Tracker Green[393], Picogreen and CyQuant assays[439].

7.2 Materials and Methods

7.2.1 Cell Culture

Stable cell lines of U87MG cell line expressing luciferase gene bearing a full length 3′-UTR from human Bmi1 was produced by lentiviral (LTV) transduction (Multiplicity of Infection, MOI = 1) and selection with Puromycin (1 µg/mL). The 3′-UTR from human Bmi1 (Length: 1943 nucleotides) contains target sequences for several miRNAs including miR-128, miR-302, miR-15, miR-16, miR-135a, miR-141, miR-203 and miR-320[440]. These cells were named as U87MG-LTV-Luc-3′UTR(Bmi1)-1MOI. For simplicity, these cell-lines will be referred as U87-Luc in this work.

7.2.2 Luciferase Assay

U87-Luc cells were seeded in a white-walled clear bottom 96-well plate (Grenier Bio). The number of cells were serially diluted (1/2) and seeded as 20000, 10000, 5000, 2500, 1250 and 625 cells per well. They were incubated overnight for attachment. StayBrite™ D-Luciferin sodium salt (MW: 302 g/mol, BioVision) was dissolved in 1x PBS to obtain the stock solution (15 mg/mL, 100x). The following day, the existing medium was replaced with DMEM with no phenol-red, supplemented with serum (10 vol.%) and D-Luciferin (0.15 mg/mL, ~500 µM, 1x)[441]. The luminescence was recorded within 20 minutes of the addition of the substrate in well-scanning mode (2 x 2 matrix), using the following settings: top optics, focal height (15 mm), temperature (37° C) and gain (3600). Background luminescence (D-luciferin medium with no cells) was subtracted from rest of the samples.

7.2.3 Estimation of Relative Cell Number (RCN) - Resazurin Assay

Background: Resazurin is a water soluble oxidized non-fluorescent blue dye which is reduced by living cells to form a red fluorescent compound resorufin which is freely soluble in aqueous medium and hence quantifiable by fluorescence measurement (Excitation: 544 nm; Emission: 590 nm)[442]. Resazurin is commercially available as Alamar Blue™ and widely used for cell proliferation and cytotoxicity assays[442,443].

Protocol: Resazurin stock solution (4400 µM, 100x) was prepared in 1x HBSS with calcium and magnesium ions. Following luciferase assay, the D-luciferin medium was replaced with DMEM with no phenol-red, supplemented with serum (10 vol.%) and resazurin (44 µM, 1x)[442,444]. The cells were incubated for 45 – 90 minutes and the fluorescence was recorded with a resorufin filter set [Excitation: 544 nm (545-20); Emission: 590 nm (600-40)]. The plate was gently [200 rpm, double orbital shaker] for 20 seconds before recording the fluorescence. The fluorescence was recorded using bottom optics, end-point mode; focal height and gain adjustments were performed for individual plates using the well with maximum fluorescence (20,000 cells/well) as the reference. Fluorescence from blank wells (resazurin medium with no cells) was subtracted from rest of the samples. The fluorescence from untreated cells or wells seeded with 20,000 cells was considered as 1 (100 % viability).

7.2.4 Total Protein Estimation - microBCA Assay

Background: The BCA assay is based on the reduction of copper salts [Cu^{2+} to Cu^{+}] under alkaline condition by certain amino acids [e.g. cysteine, tyrosine, and tryptophan] and the reducing capability of peptide bonds upon long exposure and higher temperature [2 hours at 37° C, or 1 hour at 60° C]. Reduced Cu^{+} reacts with Bicinchoninic acid (BCA) to produce an intense purple coloured complex (562 nm). The presence of reducing sugars [e.g. Glucose], reducing agents [DTT and thiols] and phospholipids interfere with measurements resulting in false-high values of protein, while copper-chelating agents produce false-low value of protein. Interference from DTT and other thiols can be overcome by pre-incubating the samples with 10 molar excess of iodoacetamide before the addition of BCA reagent[445]. Use of 2% SDS in the lysate prevents the interference from phospholipids[446].

Protocol: Following luciferase and resazurin assay, the medium was removed, the wells were washed with PBS (100 µL) and replaced with RIPA (Radio-immuno-precipitation assay) lysis buffer (100 µL). The composition of lysis buffer is as follows, Tris-Hcl, pH 8 (50 mM); NP-40 (1 wt.%); sodium deoxycholate (0.5 wt.%); sodium dodecyl sulphate (SDS, 0.1 wt.%); sodium chloride (NaCl, 150 mM); sodium fluoride (NaF, 50 mM);

Ethylenediaminetetraacetic acid (EDTA, 2 mM). After 20 min, the cells were scraped from the wells and collected in micro-centrifuge-tubes. They were vortexed for few seconds to facilitate complete lysis and centrifuged for 5 min at 3000 rpm to pellet the debris. The lysate was carefully transferred to a new tube and used for protein estimation. RIPA lysis buffer has to be diluted 1 in 10 ratios [10 vol.% RIPA Lysis Buffer] for the microBCA protein assay, however due to low protein concentrations, the cell lysate was diluted in Milli-Q water (1:5 ratio) and used for microBCA protein assay. To compensate the possible interference from lysis buffer, the standard solution was also prepared in RIPA lysis buffer [20 vol.%] to mimic the cell lysate for accurate quantification. The assay was performed in a 96-well transparent plate following the manufacturers protocol with small modifications using Pierce's Micro BCA™ Protein Assay Reagent Kit (Thermo-scientific, cat.no. 23235). Working solution of microBCA reagent was prepared by mixing Reagent A [sodium carbonate, sodium bicarbonate and sodium tartrate in 0.2 N, NaOH], Reagent B [4 wt.%, Bicinchoninic acid] and Reagent C [4 wt.%, cupric sulphate pentahydrate] at the ratio of 25:24:1. A series of BSA standard solutions, ranging from 1 to 200 µg/mL, were prepared in lysis buffer [20 vol.%] to mimic the conditions of the cell lysate. An equal volume of sample [75 µL, standard or diluted cell lysate] and microBCA reagent (75 µL) were added in each well. Each sample was prepared in duplicate. The plate was incubated at 37°C for 2 hours. The absorbance at 562 nm was measured with a CLARIOstar plate reader.

7.2.5 Statistics

Linear regression was performed for each dataset and the R-squared value for each dataset were calculated using GraphPad Prism 7.01 or Microsoft Excel 2016.

7.3 Results

7.3.1 Data Processing and Linearity

A decreasing number of U87-Luc cells were seeded as follows: 20000, 10000, 5000, 2500, 1250 and 625 cells per well. Following overnight incubation, the cells were treated with D-luciferin (0.15 mg/mL) supplemented medium and the luminescence was recorded [Arbitrary Luminescence Unit, ALU]. The raw data is presented in the top panel of **Figure 7-1**, page: 225. The D-luciferin medium was replaced with resazurin containing medium (44 µM) and incubated for 45 – 90 minutes for the reduction of resazurin to fluorescent resorufin which is released back into the medium. The fluorescence was recorded [Arbitrary Fluorescence Unit, AFU]. The cells were washed with PBS, the lysate was prepared and the protein concentration was estimated using microBCA assay. The absorbance was recorded at 562 nm. Three independent experiments (N = 3) were performed in triplicate (n = 3).

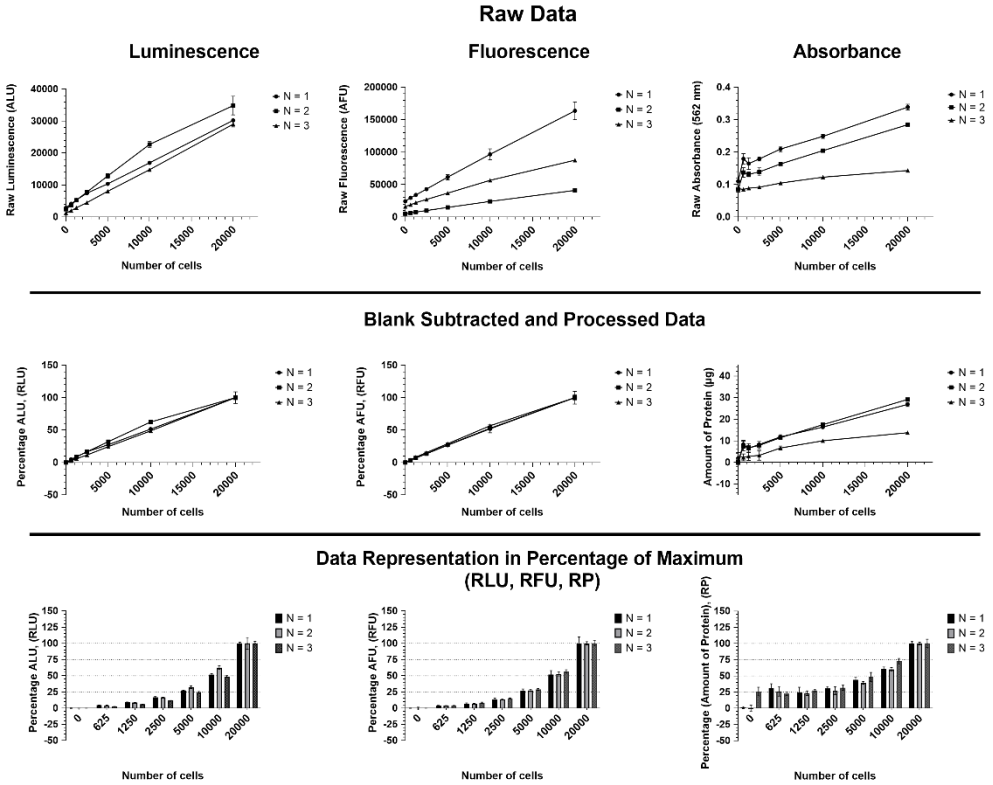

Figure 7-1: Luciferase reporter assay, step-wise data processing.
Top panel represents the raw data. **Middle panel** represents background subtracted and processed data. **Lower panel** represents the normalized data, expressed as the percentage of maximum in each group. **ALU** – Arbitrary Luminescence Unit; **RLU** – Relative Luminescence Unit; **RFL** – Relative Fluorescence Unit; **RP** – Relative Amount of Protein (w/w %). (N = 3, n = 3).

The background (blank) value was subtracted for all the samples. The luminescence and fluorescence from 20000 cells per well was assumed to be 100 %. The relative percentage luminescence and fluorescence were calculated using the mean luminescence and mean fluorescence from sample with 20000 cells/well, respectively. The relative percentages were expressed as RLU (Relative Luminescence Unit) and RFU (Relative Fluorescence Unit) in the middle panel of **Figure 7-1**, page: 225.

The amount of protein (µg) was calculated using a standard solution of Bovine Serum Albumin (BSA) with known protein concentration. The standard graph used for protein estimation is presented in the **Figure 7-4**, page: 228. The relative mass percentage of protein (RP) was obtained by assuming that the amount of protein obtained for the sample with 20000 cells/well as the 100%.

The bottom panel of **Figure 7-1** (page: 225) represents the relative quantity of measured luminescence (RLU), fluorescence (RFU) and protein (RP). This graph clearly indicates that luminescence and resazurin fluorescence decreased by 50% for each 50% decrease in the cell number throughout the tested conditions. This indicates the sensitivity of both fluorescence and luminescence methods. However, this trend was only visible at the two high cell counts (20000 and 10000 cells/well) for protein quantification. At low cell counts (from 625 to 2500 cells/well) the amount of protein quantified did not show any variation indicating that the protein assay is not sufficiently sensitive at low cell counts.

To test the linearity of the signal with respect to cell number, linear regression analysis was performed on the data, **Figure 7-2**, page: 227. This analysis fits the data in a straight line equation, $Y = m*X + C$; where X, Y are two variables, 'm' represents the slope and 'C' is the Y-intercept. This equation can be used to predict the unknown variable (e.g. X, number of cells) when information of the other data variable (e.g. Y - luminescence, fluorescence or amount of protein) is available. R-squared (r^2, from linear regression) is a measure of goodness of fit of the data with the best-fit line generated using regression analysis. An r^2 value of 1.00 would predict the unknown variable with 100% accuracy, while an r^2 value of 0 indicates a random association between the parameters. The linear regression analysis showed that all three parameters would be able to predict the

number of cells with varying degree of accuracy, RLU (r^2 = 0.9980), RFU (r^2 = 0.9985) and Amount of protein (r^2 = 0.9404).

Y	Equation (Y = m*X + C)	r^2
Amount of Protein	Y = 0.0009781*X + 4.456	**0.9404**
RLU	Y = 0.004998*X + 1.704	**0.9980**
RFU	Y = 0.005004*X + 1.373	**0.9985**

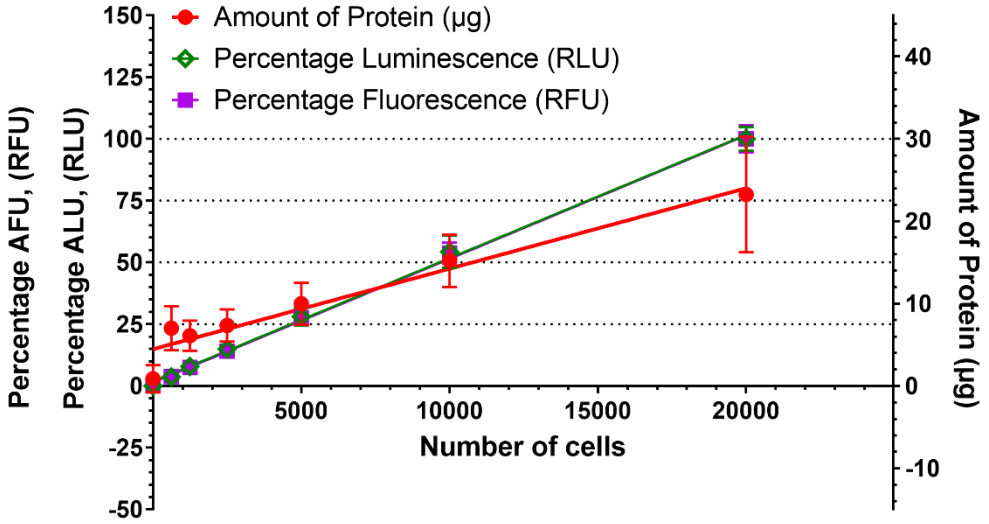

Figure 7-2: Comparison of Data Linearity with Linear Regression Analysis.

The mean and standard deviation of three experiments is represented (n = 9). R-squared values for each dataset are presented in the table presented above the graph.

It should be noted that, the best-fit line generated by linear regression analysis does not pass through the origin (X, Y = 0, 0) which is also indicated by the equations, where the y-intercept is not equal to 0 ($C \neq 0$). In fact, when there are no cells (cell number = 0), the background subtracted data points have 0 signal. Hence, the lines were constrained to pass through the origin (0,0) either using MS Excel 2016 or using non-linear regression (least-square fit, R^2) with straight line equation (Y = m*X) on GraphPad Prism 7.0, **Figure 7-3**, page:.228. R-squared values obtained from this analysis showed that luminescence (RLU, R^2 = 0.9864) and fluorescence (RFU, R^2 = 0.9912) were still able to predict the cell number with high accuracy, while the amount of protein (R^2 = 0.5618 by Prism 7.02 or r^2 = 0.6841 by MS Excel 2016) was not an accurate indicator of cell number. Although protein assay can quantify the amount of protein accurately from a pure protein solution [r^2 = 0.98, see BSA Standard Curve, **Figure 7-4**, page: 228] the amount of protein determined from the cell lysate did not reflect

the cell number accurately for the tested range, particularly when the cell count was less than 5000 cells.

Y	GraphPad Prism 7.01	
	Equation (Y = mX)	Non-Linear Regression, R^2
Amount of Protein	Y = 0.001296*X	0.5618
RLU	Y = 0.005123*X	0.9864
RFU	Y = 0.005105*X	0.9912
Y	MS Word 2016	
	Equation (Y = mX)	Linear Regression, r^2
Amount of Protein	Y = 0.0013*X	0.6841
RLU	Y = 0.0051*X	0.9965
RFU	Y = 0.0051*X	0.9976

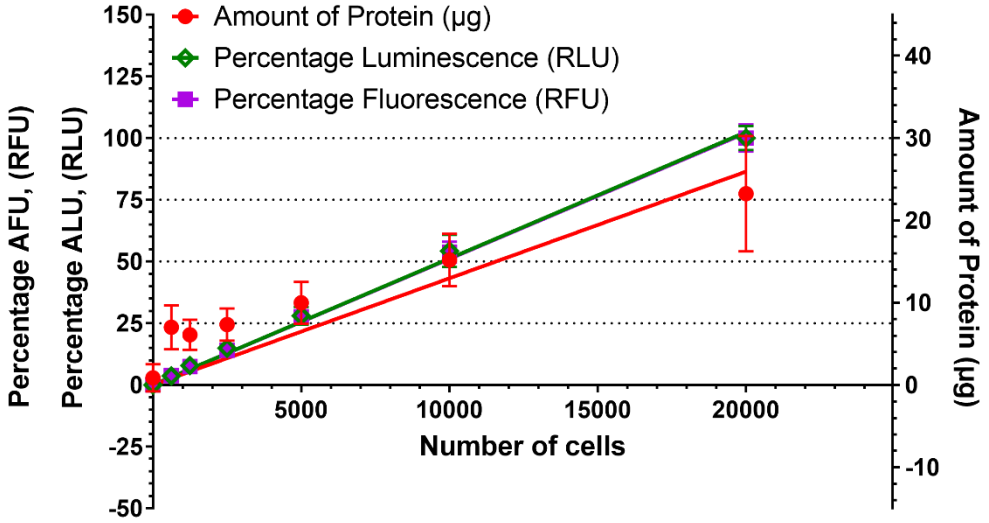

Figure 7-3: Data fitting with constraint: line passing through origin.
Data fitting technique: least-square fit with straight line equation, Y = slope.X.

Equation	R^2	
Y (Abs) = 0.004309 * (Protein Conc)	0.9883	N = 1
Y (Abs) = 0.003425 * (Protein Conc)	0.9894	N = 2
Y (Abs) = 0.002733 * (Protein Conc)	0.9798	N = 3

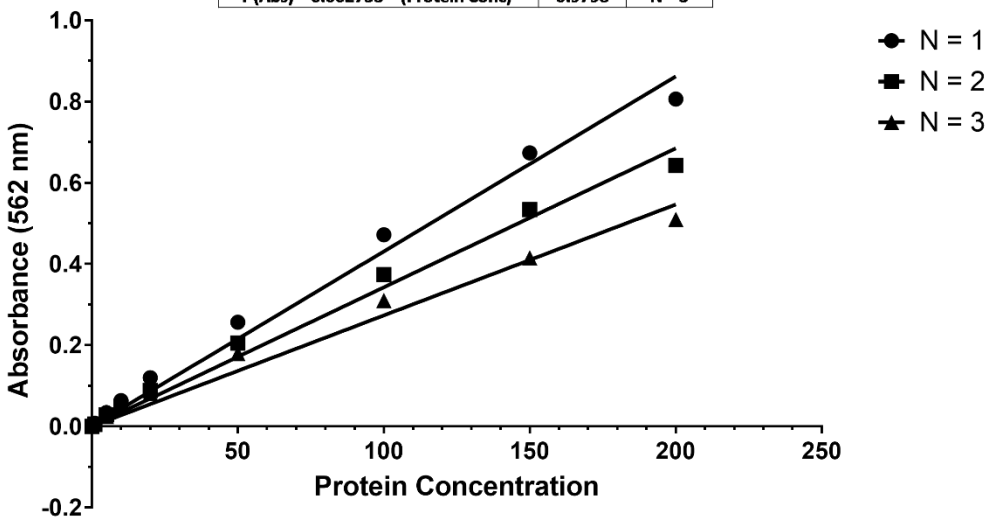

Figure 7-4: microBCA Standard Graph.

7.3.2 Normalization of Luminescence

The aim of luciferase normalization is to distinguish between a decrease in luminescence due to cell number mediated reduction from that due to a gene silencing effect caused by siRNA or microRNA. The first assumption that is made during any luciferase assay is that the luminescence is highly linear with cell number. In other words, each cell produces a constant amount of luciferase molecules, hence would produce constant amount of luminescence per cell irrespective of the number of cells seeded per well. Hence, ideally the ratio of luminescence (ALU) to cell number (CN) or relative cell number (RCN) should produce a horizontal line (slope, m = 0).

7.3.2.1 Cell number and Relative cell numbers are inter-changeable

It was assumed that the cells did not divide between seeding and luciferase assay (less than 24 hours) and hence the initial number of cells seeded were taken as the theoretical number of cells (cell number, CN-Theo) that is producing the luminescence. The ratio between the measured luminescence and cell number (ALU/CN-Theo) or luminescence and relative cell number (ALU/RCN-Theo) were plotted in **Figure 7-5** (page: 230). The figure shows that both ratios, luminescence of 1 cell (ALU/CN-Theo) or luminescence of 1% of cells (ALU/RCN-Theo), produced identical results. Luminescence produced by 1% of cells should be constant irrespective of the number of cells seeded, but the mean ratio varied between 1.4 to 1.8 (dotted lines in **Figure 7-5**) and reflected by a significant non-zero slope ($p = 0.0092$). This could be because the theoretical RCN does not reflect the exact number of cells that is actually present in the wells, which could be different due to small variations in cell counting and pipetting error.

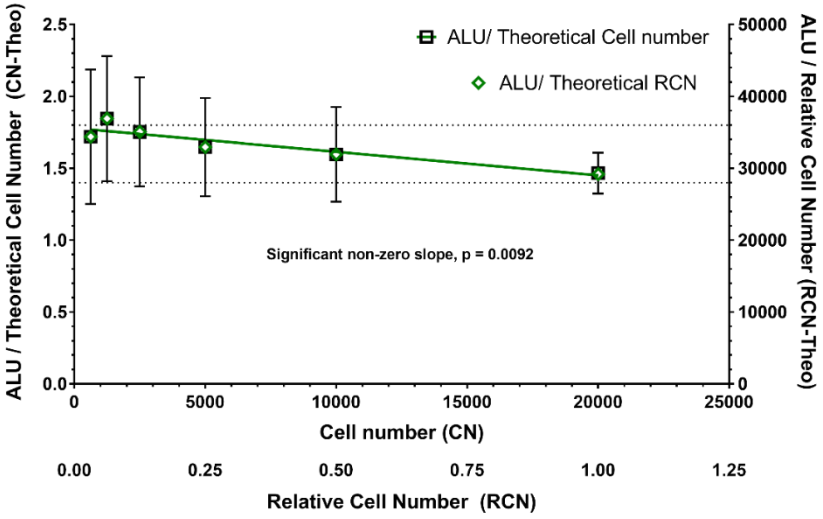

Figure 7-5: Cell number and relative cell number are inter-changeable.
(ALU/CN-Theo) represents luminescence produced by one cell; (ALU/RCN-Theo) represents the luminescence produced by 1% of cells. CN – cell number; RCN – relative cell number.

7.3.2.2 Theoretical RCN over-compensates Luciferase Data

The same data can be used to answer another simple question: Does relative cell number (RCN) based normalization of luciferase assay completely compensate the luminescence lost due to cell death?

The above experiment, cell number vs luminescence, resembles a nanoparticle treatment assay where the transfection agent (nanoparticle) is toxic to the cells resulting in a decrease in cell number, but there is no effect on gene silencing due to this treatment. As the actual decrease in cell number in the experimental setup was due to serial dilution, there is no factor (siRNA or miRNA) contributing to the decrease in the luciferase expression. It was assumed that the maximum number of cells seeded [20000 cells/well] were untreated cells representing 100% live cells. All other lower cell numbers [10000 to 0 cells/well] were assumed to be equivalent to the decrease in cellular viability due to nanoparticle treatment [(Relative cell number, RCN = Percentage viable cells: 50% (10000); 25% (5000); 12.5% (2500); 6.25% (1250); 3.125% (625 cells/ well)]. Ideally, the ratio between the luminescence and relative cell number (ALU/RCN, cell number normalized luminescence) should be a constant value. In this case, (ALU/RCN) from all lower cell numbers should be the same as the ALU/RCN obtained from the maximum number of cells. However, as the cell number decreased the value of ALU/ RCN increased indicating that the theoretical cell number was over-compensating the luminescence. Also, the standard deviation of the compensated data showed huge variation, due to the fact that the luminescence value is divided by a decimal number less than one (0.99 – 0.01), which amplified the small variation in the data.

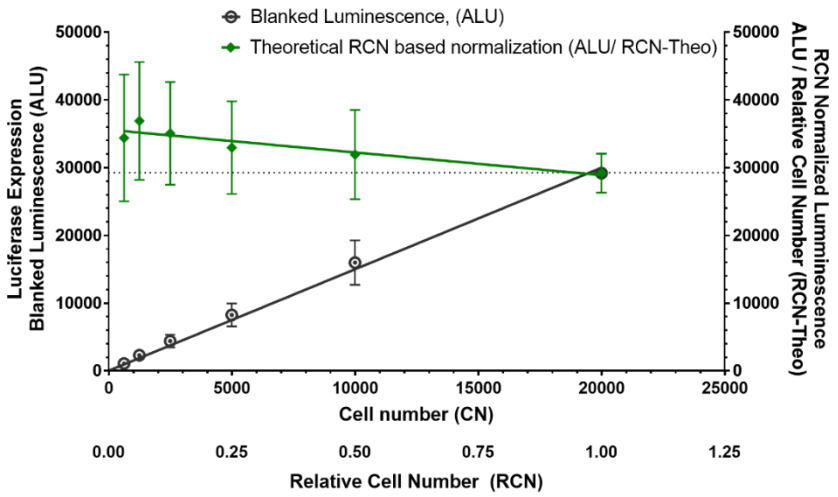

Figure 7-6: Luminescence normalized with theoretical-RCN.

The black line represents the background subtracted luminescence data (ALU), while the green line represents the normalized luminescence obtained by dividing the luminescence by the relative cell number (ALU /RCN-Theo). The dotted line represents an ideal normalization outcome (slope, m = 0).

7.3.2.3 Protein Based Normalization Under-Compensates the Data

In a typical transfection experiment, the final number of cells after treatment is not known, hence the amount of protein (mg of protein) or luminescence from a second reporter gene (*Renilla* luminescence) is generally used for data normalization. Here, the luciferase normalization was made with amount of protein (ALU/ mg of protein) and relative cell number obtained from resorufin fluorescence (ALU/ RCN-FLU), **Figure 7-7** (page: 234). The normalized luminescence obtained from resazurin based RCN produced almost a horizontal line indicated by a slope that was not significantly different from zero ($p = 0.3574$, not significant). The reason why the RCN from resazurin assay perform better than the theoretical RCN, is that the RCN calculated from resazurin assay might be more accurate representation of the actual number of cells present during the luciferase assay. The pipetting errors and well to well seeding variations could also be compensated by resazurin assay. Also, this recapitulated the normal convention that the luciferase expression is highly linear with cell number. The same data was represented in percentage luciferase expression for comparison, **Figure 7-8** (page: 234). For each condition, the mean luminescence from 20000 cells/well were assumed as 100%.

On the contrary, the luciferase normalization based on amount of protein under-compensated luminescence data for all the tested conditions, especially when the cell count was less than 10000 cells/ well. This posed a serious problem when testing RNAi-delivery systems, as there is a high chance of false positive being detected, especially when the delivery system is more toxic to the cells. This under-compensation occurs because the protein assay measures higher amount of protein at the low cell densities. It can be speculated that at low cell densities, the cells might produce higher amount of protein compared to cells seeded in high cell numbers (near confluency).

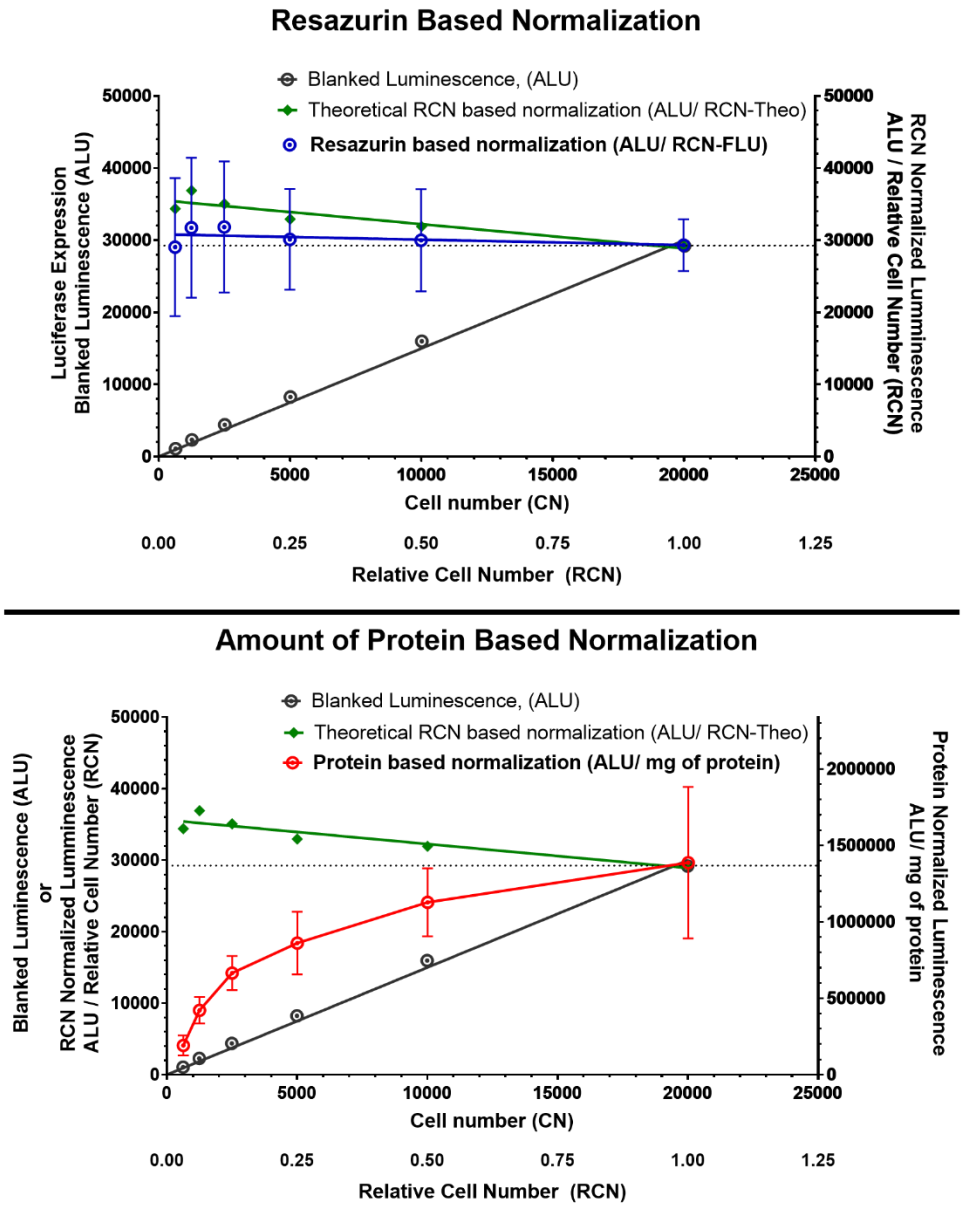

Figure 7-7: Protein- versus fluorescence-based data normalization.
The dotted line represents an ideal normalization outcome (slope, m = 0).

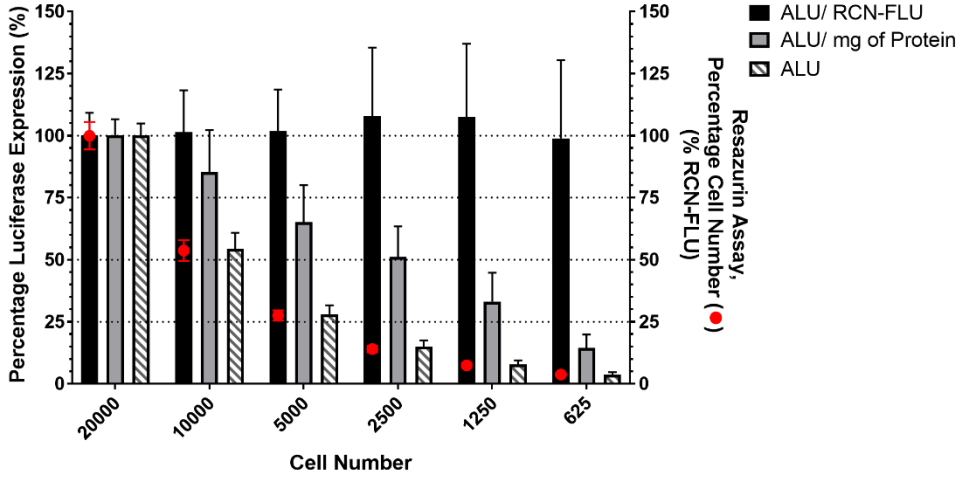

Figure 7-8: Comparison of different normalization techniques (Bar Chart).

ALU represents un-normalized background subtracted luminescence data (Striped Bar). ALU/RCN-FLU represents luciferase data normalized with relative cell number determined from resazurin assay (Black bar). This percentage RCN is presented as red dots plotted on the right-Y-axis. The grey bar represents luminescence data normalized with the amount of protein (ALU/ mg of protein), (n = 9).

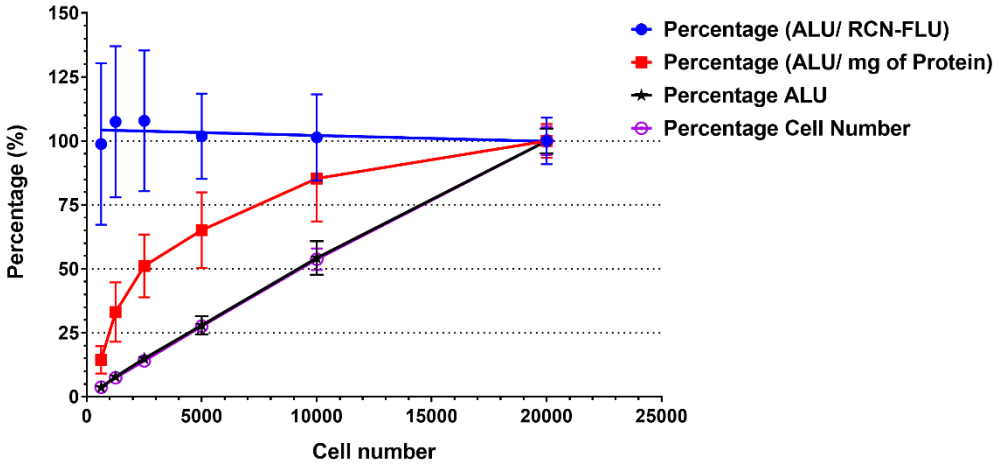

Figure 7-9: Comparison of different normalization techniques (Dot Plot).
ALU represents un-normalized background subtracted luminescence data (Star symbol, Black line). ALU/RCN-FLU represents luciferase data normalized with relative cell number determined from resazurin assay (Blue line). This percentage RCN is presented as purple open circles which exactly coincides with the percentage ALU (Black Stars). The red line represents luminescence data normalized with the amount of protein (ALU/ mg of protein), (n = 9).

7.4 Discussion

Cost-effective: Luciferase assay is one of the most widely used assay in medical research due to very high sensitivity and very low background. Luciferase assay are generally performed in a lysis (homogeneous) format using commercial assay reagents which are expensive [40 - 70 Euro/96-well plate or 35 – 55 GBP/ 96 well plate]. Alternative low cost lysis luciferase assay reagents have been proposed to reduce the cost of luciferase assay[387,388]. Live cell (non-homogeneous) luciferase assays are mostly performed when there is an availability of IVIS (*In vivo* imaging system) luminescence imaging system. Due to the advancements in the plate-reader technology, live cell luciferase quantification can be easily and cheaply performed in every lab with a luminescence plate reader with "well scan" option. The method demonstrated in this chapter uses both the quantification of luminescence and cell viability via sensitive resazurin based fluorescence method. The cost for live luciferase assay combined with live cytotoxicity assay would cost about 0.40 euros or 0.35 GBP per 96 well plate. The currently available commercial reagent that is used for the combined evaluation of cell viability and luminescence costs about 140 GBP per 96 well plate (ONE-Glo™ + Tox Luciferase Reporter and Cell Viability Assay, Promega).

Robust and Sensitive: Two different normalization techniques were tested for luciferase assay, the conventional total protein based normalization (ALU/ mg of Protein) and a novel resazurin fluorescence assay based normalization (ALU/ RCN-FLU). Both luminescence and fluorescence were found to be highly linear over the tested number of cells per well (625 to 20000 cells/ well), whereas microBCA protein assay did not accurately reflect the cell number when there were less than 10000 cells/well. Hence, protein based normalization might be suitable for nanoparticle treatments performed with large number of cells (> 10000 cells/well, U87MG). Most of the medium- and high-throughput nanoparticle screening are performed in a 96-well plate format which might contain high or low cell count at the end of the assay due to toxicity of nanoparticles. Use of protein assay for normalization might falsely identify a highly toxic formulation as a better gene-silencing formulation. RNAi delivery

system screening also includes a toxicity assay to distinguish the toxic formulation from the non-toxic but efficient gene-silencing formulation. In this work, it was demonstrated that both toxicity and luciferase normalization could be performed by using resazurin based fluorescence method with high accuracy even at very low cell count (625 cells/well).

Medium and High-throughput Capabilities: The drawback of protein estimation technique is that it requires the transfection assay to be performed in a larger format (6 or 24 well plate) in order to obtain sufficient protein concentration for data normalization. These large assay formats limit the number of samples and replicates that can be performed. Protein estimation can be performed on 96-well plates only when there are sufficient number of cells seeded. Decrease in cell number by nanoparticle mediated toxic effects can reduce the amount of protein recovered and hence affecting the quality of data normalization. Also, protein estimation for a large number of samples, like 96-well plate, is laborious, time consuming and uses a lot of additional materials like microfuge tubes, pipette tips etc. This procedure involves multiple steps like cell scraping and lysate collection, centrifugation, supernatant collection, sample dilution, protein standard preparation for each set of 96-well plate and hence increase the risk of human handling error. All these make protein assay not suitable for high-throughput or even medium throughput applications. Resazurin based quantification can be performed by simple addition of resazurin supplemented medium to the cells and the results can be directly obtained from the same plate after incubation. As this step can be automated, resazurin based quantification can be easily scaled-up for high-throughput screening.

7.5 Conclusion

A simple two-step luciferase assay procedure was developed for the assessment of luciferase expression, luciferase normalization and cytotoxicity evaluation. The assay was demonstrated to be robust, sensitive and cost-effective. This assay would also avoid possible errors at low cell number that can occur in the conventional protein based luciferase normalization. Also, this assay format can be scaled-up and can be used in high-throughput screening.

References

8 References and Bibliography

1. Types of primary brain tumours. [Document]. 2014; http://www.cancerresearchuk.org/cancer-help/type/brain-tumour/about/types-of-primary-brain-tumours?view=PrinterFriendly.
2. Facts about brain tumors in the United States. 2014; http://www.braintumor.org/brain-tumor-information/brain-tumor-information/facts-about-brain-tumors-in-the-us.html.
3. Louis DN, Perry A, Reifenberger G, et al. The 2016 World Health Organization Classification of Tumors of the Central Nervous System: a summary. *Acta Neuropathol.* 2016;131(6):803-820.
4. *AJCC Cancer Staging Handbook - From the AJCC Cancer Staging | Stephen Edge | Springer.* 7 ed2010.
5. Brain Tumor Grading System | Johns Hopkins Comprehensive Brain Tumor Center. 2016; http://www.hopkinsmedicine.org/neurology_neurosurgery/centers_clinics/brain_tumor/diagnosis/brain-tumor-grade.html.
6. Laperriere N, Zuraw L, Cairncross G. Radiotherapy for newly diagnosed malignant glioma in adults: a systematic review. *Radiotherapy and oncology : journal of the European Society for Therapeutic Radiology and Oncology.* 2002;64(3):259-273.
7. Zhang C, Moore LM, Li X, Yung WK, Zhang W. IDH1/2 mutations target a key hallmark of cancer by deregulating cellular metabolism in glioma. *Neuro-oncology.* 2013;15(9):1114-1126.
8. Wang XW, Labussiere M, Valable S, et al. IDH1(R132H) mutation increases U87 glioma cell sensitivity to radiation therapy in hypoxia. *Biomed Res Int.* 2014;2014:198697.
9. Ruggiero A, Conter V, Milani M, et al. Intrathecal chemotherapy with antineoplastic agents in children. *Paediatric drugs.* 2001;3(4):237-246.
10. Dunbar EM, Pumphrey PK, Bidari S. Unexpectedly durable palliation of metastatic olfactory neuroblastoma using anti-angiogenic therapy with Bevacizumab. *Rare tumors.* 2012;4(2):e33.
11. Debinski W, Tatter SB. Convection-enhanced delivery for the treatment of brain tumors. *Expert review of neurotherapeutics.* 2009;9(10):1519-1527.
12. Dixit S, Hingorani M, Achawal S, Scott I. The sequential use of carmustine wafers (Gliadel(R)) and post-operative radiotherapy with concomitant temozolomide followed by adjuvant temozolomide: a clinical review. *British journal of neurosurgery.* 2011;25(4):459-469.
13. Liu Y, Zhu Y, Gao L, et al. Radiation treatment for medulloblastoma: a review of 64 cases at a single institute. *Japanese journal of clinical oncology.* 2005;35(3):111-115.
14. Eriksson D, Stigbrand T. Radiation-induced cell death mechanisms. *Tumour biology : the journal of the International Society for Oncodevelopmental Biology and Medicine.* 2010;31(4):363-372.
15. Li F, Sethi G. Targeting transcription factor NF-kappaB to overcome chemoresistance and radioresistance in cancer therapy. *Biochimica et biophysica acta.* 2010;1805(2):167-180.
16. Packer RJ, Zhou T, Holmes E, Vezina G, Gajjar A. Survival and secondary tumors in children with medulloblastoma receiving radiotherapy and adjuvant chemotherapy: results of Children's Oncology Group trial A9961. *Neuro-oncology.* 2013;15(1):97-103.

17. Doskaliyev A, Yamasaki F, Kenjo M, et al. Secondary anaplastic oligodendroglioma after cranial irradiation: a case report. *Journal of neuro-oncology.* 2008;88(3):299-303.
18. Bao S, Wu Q, McLendon RE, et al. Glioma stem cells promote radioresistance by preferential activation of the DNA damage response. *Nature.* 2006;444(7120):756-760.
19. Fu J, Liu ZG, Liu XM, et al. Glioblastoma stem cells resistant to temozolomide-induced autophagy. *Chinese medical journal.* 2009;122(11):1255-1259.
20. Swift LH, Golsteyn RM. Genotoxic anti-cancer agents and their relationship to DNA damage, mitosis, and checkpoint adaptation in proliferating cancer cells. *Int J Mol Sci.* 2014;15(3):3403-3431.
21. PAYNE S, MILES D. Mechanisms of anticancer drugs. *Scott-Brown's Otorhinolaryngology: Head and Neck Surgery 7Ed: 3 volume set.* 2008:134.
22. Aggarwal BB, Vijayalekshmi RV, Sung B. Targeting inflammatory pathways for prevention and therapy of cancer: short-term friend, long-term foe. *Clinical cancer research : an official journal of the American Association for Cancer Research.* 2009;15(2):425-430.
23. Clavreul A, Guette C, Faguer R, et al. Glioblastoma-associated stromal cells (GASCs) from histologically normal surgical margins have a myofibroblast phenotype and angiogenic properties. *The Journal of pathology.* 2014;233(1):74-88.
24. Ahmed KM, Li JJ. NF-kappa B-mediated adaptive resistance to ionizing radiation. *Free radical biology & medicine.* 2008;44(1):1-13.
25. Sarkaria JN, Carlson BL, Schroeder MA, et al. Use of an orthotopic xenograft model for assessing the effect of epidermal growth factor receptor amplification on glioblastoma radiation response. *Clinical cancer research : an official journal of the American Association for Cancer Research.* 2006;12(7 Pt 1):2264-2271.
26. Zhao J. Cancer stem cells and chemoresistance: The smartest survives the raid. *Pharmacol Ther.* 2016;160:145-158.
27. Torgovnick A, Schumacher B. DNA repair mechanisms in cancer development and therapy. *Frontiers in genetics.* 2015;6:157.
28. Sehedic D, Cikankowitz A, Hindre F, Davodeau F, Garcion E. Nanomedicine to overcome radioresistance in glioblastoma stem-like cells and surviving clones. *Trends Pharmacol Sci.* 2015;36(4):236-252.
29. Buhagiar A, Ayers D. Chemoresistance, cancer stem cells, and miRNA influences: the case for neuroblastoma. *Anal Cell Pathol (Amst).* 2015;2015:150634.
30. Crowder SW, Balikov DA, Hwang YS, Sung HJ. Cancer Stem Cells under Hypoxia as a Chemoresistance Factor in Breast and Brain. *Current pathobiology reports.* 2014;2(1):33-40.
31. Schaue D, McBride WH. Counteracting tumor radioresistance by targeting DNA repair. *Mol Cancer Ther.* 2005;4(10):1548-1550.
32. Mitalipov S, Wolf D. Totipotency, pluripotency and nuclear reprogramming. *Adv Biochem Eng Biotechnol.* 2009;114:185-199.
33. Li L, Neaves WB. Normal stem cells and cancer stem cells: the niche matters. *Cancer research.* 2006;66(9):4553-4557.
34. Polyak K, Weinberg RA. Transitions between epithelial and mesenchymal states: acquisition of malignant and stem cell traits. *Nature reviews Cancer.* 2009;9(4):265-273.
35. Sabisz M, Skladanowski A. Cancer stem cells and escape from drug-induced premature senescence in human lung tumor cells: implications for drug resistance and in vitro drug screening models. *Cell Cycle.* 2009;8(19):3208-3217.

36. Kim Y, Kim KH, Lee J, et al. Wnt activation is implicated in glioblastoma radioresistance. *Lab Invest.* 2012;92(3):466-473.
37. Zahreddine HA, Culjkovic-Kraljacic B, Assouline S, et al. The sonic hedgehog factor GLI1 imparts drug resistance through inducible glucuronidation. *Nature.* 2014;511(7507):90-93.
38. Diehn M, Cho RW, Lobo NA, et al. Association of reactive oxygen species levels and radioresistance in cancer stem cells. *Nature.* 2009;458(7239):780-783.
39. Ding S, Li C, Cheng N, Cui X, Xu X, Zhou G. Redox Regulation in Cancer Stem Cells. *Oxid Med Cell Longev.* 2015;2015:750798.
40. Rahman K. Studies on free radicals, antioxidants, and co-factors. *Clin Interv Aging.* 2007;2(2):219-236.
41. Cojoc M, Peitzsch C, Kurth I, et al. Aldehyde Dehydrogenase Is Regulated by beta-Catenin/TCF and Promotes Radioresistance in Prostate Cancer Progenitor Cells. *Cancer research.* 2015;75(7):1482-1494.
42. Karim A, McCarthy K, Jawahar A, Smith D, Willis B, Nanda A. Differential cyclooxygenase-2 enzyme expression in radiosensitive versus radioresistant glioblastoma multiforme cell lines. *Anticancer research.* 2005;25(1b):675-679.
43. Wood RD, Mitchell M, Sgouros J, Lindahl T. Human DNA repair genes. *Science.* 2001;291(5507):1284-1289.
44. Hegi ME, Diserens AC, Gorlia T, et al. MGMT gene silencing and benefit from temozolomide in glioblastoma. *The New England journal of medicine.* 2005;352(10):997-1003.
45. Chapman JR, Taylor MR, Boulton SJ. Playing the end game: DNA double-strand break repair pathway choice. *Mol Cell.* 2012;47(4):497-510.
46. Farmer H, McCabe N, Lord CJ, et al. Targeting the DNA repair defect in BRCA mutant cells as a therapeutic strategy. *Nature.* 2005;434(7035):917-921.
47. Fece de la Cruz F, Gapp BV, Nijman SM. Synthetic lethal vulnerabilities of cancer. *Annu Rev Pharmacol Toxicol.* 2015;55:513-531.
48. Takebe N, Miele L, Harris PJ, et al. Targeting Notch, Hedgehog, and Wnt pathways in cancer stem cells: clinical update. *Nat Rev Clin Oncol.* 2015;12(8):445-464.
49. Lee Y, Lee JK, Ahn SH, Lee J, Nam DH. WNT signaling in glioblastoma and therapeutic opportunities. *Lab Invest.* 2016;96(2):137-150.
50. Schiefer L, Visweswaran M, Perumal V, et al. Epigenetic regulation of the secreted frizzled-related protein family in human glioblastoma multiforme. *Cancer Gene Ther.* 2014;21(7):297-303.
51. Foltz G, Yoon JG, Lee H, et al. Epigenetic regulation of wnt pathway antagonists in human glioblastoma multiforme. *Genes Cancer.* 2010;1(1):81-90.
52. Zheng H, Ying H, Wiedemeyer R, et al. PLAGL2 regulates Wnt signaling to impede differentiation in neural stem cells and gliomas. *Cancer cell.* 2010;17(5):497-509.
53. Rheinbay E, Suva ML, Gillespie SM, et al. An aberrant transcription factor network essential for Wnt signaling and stem cell maintenance in glioblastoma. *Cell reports.* 2013;3(5):1567-1579.
54. Joshi K, Banasavadi-Siddegowda Y, Mo X, et al. MELK-dependent FOXM1 phosphorylation is essential for proliferation of glioma stem cells. *Stem cells (Dayton, Ohio).* 2013;31(6):1051-1063.
55. Augustin I, Goidts V, Bongers A, et al. The Wnt secretion protein Evi/Gpr177 promotes glioma tumourigenesis. *EMBO molecular medicine.* 2012;4(1):38-51.

56. Peng C, Zhang X, Yu H, Wu D, Zheng J. Wnt5a as a predictor in poor clinical outcome of patients and a mediator in chemoresistance of ovarian cancer. *Int J Gynecol Cancer.* 2011;21(2):280-288.
57. Munoz JL, Rodriguez-Cruz V, Walker ND, Greco SJ, Rameshwar P. Temozolomide resistance and tumor recurrence: Halting the Hedgehog. *Cancer Cell Microenviron.* 2015;2(2).
58. Santoni M, Burattini L, Nabissi M, et al. Essential role of Gli proteins in glioblastoma multiforme. *Curr Protein Pept Sci.* 2013;14(2):133-140.
59. Regad T. Targeting RTK Signaling Pathways in Cancer. *Cancers (Basel).* 2015;7(3):1758-1784.
60. Zhou H, Li XM, Meinkoth J, Pittman RN. Akt regulates cell survival and apoptosis at a postmitochondrial level. *J Cell Biol.* 2000;151(3):483-494.
61. Song G, Ouyang G, Bao S. The activation of Akt/PKB signaling pathway and cell survival. *Journal of cellular and molecular medicine.* 2005;9(1):59-71.
62. Spitzner M, Ebner R, Wolff HA, Ghadimi BM, Wienands J, Grade M. STAT3: A Novel Molecular Mediator of Resistance to Chemoradiotherapy. *Cancers (Basel).* 2014;6(4):1986-2011.
63. Kelley K, Knisely J, Symons M, Ruggieri R. Radioresistance of Brain Tumors. *Cancers (Basel).* 2016;8(4).
64. Joseph JV, Balasubramaniyan V, Walenkamp A, Kruyt FA. TGF-beta as a therapeutic target in high grade gliomas - promises and challenges. *Biochem Pharmacol.* 2013;85(4):478-485.
65. Barker HE, Paget JT, Khan AA, Harrington KJ. The tumour microenvironment after radiotherapy: mechanisms of resistance and recurrence. *Nature reviews Cancer.* 2015;15(7):409-425.
66. Yang L, Lin C, Wang L, Guo H, Wang X. Hypoxia and hypoxia-inducible factors in glioblastoma multiforme progression and therapeutic implications. *Exp Cell Res.* 2012;318(19):2417-2426.
67. Ganat Y, Soni S, Chacon M, Schwartz ML, Vaccarino FM. Chronic hypoxia up-regulates fibroblast growth factor ligands in the perinatal brain and induces fibroblast growth factor-responsive radial glial cells in the sub-ependymal zone. *Neuroscience.* 2002;112(4):977-991.
68. Skuli N, Monferran S, Delmas C, et al. Alphavbeta3/alphavbeta5 integrins-FAK-RhoB: a novel pathway for hypoxia regulation in glioblastoma. *Cancer research.* 2009;69(8):3308-3316.
69. Milia J, Teyssier F, Dalenc F, et al. Farnesylated RhoB inhibits radiation-induced mitotic cell death and controls radiation-induced centrosome overduplication. *Cell Death Differ.* 2005;12(5):492-501.
70. Zitvogel L, Rusakiewicz S, Routy B, Ayyoub M, Kroemer G. Immunological off-target effects of imatinib. *Nat Rev Clin Oncol.* 2016;13(7):431-446.
71. Lipchick BC, Fink EE, Nikiforov MA. Oxidative stress and proteasome inhibitors in multiple myeloma. *Pharmacol Res.* 2016;105:210-215.
72. Kiprianova I, Remy J, Milosch N, et al. Sorafenib Sensitizes Glioma Cells to the BH3 Mimetic ABT-737 by Targeting MCL1 in a STAT3-Dependent Manner. *Neoplasia.* 2015;17(7):564-573.
73. Pollack IF, Stewart CF, Kocak M, et al. A phase II study of gefitinib and irradiation in children with newly diagnosed brainstem gliomas: a report from the Pediatric Brain Tumor Consortium. *Neuro-oncology.* 2011;13(3):290-297.
74. Zheng MH, Sun HT, Xu JG, et al. Combining Whole-Brain Radiotherapy with Gefitinib/Erlotinib for Brain Metastases from Non-Small-Cell Lung Cancer: A Meta-Analysis. *Biomed Res Int.* 2016;2016:5807346.

75. Drazin D, Al-Khouja L, Patel A, Hu J, Phuphanich S. Long-term Remission Over Six Years for a Patient with Recurrent Glioblastoma Treated with Cediranib/Lomustine. *Cureus.* 2016;8(1):e460.
76. Hottinger AF, Aissa AB, Espeli V, et al. Phase I study of sorafenib combined with radiation therapy and temozolomide as first-line treatment of high-grade glioma. *British journal of cancer.* 2014;110(11):2655-2661.
77. Roviello G, Ravelli A, Polom K, et al. Apatinib: A novel receptor tyrosine kinase inhibitor for the treatment of gastric cancer. *Cancer letters.* 2016;372(2):187-191.
78. Lee Y, Kim M, Han J, et al. MicroRNA genes are transcribed by RNA polymerase II. *Embo j.* 2004;23(20):4051-4060.
79. Han J, Lee Y, Yeom KH, et al. Molecular basis for the recognition of primary microRNAs by the Drosha-DGCR8 complex. *Cell.* 2006;125(5):887-901.
80. Lund E, Guttinger S, Calado A, Dahlberg JE, Kutay U. Nuclear export of microRNA precursors. *Science.* 2004;303(5654):95-98.
81. Wilson RC, Tambe A, Kidwell MA, Noland CL, Schneider CP, Doudna JA. Dicer-TRBP complex formation ensures accurate mammalian microRNA biogenesis. *Mol Cell.* 2015;57(3):397-407.
82. Frank F, Sonenberg N, Nagar B. Structural basis for 5'-nucleotide base-specific recognition of guide RNA by human AGO2. *Nature.* 2010;465(7299):818-822.
83. Khvorova A, Reynolds A, Jayasena SD. Functional siRNAs and miRNAs exhibit strand bias. *Cell.* 2003;115(2):209-216.
84. Schwarz DS, Hutvagner G, Du T, Xu Z, Aronin N, Zamore PD. Asymmetry in the assembly of the RNAi enzyme complex. *Cell.* 2003;115(2):199-208.
85. Grimson AaFKK-HaJWKaG-EPaLLPaBDP. MicroRNA targeting specificity in mammals: determinants beyond seed pairing. *Molecular cell.* 2007;27(1):91--105.
86. Jonas S, Izaurralde E. Towards a molecular understanding of microRNA-mediated gene silencing. *Nat Rev Genet.* 2015;16(7):421-433.
87. Sicard F, Gayral M, Lulka H, Buscail L, Cordelier P. Targeting miR-21 for the Therapy of Pancreatic Cancer. *Molecular Therapy.* 2013;21(5):986-994.
88. Buscaglia LE, Li Y. Apoptosis and the target genes of microRNA-21. *Chinese journal of cancer.* 2011;30(6):371-380.
89. Bader AG. miR-34 - a microRNA replacement therapy is headed to the clinic. *Frontiers in genetics.* 2012;3:120.
90. Buechner J, Tomte E, Haug BH, et al. Tumour-suppressor microRNAs let-7 and mir-101 target the proto-oncogene MYCN and inhibit cell proliferation in MYCN-amplified neuroblastoma. *British journal of cancer.* 2011;105(2):296-303.
91. He Q, Ren X, Chen J, et al. miR-16 targets fibroblast growth factor 2 to inhibit NPC cell proliferation and invasion via PI3K/AKT and MAPK signaling pathways. *Oncotarget.* 2016;7(3):3047-3058.
92. Li X, Ling N, Bai Y, et al. MiR-16-1 plays a role in reducing migration and invasion of glioma cells. *Anat Rec (Hoboken).* 2013;296(3):427-432.
93. Jiang H, Zhang G, Wu JH, Jiang CP. Diverse roles of miR-29 in cancer (review). *Oncol Rep.* 2014;31(4):1509-1516.
94. Zheng F, Liao YJ, Cai MY, et al. Systemic delivery of microRNA-101 potently inhibits hepatocellular carcinoma in vivo by repressing multiple targets. *PLoS genetics.* 2015;11(2):e1004873.

95. Bandiera S, Pfeffer S, Baumert TF, Zeisel MB. miR-122--a key factor and therapeutic target in liver disease. *J Hepatol.* 2015;62(2):448-457.
96. Li W, Huang H, Su J, et al. miR-124 Acts as a Tumor Suppressor in Glioblastoma via the Inhibition of Signal Transducer and Activator of Transcription 3. *Mol Neurobiol.* 2016.
97. Adlakha YK, Saini N. Brain microRNAs and insights into biological functions and therapeutic potential of brain enriched miRNA-128. *Mol Cancer.* 2014;13:33.
98. Cioce M, Strano S, Muti P, Blandino G. Mir 145/143: tumor suppressor, oncogenic microenvironmental factor or ...both? *Aging (Albany NY).* 2016.
99. Zhao D, Wang R, Fang J, et al. MiR-154 Functions as a Tumor Suppressor in Glioblastoma by Targeting Wnt5a. *Mol Neurobiol.* 2016.
100. Shi L, Cheng Z, Zhang J, et al. hsa-mir-181a and hsa-mir-181b function as tumor suppressors in human glioma cells. *Brain research.* 2008;1236:185-193.
101. Jun GJ, Zhong GG, Ming ZS. miR-218 inhibits the proliferation of glioma U87 cells through the inactivation of the CDK6/cyclin D1/p21Cip1/Waf1 pathway. *Oncol Lett.* 2015;9(6):2743-2749.
102. Fareh MaTLaVVaDDaAFad-l-FDSaPPaP-SO. The miR 302-367 cluster drastically affects self-renewal and infiltration properties of glioma-initiating cells through CXCR4 repression and consequent disruption of the SHH-GLI-NANOG network. *Cell death and differentiation.* 2012;19(2):232--244.
103. Zhu Y, Yu F, Jiao Y, et al. Reduced miR-128 in Breast Tumor-Initiating Cells Induces Chemotherapeutic Resistance via Bmi-1 and ABCC5. *Clin Cancer Res.* 2011;17(22):7105-7115.
104. Adlakha YK, Khanna S, Singh R, Singh VP, Agrawal A, Saini N. Pro-apoptotic miRNA-128-2 modulates ABCA1, ABCG1 and RXRα expression and cholesterol homeostasis. *Cell Death Dis.* 2013;4:e780.
105. Ye C, Sun NX, Ma Y, et al. MicroRNA-145 contributes to enhancing radiosensitivity of cervical cancer cells. *FEBS Lett.* 2015.
106. Liu H, Liu Z, Jiang B, Huo L, Liu J, Lu J. Synthetic miR-145 Mimic Enhances the Cytotoxic Effect of the Antiangiogenic Drug Sunitinib in Glioblastoma. *Cell Biochem Biophys.* 2015.
107. Liang Z, Ahn J, Guo D, Votaw JR, Shim H. MicroRNA-302 replacement therapy sensitizes breast cancer cells to ionizing radiation. *Pharm Res.* 2013;30(4):1008-1016.
108. Zhang GM, Bao CY, Wan FN, et al. MicroRNA-302a Suppresses Tumor Cell Proliferation by Inhibiting AKT in Prostate Cancer. *PLoS One.* 2015;10(4):e0124410.
109. Ciafre SA, Galardi S, Mangiola A, et al. Extensive modulation of a set of microRNAs in primary glioblastoma. *Biochem Biophys Res Commun.* 2005;334(4):1351-1358.
110. Shi Z-M, Wang J, Yan Z, et al. MiR-128 inhibits tumor growth and angiogenesis by targeting p70S6K1. *PLoS One.* 2012;7(3):e32709.
111. Kotani A, Ha D, Hsieh J, et al. miR-128b is a potent glucocorticoid sensitizer in MLL-AF4 acute lymphocytic leukemia cells and exerts cooperative effects with miR-221. *Blood.* 2009;114(19):4169-4178.
112. Yang J, Li J, Le Y, Zhou C, Zhang S, Gong Z. PFKL/miR-128 axis regulates glycolysis by inhibiting AKT phosphorylation and predicts poor survival in lung cancer. *American journal of cancer research.* 2016;6(2):473-485.

113. Palumbo T, Faucz FR, Azevedo M, Xekouki P, Iliopoulos D, Stratakis CA. Functional screen analysis reveals miR-26b and miR-128 as central regulators of pituitary somatomammotrophic tumor growth through activation of the PTEN-AKT pathway. *Oncogene.* 2013;32(13):1651-1659.
114. Adlakha YK, Saini N. miR-128 exerts pro-apoptotic effect in a p53 transcription-dependent and -independent manner via PUMA-Bak axis. *Cell Death Dis.* 2013;4(March):e542.
115. Lam SS, Ip CK, Mak AS, Wong AS. A novel p70 S6 kinase-microRNA biogenesis axis mediates multicellular spheroid formation in ovarian cancer progression. *Oncotarget.* 2016.
116. Zhang Y, Chao T, Li R, et al. MicroRNA-128 inhibits glioma cells proliferation by targeting transcription factor E2F3a. *J Mol Med (Heidelberg, Ger).* 2009;87(1):43-51.
117. Godlewski J, Nowicki MO, Bronisz A, et al. Targeting of the Bmi-1 Oncogene/Stem Cell Renewal Factor by MicroRNA-128 Inhibits Glioma Proliferation and Self-Renewal. *Cancer Res.* 2008;68(22):9125-9130.
118. Zhou XU, Qi L, Tong S, et al. miR-128 downregulation promotes growth and metastasis of bladder cancer cells and involves VEGF-C upregulation. *Oncol Lett.* 2015;10(5):3183-3190.
119. Papagiannakopoulos T, Friedmann-Morvinski D, Neveu P, et al. Pro-neural miR-128 is a glioma tumor suppressor that targets mitogenic kinases. *Oncogene.* 2012;31(15):1884-1895.
120. Butz H, Liko I, Czirjak S, et al. Down-regulation of Wee1 kinase by a specific subset of microRNA in human sporadic pituitary adenomas. *The Journal of clinical endocrinology and metabolism.* 2010;95(10):E181-191.
121. Shang C, Hong Y, Guo Y, Liu YH, Xue YX. miR-128 regulates the apoptosis and proliferation of glioma cells by targeting RhoE. *Oncol Lett.* 2016;11(1):904-908.
122. Wang Z, Pang L, Zhao H, et al. miR-128 regulates differentiation of hair follicle mesenchymal stem cells into smooth muscle cells by targeting SMAD2. *Acta Histochem.* 2016;118(4):393-400.
123. Adlakha YK, Saini N. MicroRNA-128 downregulates Bax and induces apoptosis in human embryonic kidney cells. *Cell Mol Life Sci.* 2011;68(8):1415-1428.
124. Guidi M, Muinos-Gimeno M, Kagerbauer B, Marti E, Estivill X, Espinosa-Parrilla Y. Overexpression of miR-128 specifically inhibits the truncated isoform of NTRK3 and upregulates BCL2 in SH-SY5Y neuroblastoma cells. *BMC Mol Biol.* 2010;11:95.
125. Evangelisti C, Florian MC, Massimi I, et al. MiR-128 up-regulation inhibits Reelin and DCX expression and reduces neuroblastoma cell motility and invasiveness. *FASEB J.* 2009;23(12):4276-4287, 4210.1096/fj.4209-134965.
126. Venkataraman S, Alimova I, Fan R, Harris P, Foreman N, Vibhakar R. MicroRNA 128a increases intracellular ROS level by targeting Bmi-1 and inhibits medulloblastoma cancer cell growth by promoting senescence. *PLoS One.* 2010;5(6):e10748.
127. Na HS, Park MH, Song YR, et al. Elevated miR-128 in Periodontitis Mitigates Tumor Necrosis Factor-Alpha Response via P38 Signaling Pathway in Macrophages. *J Periodontol.* 2016:1-18.
128. Xu N, Papagiannakopoulos T, Pan G, Thomson JA, Kosik KS. MicroRNA-145 regulates OCT4, SOX2, and KLF4 and represses pluripotency in human embryonic stem cells. *Cell.* 2009;137(4):647-658.

129. Speranza MC, Frattini V, Pisati F, et al. NEDD9, a novel target of miR-145, increases the invasiveness of glioblastoma. *Oncotarget.* 2012;3(7):723-734.
130. Shi B, Sepp-Lorenzino L, Prisco M, Linsley P, deAngelis T, Baserga R. Micro RNA 145 targets the insulin receptor substrate-1 and inhibits the growth of colon cancer cells. *J Biol Chem.* 2007;282(45):32582-32590.
131. Zhu Z, Xu T, Wang L, et al. MicroRNA-145 directly targets the insulin-like growth factor receptor I in human bladder cancer cells. *FEBS Lett.* 2014.
132. Villadsen SB, Bramsen JB, Ostenfeld MS, et al. The miR-143/-145 cluster regulates plasminogen activator inhibitor-1 in bladder cancer. *British journal of cancer.* 2012;106(2):366-374.
133. Xu Q, Liu LZ, Qian X, et al. MiR-145 directly targets p70S6K1 in cancer cells to inhibit tumor growth and angiogenesis. *Nucleic Acids Res.* 2012;40(2):761-774.
134. Zhu X, Li Y, Xie C, et al. miR-145 sensitizes ovarian cancer cells to paclitaxel by targeting Sp1 and Cdk6. *Int J Cancer.* 2014;135(6):1286-1296.
135. Zhang J, Wang L, Li B, et al. miR-145 downregulates the expression of cyclin-dependent kinase 6 in human cervical carcinoma cells. *Experimental and therapeutic medicine.* 2014;8(2):591-594.
136. Shao Y, Qu Y, Dang S, Yao B, Ji M. MiR-145 inhibits oral squamous cell carcinoma (OSCC) cell growth by targeting c-Myc and Cdk6. *Cancer Cell Int.* 2013;13(1):51.
137. Cui XB, Li S, Li TT, et al. Targeting oncogenic PLCE1 by miR-145 impairs tumor proliferation and metastasis of esophageal squamous cell carcinoma. *Oncotarget.* 2016;7(2):1777-1795.
138. Gregersen LH, Jacobsen AB, Frankel LB, Wen J, Krogh A, Lund AH. MicroRNA-145 targets YES and STAT1 in colon cancer cells. *PLoS One.* 2010;5(1):e8836.
139. Wang S, Bian C, Yang Z, et al. miR-145 inhibits breast cancer cell growth through RTKN. *International journal of oncology.* 2009;34(5):1461-1466.
140. Zheng H, Liu Z, Liu T, et al. Fas signaling promotes chemoresistance in gastrointestinal cancer by up-regulating P-glycoprotein. *Oncotarget.* 2014.
141. Gong P, Zhang T, He D, Hsieh JT. MicroRNA-145 Modulates Tumor Sensitivity to Radiation in Prostate Cancer. *Radiat Res.* 2015;184(6):630-638.
142. Rani SB, Rathod SS, Karthik S, Kaur N, Muzumdar D, Shiras AS. MiR-145 functions as a tumor-suppressive RNA by targeting Sox9 and adducin 3 in human glioma cells. *Neuro-oncology.* 2013;15(10):1302-1316.
143. Sachdeva M, Mo YY. MicroRNA-145 suppresses cell invasion and metastasis by directly targeting mucin 1. *Cancer research.* 2010;70(1):378-387.
144. Tan J, Qiu K, Li M, Liang Y. Double-negative feedback loop between long non-coding RNA TUG1 and miR-145 promotes epithelial to mesenchymal transition and radioresistance in human bladder cancer cells. *FEBS Lett.* 2015;589(20 Pt B):3175-3181.
145. Wang M, Wang J, Deng J, Li X, Long W, Chang Y. MiR-145 acts as a metastasis suppressor by targeting metadherin in lung cancer. *Med Oncol.* 2015;32(1):344.
146. Dong R, Liu X, Zhang Q, et al. miR-145 inhibits tumor growth and metastasis by targeting metadherin in high-grade serous ovarian carcinoma. *Oncotarget.* 2014.

147. Chiyomaru T, Enokida H, Tatarano S, et al. miR-145 and miR-133a function as tumour suppressors and directly regulate FSCN1 expression in bladder cancer. *British journal of cancer.* 2010;102(5):883-891.
148. Hu H, Xu Z, Li C, et al. MiR-145 and miR-203 represses TGF-beta-induced epithelial-mesenchymal transition and invasion by inhibiting SMAD3 in non-small cell lung cancer cells. *Lung Cancer.* 2016;97:87-94.
149. Li Y, Huang J, Jiang Z, et al. MicroRNA-145 regulates platelet-derived growth factor-induced human aortic vascular smooth muscle cell proliferation and migration by targeting CD40. *American journal of translational research.* 2016;8(4):1813-1825.
150. Lu H, He Y, Lin L, et al. Long non-coding RNA MALAT1 modulates radiosensitivity of HR-HPV+ cervical cancer via sponging miR-145. *Tumour biology : the journal of the International Society for Oncodevelopmental Biology and Medicine.* 2016;37(2):1683-1691.
151. Gao Z, Zhu X, Dou Y. The miR-302/367 cluster: a comprehensive update on its evolution and functions. *Open Biol.* 2015;5(12):150138.
152. Subramanyam DaLSaJRLaLJYaBNaDRaBR. Multiple targets of miR-302 and miR-372 promote reprogramming of human fibroblasts to induced pluripotent stem cells. *Nature biotechnology.* 2011;29(5):443--448.
153. Lin SL, Chang DC, Ying SY, Leu D, Wu DT. MicroRNA miR-302 inhibits the tumorigenecity of human pluripotent stem cells by coordinate suppression of the CDK2 and CDK4/6 cell cycle pathways. *Cancer research.* 2010;70(22):9473-9482.
154. Wang L, Yao J, Shi X, et al. MicroRNA-302b suppresses cell proliferation by targeting EGFR in human hepatocellular carcinoma SMMC-7721 cells. *BMC Cancer.* 2013;13:448.
155. Zhang M, Yang Q, Zhang L, et al. miR-302b is a potential molecular marker of esophageal squamous cell carcinoma and functions as a tumor suppressor by targeting ErbB4. *Journal of experimental & clinical cancer research : CR.* 2014;33:10.
156. Rosa AaBAH. A regulatory circuitry comprised of miR-302 and the transcription factors OCT4 and NR2F2 regulates human embryonic stem cell differentiation. *The EMBO journal.* 2011;30(2):237--248.
157. Card DaGaHPBaLLaTKWaKYaMYaATK. Oct4/Sox2-regulated miR-302 targets cyclin D1 in human embryonic stem cells. *Molecular and cellular biology.* 2008;28(20):6426--6438.
158. Kumar MGaPNMaNAMaKALaSEHaGPC. Reactive oxygen species mediate microRNA-302 regulation of AT-rich interacting domain 4a and C-C motif ligand 5 expression during transitions between quiescence and proliferation. Vol 532012:974--982.
159. Lipchina IaEYaHMaSRaMAaTTaSCaSLaBD. Genome-wide identification of microRNA targets in human ES cells reveals a role for miR-302 in modulating BMP response. 2011;2:2173--2186.
160. Lin S-LaCDCaLC-HaYS-YaLDaWDTS. Regulation of somatic cell reprogramming through inducible mir-302 expression. *Nucleic acids research.* 2011;39(3):1054--1065.
161. Lee MR, Prasain N, Chae HD, et al. Epigenetic regulation of NANOG by miR-302 cluster-MBD2 completes induced pluripotent stem cell reprogramming. *Stem cells (Dayton, Ohio).* 2013;31(4):666-681.
162. Meiler S, Baumer Y, Toulmin E, Seng K, Boisvert WA. MicroRNA 302a is a novel modulator of cholesterol homeostasis and atherosclerosis. *Arterioscler Thromb Vasc Biol.* 2015;35(2):323-331.

163. Longmire M, Choyke PL, Kobayashi H. Clearance properties of nano-sized particles and molecules as imaging agents: considerations and caveats. *Nanomedicine (Lond).* 2008;3(5):703-717.
164. Laufer SD, Detzer A, Sczakiel G, Restle T. Selected Strategies for the Delivery of siRNA In Vitro and In Vivo. In: Erdmann AV, Barciszewski J, eds. *RNA Technologies and Their Applications*. Berlin, Heidelberg: Springer Berlin Heidelberg; 2010:29-58.
165. Juliano RL, Carver K. Cellular uptake and intracellular trafficking of oligonucleotides. *Advanced drug delivery reviews.* 2015;87:35-45.
166. Kim YJ, Maizel A, Chen X. Traffic into silence: endomembranes and post-transcriptional RNA silencing. *EMBO J.* 2014;33(9):968-980.
167. Thomson DW, Dinger ME. Endogenous microRNA sponges: evidence and controversy. *Nat Rev Genet.* 2016;17(5):272-283.
168. Gilleron J, Paramasivam P, Zeigerer A, et al. Identification of siRNA delivery enhancers by a chemical library screen. *Nucleic Acids Research.* 2015.
169. Liu YM, Xia Y, Dai W, et al. Cholesterol-conjugated let-7a mimics: antitumor efficacy on hepatocellular carcinoma in vitro and in a preclinical orthotopic xenograft model of systemic therapy. *BMC Cancer.* 2014;14:889.
170. Urbinati G, Ali HM, Rousseau Q, et al. Antineoplastic Effects of siRNA against TMPRSS2-ERG Junction Oncogene in Prostate Cancer. *PLoS One.* 2015;10(5):e0125277.
171. Ugarte-Uribe B, Grijalvo S, Busto JV, et al. Double-tailed lipid modification as a promising candidate for oligonucleotide delivery in mammalian cells. *Biochimica et biophysica acta.* 2013;1830(10):4872-4884.
172. Nishina K, Unno T, Uno Y, et al. Efficient in vivo delivery of siRNA to the liver by conjugation of alpha-tocopherol. *Molecular therapy : the journal of the American Society of Gene Therapy.* 2008;16(4):734-740.
173. Alam MR, Ming X, Fisher M, et al. Multivalent cyclic RGD conjugates for targeted delivery of small interfering RNA. *Bioconjugate chemistry.* 2011;22(8):1673-1681.
174. Rozema DB, Lewis DL, Wakefield DH, et al. Dynamic PolyConjugates for targeted in vivo delivery of siRNA to hepatocytes. *Proc Natl Acad Sci U S A.* 2007;104(32):12982-12987.
175. Kortylewski M, Swiderski P, Herrmann A, et al. In vivo delivery of siRNA to immune cells by conjugation to a TLR9 agonist enhances antitumor immune responses. *Nat Biotechnol.* 2009;27(10):925-932.
176. Asseline U, Goncalves C, Pichon C, Midoux P. Improved nuclear delivery of antisense 2'-Ome RNA by conjugation with the histidine-rich peptide H5WYG. *The journal of gene medicine.* 2014;16(7-8):157-165.
177. Xia CF, Zhang Y, Boado RJ, Pardridge WM. Intravenous siRNA of brain cancer with receptor targeting and avidin-biotin technology. *Pharm Res.* 2007;24(12):2309-2316.
178. Esposito CL, Cerchia L, Catuogno S, et al. Multifunctional aptamer-miRNA conjugates for targeted cancer therapy. *Molecular therapy : the journal of the American Society of Gene Therapy.* 2014;22(6):1151-1163.
179. Juliano RL, Ming X, Carver K, Laing B. Cellular uptake and intracellular trafficking of oligonucleotides: implications for oligonucleotide pharmacology. *Nucleic Acid Ther.* 2014;24(2):101-113.

180. Crombez L, Morris MC, Dufort S, et al. Targeting cyclin B1 through peptide-based delivery of siRNA prevents tumour growth. *Nucleic Acids Res.* 2009;37(14):4559-4569.
181. Crombez L, Aldrian-Herrada G, Konate K, et al. A new potent secondary amphipathic cell-penetrating peptide for siRNA delivery into mammalian cells. *Molecular therapy : the journal of the American Society of Gene Therapy.* 2009;17(1):95-103.
182. Kumar P, Wu H, McBride JL, et al. Transvascular delivery of small interfering RNA to the central nervous system. *Nature.* 2007;448(7149):39-43.
183. Morris MC, Vidal P, Chaloin L, Heitz F, Divita G. A new peptide vector for efficient delivery of oligonucleotides into mammalian cells. *Nucleic Acids Res.* 1997;25(14):2730-2736.
184. Kouri FM, Hurley LA, Daniel WL, et al. miR-182 integrates apoptosis, growth, and differentiation programs in glioblastoma. *Genes & development.* 2015;29(7):732-745.
185. Ghosh R, Singh LC, Shohet JM, Gunaratne PH. A gold nanoparticle platform for the delivery of functional microRNAs into cancer cells. *Biomaterials.* 2013;34(3):807-816.
186. Schade A, Delyagina E, Scharfenberg D, et al. Innovative Strategy for MicroRNA Delivery in Human Mesenchymal Stem Cells via Magnetic Nanoparticles. *Int J Mol Sci.* 2013;14(6):10710-10726.
187. Yang HW, Huang CY, Lin CW, et al. Gadolinium-functionalized nanographene oxide for combined drug and microRNA delivery and magnetic resonance imaging. *Biomaterials.* 2014;35(24):6534-6542.
188. Gujrati M, Vaidya A, Lu ZR. Multifunctional pH-Sensitive Amino Lipids for siRNA Delivery. *Bioconjugate chemistry.* 2016;27(1):19-35.
189. Hsu SH, Yu B, Wang X, et al. Cationic lipid nanoparticles for therapeutic delivery of siRNA and miRNA to murine liver tumor. *Nanomedicine.* 2013.
190. Belliveau NM, Huft J, Lin PJ, et al. Microfluidic Synthesis of Highly Potent Limit-size Lipid Nanoparticles for In Vivo Delivery of siRNA. *Molecular therapy Nucleic acids.* 2012;1:e37.
191. Costa PM, Cardoso AL, Custodia C, Cunha P, Pereira de Almeida L, Pedroso de Lima MC. MiRNA-21 silencing mediated by tumor-targeted nanoparticles combined with sunitinib: A new multimodal gene therapy approach for glioblastoma. *J Control Release.* 2015;207:31-39.
192. Xiao H, Altangerel A, Gerile G, Wu Y, Baigude H. Design of Highly Potent Lipid-Functionalized Peptidomimetics for Efficient in Vivo siRNA Delivery. *ACS applied materials & interfaces.* 2016;8(12):7638-7645.
193. Chu Y, Masoud M, Gebeyehu G. Transfection reagents. Google Patents; 2009.
194. Han SE, Kang H, Shim GY, et al. Novel cationic cholesterol derivative-based liposomes for serum-enhanced delivery of siRNA. *Int J Pharm.* 2008;353(1-2):260-269.
195. Sahay G, Querbes W, Alabi C, et al. Efficiency of siRNA delivery by lipid nanoparticles is limited by endocytic recycling. *Nat Biotechnol.* 2013;31(7):653-658.
196. Gilleron J, Querbes W, Zeigerer A, et al. Image-based analysis of lipid nanoparticle-mediated siRNA delivery, intracellular trafficking and endosomal escape. *Nat Biotechnol.* 2013;31(7):638-646.
197. David S, Resnier P, Guillot A, Pitard B, Benoit JP, Passirani C. siRNA LNCs--a novel platform of lipid nanocapsules for systemic siRNA administration. *European journal of pharmaceutics and*

biopharmaceutics : official journal of Arbeitsgemeinschaft fur Pharmazeutische Verfahrenstechnik eV. 2012;81(2):448-452.
198. Griveau A, Bejaud J, Anthiya S, Avril S, Autret D, Garcion E. Silencing of miR-21 by locked nucleic acid-lipid nanocapsule complexes sensitize human glioblastoma cells to radiation-induced cell death. *Int J Pharm.* 2013.
199. Midoux P, Pichon C. Lipid-based mRNA vaccine delivery systems. *Expert Rev Vaccines.* 2015;14(2):221-234.
200. Goncalves C, Berchel M, Gosselin MP, et al. Lipopolyplexes comprising imidazole/imidazolium lipophosphoramidate, histidinylated polyethyleneimine and siRNA as efficient formulation for siRNA transfection. *Int J Pharm.* 2014;460(1-2):264-272.
201. Wang TY, Choe JW, Pu K, et al. Ultrasound-guided delivery of microRNA loaded nanoparticles into cancer. *J Control Release.* 2015;203:99-108.
202. Sanpui P, Paul A, Chattopadhyay A. Theranostic potential of gold nanoparticle-protein agglomerates. *Nanoscale.* 2015;7(44):18411-18423.
203. Louw AM, Kolar MK, Novikova LN, et al. Chitosan polyplex mediated delivery of miRNA-124 reduces activation of microglial cells in vitro and in rat models of spinal cord injury. *Nanomedicine.* 2015.
204. Deng X, Cao M, Zhang J, et al. Hyaluronic acid-chitosan nanoparticles for co-delivery of MiR-34a and doxorubicin in therapy against triple negative breast cancer. *Biomaterials.* 2014;35(14):4333-4344.
205. Mei M, Ren Y, Zhou X, et al. Downregulation of miR-21 enhances chemotherapeutic effect of taxol in breast carcinoma cells. *Technol Cancer Res Treat.* 2010;9(1):77-86.
206. Tripathi SK, Goyal R, Kumar P, Gupta KC. Linear polyethylenimine-graft-chitosan copolymers as efficient DNA/siRNA delivery vectors in vitro and in vivo. *Nanomedicine.* 2012;8(3):337-345.
207. Hwang do W, Son S, Jang J, et al. A brain-targeted rabies virus glycoprotein-disulfide linked PEI nanocarrier for delivery of neurogenic microRNA. *Biomaterials.* 2011;32(21):4968-4975.
208. Wahlgren J, Statello L, Skogberg G, Telemo E, Valadi H. Delivery of Small Interfering RNAs to Cells via Exosomes. *Methods in molecular biology (Clifton, NJ).* 2016;1364:105-125.
209. Lunavat TR, Jang SC, Nilsson L, et al. RNAi delivery by exosome-mimetic nanovesicles - Implications for targeting c-Myc in cancer. *Biomaterials.* 2016;102:231-238.
210. Huang RQ, Qu YH, Ke WL, Zhu JH, Pei YY, Jiang C. Efficient gene delivery targeted to the brain using a transferrin-conjugated polyethyleneglycol-modified polyamidoamine dendrimer. *Faseb j.* 2007;21(4):1117-1125.
211. Huang R, Ke W, Han L, et al. Lactoferrin-modified nanoparticles could mediate efficient gene delivery to the brain in vivo. *Brain research bulletin.* 2010;81(6):600-604.
212. Ke W, Shao K, Huang R, et al. Gene delivery targeted to the brain using an Angiopep-conjugated polyethyleneglycol-modified polyamidoamine dendrimer. *Biomaterials.* 2009;30(36):6976-6985.
213. Wang L, Hao Y, Li H, et al. Co-delivery of doxorubicin and siRNA for glioma therapy by a brain targeting system: angiopep-2-modified poly(lactic-co-glycolic acid) nanoparticles. *Journal of drug targeting.* 2015;23(9):832-846.
214. Liu Y, Li J, Shao K, et al. A leptin derived 30-amino-acid peptide modified pegylated poly-L-lysine dendrigraft for brain targeted gene delivery. *Biomaterials.* 2010;31(19):5246-5257.

215. Zhan C, Wei X, Qian J, Feng L, Zhu J, Lu W. Co-delivery of TRAIL gene enhances the anti-glioblastoma effect of paclitaxel in vitro and in vivo. *J Control Release.* 2012;160(3):630-636.
216. Kanazawa T, Akiyama F, Kakizaki S, Takashima Y, Seta Y. Delivery of siRNA to the brain using a combination of nose-to-brain delivery and cell-penetrating peptide-modified nano-micelles. *Biomaterials.* 2013;34(36):9220-9226.
217. Du L, Kayali R, Bertoni C, et al. Arginine-rich cell-penetrating peptide dramatically enhances AMO-mediated ATM aberrant splicing correction and enables delivery to brain and cerebellum. *Human molecular genetics.* 2011;20(16):3151-3160.
218. Alvarez-Erviti L, Seow Y, Yin H, Betts C, Lakhal S, Wood MJ. Delivery of siRNA to the mouse brain by systemic injection of targeted exosomes. *Nat Biotechnol.* 2011;29(4):341-345.
219. Fu A, Zhang M, Gao F, Xu X, Chen Z. A novel peptide delivers plasmids across blood-brain barrier into neuronal cells as a single-component transfer vector. *PLoS One.* 2013;8(3):e59642.
220. Alexis F, Pridgen E, Molnar LK, Farokhzad OC. Factors affecting the clearance and biodistribution of polymeric nanoparticles. *Mol Pharm.* 2008;5(4):505-515.
221. Gulyaev AE, Gelperina SE, Skidan IN, Antropov AS, Kivman GY, Kreuter J. Significant transport of doxorubicin into the brain with polysorbate 80-coated nanoparticles. *Pharm Res.* 1999;16(10):1564-1569.
222. van der Ree MH, van der Meer AJ, van Nuenen AC, et al. Miravirsen dosing in chronic hepatitis C patients results in decreased microRNA-122 levels without affecting other microRNAs in plasma. *Aliment Pharmacol Ther.* 2016;43(1):102-113.
223. Yin H, Kanasty RL, Eltoukhy AA, Vegas AJ, Dorkin JR, Anderson DG. Non-viral vectors for gene-based therapy. *Nat Rev Genet.* 2014;15(8):541-555.
224. Ozcan G, Ozpolat B, Coleman RL, Sood AK, Lopez-Berestein G. Preclinical and clinical development of siRNA-based therapeutics. *Advanced drug delivery reviews.* 2015;87:108-119.
225. Van Der Ree M, de Vree ML, Stelma F, et al. LO7 : A single subcutaneous dose of 2mg/kg or 4mg/kg of RG-101, a GalNAc-conjugated oligonucleotide with antagonist activity against MIR-122, results in significant viral load reductions in chronic hepatitis C patients. *Journal of Hepatology.*62:S261.
226. Burnett JC, Rossi JJ, Tiemann K. Current progress of siRNA/shRNA therapeutics in clinical trials. *Biotechnol J.* 2011;6(9):1130-1146.
227. Bellocq NC, Pun SH, Jensen GS, Davis ME. Transferrin-containing, cyclodextrin polymer-based particles for tumor-targeted gene delivery. *Bioconjugate chemistry.* 2003;14(6):1122-1132.
228. Hwang SJ, Bellocq NC, Davis ME. Effects of structure of beta-cyclodextrin-containing polymers on gene delivery. *Bioconjugate chemistry.* 2001;12(2):280-290.
229. Davis ME, Zuckerman JE, Choi CH, et al. Evidence of RNAi in humans from systemically administered siRNA via targeted nanoparticles. *Nature.* 2010;464(7291):1067-1070.
230. Shemi A. Methods, compositions and systems for local delivery of drugs. Google Patents; 2011.
231. Zorde Khvalevsky E, Gabai R, Rachmut IH, et al. Mutant KRAS is a druggable target for pancreatic cancer. *Proc Natl Acad Sci U S A.* 2013;110(51):20723-20728.

232. French JM. Marina Biotech Achieves Broad Patent Coverage for DiLA2 Nucleic Acid Delivery Technology in U.S., Europe and Japan. 2014; http://www.marketwired.com/printer_friendly?id=1871761.
233. Panzner S, Siepi E, Lutz S, Reinsch C, Müller C. Lipids and lipid assemblies comprising transfection enhancer elements. Google Patents; 2012.
234. Endert G, Kerwitz Y, Fellermeier M. Serum-stable amphoteric liposomes. Google Patents; 2012.
235. Panzner S, Fankhänel S, Essler F, Panzner C. Amphoteric liposomes containing positive and negative membrane-based or membrane forming charge carriers and having an isoelectric point of between 4 and 8. Google Patents; 2008.
236. Essler F, Panzner S, Endert G. Ph-sensitive cationic lipids, and liposomes and nanocapsules containing the same. Google Patents; 2006.
237. Jung K O, Ray D, Daniel J S, Krzysztof M. The development of microgels/nanogels for drug delivery applications. *Progress in Polymer Science, Vol 33, No 4 (April 2008), pp 448-477, doi:101016/jprogpolymsci200801002.* 2008.
238. Molina M, Asadian-Birjand M, Balach J, Bergueiro J, Miceli E, Calderon M. Stimuli-responsive nanogel composites and their application in nanomedicine. *Chemical Society reviews.* 2015;44(17):6161-6186.
239. Lin C, Zhong Z, Lok MC, et al. Linear poly(amido amine)s with secondary and tertiary amino groups and variable amounts of disulfide linkages: synthesis and in vitro gene transfer properties. *J Control Release.* 2006;116(2):130-137.
240. Raemdonck K, Demeester J, De Smedt S. Advanced nanogel engineering for drug delivery. *Soft Matter.* 2008;5:707-715.
241. Zhang X, Malhotra S, Molina M, Haag R. Micro- and nanogels with labile crosslinks - from synthesis to biomedical applications. *Chemical Society reviews.* 2015;44(7):1948-1973.
242. McKenzie DL, Kwok KY, Rice KG. A potent new class of reductively activated peptide gene delivery agents. *J Biol Chem.* 2000;275(14):9970-9977.
243. Read ML, Singh S, Ahmed Z, et al. A versatile reducible polycation-based system for efficient delivery of a broad range of nucleic acids. *Nucleic Acids Res.* 2005;33(9):e86.
244. Matsumoto S, Christie RJ, Nishiyama N, et al. Environment-responsive block copolymer micelles with a disulfide cross-linked core for enhanced siRNA delivery. *Biomacromolecules.* 2009;10(1):119-127.
245. Garnett MC, Ferruti P, Ranucci E, Suardi MA, Heyde M, Sleat R. Sterically stabilized self-assembling reversibly cross-linked polyelectrolyte complexes with nucleic acids for environmental and medical applications. *Biochem Soc Trans.* 2009;37(Pt 4):713-716.
246. Gosselin MA, Guo W, Lee RJ. Efficient gene transfer using reversibly cross-linked low molecular weight polyethylenimine. *Bioconjugate chemistry.* 2001;12(6):989-994.
247. Trubetskoy VS, Loomis A, Slattum PM, Hagstrom JE, Budker VG, Wolff JA. Caged DNA does not aggregate in high ionic strength solutions. *Bioconjugate chemistry.* 1999;10(4):624-628.
248. Breunig M, Lungwitz U, Liebl R, Goepferich A. Breaking up the correlation between efficacy and toxicity for nonviral gene delivery. *Proc Natl Acad Sci U S A.* 2007;104(36):14454-14459.
249. Parker AL, Eckley L, Singh S, Preece JA, Collins L, Fabre JW. (LYS)(16)-based reducible polycations provide stable polyplexes with

anionic fusogenic peptides and efficient gene delivery to post mitotic cells. *Biochimica et biophysica acta.* 2007;1770(9):1331-1337.
250. Stevenson M, Ramos-Perez V, Singh S, et al. Delivery of siRNA mediated by histidine-containing reducible polycations. *J Control Release.* 2008;130(1):46-56.
251. McKenzie DL, Smiley E, Kwok KY, Rice KG. Low molecular weight disulfide cross-linking peptides as nonviral gene delivery carriers. *Bioconjugate chemistry.* 2000;11(6):901-909.
252. Kwok KY, Park Y, Yang Y, McKenzie DL, Liu Y, Rice KG. In vivo gene transfer using sulfhydryl cross-linked PEG-peptide/glycopeptide DNA co-condensates. *J Pharm Sci.* 2003;92(6):1174-1185.
253. Khargharia S, Kizzire K, Ericson MD, Baumhover NJ, Rice KG. PEG length and chemical linkage controls polyacridine peptide DNA polyplex pharmacokinetics, biodistribution, metabolic stability and in vivo gene expression. *J Control Release.* 2013;170(3):325-333.
254. Zheng N, Song Z, Liu Y, et al. Redox-responsive, reversibly-crosslinked thiolated cationic helical polypeptides for efficient siRNA encapsulation and delivery. *J Control Release.* 2015;205:231-239.
255. Klein PM, Muller K, Gutmann C, et al. Twin disulfides as opportunity for improving stability and transfection efficiency of oligoaminoethane polyplexes. *J Control Release.* 2015;205:109-119.
256. Dauty E, Remy JS, Blessing T, Behr JP. Dimerizable cationic detergents with a low cmc condense plasmid DNA into nanometric particles and transfect cells in culture. *Journal of the American Chemical Society.* 2001;123(38):9227-9234.
257. Gosselin MA, Guo W, Lee RJ. Incorporation of reversibly cross-linked polyplexes into LPDII vectors for gene delivery. *Bioconjugate chemistry.* 2002;13(5):1044-1053.
258. Candiani G, Pezzoli D, Ciani L, Chiesa R, Ristori S. Bioreducible liposomes for gene delivery: from the formulation to the mechanism of action. *PLoS One.* 2010;5(10):e13430.
259. Wang XL, Ramusovic S, Nguyen T, Lu ZR. Novel polymerizable surfactants with pH-sensitive amphiphilicity and cell membrane disruption for efficient siRNA delivery. *Bioconjugate chemistry.* 2007;18(6):2169-2177.
260. Neu M, Sitterberg J, Bakowsky U, Kissel T. Stabilized nanocarriers for plasmids based upon cross-linked poly(ethylene imine). *Biomacromolecules.* 2006;7(12):3428-3438.
261. Neu M, Germershaus O, Behe M, Kissel T. Bioreversibly crosslinked polyplexes of PEI and high molecular weight PEG show extended circulation times in vivo. *J Control Release.* 2007;124(1-2):69-80.
262. Xia W, Wang P, Lin C, et al. Bioreducible polyethylenimine-delivered siRNA targeting human telomerase reverse transcriptase inhibits HepG2 cell growth in vitro and in vivo. *J Control Release.* 2012;157(3):427-436.
263. Breunig M, Hozsa C, Lungwitz U, et al. Mechanistic investigation of poly(ethylene imine)-based siRNA delivery: disulfide bonds boost intracellular release of the cargo. *J Control Release.* 2008;130(1):57-63.
264. Peng Q, Hu C, Cheng J, Zhong Z, Zhuo R. Influence of disulfide density and molecular weight on disulfide cross-linked polyethylenimine as gene vectors. *Bioconjugate chemistry.* 2009;20(2):340-346.
265. Li D, Tang X, Pulli B, et al. Theranostic nanoparticles based on bioreducible polyethylenimine-coated iron oxide for reduction-responsive gene delivery and magnetic resonance imaging. *Int J Nanomedicine.* 2014;9:3347-3361.

266. Fang H, Zhang K, Shen G, Wooley KL, Taylor JS. Cationic shell-cross-linked knedel-like (cSCK) nanoparticles for highly efficient PNA delivery. *Mol Pharm.* 2009;6(2):615-626.
267. Shi J, Johnson RN, Schellinger JG, Carlson PM, Pun SH. Reducible HPMA-co-oligolysine copolymers for nucleic acid delivery. *Int J Pharm.* 2012;427(1):113-122.
268. Novo L, Rizzo LY, Golombek SK, et al. Decationized polyplexes as stable and safe carrier systems for improved biodistribution in systemic gene therapy. *J Control Release.* 2014;195:162-175.
269. Novo L, Takeda KM, Petteta T, et al. Targeted decationized polyplexes for siRNA delivery. *Mol Pharm.* 2015;12(1):150-161.
270. Liu J, Xu Y, Yang Q, et al. Reduction biodegradable brushed PDMAEMA derivatives synthesized by atom transfer radical polymerization and click chemistry for gene delivery. *Acta biomaterialia.* 2013;9(8):7758-7766.
271. Zhu C, Zheng M, Meng F, et al. Reversibly shielded DNA polyplexes based on bioreducible PDMAEMA-SS-PEG-SS-PDMAEMA triblock copolymers mediate markedly enhanced nonviral gene transfection. *Biomacromolecules.* 2012;13(3):769-778.
272. Lee SJ, Huh MS, Lee SY, et al. Tumor-homing poly-siRNA/glycol chitosan self-cross-linked nanoparticles for systemic siRNA delivery in cancer treatment. *Angewandte Chemie (International ed in English).* 2012;51(29):7203-7207.
273. Yhee JY, Song S, Lee SJ, et al. Cancer-targeted MDR-1 siRNA delivery using self-cross-linked glycol chitosan nanoparticles to overcome drug resistance. *J Control Release.* 2015;198:1-9.
274. Aljaeid BM. *Formulation of novel cross-linked sterically stabilised polyplexes with polyethylene glycol for DNA delivery*: School of Pharmacy, University of Nottingham 2012.
275. Danish MZ. *Formulation and characterization of self-assembling, bio-reducible cross-linked siRNA polyplexes*: Pharmacy, University of Nottingham; 2014.
276. Martello F, Piest M, Engbersen JF, Ferruti P. Effects of branched or linear architecture of bioreducible poly(amido amine)s on their in vitro gene delivery properties. *J Control Release.* 2012;164(3):372-379.
277. van der Aa LJ, Vader P, Storm G, Schiffelers RM, Engbersen JF. Optimization of poly(amido amine)s as vectors for siRNA delivery. *J Control Release.* 2011;150(2):177-186.
278. Manickam DS, Li J, Putt DA, et al. Effect of innate glutathione levels on activity of redox-responsive gene delivery vectors. *J Control Release.* 2010;141(1):77-84.
279. Li J, Manickam DS, Chen J, Oupicky D. Effect of cell membrane thiols and reduction-triggered disassembly on transfection activity of bioreducible polyplexes. *Eur J Pharm Sci.* 2012;46(3):173-180.
280. Lin C, Zhong Z, Lok MC, et al. Novel bioreducible poly(amido amine)s for highly efficient gene delivery. *Bioconjugate chemistry.* 2007;18(1):138-145.
281. Lin C, Blaauboer CJ, Timoneda MM, et al. Bioreducible poly(amido amine)s with oligoamine side chains: synthesis, characterization, and structural effects on gene delivery. *J Control Release.* 2008;126(2):166-174.
282. Piest M, Lin C, Mateos-Timoneda MA, et al. Novel poly(amido amine)s with bioreducible disulfide linkages in their diamino-units: structure effects and in vitro gene transfer properties. *J Control Release.* 2008;130(1):38-45.

283. Lin C, Zhong Z, Lok MC, et al. Random and block copolymers of bioreducible poly(amido amine)s with high- and low-basicity amino groups: study of DNA condensation and buffer capacity on gene transfection. *J Control Release.* 2007;123(1):67-75.
284. Kim TI, Ou M, Lee M, Kim SW. Arginine-grafted bioreducible poly(disulfide amine) for gene delivery systems. *Biomaterials.* 2009;30(4):658-664.
285. Nam HY, Lee Y, Lee M, et al. Erythropoietin gene delivery using an arginine-grafted bioreducible polymer system. *J Control Release.* 2012;157(3):437-444.
286. Nam K, Nam HY, Kim PH, Kim SW. Paclitaxel-conjugated PEG and arginine-grafted bioreducible poly (disulfide amine) micelles for co-delivery of drug and gene. *Biomaterials.* 2012;33(32):8122-8130.
287. Nam JP, Nam K, Nah JW, Kim SW. Evaluation of Histidylated Arginine-Grafted Bioreducible Polymer To Enhance Transfection Efficiency for Use as a Gene Carrier. *Mol Pharm.* 2015;12(7):2352-2364.
288. Kim TI, Lee M, Kim SW. A guanidinylated bioreducible polymer with high nuclear localization ability for gene delivery systems. *Biomaterials.* 2010;31(7):1798-1804.
289. Nam HY, Nam K, Lee M, Kim SW, Bull DA. Dendrimer type bio-reducible polymer for efficient gene delivery. *J Control Release.* 2012;160(3):592-600.
290. Kim HA, Nam K, Kim SW. Tumor targeting RGD conjugated bio-reducible polymer for VEGF siRNA expressing plasmid delivery. *Biomaterials.* 2014;35(26):7543-7552.
291. Kim SH, Jeong JH, Kim TI, Kim SW, Bull DA. VEGF siRNA delivery system using arginine-grafted bioreducible poly(disulfide amine). *Mol Pharm.* 2009;6(3):718-726.
292. Mateos-Timoneda MA, Lok MC, Hennink WE, Feijen J, Engbersen JF. Poly(amido amine)s as gene delivery vectors: effects of quaternary nicotinamide moieties in the side chains. *ChemMedChem.* 2008;3(3):478-486.
293. Ferruti P. Poly(amidoamine)s: Past, present, and perspectives. *Journal of Polymer Science Part A: Polymer Chemistry.* 2013;51(11):2319-2353.
294. Ranucci E, Ferruti P, Suardi MA, Manfredi A. Poly(amidoamine)s with 2-Dithiopyridine Side Substituents as Intermediates to Peptide–Polymer Conjugates. *Macromolecular Rapid Communications.* 2007;28(11):1243-1250.
295. Ranucci E, Ferruti P. Block copolymers containing poly(ethylene glycol) and poly(amido-amine) or poly(amido-thioether-amine) segments. *Macromolecules.* 1991;24(13):3747-3752.
296. Rackstraw BJ, Stolnik S, Davis SS, Bignotti F, Garnett MC. Development of multicomponent DNA delivery systems based upon poly(amidoamine)-PEG co-polymers. *Biochimica et biophysica acta.* 2002;1576(3):269-286.
297. Jones NA, Hill IR, Stolnik S, Bignotti F, Davis SS, Garnett MC. Polymer chemical structure is a key determinant of physicochemical and colloidal properties of polymer-DNA complexes for gene delivery. *Biochimica et biophysica acta.* 2000;1517(1):1-18.
298. Hill IRC, Garnett MC, Bignotti F, Davis SS. In vitro cytotoxicity of poly(amidoamine)s: relevance to DNA delivery. *Biochimica et Biophysica Acta (BBA) - General Subjects.* 1999;1427(2):161-174.
299. Ranucci E, Suardi MA, Annunziata R, Ferruti P, Chiellini F, Bartoli C. Poly(amidoamine) conjugates with disulfide-linked cholesterol pendants self-assembling into redox-sensitive nanoparticles. *Biomacromolecules.* 2008;9(10):2693-2704.

300. Vinall RL, Ripoll AZ, Wang S, Pan CX, deVere White RW. MiR-34a chemosensitizes bladder cancer cells to cisplatin treatment regardless of p53-Rb pathway status. *Int J Cancer.* 2012;130(11):2526-2538.
301. Zhang YH, Wang QQ, Li H, Ye T, Gao F, Liu YC. miR-124 radiosensitizes human esophageal cancer cell TE-1 by targeting CDK4. *Genet Mol Res.* 2016;15(2).
302. Sun X, Li Y, Yu J, Pei H, Luo P, Zhang J. miR-128 modulates chemosensitivity and invasion of prostate cancer cells through targeting ZEB1. *Japanese journal of clinical oncology.* 2015;45(5):474-482.
303. Gebhardt BJ, Dobelbower MC, Ennis WH, Bag AK, Markert JM, Fiveash JB. Patterns of failure for glioblastoma multiforme following limited-margin radiation and concurrent temozolomide. *Radiation oncology (London, England).* 2014;9:130.
304. Menei P, Jadaud E, Faisant N, et al. Stereotaxic implantation of 5-fluorouracil-releasing microspheres in malignant glioma. *Cancer.* 2004;100(2):405-410.
305. Menei P, Capelle L, Guyotat J, et al. Local and sustained delivery of 5-fluorouracil from biodegradable microspheres for the radiosensitization of malignant glioma: a randomized phase II trial. *Neurosurgery.* 2005;56(2):242-248; discussion 242-248.
306. Ellman's Reagent (FDAA). 2014; http://www.piercenet.com/product/ellmans-reagent-fdaa.
307. Wong DM, Jameson SS. *Chemistry of Protein and Nucleic Acid Cross-Linking and Conjugation.* Second Edition ed: CRC Press 2011; 2011.
308. Le Pecq JB, Paoletti C. A new fluorometric method for RNA and DNA determination. *Analytical biochemistry.* 1966;17(1):100-107.
309. Olmsted J, 3rd, Kearns DR. Mechanism of ethidium bromide fluorescence enhancement on binding to nucleic acids. *Biochemistry.* 1977;16(16):3647-3654.
310. Zetasizer Nano series User Manual (Man0485-1.1). MAN0485 Issue 1.1 ed: Malvern Instruments Ltd; 2013:250.
311. Quinten M. Limitations of Mie's Theory – Size and Quantum Size Effects in Very Small Nanoparticles. 2011:233-244.
312. Troiber C, Kasper JC, Milani S, et al. Comparison of four different particle sizing methods for siRNA polyplex characterization. *European journal of pharmaceutics and biopharmaceutics : official journal of Arbeitsgemeinschaft fur Pharmazeutische Verfahrenstechnik eV.* 2013;84(2):255-264.
313. Corporaton V. Viscotek 802 DLS - OmniSIZE 3.0 - User Manual - Help Menu. 2006:20.
314. Limited MI. Dynamic Light Scattering - Common terms defined - INFORM WHITE PAPER - MRK1764-01. 2011.
315. Phillips DJ, Gibson MI. Degradable thermoresponsive polymers which display redox-responsive LCST behaviour. *Chemical communications (Cambridge, England).* 2012;48(7):1054-1056.
316. Kabanov AV, Astafyeva IV, Chikindas ML, et al. DNA interpolyelectrolyte complexes as a tool for efficient cell transformation. *Biopolymers.* 1991;31(12):1437-1443.
317. Garnett MC. Gene-delivery systems using cationic polymers. *Crit Rev Ther Drug Carrier Syst.* 1999;16(2):147-207.
318. Dautzenberg H. Polyelectrolyte Complex Formation in Highly Aggregating Systems. 1. Effect of Salt: Polyelectrolyte Complex Formation in the Presence of NaCl. *Macromolecules.* 1997;30(25):7810-7815.

319. Perry LS, Li Y, Priftis D, Leon L, Tirrell M. The Effect of Salt on the Complex Coacervation of Vinyl Polyelectrolytes. *Polymers.* 2014;6(6).
320. Scientific T. Crosslinking Technical Handbook.
321. Benjaminsen RV, Mattebjerg MA, Henriksen JR, Moghimi SM, Andresen TL. The possible "proton sponge " effect of polyethylenimine (PEI) does not include change in lysosomal pH. *Molecular therapy : the journal of the American Society of Gene Therapy.* 2013;21(1):149-157.
322. Akinc A, Thomas M, Klibanov AM, Langer R. Exploring polyethylenimine-mediated DNA transfection and the proton sponge hypothesis. *The journal of gene medicine.* 2005;7(5):657-663.
323. Richard I, Thibault M, De Crescenzo G, Buschmann MD, Lavertu M. Ionization behavior of chitosan and chitosan-DNA polyplexes indicate that chitosan has a similar capability to induce a proton-sponge effect as PEI. *Biomacromolecules.* 2013;14(6):1732-1740.
324. Hill IR, Garnett MC, Bignotti F, Davis SS. In vitro cytotoxicity of poly(amidoamine)s: relevance to DNA delivery. *Biochimica et biophysica acta.* 1999;1427(2):161-174.
325. Barbucci R, Ferruti P, Improta C, Delfini M, Segre A, Conti F. Protonation studies of multifunctional polymers with a poly (amido-amine) structure. *Polymer.* 1978;19(11):1329-1334.
326. Meng W, Garnett MC, Walker DA, Parker TL. Penetration and intracellular uptake of poly(glycerol-adipate) nanoparticles into three-dimensional brain tumour cell culture models. *Exp Biol Med (Maywood).* 2016;241(5):466-477.
327. Sims LB, Curtis LT, Frieboes HB, Steinbach-Rankins JM. Enhanced uptake and transport of PLGA-modified nanoparticles in cervical cancer. *J Nanobiotechnology.* 2016;14:33.
328. Centonze VE, White JG. Multiphoton excitation provides optical sections from deeper within scattering specimens than confocal imaging. *Biophys J.* 1998;75(4):2015-2024.
329. Priftis D, Tirrell M. Phase behaviour and complex coacervation of aqueous polypeptide solutions. *Soft Matter.* 2012;8(36):9396-9405.
330. Ranucci E, Ferruti P, Lattanzio E, et al. Acid-base properties of poly(amidoamine)s. *Journal of Polymer Science Part A: Polymer Chemistry.* 2009;47(24):6977-6991.
331. Wan KW, Malgesini B, Verpilio I, et al. Poly(amidoamine) salt form: effect on pH-dependent membrane activity and polymer conformation in solution. *Biomacromolecules.* 2004;5(3):1102-1109.
332. van Bergen LA, Roos G, De Proft F. From thiol to sulfonic acid: modeling the oxidation pathway of protein thiols by hydrogen peroxide. *J Phys Chem A.* 2014;118(31):6078-6084.
333. Sigma-Aldrich, N-TER Nanoparticle siRNA Transfection System (N2913) - TECHNICAL BULLETIN.
334. Invitrogen, Life-Technologies, Lipofectamine® RNAiMAX Reagent (Cat: 13778), Protocol Pub. No. MAN0007825 Rev.1.0. 2013.
335. Morishita Y, Imai T, Yoshizawa H, et al. Delivery of microRNA-146a with polyethylenimine nanoparticles inhibits renal fibrosis in vivo. *Int J Nanomedicine.* 2015;10:3475-3488.
336. Santos-Carballal B, Aaldering LJ, Ritzefeld M, et al. Physicochemical and biological characterization of chitosan-microRNA nanocomplexes for gene delivery to MCF-7 breast cancer cells. *Sci Rep.* 2015;5:13567.
337. Xu S, Dong M, Liu X, Howard KA, Kjems J, Besenbacher F. Direct force measurements between siRNA and chitosan molecules using force spectroscopy. *Biophys J.* 2007;93(3):952-959.

338. Weitz DA, Lin MY, Lindsay HM. Universality laws in coagulation. *Chemometrics and Intelligent Laboratory Systems.* 1991;10(1):133-140.
339. Przybycien TM, Bailey JE. Aggregation kinetics in salt-induced protein precipitation. *AIChE Journal.* 1989;35(11):1779-1790.
340. Sun M, Liu F, Zhu Y, et al. Salt-induced aggregation of gold nanoparticles for photoacoustic imaging and photothermal therapy of cancer. *Nanoscale.* 2016;8(8):4452-4457.
341. Albanese A, Chan WC. Effect of gold nanoparticle aggregation on cell uptake and toxicity. *ACS Nano.* 2011;5(7):5478-5489.
342. Moore TL, Rodriguez-Lorenzo L, Hirsch V, et al. Nanoparticle colloidal stability in cell culture media and impact on cellular interactions. *Chemical Society reviews.* 2015;44(17):6287-6305.
343. Carlsson J, Drevin H, Axen R. Protein thiolation and reversible protein-protein conjugation. N-Succinimidyl 3-(2-pyridyldithio)propionate, a new heterobifunctional reagent. *Biochem J.* 1978;173(3):723-737.
344. Hong P, Koza S, Bouvier ES. Size-Exclusion Chromatography for the Analysis of Protein Biotherapeutics and their Aggregates. *J Liq Chromatogr Relat Technol.* 2012;35(20):2923-2950.
345. Moenner M, Hatzi E, Badet J. Secretion of ribonucleases by normal and immortalized cells grown in serum-free culture conditions. *In Vitro Cell Dev Biol Anim.* 1997;33(7):553-561.
346. Schmidtke C, Poselt E, Ostermann J, et al. Amphiphilic, cross-linkable diblock copolymers for multifunctionalized nanoparticles as biological probes. *Nanoscale.* 2013;5(16):7433-7444.
347. Hirsjarvi S, Belloche C, Hindre F, Garcion E, Benoit JP. Tumour targeting of lipid nanocapsules grafted with cRGD peptides. *European journal of pharmaceutics and biopharmaceutics : official journal of Arbeitsgemeinschaft fur Pharmazeutische Verfahrenstechnik eV.* 2014;87(1):152-159.
348. Jain N, Smith SW, Ghone S, Tomczuk B. Current ADC Linker Chemistry. *Pharmaceutical Research.* 2015;32(11):3526-3540.
349. Russell-Jones G, McTavish K, McEwan J, Rice J, Nowotnik D. Vitamin-mediated targeting as a potential mechanism to increase drug uptake by tumours. *J Inorg Biochem.* 2004;98(10):1625-1633.
350. Yellepeddi VK, Kumar A, Palakurthi S. Biotinylated poly(amido)amine (PAMAM) dendrimers as carriers for drug delivery to ovarian cancer cells in vitro. *Anticancer research.* 2009;29(8):2933-2943.
351. Jiang G, Tang S, Chen X, Ding F. Enhancing the receptor-mediated cell uptake of PLGA nanoparticle for targeted drug delivery by incorporation chitosan onto the particle surface. *Journal of Nanoparticle Research.* 2014;16(6):1-10.
352. Chen CJ, Wang JC, Zhao EY, et al. Self-assembly cationic nanoparticles based on cholesterol-grafted bioreducible poly(amidoamine) for siRNA delivery. *Biomaterials.* 2013;34(21):5303-5316.
353. Getz EB, Xiao M, Chakrabarty T, Cooke R, Selvin PR. A comparison between the sulfhydryl reductants tris(2-carboxyethyl)phosphine and dithiothreitol for use in protein biochemistry. *Analytical biochemistry.* 1999;273(1):73-80.
354. Shafer DE, Inman JK, Lees A. Reaction of Tris(2-carboxyethyl)phosphine (TCEP) with maleimide and alpha-haloacyl groups: anomalous elution of TCEP by gel filtration. *Analytical biochemistry.* 2000;282(1):161-164.

355. Tyagarajan K, Pretzer E, Wiktorowicz JE. Thiol-reactive dyes for fluorescence labeling of proteomic samples. *Electrophoresis.* 2003;24(14):2348-2358.
356. Chandrasekhar S, Topp EM. Thiol-disulfide exchange in peptides derived from human growth hormone during lyophilization and storage in the solid state. *J Pharm Sci.* 2015;104(4):1291-1302.
357. Raja MA, Katas H, Jing Wen T. Stability, Intracellular Delivery, and Release of siRNA from Chitosan Nanoparticles Using Different Cross-Linkers. *PLoS One.* 2015;10(6):e0128963.
358. Zhang Y, Zhou C, Kwak KJ, et al. Efficient siRNA delivery using a polyamidoamine dendrimer with a modified pentaerythritol core. *Pharm Res.* 2012;29(6):1627-1636.
359. Strand SP, Issa MM, Christensen BE, Varum KM, Artursson P. Tailoring of chitosans for gene delivery: novel self-branched glycosylated chitosan oligomers with improved functional properties. *Biomacromolecules.* 2008;9(11):3268-3276.
360. Draper DE, Grilley D, Soto AM. Ions and RNA folding. *Annu Rev Biophys Biomol Struct.* 2005;34:221-243.
361. Draper DE. A guide to ions and RNA structure. *RNA.* 2004;10(3):335-343.
362. Brulisauer L, Gauthier MA, Leroux JC. Disulfide-containing parenteral delivery systems and their redox-biological fate. *J Control Release.* 2014;195:147-154.
363. Gref R, Luck M, Quellec P, et al. 'Stealth' corona-core nanoparticles surface modified by polyethylene glycol (PEG): influences of the corona (PEG chain length and surface density) and of the core composition on phagocytic uptake and plasma protein adsorption. *Colloids Surf B Biointerfaces.* 2000;18(3-4):301-313.
364. Hu Y, Xie J, Tong YW, Wang CH. Effect of PEG conformation and particle size on the cellular uptake efficiency of nanoparticles with the HepG2 cells. *J Control Release.* 2007;118(1):7-17.
365. Cruje C, Chithrani DB. Polyethylene Glycol Density and Length Affects Nanoparticle Uptake by Cancer Cells. *Journal of Nanomedicine Research.* 2014;1(1):1-6.
366. Pelaz B, del Pino P, Maffre P, et al. Surface Functionalization of Nanoparticles with Polyethylene Glycol: Effects on Protein Adsorption and Cellular Uptake. *ACS Nano.* 2015;9(7):6996-7008.
367. Holland JW, Hui C, Cullis PR, Madden TD. Poly(ethylene glycol)--lipid conjugates regulate the calcium-induced fusion of liposomes composed of phosphatidylethanolamine and phosphatidylserine. *Biochemistry.* 1996;35(8):2618-2624.
368. Mishra S, Webster P, Davis ME. PEGylation significantly affects cellular uptake and intracellular trafficking of non-viral gene delivery particles. *European journal of cell biology.* 2004;83(3):97-111.
369. Hak S, Helgesen E, Hektoen HH, et al. The effect of nanoparticle polyethylene glycol surface density on ligand-directed tumor targeting studied in vivo by dual modality imaging. *ACS Nano.* 2012;6(6):5648-5658.
370. Vonarbourg A, Passirani C, Saulnier P, Benoit JP. Parameters influencing the stealthiness of colloidal drug delivery systems. *Biomaterials.* 2006;27(24):4356-4373.
371. Suk JS, Xu Q, Kim N, Hanes J, Ensign LM. PEGylation as a strategy for improving nanoparticle-based drug and gene delivery. *Advanced drug delivery reviews.* 2016;99(Pt A):28-51.
372. Maisel K, Reddy M, Xu Q, et al. Nanoparticles coated with high molecular weight PEG penetrate mucus and provide uniform vaginal

and colorectal distribution in vivo. *Nanomedicine (Lond).* 2016;11(11):1337-1343.
373. Wolinsky JB, Colson YL, Grinstaff MW. Local drug delivery strategies for cancer treatment: gels, nanoparticles, polymeric films, rods, and wafers. *J Control Release.* 2012;159(1):14-26.
374. Nance E, Zhang C, Shih TY, Xu Q, Schuster BS, Hanes J. Brain-penetrating nanoparticles improve paclitaxel efficacy in malignant glioma following local administration. *ACS Nano.* 2014;8(10):10655-10664.
375. Mastorakos P, Song E, Zhang C, et al. Biodegradable DNA Nanoparticles that Provide Widespread Gene Delivery in the Brain. *Small.* 2016;12(5):678-685.
376. Mastorakos P, Zhang C, Berry S, et al. Highly PEGylated DNA Nanoparticles Provide Uniform and Widespread Gene Transfer in the Brain. *Adv Healthc Mater.* 2015;4(7):1023-1033.
377. Yang W, Cheng Y, Xu T, Wang X, Wen LP. Targeting cancer cells with biotin-dendrimer conjugates. *Eur J Med Chem.* 2009;44(2):862-868.
378. Yellepeddi VK, Kumar A, Maher DM, Chauhan SC, Vangara KK, Palakurthi S. Biotinylated PAMAM dendrimers for intracellular delivery of cisplatin to ovarian cancer: role of SMVT. *Anticancer research.* 2011;31(3):897-906.
379. Vadlapudi AD, Vadlapatla RK, Pal D, Mitra AK. Biotin uptake by T47D breast cancer cells: functional and molecular evidence of sodium-dependent multivitamin transporter (SMVT). *Int J Pharm.* 2013;441(1-2):535-543.
380. Russell-Jones G, McEwan J. Amplification of biotin-mediated targeting. Google Patents; 2006.
381. Vadlapudi AD, Vadlapatla RK, Mitra AK. Sodium dependent multivitamin transporter (SMVT): a potential target for drug delivery. *Curr Drug Targets.* 2012;13(7):994-1003.
382. Klibanov AL, Maruyama K, Beckerleg AM, Torchilin VP, Huang L. Activity of amphipathic poly(ethylene glycol) 5000 to prolong the circulation time of liposomes depends on the liposome size and is unfavorable for immunoliposome binding to target. *Biochimica et biophysica acta.* 1991;1062(2):142-148.
383. Salvati A, Pitek AS, Monopoli MP, et al. Transferrin-functionalized nanoparticles lose their targeting capabilities when a biomolecule corona adsorbs on the surface. *Nat Nanotechnol.* 2013;8(2):137-143.
384. Parkhouse SM, Garnett MC, Chan WC. Targeting of polyamidoamine-DNA nanoparticles using the Staudinger ligation: attachment of an RGD motif either before or after complexation. *Bioorg Med Chem.* 2008;16(13):6641-6650.
385. Moradi E, Vllasaliu D, Garnett M, Falcone F, Stolnik S. Ligand density and clustering effects on endocytosis of folate modified nanoparticles. *RSC Advances.* 2012;2(7):3025-3033.
386. Ezzine S, Vassaux G, Pitard B, et al. RILES, a novel method for temporal analysis of the in vivo regulation of miRNA expression. *Nucleic Acids Res.* 2013;41(20):e192.
387. Hampf M, Gossen M. A protocol for combined Photinus and Renilla luciferase quantification compatible with protein assays. *Analytical biochemistry.* 2006;356(1):94-99.
388. SiebringvanOlst E, Vermeulen C, de Menezes RX, Howell M, Smit EF, van Beusechem VW. Affordable luciferase reporter assay for cell-based high-throughput screening. *Journal of biomolecular screening.* 2013;18(4):453-461.

389. Patel DA, Patel AC, Nolan WC, et al. High-throughput screening normalized to biological response: application to antiviral drug discovery. *Journal of biomolecular screening.* 2014;19(1):119-130.
390. Aldred SF, Collins P, Trinklein N. Identifying targets of human microrna with the LightSwitch Luciferase Assay System using 3'UTR-reporter constructs and a microRNA mimic in adherent cells. *Journal of visualized experiments : JoVE.* 2011(55).
391. Barriscale KA, O'Sullivan SA, McCarthy TV. A single secreted luciferase-based gene reporter assay. *Analytical biochemistry.* 2014;453:44-49.
392. Schagat T, Paguio A, Kopish K. Normalizing genetic reporter assays: approaches and considerations for increasing consistency and statistical significance. *CELL NOTES*. www.promega.com: *Promega Corporation*; 2007:9 - 12.
393. Tran TV, Malainer C, Schwaiger S, et al. Screening of Vietnamese medicinal plants for NF-kappaB signaling inhibitors: assessing the activity of flavonoids from the stem bark of Oroxylum indicum. *J Ethnopharmacol.* 2015;159:36-42.
394. Hobel S, Aigner A. Polyethylenimine (PEI)/siRNA-mediated gene knockdown in vitro and in vivo. *Methods in molecular biology (Clifton, NJ).* 2010;623:283-297.
395. Creusat G, Thomann JS, Maglott A, et al. Pyridylthiourea-grafted polyethylenimine offers an effective assistance to siRNA-mediated gene silencing in vitro and in vivo. *J Control Release.* 2012;157(3):418-426.
396. Goyal R, Bansal R, Tyagi S, Shukla Y, Kumar P, Gupta KC. 1,4-Butanediol diglycidyl ether (BDE)-crosslinked PEI-g-imidazole nanoparticles as nucleic acid-carriers in vitro and in vivo. *Molecular bioSystems.* 2011;7(6):2055-2065.
397. Buschmann MD, Merzouki A, Lavertu M, Thibault M, Jean M, Darras V. Chitosans for delivery of nucleic acids. *Advanced drug delivery reviews.* 2013;65(9):1234-1270.
398. Midoux P, Pichon C, Yaouanc JJ, Jaffres PA. Chemical vectors for gene delivery: a current review on polymers, peptides and lipids containing histidine or imidazole as nucleic acids carriers. *Br J Pharmacol.* 2009;157(2):166-178.
399. El-Sayed A, Futaki S, Harashima H. Delivery of macromolecules using arginine-rich cell-penetrating peptides: ways to overcome endosomal entrapment. *AAPS J.* 2009;11(1):13-22.
400. Styslinger TJ, Zhang N, Bhatt VS, Pettit N, Palmer AF, Wang PG. Site-selective glycosylation of hemoglobin with variable molecular weight oligosaccharides: potential alternative to PEGylation. *Journal of the American Chemical Society.* 2012;134(17):7507-7515.
401. Schlapschy M, Binder U, Borger C, et al. PASylation: a biological alternative to PEGylation for extending the plasma half-life of pharmaceutically active proteins. *Protein Eng Des Sel.* 2013;26(8):489-501.
402. Wang X, Cai X, Hu J, et al. Glutathione-triggered "off-on" release of anticancer drugs from dendrimer-encapsulated gold nanoparticles. *Journal of the American Chemical Society.* 2013;135(26):9805-9810.
403. Sarrazin A, Gontier A, Plaud A, et al. Single step synthesis and organization of gold colloids assisted by copolymer templates. *Nanotechnology.* 2014;25(22):225603.
404. Azubel M, Kornberg RD. Synthesis of Water-Soluble, Thiolate-Protected Gold Nanoparticles Uniform in Size. *Nano Lett.* 2016;16(5):3348-3351.

405. Chen H, Zou H, Paholak HJ, et al. Thiol-reactive amphiphilic block copolymer for coating gold nanoparticles with neutral and functionable surfaces. *Polym Chem.* 2014;5(8):2768-2773.
406. Xie M, Ding L, You Z, Gao D, Yang G, Han H. Robust hybrid nanostructures comprising gold and thiol-functionalized polymer nanoparticles: facile preparation, diverse morphologies and unique properties. *Journal of Materials Chemistry.* 2012;22(28):14108-14118.
407. Gorman CM, Moffat LF, Howard BH. Recombinant genomes which express chloramphenicol acetyltransferase in mammalian cells. *Mol Cell Biol.* 1982;2(9):1044-1051.
408. Howcroft TK, Kirshner SL, Singer DS. Measure of transient transfection efficiency using beta-galactosidase protein. *Analytical biochemistry.* 1997;244(1):22-27.
409. Rutter GA, Kennedy HJ, Wood CD, White MR, Tavare JM. Real-time imaging of gene expression in single living cells. *Chemistry & biology.* 1998;5(11):R285-290.
410. Zhang G, Gurtu V, Kain SR. An enhanced green fluorescent protein allows sensitive detection of gene transfer in mammalian cells. *Biochem Biophys Res Commun.* 1996;227(3):707-711.
411. Bronstein I, Fortin J, Stanley PE, Stewart GS, Kricka LJ. Chemiluminescent and bioluminescent reporter gene assays. *Analytical biochemistry.* 1994;219(2):169-181.
412. Fan F, Wood KV. Bioluminescent assays for high-throughput screening. *Assay and drug development technologies.* 2007;5(1):127-136.
413. Ignowski JM, Schaffer DV. Kinetic analysis and modeling of firefly luciferase as a quantitative reporter gene in live mammalian cells. *Biotechnology and bioengineering.* 2004;86(7):827-834.
414. Leclerc GM, Boockfor FR, Faught WJ, Frawley LS. Development of a destabilized firefly luciferase enzyme for measurement of gene expression. *BioTechniques.* 2000;29(3):590-591, 594-596, 598 passim.
415. Corish P, Tyler-Smith C. Attenuation of green fluorescent protein half-life in mammalian cells. *Protein engineering.* 1999;12(12):1035-1040.
416. Welsh S, Kay SA. Reporter gene expression for monitoring gene transfer. *Curr Opin Biotechnol.* 1997;8(5):617-622.
417. Pannier AK, Ariazi EA, Bellis AD, Bengali Z, Jordan VC, Shea LD. Bioluminescence imaging for assessment and normalization in transfected cell arrays. *Biotechnology and bioengineering.* 2007;98(2):486-497.
418. Mourtada-Maarabouni M, Williams GT. Protein phosphatase 4 regulates apoptosis, proliferation and mutation rate of human cells. *Biochimica et biophysica acta.* 2008;1783(8):1490-1502.
419. Tian Y, Liu Y, Wang T, et al. A microRNA-Hippo pathway that promotes cardiomyocyte proliferation and cardiac regeneration in mice. *Science translational medicine.* 2015;7(279):279ra238.
420. Kim JY, Shin KK, Lee AL, et al. MicroRNA-302 induces proliferation and inhibits oxidant-induced cell death in human adipose tissue-derived mesenchymal stem cells. *Cell Death Dis.* 2014;5:e1385.
421. Campos-Melo D, Droppelmann CA, Volkening K, Strong MJ. Comprehensive luciferase-based reporter gene assay reveals previously masked up-regulatory effects of miRNAs. *Int J Mol Sci.* 2014;15(9):15592-15602.
422. Arif T, Vasilkovsky L, Refaely Y, Konson A, Shoshan-Barmatz V. Silencing VDAC1 Expression by siRNA Inhibits Cancer Cell

Proliferation and Tumor Growth In Vivo. *Molecular therapy Nucleic acids.* 2014;3:e159.
423. Chen SM, Chen HC, Chen SJ, et al. MicroRNA-495 inhibits proliferation of glioblastoma multiforme cells by downregulating cyclin-dependent kinase 6. *World journal of surgical oncology.* 2013;11:87.
424. Smart N, Scambler PJ, Riley PR. A rapid and sensitive assay for quantification of siRNA efficiency and specificity. *Biol Proced Online.* 2005;7:1-7.
425. Dandekar DH, Kumar M, Ladha JS, Ganesh KN, Mitra D. A quantitative method for normalization of transfection efficiency using enhanced green fluorescent protein. *Analytical biochemistry.* 2005;342(2):341-344.
426. Vesuna F, Winnard P, Jr., Raman V. Enhanced green fluorescent protein as an alternative control reporter to Renilla luciferase. *Analytical biochemistry.* 2005;342(2):345-347.
427. Sims RJ, 3rd, Liss AS, Gottlieb PD. Normalization of luciferase reporter assays under conditions that alter internal controls. *BioTechniques.* 2003;34(5):938-940.
428. Siedow A, Gratchev A, Hanski C. Correct evaluation of reporter assays in different cell lines by direct determination of the introduced plasmid amount. *European journal of cell biology.* 2000;79(2):150-153.
429. O'Mahoney JV, Adams TE. Optimization of experimental variables influencing reporter gene expression in hepatoma cells following calcium phosphate transfection. *DNA and cell biology.* 1994;13(12):1227-1232.
430. Connelly CM, Thomas M, Deiters A. High-throughput luciferase reporter assay for small-molecule inhibitors of microRNA function. *Journal of biomolecular screening.* 2012;17(6):822-828.
431. Huszar T, Mucsi I, Terebessy T, et al. The use of a second reporter plasmid as an internal standard to normalize luciferase activity in transient transfection experiments may lead to a systematic error. *Journal of biotechnology.* 2001;88(3):251-258.
432. Zhang X, Chen HZ, Rovin BH. Unexpected sensitivity of synthetic Renilla luciferase control vectors to treatment with a cyclopentenone prostaglandin. *BioTechniques.* 2003;35(6):1144-1146, 1148.
433. Ho CK, Strauss JF, 3rd. Activation of the control reporter plasmids pRL-TK and pRL-SV40 by multiple GATA transcription factors can lead to aberrant normalization of transfection efficiency. *BMC biotechnology.* 2004;4:10.
434. Theile D, Spalwisz A, Weiss J. Watch out for reporter gene assays with Renilla luciferase and paclitaxel. *Analytical biochemistry.* 2013;437(2):109-110.
435. Wu GQ, Wang X, Zhou HY, et al. Evidence for transcriptional interference in a dual-luciferase reporter system. *Sci Rep.* 2015;5:17675.
436. Kreiss P, Cameron B, Rangara R, et al. Plasmid DNA size does not affect the physicochemical properties of lipoplexes but modulates gene transfer efficiency. *Nucleic Acids Res.* 1999;27(19):3792-3798.
437. Yin W, Xiang P, Li Q. Investigations of the effect of DNA size in transient transfection assay using dual luciferase system. *Analytical biochemistry.* 2005;346(2):289-294.
438. Sapan CV, Lundblad RL, Price NC. Colorimetric protein assay techniques. *Biotechnology and applied biochemistry.* 1999;29 (Pt 2):99-108.

439. Quent VM, Loessner D, Friis T, Reichert JC, Hutmacher DW. Discrepancies between metabolic activity and DNA content as tool to assess cell proliferation in cancer research. *Journal of cellular and molecular medicine.* 2010;14(4):1003-1013.
440. Bhattacharya R, Mustafi SB, Street M, Dey A, Dwivedi SK. Bmi-1: At the crossroads of physiological and pathological biology. *Genes Dis.* 2015;2(3):225-239.
441. Shinde R, Perkins J, Contag CH. Luciferin derivatives for enhanced in vitro and in vivo bioluminescence assays. *Biochemistry.* 2006;45(37):11103-11112.
442. O'Brien J, Wilson I, Orton T, Pognan F. Investigation of the Alamar Blue (resazurin) fluorescent dye for the assessment of mammalian cell cytotoxicity. *Eur J Biochem.* 2000;267(17):5421-5426.
443. Rampersad SN. Multiple applications of Alamar Blue as an indicator of metabolic function and cellular health in cell viability bioassays. *Sensors (Basel).* 2012;12(9):12347-12360.
444. Ivanov DP, Parker TL, Walker DA, et al. Multiplexing spheroid volume, resazurin and acid phosphatase viability assays for high-throughput screening of tumour spheroids and stem cell neurospheres. *PLoS One.* 2014;9(8):e103817.
445. Hill HD, Straka JG. Protein determination using bicinchoninic acid in the presence of sulfhydryl reagents. *Analytical biochemistry.* 1988;170(1):203-208.
446. Morton RE, Evans TA. Modification of the bicinchoninic acid protein assay to eliminate lipid interference in determining lipoprotein protein content. *Analytical biochemistry.* 1992;204(2):332-334.

9 Miscellaneous

COURSES ATTENDED, PUBLICATIONS AND PRESENTATIONS, CURRICULUM VITAE

Training Courses (University of Nottingham)	**Length of course**	**Credits***
Demonstrating in Laboratory Practical	½ day	1.0
Essential information skills for new researchers in pharmacy	½ day	1.0
Introduction to library services for new Pharmacy postgraduates	½ day	0.0
Microsoft PowerPoint: Advanced	1 day	2.0
Radiation - Safe Working with Ionising Radiations	½ day	0.0
Marking and Assessment for Scientists	½ day	1.0
Biological Safety	½ day	0.0
Creating a Poster in PowerPoint	½ day	1.0
Introduction to Database Design	½ day	1.0
Creating and Managing Long Documents in Microsoft Word	1 day	2.0
Creating Macros in Excel	½ day	1.0
Microsoft Access: Introduction	2 days	4.0
Microsoft Outlook: Introduction to email	½ day	1.0
Working with Photographs using GIMP	½ day	1.0
Simple Calculations in Excel	½ day	1.0
Using Excel as a Database	1 day	2.0
Endnote introduction for referencing and citing (any discipline)	½ day	1.0
Keeping up to date with research in engineering, medicine & science	½ day	1.0
More Functions in Excel	1 day	2.0
Introduction to MATLAB for Engineers	2 days	4.0
Getting into the habit of writing	½ day	1.0
Assertiveness - an Introduction	½ day	0.0
Introduction to Flow Cytometry	½ day	1.0
	45 hours	**29 credits**
Scientific / Technical Courses		
Report Writing (Compulsory) (Professor Morgan Alexander)	½ day	1.0
Scanning Probe Techniques (Dr Stephanie Allen)	½ day	1.0
Solid-Phase Peptide Synthesis (Dr Weng Chan)	½ day	1.0
Cancer Biology and Current Chemotherapy (Dr Tracey Bradshaw)	½ day	1.0
Targeted Therapeutics (Professor Cameron Alexander)	½ day	1.0
Nanoparticles - Production, Characterisation and Applications (Dr Snow Stolnik)	½ day	1.0
Cell Culture Techniques/ Stem cells (Dr Lisa White)	½ day	1.0
Practical Techniques in Gene Regulation Course	½ day	1.0
Introduction to Unix (Dr Ian Withers)	2X½ day	2.0
Statistics Course (Dr Murray Smith)	2X½ day	2.0
	18 hours	**12 credits**
	63 hours	**41 credits**

*** - One credit is awarded per half-day session**

WORKSHOPS, TRAININGS AND AUTUMN SCHOOLS

1. **NanoFar Autumn School 2012**

Place: University of Angers, France.
Duration: 1 week (18 – 27 October 2012)
Total Teaching Time: 40 hours

2. **NanoFar Autumn School 2013**

Place: University of Santiago de Compostela, Spain.
Duration: 1 week (21 – 25 October 2013)
Total Teaching Time: 24 hours

3. **NanoFar Autumn School 2014**

Place: Université Catholique de Louvain, Brussels, Belgium.
Duration: 1 week (20 – 24 October 2014)
Total Teaching Time: 26 hours

4. **Animal Experimentation – Stage II (Training)**

Course: Expérimentation Animale Mammiferes – Niveau II
Place : ONIRIS, Ecole Nationale, Nantes Atlantique, France.
French National Certification for Animal Handling: January 2013.
Duration: 1 week (14 - 19 January 2013)

5. **Cancéropole Grand Ouest Workshop (8th Edition)**

Theme : Immune and stromal responses in cancerology: new challenges for therapeutic targeting
Place : Pen Bron, La Turballe, France.
Duration: 1 week (1 – 4 October 2014)

6. **Bio Business Week (Workshop and Training)**

Theme : How to turn Bioscience into Biobusiness?
Place : Angers, France.
Duration: 1 week (8 - 12 June 2015)

Appendix II-B – Publications and Presentations

Publication

Griveau A, Bejaud J, **Anthiya S**, Avril S, Autret D, Garcion E. Silencing of miR-21 by locked nucleic acid-lipid nanocapsule complexes sensitize human glioblastoma cells to radiation-induced cell death. Int J Pharm. 2013.

My Contribution: Co-author. Locked-Nucleic Acid – Lipid Nanocapsule (LNA-LNC) interaction analysis by gel electrophoresis; Discussion and writing of the manuscript.

Manuscripts Under Preparation

Review Article

Griveau A, **Anthiya S**, Loussouarn C, Baril P, Garnett M, Issartel JP, Garcion E*. MicroRNA therapeutics and nanomedicine for brain tumour treatment.

My Contribution: Joint-first author. Preparation of the manuscript.

Research Articles

Anthiya S, Najberg M, …., Coyle B, Garnett M*, Garcion E*. Development of Normalization Technique for Live Cell Luciferase Assay with High Throughput Compatibility

My Contribution: First author. Planning and performing the experiments. Preparation of the manuscript.

Anthiya S, ….., Coyle B, Garcion E*, Garnett M*. Development of miRNA nanoparticles with crosslinkable poly(amidoamine) polymers for brain tumour treatment.

My Contribution: First author. Planning and performing the experiments. Preparation of the manuscript.

Presentation at conferences

Anthiya S, Coyle B, Garcion E*, Garnett M*. Making stable cross-linked microRNA nanoparticles for brain tumour treatment, **SFNano Grenoble** (7-9 December 2015). – **[Poster Presentation].**

Anthiya S, Garcion E, Coyle B, Garnett M*. Delivering microRNA Therapeutics for Un-druggable Cancer Targets, **NCRI Cancer Conference,** Liverpool (3-4, November 2014). – **[Poster Presentation].**

Anthiya S, Coyle B, Garnett M, Garcion E*. Assessment of microRNA mimics as radio-sensitizers in a high grade brain tumour model, "Immune and stromal responses in cancerology: new challenges for therapeutic targeting" Workshop, La Turballe, France (1-4, October 2014) – **[Poster Presentation].**

Anthiya S, Garcion E, Coyle B, Garnett M*. Developing microRNA Delivery Systems, Science Day – SFR-ICAT4208, Angers, France (27, March 2015) – **[Poster Presentation].**

PERSONAL INFORMATION

Shubaash Anthiya Ramamoorthi Gopalram

12 Rue Boileau, 49100 Angers (France)

(+33) 7 83 95 84 96

shubaash87@gmail.com

EDUCATION AND TRAINING

2012–Present

Doctoral Programme

EQF level 8

University of Nottingham, UK and University of Angers, France

Title: Development of miRNA-mimic nanoparticles for the treatment of brain tumours

- Thiol-crosslinked miRNA-polymer nanoparticles - Formulation, Characterization and *in vitro* testing

2009–2011

Master of Technology (M.Tech.) in Biotechnology

EQF level 7

Indian Institute of Technology (IIT-G), Guwahati (India)

C.P.I. **9.42 / 10.00** (C.P.I. – Cumulative Performance Index)

Bio-techniques, Genetic Engineering, Gene Therapy, Quantitative and Systems Biology.

2005–2009

Bachelor of Technology (B.Tech.) in Biotechnology

EQF level 6

Arulmigu Kalasalingam College of Engineering, Krishnankoil (India)

Percentage: **84.45 / 100.00** (First class with distinction)

Biochemistry, Cell and Molecular Biology, Biotechnology and Chemical Engineering subjects.

2003–2005

Higher Secondary Course Certificate

Swamy Matriculation Higher Secondary School., Palani, Tamil Nadu (India)

Percentage: **89.25 / 100.00**

Physics, Chemistry, Mathematics and Biology.

2002–2003

Secondary School Examination Certificate

Swamy Matriculation School., Palani, Tamil Nadu (India)

Percentage: **89.09 / 100.00**

Science, Mathematics, History and Geography.

EQF - European Qualifications Framework

PERSONAL SKILLS

Language skills

Sourashtra (Native Proficiency)

Tamil (Native Proficiency)

English (Professional Proficiency)

French (Basic Proficiency)

Hindi (Basic Proficiency)

Communication skills

- Good communication and presentation skills.
- Able to explain complex scientific concepts to a wide audience
- Good at making schematics and diagrams.

Job-related skills	- Small animal model handling and brain stereotaxic injections. - Nanoparticle Formulation - Method development, Thiol chemistry and analytical assays. - Nanoparticle Characterization - Dynamic Light Scattering (DLS), Nanoparticle Tracking Analysis (NTA), Scanning and Transmission Electron Microscopy, Atomic Force Microscope (AFM) – non-contact mode. - *In vitro* testing - Mammalian cell culture, media preparation, cell-line maintenance, Luciferase and Cytotoxicity assays, Flowcytometry, Confocal LASER Scanning Microscopy, Fluorescence Microscopy. - Spectroscopy Techniques: UV-Visible Spectrophotometry, Spectrofluorometry, Powder and thin film X-ray Diffraction (XRD) analysis, Atomic Absorption Spectroscopy, Fourier Transform Infrared Spectroscopy (FT-IR); Nuclear Magnetic Resonance Spectroscopy. - Bacterial aseptic culture techniques. - Molecular Biology Techniques: Isolation of genomic DNA from bacterial, plant and animal cells, plasmid isolation, Agarose gel electrophoresis, competent cells preparation and transformation, Polymerase Chain Reaction (PCR), cloning and restriction analysis, induction and over-expression of proteins; - Techniques in Protein Analysis: Protein purification, SDS & Native Polyacrylamide Gel Electrophoresis (PAGE), Western Blot, - Chromatography Techniques: Analytical (Thin Layer and Paper Chromatography) and Preparatory (Size Exclusion chromatography; Ion Exchange and Glutathione S-transferase (GST) affinity column chromatography).
Digital competence	- Proficient in handling academic and research softwares: EndNote, GraphPad Prism, FlowJo, ImageJ. - Proficient with Windows Operating System and Microsoft Office. - Keen and quick in learning new software tools.

RÉSUMÉ

Les glioblastomes sont des tumeurs cérébrales très agressives présentant une médiane de survie de 15 mois malgré l'usage du traitement de référence. Parmi les stratégies innovantes anti-glioblastome, les microARNs (miARN) constituent de nouvelles cibles et des outils thérapeutiques à fort potentiel. En outre, pour atteindre les cellules tumorales notamment au niveau loco-régional, les miARNs nécessitent d'être administrés grâce à dese vecteurs sûrs et efficaces. L'objectif de ce travail a été de développer un système nanoparticulaire original de polyamidoamine réticulé (PAA) capable de véhiculer des miARNs au niveau cellulaire et tissulaire. Dans un premier temps, un test basé sur l'expression de la luciférase a été mis au point afin d'étudier la cytotoxicité et l'efficacité de nanoparticules des miARNs. Dans un second temps, des nanoparticules PAA-miARN ont été développées. Différentes conditions de formulation ont été testées afin d'optimiser la complexation entre miARNs et polymères. En l'absence d'efficacité cellulaire significative des premiers objets obtenus, des modifications du procédé de formulation ont été apportées, permettant une plus grande stabilité et une meilleure efficacité. Une fonctionnalisation par greffage de groupements biotine à des complexes PAA thio-réticulés a amélioré l'efficacité des internalisations. En conclusion, ce travail a permis le développement d'une méthode simple et rapide pour l'évaluation de l'efficacité et de la cytotoxicité de nanoparticules de miARN. La stabilité des nanoparticules a été augmentée par réticulation de thiol et leur internalisation a été améliorée par le greffage, adapté et modulable, d'un ligand cellulaire.

mots-clés : vectorisation de microARN, glioblastomes, Poly(amidoamine), réticulation de thiol, greffage d'un ligand, nanomédecine, test de luciférase.

ABSTRACT

Glioblastoma are aggressive brain tumours with a median survival of 15 months even with the best currently available treatment options. microRNAs (miRNA) are ~23 nucleotide natural silencing RNAs that have great potentials to improve cancer treatment outcomes. Lack of a safe, stable and efficient delivery system has, however, hindered the use of miRNAs in clinical applications. The aim is therefore to develop a miRNA delivery system adapted to glioblastoma using linear chain cationic polyamidoamine (PAA) polymers. The first part involved the development of luciferase assay that combined the measurement of gene-knockdown efficiency and cytotoxicity of miRNA nanoparticles. The simple two-step procedure was more effective and sensitive compared to the conventional protein-based normalization method. The second part was focused on the development of miRNA nanoparticles. In the initial phase, conditions required for maximum miRNA-polymer binding was achieved, however, the newly developed miRNA-PAA-nanoparticles did not produce significant functional gene-knockdown after cell treatment. The second stage was focused on the optimization of nanoparticle formulation as a function of stability in physiological ionic concentration. Stable PAA-nanoparticles displaying moderate cellular uptake and gene-knockdown were obtained. The final stage of development was focused on PAA-nanoparticle tagging with biotin, which improved their cellular uptake. This work developed simple and informative luciferase assay; the stability of miRNA-PAA-nanoparticles was improved by thiol-crosslinking and the functional performance was strongly enhanced by a simple but smart method of ligand tagging.

keywords : miRNA Delivery, Glioblastoma, Poly(amidoamine), thiol crosslinking, ligand targeting, nanomedicine, luciferase assay.

Présidence de l'université
40 rue de rennes – BP 73532
49035 Angers cedex
Tél. 02 41 96 23 23 | Fax 02 41 96 23 00

ENGAGEMENT DE NON PLAGIAT

Je, soussigné(e) Shubaash Anthiya Ramamoorthi Gopalram.....
déclare être pleinement conscient(e) que le plagiat de documents ou d'une partie d'un document publiée sur toutes formes de support, y compris l'internet, constitue une violation des droits d'auteur ainsi qu'une fraude caractérisée.
En conséquence, je m'engage à citer toutes les sources que j'ai utilisées pour écrire ce rapport ou mémoire.

signé par l'étudiant(e) le **09** / **12** / **2016**

Cet engagement de non plagiat doit être signé et joint à tous les rapports, dossiers, mémoires.

Présidence de l'université
40 rue de rennes – BP 73532
49035 Angers cedex
Tél. 02 41 96 23 23 | Fax 02 41 96 23 00

université angers

Thèse de Doctorat

Shubaash
ANTHIYA RAMAMOORTHI GOPALRAM

Development of miRNA-mimic nanoparticles for the treatment of brain tumours

Résumé

Les glioblastomes sont des tumeurs cérébrales très agressives présentant une médiane de survie de 15 mois malgré l'usage du traitement de référence. Parmi les stratégies innovantes anti-glioblastome, les microARNs (miARN) constituent de nouvelles cibles et des outils thérapeutiques à fort potentiel. En outre, pour atteindre les cellules tumorales notamment au niveau loco-régional, les miARNs nécessitent d'être administrés grâce à dese vecteurs sûrs et efficaces. L'objectif de ce travail a été de développer un système nanoparticulaire original de polyamidoamine réticulé (PAA) capable de véhiculer des miARNs au niveau cellulaire et tissulaire. Dans un premier temps, un test basé sur l'expression de la luciférase a été mis au point afin d'étudier la cytotoxicité et l'efficacité de nanoparticules des miARNs. Dans un second temps, des nanoparticules PAA-miARN ont été développées. Différentes conditions de formulation ont été testées afin d'optimiser la complexation entre miARNs et polymères. En l'absence d'efficacité cellulaire significative des premiers objets obtenus, des modifications du procédé de formulation ont été apportées, permettant une plus grande stabilité et une meilleure efficacité. Une fonctionnalisation par greffage de groupements biotine à des complexes PAA thio-réticulés a amélioré l'efficacité des internalisations. En conclusion, ce travail a permis le développement d'une méthode simple et rapide pour l'évaluation de l'efficacité et de la cytotoxicité de nanoparticules de miARN. La stabilité des nanoparticules a été augmentée par réticulation de thiol et leur internalisation a été améliorée par le greffage, adapté et modulable, d'un ligand cellulaire.

Mots clés
vectorisation de microARN, glioblastomes, Poly(amidoamine), réticulation de thiol, greffage d'un ligand, nanomédecine, test de luciférase

Abstract

Glioblastoma are aggressive brain tumours with a median survival of 15 months even with the best currently available treatment options. microRNAs (miRNA) are ~23 nucleotide natural silencing RNAs that have great potentials to improve cancer treatment outcomes. Lack of a safe, stable and efficient delivery system has, however, hindered the use of miRNAs in clinical applications. The aim is therefore to develop a miRNA delivery system adapted to glioblastoma using linear chain cationic polyamidoamine (PAA) polymers. The first part involved the development of luciferase assay that combined the measurement of gene-knockdown efficiency and cytotoxicity of miRNA nanoparticles. The simple two-step procedure was more effective and sensitive compared to the conventional protein-based normalization method. The second part was focused on the development of miRNA nanoparticles. In the initial phase, conditions required for maximum miRNA-polymer binding was achieved, however, the newly developed miRNA-PAA-nanoparticles did not produce significant functional gene-knockdown after cell treatment. The second stage was focused on the optimization of nanoparticle formulation as a function of stability in physiological ionic concentration. Stable PAA-nanoparticles displaying moderate cellular uptake and gene-knockdown were obtained. The final stage of development was focused on PAA-nanoparticle tagging with biotin, which improved their cellular uptake. This work developed simple and informative luciferase assay; the stability of miRNA-PAA-nanoparticles was improved by thiol-crosslinking and the functional performance was strongly enhanced by a simple but smart method of ligand tagging.

Key Words
miRNA Delivery, Glioblastoma, Poly(amidoamine), thiol crosslinking, ligand targeting, nanomedicine, luciferase assay.